Evaluating the Effect of Titanium-Based PVD Metallic Thin Films on Nitrogen Diffusion Efficiency in Duplex Plasma Diffusion/Coating Systems

by:

Gorkem Yumusak

A dissertation submitted in fulfilment of the requirements for the degree of

Doctor of Philosophy

Department of Materials Science and Engineering

AUGUST 2018

ACKNOWLEDGEMENTS

ABSTRACT

Titanium is a very popular engineering metal due to its outstanding properties, such as low density and high specific strength. However, the wear resistance of titanium is very poor in many industrial environments. Wear-resistant hard coatings can be used to increase the service lifetime of manufactured products, but the effectiveness of these coatings on titanium is sometimes low due to the inadequate load-bearing capacity of the substrate. Therefore, titanium alloys benefit from a substrate strengthening thermochemical diffusion pre-treatment before the Physical Vapour Deposition (PVD) of hard ceramic coatings.

In this work, triode plasma nitriding (TPN) has been applied to increase the load-bearing capacity of titanium alloys. It is known that the effective adhesion between PVD hard coatings and titanium alloy substrates can be improved significantly after substrate diffusion pre-treatment. TPN treatments were used in this work because the diffusion of the nitrogen can be achieved more efficiently (than conventional nitriding techniques) at lower temperatures and shorter times, without the need for hydrogen in the gas mixture. Also, the (low) treatment pressure regime allows the coating and diffusion treatment stage to be combined and integrated into the same treatment equipment. Thus, the risk of hydrogen embrittlement is entirely avoided, and the treatment temperatures well below the alloy beta-transus minimise the grain growth (that can reduce the core strength and the fatigue life of the materials).

The effectiveness of triode-plasma diffusion treatment can, however, be increased by applying a thin PVD metallic layer on titanium alloy substrates before the plasma nitriding stage. In this context, different compositions of β-titanium coating (stabilised by addition of Nb) were produced on α+β Ti-6Al-4V and β Ti-4Al-10V-22Mo substrate materials; the effect of formation of the β phase in Ti-Nb coatings before nitriding on diffusion treatment efficiency (and on nitride phase formation after TPN treatment at 700°C) was analysed.

The hardening effect for Ti-Nb coated Ti-6Al-4V substrate was found higher than the other (uncoated and Ti coated) Ti-6Al-4V substrates after 4-hour triode plasma nitriding treatment. On the other hand, the hardening effect for Ti coated Ti-4Al-10V-22Mo substrate was found higher than other (uncoated and Ti-Nb coated) Ti-4Al-10V-22Mo substrates. Besides the hardness results, the wear coefficients of the Ti-Nb coated Ti-6Al-4V, and Ti coated Ti-4Al-10V-22Mo substrates (after 4-hour triode plasma nitriding treatment at 700 ℃) were found approximately 16% and 31% lower (compared to their untreated counterparts) respectively. The enhanced performance of the duplex treated samples suggested that the coating deposition process (prior to diffusion treatments) needs to be optimised for each Ti alloy to attain adequate results.

TABLE OF CONTENTS

LIST OF FIGURES

LIST OF TABLES

SYMBOLS AND ABBREVIATIONS

Symbols (Greek letters)

α	Hexagonal phase of titanium
	Face angle for long edge of Knoop indenter
α''	Martensitic phase of titanium
β	Cubic phase of titanium
	Face angle for short edge of Knoop indenter
θ	Incidence angle of X-ray
$\boldsymbol{\kappa}$	Wear coefficient
$\boldsymbol{\kappa}_c$	Coating specific wear rate
$\boldsymbol{\kappa}_s$	Substrate specific wear rate
λ	Mean free path
	Wavelength

Symbols (Latin letters)

a	Lattice parameter
b	Crater diameter
c	Interbasal lattice parameter
d	Interplanar distance
d_1, d_2	Knoop impression lengths
	Vickers impression lengths
D	Diffusivity
D_0	Pre-exponential factor
D_T	Diffusion coefficient at treatment temperature
E	Elastic modulus
h_f	Final depth after unloading
h_{max}	Indenter displacement at maximum load

H	Hardness
HK	Knoop hardness
L	Cathode sheath thickness
n	Whole number multiplier
N	Normal Load
Q	Activation energy
P_{max}	Maximum load
R	Radius of ball
	Gas constant
R_a	Arithmetic mean surface roughness
S	Abrading distance
	Slope of load-displacement curve
	Unloading stiffness
T	Temperature
V	Total wear scar volume
V_c	Wear volume of the coating
V_f	Volume fraction
V_s	Wear volume of the substrate

Abbreviations

2D	Two-dimensional
3D	Three-dimensional
AC	Alternating current
AFM	Atomic force microscopy
ASTM	American Society for Testing and Materials
BCC	Body-centred cubic
BS	British Standards

CoF	Coefficient of friction
DC	Direct Current
EDX	Energy Dispersive X-ray Spectrometer
GAXRD	Glancing angle X-ray diffraction
GDOES	Glow-discharge optical emission spectroscopy
HCP	Hexagonal close-packed
HIPIMS	High power impulse magnetron sputtering
ICDD	International Centre of Diffraction Data
ISO	International Organization for Standardization
IVD	Ion vapour deposition
PBII	Plasma-based ion implantation
PDF	Powder diffraction file
PVD	Physical vapour deposition
RF	Radiofrequency
SAE	Society of Automotive Engineers
SEM	Scanning electron microscopy
SPD	Severe plastic deformation
TPN	Triode plasma nitriding
XRD	X-Ray Diffraction

1 INTRODUCTION

Wear is one of the most harmful forms of deterioration sustained by the surface of engineering materials. The reduction of such surface damage is thus very important because it directly affects the lifetime costs of the component. Conversely, increased product service life decreases the number of part replacements, which in turn reduces the maintenance cost. Surface modification techniques are used to improve wear-resistance of materials, especially in the transport sector where the use of light alloys, such as titanium, is increasing year after year, and in many other industries (e.g. food & chemical processing, biomedical implants and devices) due to the superior properties such alloys exhibit. However, it is almost impossible to use these alloys for moving parts without surface modification technology. In this study, PVD surface pre-modification followed by Triode Plasma Nitriding (i.e. deposition of a thin α-Ti or β-Ti PVD surface layer before TPN treatment) was applied at 700°C on different titanium alloy substrates. The thermochemical treatment was applied on uncoated, Ti coated, and Ti-Nb coated titanium alloy substrates (α+β Ti-6Al-4V and β Ti-4Al-10V-22Mo).

To date, numerous examples relating to coating layers combined with diffusion treatment (or alone) can be found in the literature for titanium alloys [1]. Examples are; PVD metal layers deposited on titanium alloy substrates prior to plasma thermochemical treatment to decrease surface roughening during the TPN process [2], [3], NiTi (superelastic) interlayer deposited between an aluminium substrate and a CrN hard coating to increase tribological performance of hard and wear resistant coatings on soft compliant substrates [4], Ni deposited before TiN coating on 304 stainless steel to improve corrosion protection [5], and Ti interlayer deposition on steel before diamond coating to enhance coating adhesion [6], pre-coating of Ti-6Al-4V with IVD Al-Mg followed by PEO oxidation [7].

1

Titanium is an allotropic metal which can be found in different crystal structures (HCP= α phase and BCC= β phase) at specific temperature ranges. In normal equilibrium conditions, the alpha to beta phase transformation temperature is 882.5°C [8]. The beta phase can be stabilised by using suitable amounts of alloying elements (such as Nb, V, Mo) at room temperature. Achache et al. [9] reported the deposition of the β phase titanium alloy coatings (Ti-Nb) on glass substrates by sputtering of pure metallic targets. They found a fully α phase structure when the Nb concentration is between 3 and 9 at.%. A mixture of α and β phases was seen above 17 at. % Nb. The fully β-stabilised structure appeared at 34 at. % Nb. The amount of α phase progressively decreases with Nb addition ≥ 10 at. % because of the beta stabilisation effect of the Nb. The polymorphic structure of Ti can also provide some advantages to the TPN process. The literature suggests that nitrogen diffusion coefficients in β-Ti are about three orders of magnitude higher than in α-Ti [10,11]. On the other hand, the rate of nitrogen diffusion in a surface nitride compound layer is claimed to be 20-30 times lower than for α-Ti [12].

1.1   Aims and Objectives

- The aim of this research was to improve the efficiency of the nitriding process of different titanium alloy substrates by depositing PVD metallic surface layers (before nitriding) to increase the load-bearing capacity and the wear performance of the titanium alloy substrates.

The research involves two main stages. The first stage was to deposit a PVD metallic Ti and Ti-Nb coatings on different titanium alloy substrates. The second stage was to apply Triode Plasma Nitriding process on uncoated and previously coated titanium alloy substrates. The four main objectives to achieve the aim described above were thus:

- Designing Ti and Ti-Nb PVD metallic coatings considering their phase structures depending on their compositions and deposited substrate types. The first objective was to find almost fully β phase for Ti-Nb coatings by doping a minimum amount of Nb. The redundant increase of Nb may have detrimental effect on further nitrogen diffusion efficiency.

- Pre-depositing a pure Ti (α phase) coating layer on titanium alloy (with better results expected on β-Ti alloy substrate) before nitriding to decrease N diffusion rate (maintain nitrogen supersaturation at the near surface) and provide improved strengthening by N interstitial solid solution.

- Pre-depositing a Ti-Nb (β phase) alloy layer on titanium alloy (with better results expected on α-Ti or α+β-Ti alloy substrates) before nitriding to speed up N diffusion rates inside the substrate and to provide deep hardened zone.

- Applying Triode Plasma Nitriding (plasma assisted diffusion treatment) on uncoated and previously coated titanium alloy substrates to modify the surface by changing its chemical composition (with acceptable surface roughness) and to provide hardened diffusion layer.

1.2 Structure of this Thesis

Chapter 2 focuses on the literature work which is related to the story of this study. The starting point is titanium metal and its insufficient wear performance. This is followed by the surface engineering methods which can be used to improve wear properties. The nitriding process is then investigated deeply, by searching the nitrogen diffusion mechanisms in titanium metal and the required process parameters. Finally, new attempts to improve the nitriding efficiency are discussed, one of which is the main idea of this thesis.

Chapter 3 describes the production and testing methods (used in this study), with their brief theoretical backgrounds and their experimental procedures. The production stage consists of two steps: the deposition of metallic surface layers on the various substrates and the subsequent nitriding of them. Characterisation techniques (such as XRD, SEM, EDX, nanoindentation) were used to demonstrate the change on the surface (or near-surface) after coating and nitriding processes.

Chapter 4 presents the results related to the first production stage of this study which includes the Ti and Ti-Nb coating deposition. The optimisation of the Ti-Nb coatings, the effect of the type of substrate and working distance on the Nb concentration were described. The deposition rate of the coatings was estimated by measuring the coating thickness for different process durations.

Chapter 5 focuses on the results related to the nitriding process of uncoated, Ti coated, and Ti-Nb coated titanium alloy substrates. The effect of nitriding temperature and process duration were analysed. The effect of the thickness of the PVD metallic surface layer on titanium alloy nitriding performance was investigated.

Chapter 6 describes the results related to the wear performance of the uncoated, Ti coated, and Ti-Nb coated titanium alloy substrates after various nitriding process by applying the micro-abrasion test.

Chapter 7 (the final chapter) presents the main conclusions which can be obtained from this study. It is followed by the future work plan.

2 LITERATURE REVIEW

2.1 Titanium Metal

Titanium is one of the more abundant metals in the world. Its content in the Earth's crust is about 0.63% by mass [13]. This occurrence means that titanium comes ninth in all elements and seventh in all metals. It is a transition metal which is found in the fourth period and IVb group in the periodic table. Titanium is increasingly used because of its unique and superior properties (Table 2-1). Its density is lower than many other commonly available metals such as iron, nickel, and copper. It is also very corrosion resistant in many environments and can be used in the human body with its favourable biocompatibility.

Table 2-1 Physical properties of pure α titanium at 25°C [8], [14], [15]

Property	Value
Atomic number	22
Atomic weight	47.88
Melting point (°C)	1668
Density (kg/m^3)	4540
Lattice parameters	a=0.295 nm c=0.468 nm c/a=1.587
β-transus temperature (°C)	882
Elastic modulus (GPa)	115
Shear modulus (GPa)	44
Thermal expansion coefficient ($10^{-6}K^{-1}$)	8.36
Thermal conductivity (W/mK)	14.99
Specific heat capacity (J/kgK)	523
Electrical resistance (10^{-9} Ωm)	564.9

Titanium was discovered by William Gregor (British mineralogist) in 1791 as a "black sand" which is now known as "ilmenite ($FeTiO_3$)". The iron was then removed with a magnet, and the sand was treated with HCl (hydrochloric acid) in order to produce an oxide of a new element. After more than 100 years later (in 1910), Matthew Albert Hunter, isolated the metal by heating $TiCl_4$ (titanium tetrachloride) with Na (sodium). Finally, in 1932, Wilhelm Justin Kroll (known as the father of the titanium industry) produced some amount of titanium by treating $TiCl_4$ with Ca (calcium). He then showed reducing $TiCl_4$ with Mg (magnesium) commercially in the USA in 1940. Today, it is the most widely used method which is known as the "Kroll Process" [14]. DuPont Company (in 1948) was the first to produce titanium commercially. Titanium cannot be found in a pure state, and the difficult processing makes it expensive metal. Besides the form of ilmenite (inside the mineral sands), titanium can be found as TiO_2 (titanium dioxide or rutile) in Mexico, India and Australia. The production routes for titanium are very versatile. It can be forged, cast (investment casting), formed and machined. Powder metallurgy and additive layer manufacturing are also used to produce titanium components [8], [16]–[18].

Besides its high corrosion resistance, titanium also shows high specific strength. Aerospace, chemical, medical and leisure sectors of industry all use titanium alloys because of these two salient properties. Only a few engineering materials (such as fibre-reinforced plastics) exhibit higher specific strength than titanium below 300ºC. Titanium alloys are eligible for higher temperature applications up to 600-700ºC, in principle. However, the high specific strength property is limited for many titanium alloys when the temperature is above 500ºC because of the adverse effects of oxidation on ductility and fatigue strength. Ti-Al intermetallic alloys overcome this problem and show higher specific strength than steels and superalloys up to 1000ºC, but their low-temperature ductility is poor. Continued efforts are needed to develop titanium-based alloys to satisfy high temperature requirements [14], [19].

2.1.1 Crystal Structure

Pure titanium has hexagonal close-packed (α) crystal structure at room temperature. The atoms are changing their position at higher temperatures and form the body-centred cubic structure (β). In normal equilibrium conditions, the alpha to beta phase transformation temperature is 882.5°C [8], but titanium can be alloyed with different elements to maintain beta phase stability at lower temperatures. Titanium alloys are categorised as α, near-α, α+β, metastable-β and β alloys (Figure 2-1). Therefore, titanium is a critical material having two crystal structures and adjustable transformation temperatures to create various types of alloys having different properties.
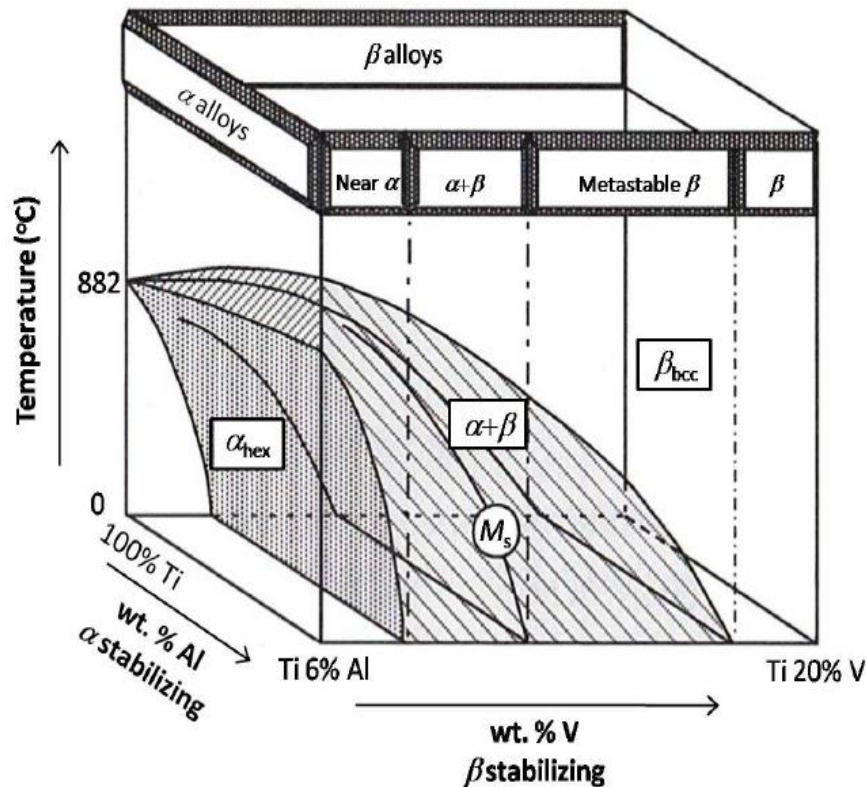
Figure 2-1 Titanium alloy classification [14]

The addition of elements which change the α/β transformation temperature can be divided into two main groups: alpha and beta stabiliser. Al, O, N, C, B, Ga, Ge are α stabilisers and can increase the transus temperature. On the other hand, β stabilisers decrease the transformation

temperature. They are categorised into two groups: β isomorphous and β eutectoid elements. V, Mo, Nb, Ta are used as β isomorphous elements. The beta phase can be stabilised by using a suitable amount of these elements at room temperature. Cr, Fe, Si, Ni, Cu, H, Mn, W, Pd, Bi are used as β eutectoid elements. Also, there are some elements which behave neutrally such as Zr, Hf, Sn decreasing the transus temperature a little at smaller amounts, then increasing it when they are added in high amounts [20].

Because of the different crystal structures and phases, Ti alloys have various characteristics. The hexagonal crystal structure of titanium shows anisotropic mechanical properties. The elastic modulus of an α titanium single crystal is 145 GPa when the load is perpendicular to the basal plane, and it is 100 GPa when the load is parallel to the basal plane. The alpha phase is more closely-packed, and this tends to affect the diffusion properties inversely. The bulk diffusion coefficient of β-Ti is reported to be significantly higher than the alpha phase of Ti. The self-diffusion of Ti is 100 times bigger in beta phase at 1000°C ($D_{\alpha Ti}= 10^{-15}$ m/s, $D_{\beta Ti}= 10^{-13}$ m/s). The different diffusion rate of the two phases is dependent on the microstructure, and this affects mechanical properties such as creep resistance and superplasticity [14].

2.1.2 Plastic Deformation

The plastic deformation of metals depends on their crystal structure. It can be clarified with three factors. The first of these is the total number of available slip systems. The total is 3 in the α phase crystal structure and 12 in the β phase crystal structure. The slip planes and directions determine the number of slip systems. It can be derived from this information that plastic deformation is easier in BCC structures than in HCP structures [14], [21].

The HCP alpha phase has a different c/a ratio than ideal hexagonal lattices. The lattice parameters for Ti are a= 0.295 nm, and c= 0.468 nm and this value give a c/a ratio of 1.587. In the ideal case, the c/a ratio is 1.633. The ratio is different from the ideal case because of the

phase transformation (β to α), in which {110} planes in BCC structure transform to {0001} basal planes in HCP structure. The distance between {110} planes is different from the corresponding distance between the basal planes, so the c axis is shrunk. The reduced ratio can be increased by diffusion of some interstitial elements into Ti or substitution of some elements which have a smaller atomic radius. When the c/a ratio is small, the space between the prismatic planes become high. In this condition, titanium can exhibit slip on prismatic planes [14].

2.2   The Necessity of Surface Engineering for Ti

With its mechanical and physical properties, such as low density and good strength to weight ratio, titanium is always an active candidate in many structural engineering material applications. However, the wear performance of Ti is inadequate for tribological environments. When titanium and other metals come together, the oxide film on the titanium can easily break and then surface damage occurs. There are some reasons to explain why Ti has a weak performance in tribological systems:

The atomic number of Ti is 22, and it is a transition metal. The electronic configuration of Ti finishes with $3d^2$. Because of this low d bond character (the relation between d bond character and friction coefficient is seen in Figure 2-2), the surface of the Ti is more active and needs to create adhesive bonding when the contact occurs. This will tend to result in a high CoF and poor wear resistance [22].
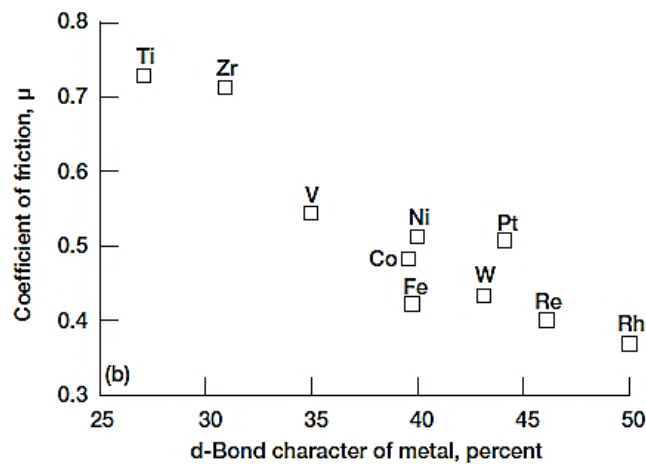
Figure 2-2 Coefficient of friction for various transition metals in contact with the diamond surface as a function of percent of metal's d-Bond character [23]

The shear modulus of Ti also affects the friction behaviour [23]. Materials which have a low shear modulus, tend to show more adhesion with a high coefficient of friction. Figure 2-3 shows the relationship between the shear modulus and coefficient of friction. The reduced c/a ratio affects the shear property of Ti because of the different slip type. On the other hand, HCP metals with c/a ratios closer to the ideal value of 1.633, show lower friction coefficients.
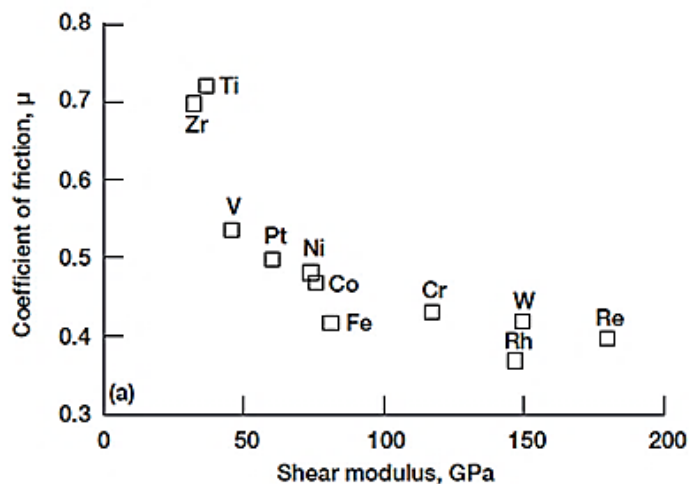
Figure 2-3 Coefficient of friction for various transition metals in contact with the diamond surface as a function of shear modulus [23]

The friction coefficient of pure Ti is 0.47 when in contact with itself, and it would be commented at the end of the measurement that some transfer and deformation had occurred. On the other hand, the Ti6Al4V alloy (α+β) has a friction coefficient of 0.36 when it contacts

itself under the same test conditions [24]. Alloying of Ti with other metals can reduce the friction coefficient. The weak tribological property of Ti and its alloys needs some surface engineering modification to increase the wear resistance property and the range of application. The lifetime of the moving parts of the engineering application, such as bearings, can also be increased in this way.

2.3   Surface Engineering Methods

Surface engineering methods are used in many industrial sectors, such as aerospace and biomedical, which often require components with an excellent tribological performance in applications on moving parts under load. There are lots of methods available to harden the surface of materials for better wear properties. However, these methods will not always work, or give only a small improvement on substrates such as titanium and its alloys, because of its lower load-bearing capacity. Before starting the coating process, it is critically important to analyse the substrate properties because this will affect the quality of the modification. In this context, the hardness of the substrate plays a prominent role in tribological coatings. When the substrate, which has low hardness, is coated with hard materials, the substrate cannot support the coatings because of the contact stress level. This phenomenon is called the egg-shell effect [25]. The solution for this undesirable condition is to apply a preliminary treatment (such as nitriding) before hard coatings deposition. In addition to this, the nitriding treatment can increase the surface hardness, but it often cannot significantly change the surface tribochemistry of the substrate and may have little effect on the wear properties. It is preferred that multi-layered coatings, duplex or hybrid techniques be used for this purpose. The combination of thermochemical diffusion treatments and coatings deposited by plasma-assisted physical vapour deposition is an example of hybrid techniques [26]. On the other hand, to increase the efficiency of this preliminary thermochemical treatment (and/or control surface finish more precisely), the substrates can be coated with a (pure or alloy) metallic thin PVD

11

coating. After deposition of this metallic layer, nitriding treatments can be applied to them, and the effect on surface properties can be compared with the requirements of the area in which the material will be used. The formation of nitride phase (after diffusion treatment) can be different depending on the pre-deposited metallic thin PVD coatings. For example, nitriding of PVD Ti-coated titanium alloys could result in a Ti_2N or TiN nitride layer of low surface roughness; on the other hand, Ti-Nb alloy layer coated Ti alloys could result with TiNbN nitride layer. It should be noted that there could be no or very thin compound layers on the surface if the correct processing parameters are chosen. Besides this, the nitrogen diffusion zone thickness inside the substrate can be improved by using this pre-deposited metallic coating before nitriding. The different phases of titanium and its alloys have different behaviour in terms of nitrogen interstitial diffusion. If the formation of a thick compound layer occurs rapidly (at the beginning of the process), nitrogen will not diffuse into the substrate material easily because the compound (ceramic) layers inhibit further nitrogen diffusion. The surface layer coatings deposited before nitriding can increase or decrease the nitrogen diffusion rate. It will depend on which surface layer coating is chosen for which titanium alloy. If the titanium alloy (desired to be nitrided) has fully or almost β structure, it should be considered that the nitrogen diffusion coefficient is very high for this alloy and a pure α-Ti surface layer coating can be deposited on it to keep the nitrogen concentration sufficiently high near the surface (increased the hardenability). If the titanium alloy which is desired to be nitrided contains a large quantity of α phase, a cubic phase of titanium surface layer should preferentially be deposited. In this condition, the nitrogen is considered to diffuse faster into the α or α+β Ti alloys, and the onset of compound layer formation can be delayed. This is the main logic and novelty of the work performed in this thesis for improving the nitrogen diffusion efficiency in both α-rich and β-rich Ti alloys.

2.3.1 Physical Vapour Deposition

Physical Vapour Deposition (PVD) is a process that evaporates a solid material source under vacuum and condenses this vapour on a chosen substrate material to create a coating. The PVD method is classified into three main categories:

- Thermal Evaporation

- Sputtering

- Cathodic Arc Evaporation

2.3.1.1 Evaporation Deposition

Evaporative PVD (Figure 2-4) is a process which uses a heating source (thermal) such as resistive heating [27], e-beam [28], inductive heating [29] or laser (ablation) [30] to evaporate the material to be coated on the desired substrate. This method needs vacuum levels better than 10^{-5} mbar. The main principle of this method can be explained as basically: a generation of the vapour; transportation of the vapour and finally condensation of the vapour. The different vapour pressure of each material at a particular temperature will help to manage the process and adjust the final product's specifications. The advantages of this method are: vaporisation materials can be in different geometries (bulk, powder, wire, etc.) so it is easy to maintain source materials for this technique, and it makes this process cheaper when compared to others. The control of the power supply on the vaporisation source allows to monitor the deposition rate easily, and it is easy to reach higher deposition rates. On the other hand, the major drawback of purely thermal evaporation is that the density of the packing (during condensation), and the adhesion of the coating to the substrate, are not very good. This is because of the mean free path (λ) of the low-energy vaporised species which travel from source to substrate is bigger than the distance between source and substrate, and so the energy of the incoming particles is low due to self-scattering and "thermalisation" of the vapour species. The

flight path of the vaporised particle is also "line of sight". It means that the side and back of the substrates often cannot be coated effectively. Moreover, the deposition of some alloys or compounds could be tricky because the evaporation rates of the components of a mixture are related to their vapour pressure therefore high vapour pressure component will have vaporised faster. In this condition, one of the components could vaporise completely while the other one remains in the molten pool and it can be difficult to obtain the desired concentration of final coatings.
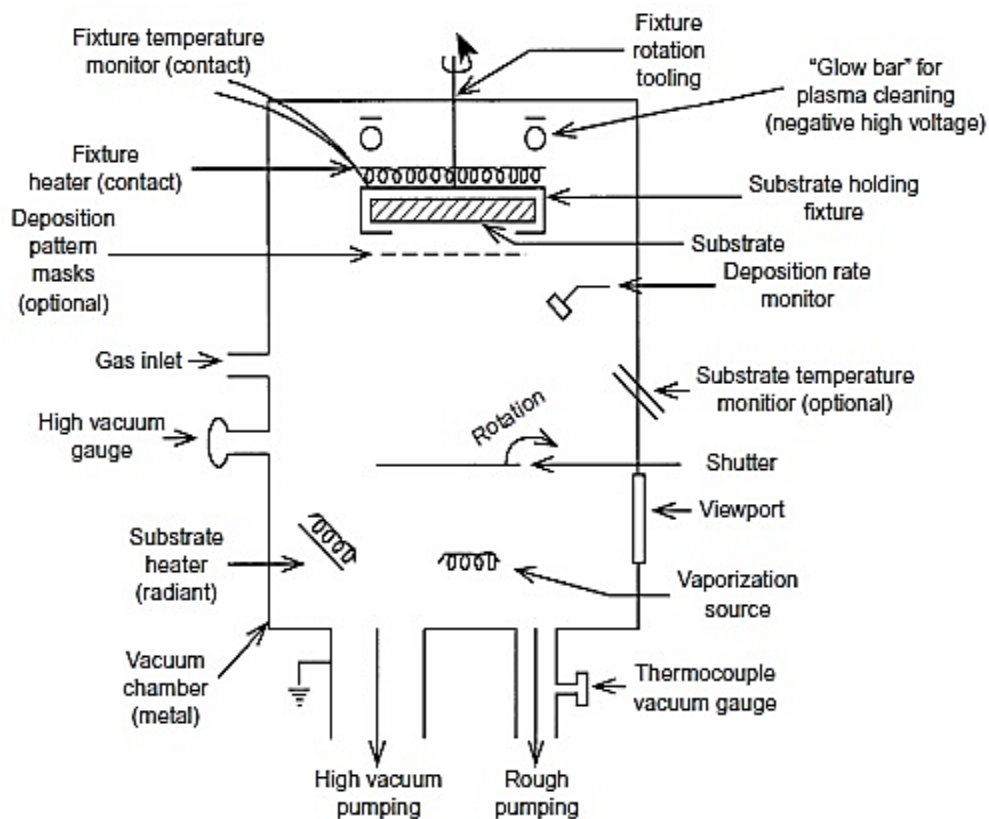
Figure 2-4 Components of an Evaporative Deposition Chamber [31]

The high melting temperature of vaporised material such as Mo and Nb could cause some difficulties to transfer from solid to vapour phase, and it needs more energy and time to complete the process. It can be advised that some eutectic alloys have lower melting temperatures than the melting temperatures of individual components. The usage of this kind of alloy makes the process more applicable. The hard-ceramic compounds (such as Al_2O_3,

14

TiO$_2$) can be deposited on desired substrates by evaporating the compound directly and condensing onto the substrate [32]. By evaporating only metal (such as Fe, Ti, Al, Cr) and supplying reactive gas (such as N, O$_2$, CO$_2$) into the evaporation chamber (to create a reaction between metal vapour and reactive gas) will have a reactive product onto the substrate surface [33]. This method is called reactive evaporative deposition. The decorative coatings (gold on plastic or other materials) [34], corrosion resistance coatings (Al or Ti on steel) [35], electrically conductive coatings (Ti-Pd-Au on ceramic substrates) [36] can be examples of some applications which use thermal evaporation as a vapour generating source.

2.3.1.2 Sputtering

Sputtering (Figure 2-5) is another type of PVD method that includes physical vaporisation of atoms from a target surface to create a flux of coating material atoms for deposition. It works by a momentum transfer mechanism through the bombardment of a target surface with energetic particles (ions of gas) -which is called sputtering- and the deposition of the sputtered material onto the substrate surface which is referred to as sputter deposition. The sputter deposition method needs vacuum levels better than 10^{-5} mbar. This technique can be classified as magnetron sputtering (conventional balanced magnetron, Type 1 unbalanced magnetron, and Type 2 unbalanced magnetron) (Figure 2-6) [37], RF sputtering [38], high power impulse magnetron sputtering (HIPIMS) and ion beam sputtering [39]. If any compound material desired to be coated, it can be used as a compound target material or elemental target material in a reactive gas environment (reactive sputter deposition). Compound materials have stronger chemical bonding, and they have a lower sputter yield (i.e. compared to TiO$_2$ and Ti). Sputter yield is a very important term for this technique and can be explained as a ratio of the number of ejected atoms from the target surface to the number of the incident particles to the target surface.
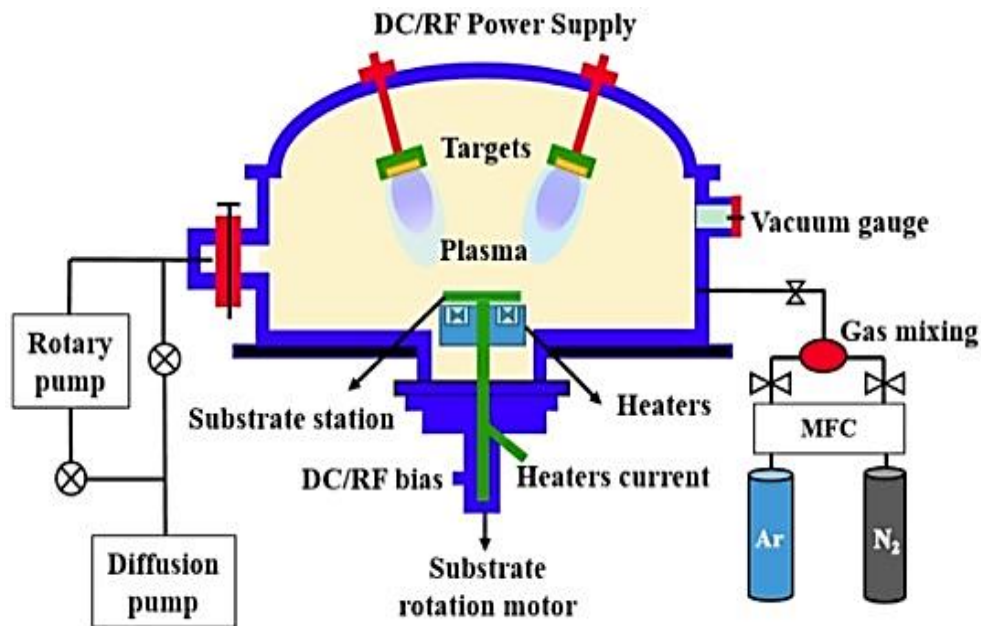
Figure 2-5 Schematic of a Sputter System [40]
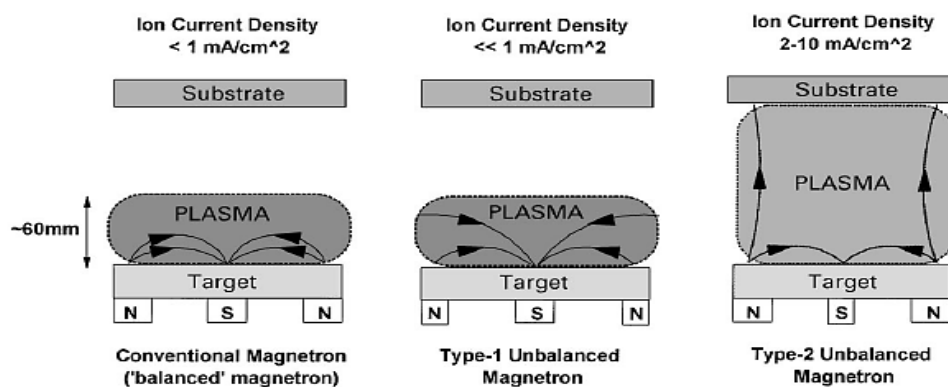
Figure 2-6 Schematic representation of the plasma confinement in balanced and unbalanced magnetrons [37]

It is related to the degree of chemical bonding of the target materials and the degree of energy which the incident particles have. The deposition rate and composition of sputtered alloy films (e.g. Ti-Nb, Cu-Al) can be controlled by using the metallic target element's sputtering yield value, the distance between target-substrate and the amount of applied power on the target. If multiple targets are used, the chemical composition of the sputtered films can be controlled by applied power on each target. The other parameters such as total gas pressure, the composition

of the reactive gas, the geometry of the chamber and substrate holder, substrate temperature are also critical to obtain reproducible processes.

The advantages of this method are: very wide selection of materials can be used as a target (alloys, compounds) and it is possible to use metals which have high melting temperature as a target material. The system has less radiant heating (by using target cooling system) when compared to the evaporation deposition, and so the distance between target and substrate can be adjusted shorter, and the substrate materials whose melting temperature are low (such as polymeric materials) can be coated without any degradation. Sputtering conditions can be set easily, and it increases the reproducibility of this technique. On the other hand, the target materials could be more expensive, and the energy usage could be higher when compared to other PVD techniques. Also, poor target utilisation due to the "race track" effect in magnetron sputtering can make this technique less efficient. The electrical coatings (e.g. ITO) [41], magnetic coatings (e.g. Fe-Al-Si-N) [42] can be examples of some applications which use sputtering as a vapour generating source.

2.3.1.3 Cathodic Arc Evaporation

Arc Evaporation (Figure 2-7) is another type of PVD method where an electrode (target) is vaporised under the arcing condition to obtain highly energetic vaporised material. The principle of cathodic arc evaporation is that gas cations (from the flux of ionised vapour) bombard the negatively polarised cathode, and this will eject of electrons from the cathode surface. The ejected electrons will move to the positively polarised anode. Because of this motion, an arc discharge will be struck between cathode and anode. Then, it will result in evaporation of the cathode material. The evaporated metal atoms will be ionised (because of the high electron density). It is not only evaporating the material, but also it is provided high ion energy. The main difference between the arc vapour deposition and the conventional

evaporation system is that, because an arc discharge produces the vapour, the target metal flux is mostly in an ionised state.
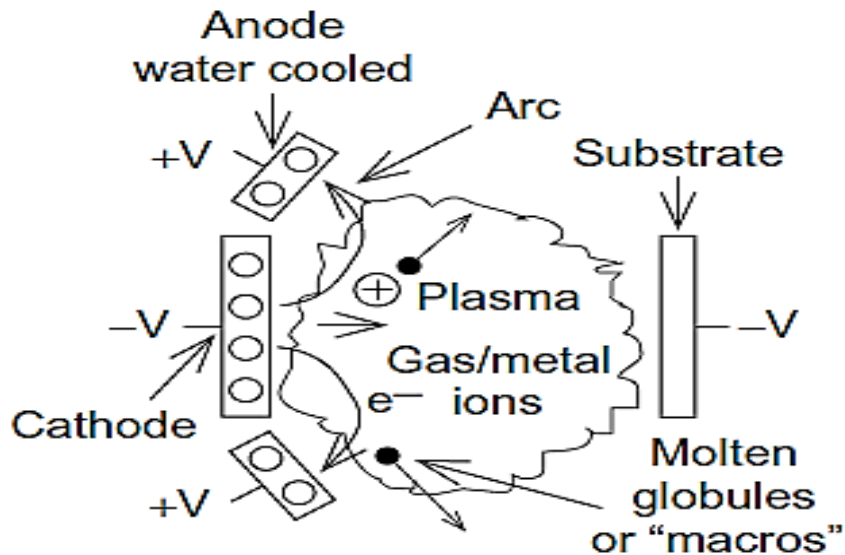
Figure 2-7 Components of Cathodic Arc Vapour Deposition System [31]

On the other hand, the material is directly heated for conventional evaporation, and the metal flux is mostly in the neutral (thermalized) atomic level. The reactive arc deposition can be applied by supplying the reactive gas into the deposition chamber. The advantages of arc vapour deposition are: the flux of ion which arrives at the substrate surface has high ion energy (10-100 eV). The densification of the coating (reflects its hardness) and the adhesion of the coating (how long it can work as a functional coating) are beneficial for this method because of a high ion energy of incoming flux. It does not need a high substrate temperature which allows this use of a polymeric substrate (with no damage to the substrate) to be coated. The formulations of the source material and the formulation of film material can be held same (for alloy deposition). The possibility of the formation of molten globules (because of the erosion from the cathode spots) and deposition of these droplets onto the substrate surface can be a disadvantage of this technique. A plasma duct can be used to solve this problem by directing the charged particles onto the walls of the duct. The corrosion resistant coatings (TiN/TiAlN

on steel) [43], decorative coatings (TiN as a replacement for gold) [44], protective coatings (hard carbon films) [45] can be examples of some applications which use cathodic arc evaporation as a vapour generating source.

2.3.1.4 Ion Plating

Ion Plating is an "atomistic film deposition process" [46] in which the substrate (and depositing film) is bombarded by energetic particles (inert or reactive) before and during film formation. The bombardment before the film formation cleans the substrate surface (sputter cleaning). The depositing atoms can be obtained by vacuum evaporation (vacuum ion plating), sputtering (sputter ion plating) or arc evaporation (arc ion plating). The ion plating process was (initially) used to obtain better adhesion and increase the density of the PVD films [47]. Then, it was shown that the continuous or periodic bombardment could control the film properties such as morphology, growth, density, residual stresses. Ion plating can be categorised which related its ion source: plasma-based ion plating (Figure 2-8) and vacuum-based ion plating (Figure 2-9). In plasma-based ion plating system, the bombarding particles (ions) are supplied from plasma. On the other hand, the ions are supplied from an ion source for vacuum-based ion plating. The bombardment stages which happen in ion plating process can be sorted as: bombardment for substrate sputter cleaning (surface activation), bombardment during the nucleation (the density of nucleation is increased), bombardment during interface formation (the thermal energy on the substrate surface is increased, and diffusion is incited), bombardment during film formation (the film density is improved and supply thermal energy to the surface). The deposition of the compound materials can be applied by reactive ion plating system which the reactive species (such as N) are activated by a plasma, or an ion source can produce the reactive and inert ions. The chemical reactions and density of the compound films can be improved by bombardment during the process. The concentration of the coating films can be controlled by adjusting the reactive species availability in the system, and this will give a chance to produce graded

coatings. The advantages of ion plating system are: the substrate surface can be cleaned during

the process (in situ).
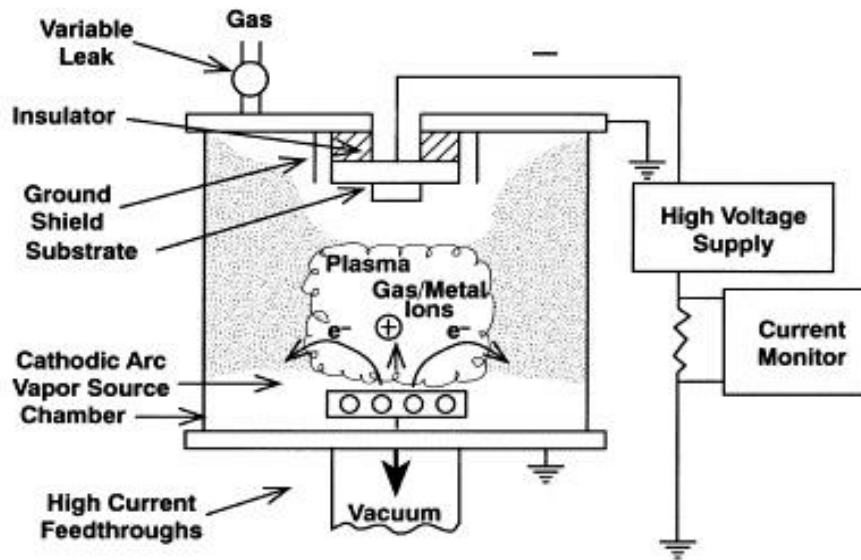
Figure 2-8 Plasma-based ion plating system using a cathodic arc vaporisation source with bombardment from the plasma [48].
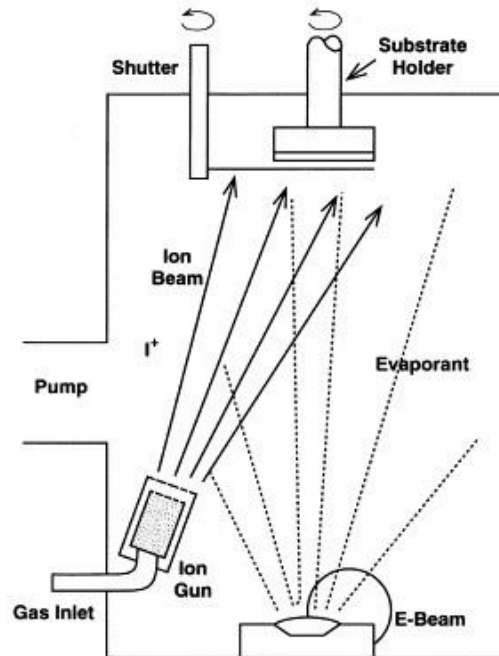
Figure 2-9 Vacuum-based ion plating system using a thermal evaporation source and an 'ion gun' for bombardment [48].

The deposition material can be supplied from various sources (sputtering, evaporation, etc.).

The film properties can be controlled flexibly by changing the bombardment condition. On the

other hand, the number of process parameter which must be controlled is high. The substrate heating can be extreme (related to other processes) so materials which are not durable at high temperatures cannot be suitable for this process (or the process parameters must be adjusted carefully). The geometry of the substrate and the position of the substrate in the chamber are very important criteria because the establishment of the bombardment uniformity is difficult. The hard decorative coatings (gold coloured TiN) [49], wear and oxidation resistance coatings (Ti-Al-N, TiN) [50], [51] can be examples of some applications for ion plating process.

2.3.2 Thermochemical Treatment Methods: Nitriding

The tribological performance of titanium and titanium alloys can be enhanced by thermochemical treatments (such as nitriding), to allow better load-bearing capacity (by diffusion of interstitial materials from the surface) and thereby improved adhesion between titanium alloys (substrate) and subsequent coatings. The surface of titanium can be hardened by the formation of hard nitrides, and the following nitrogen diffusion zone can support the compound layer. Nitriding is the most widely used method for this purpose. There are several methods by which nitrogen can be diffused into titanium and its alloys, to harden the surface of the substrate:

2.3.2.1 Gas Nitriding

Gas nitriding is one of the thermochemical methods and is applied to titanium at higher temperatures to maintain the proper diffusion rate. The main advantages of this method are that the initial equipment cost is low and does not require a special rig. It is easy to treat any size of materials (limited only the size of the furnace), and it is suitable for complex geometries. On the other hand, when the working temperature (750°C-1150°C) passes the beta-transus temperature, this affects the microstructure of the bulk materials irregularly. The high temperature and long working time (it is always increased when the temperature is decreased)

are the main disadvantages of this method. Also, gas nitriding can increase the surface roughness of the substrate materials (compared to plasma nitriding), partly because the gas nitriding process is generally applied at higher temperatures [52]–[54] where surface adatom mobility and surface diffusion kinetics are also higher.

2.3.2.2 Laser Nitriding

Laser nitriding is a thermochemical method where laser heating melts the surface of the substrate in a nitrogen environment. It is a relatively rapid method (followed by rapid cooling) that forms nitride layers on the surface of the samples. The composition of the nitride layer can be controlled, and the microstructure of the near surface region can be rearranged (it does not alter the bulk properties). The bonding between the substrate and nitride layers can be better because this method allows for melting of the surface and it is possible to have metallurgical bonding with nitrogen. On the other hand, the formation of surface cracking, the requirement of special equipment and the dependency on the shape of the materials are the disadvantages of this method [55]–[57].

2.3.2.3 Ion Beam Nitriding

Ion beam nitriding is another choice of the thermochemical technique that is used for producing hard nitrides on the surface of the substrate which is exposed to an ion beam. The ion beam can contain argon (besides nitrogen) to control the partial pressure of the gases. The method has some advantages, such as having controlled parameters, using the shorter time for treatment and having less distorted materials over conventional nitriding methods. It can be applied at low temperatures (such as 400-600ºC) and lower pressures (around 10^{-5}-10^{-6} mbar) which inhibit the possibility of contamination from oxygen. On the other hand, the different angle of incidence for ion beam can affect the film thickness and diffusion depth for complex shaped samples. The relatively high surface roughness after nitriding and the sputtering off the nitrided

layer (which is formed during the nitriding process) from the surface can be the main disadvantages of this method [58], [59].

2.3.2.4 Plasma Nitriding (Fundamentals)

Plasma (ion) nitriding is one of the thermochemical methods in which a voltage (from an external source) is introduced between the substrate (cathode) and process chamber (anode). The working/reactive gases (such as argon, nitrogen) are ionised which supplies active gases to the nitriding environment for surface treatment [60]. The power supply for plasma generation can be direct current (DC), alternating current (AC), radio frequency, microwave, etc. The temperature for the conventional nitriding process is generally selected high (around 1000°C) to possess fast nitriding kinetics. However, the high process temperatures can cause grain growth and microstructural change in substrates, and this affects the mechanical properties of the substrates (it can reduce the ductility and fatigue strength). Therefore, plasma nitriding is preferred because it is practicable at low temperatures [61], [62]. Moreover, easy control of the compound phase formation such as TiN or Ti_2N (by controlling the process parameters such as temperature, duration, pressure or applied cathode bias voltage), requiring a shorter time for nitriding than conventional methods. It is also more efficient and clean process [63], [64].

In the diode plasma system, the applied voltage provides the ionisation of the gas (such as Ar) and initiate a plasma. By this happening, the activity of the gases is increasing, and they are colliding with each other. Therefore, positively charged ions are formed. After the interaction of these ions with the cathode, secondary electrons will be emitted from the cathode. These secondary electrons travel back to the anode direction and will provide the plasma stabilisation through ionising collisions with the gas atoms. The average travel distance of these secondary electrons before collision (with an atom while they are travelling to the anode) is referred to as "cathode sheath area" or "dark space area" which is one of the main regions of the ion plating

discharge system [65]. The dependence of electron emission from the cathode can result in low ionisation in the diode plasma system. The possibility of the collision of the energetic ions with gas atoms is high in this system. Therefore, the energy of the ions could decrease before reaching the cathode (substrate) surface. The loss of this energy will affect the process performance such as the formation of any chemical reaction on the surface. For obtaining higher ionisation, plasma potential distribution can be controlled by changing the ratio of sheath thickness (L), and ion mean free path (λ). With an increase in the L/λ ratio, more collisions will happen, and the average energy of the ions will drop. Other than the energy of the species inside the plasma, the average energy of these species reaching the substrate surface is also important. Figure 2-10 shows the energy distribution of ions depends on the L/λ ratio [66], [67].
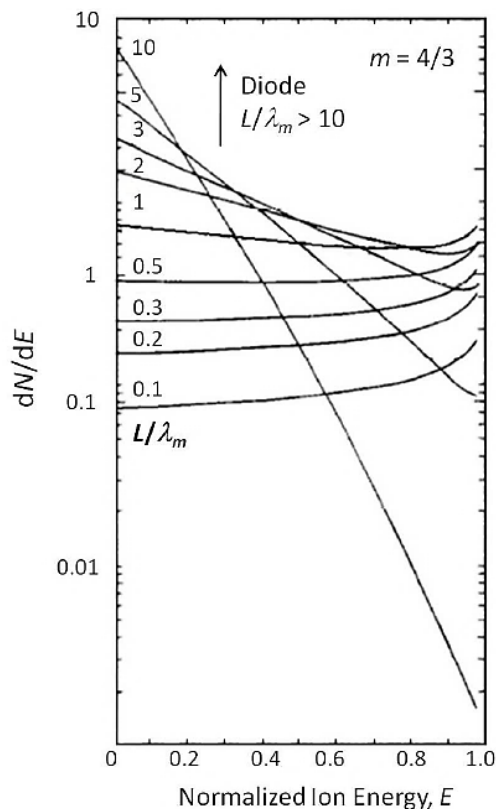
Figure 2-10 Energy distribution of ions at various values of L/λ [67]

A decrease of this ratio will allow increase of the energy transported to the cathode and the fraction of ions with maximum energy. Therefore, this ratio needs to be decreased to get less

collision in the cathode sheath, and the cathode surface would be bombarded with higher energy. However, this is not possible for the diode plasma system because gas pressure and applied voltage both need to be decreased to reduce the L/λ_m ratio. If these process parameters are reduced, the secondary electrons in the system are also decreased, affecting the plasma stability, and it will result in quenching of plasma [68]. As a result, to obtain a lower L/λ_m ratio, an auxiliary energetic electron source should be provided.

The advanced (more recently) method allows increasing the control of the ionisation in plasma nitriding by intensifying the glow discharge with a thermionic electron emitter. It is generally referred to as "triode configuration". This addition supplies extra energetic electrons, which collide with gas molecules. Therefore, the glow discharge can be maintained at a lower pressure, and the degree of ionisation is increased (which means that the number of the energetic particles is high) [69]. With this type of plasma configuration, the dependence on the secondary electrons which are ejected from the cathode surface to maintain the plasma will disappear. Regarding the negative bias voltage applied to the substrate, it was reported that values below 1000 V provide some improvement for triode system and the values between 500V and 200V will give superior nitriding performance [70]. The development of the plasma nitriding incites diffusion of the nitrogen at lower temperatures and shorter time (improved the efficiency and the kinetics of nitriding). The triode nitriding mechanism also has more advantages that the gas discharge is controlled better and the substrate heating is reduced, and the nitriding of the complex shape substrate (a thin sheath is needed for better recess penetration) is possible with triode plasma nitriding because the cathode voltage can be decreased to very low values [70]–[72].

2.4   The nitrogen diffusion in titanium and titanium alloys

When nitrogen penetrates the surface of pure titanium, the formation of an interstitial solid solution is seen (by dissolving nitrogen in Ti). The α titanium can only dissolve a limited amount of nitrogen in solid solution. It is seen from the Ti-N binary phase diagram (Figure 2-11) that a maximum of 23 at. % N can be dissolved in α titanium at around 1000°C. When the concentration of the nitrogen exceeds the amount which α titanium can dissolve, the development of new structures (i.e., nitride phases) by titanium and nitrogen reaction is seen. The (hexagonal phase) titanium nitride has the chemical formula γ-Ti_2N. In this condition, titanium substrate has a nitrided layer which involves titanium-nitrogen precipitates (Ti_2N) embedded in a nitrogen-saturated diffusion zone. Ti_2N has a solubility limit of about 34 at. % N at 850°C. When the nitriding time further increased, and the nitrogen concentration goes up, the nitride phase will change at the surface of the titanium substrate. A new face-centred cubic compound forms (with the chemical formula TiN). The schematic representation of the formation of the nitride layers on α titanium and the nitrogen diffusion zone is seen in Figure 2-12 [56], [73].
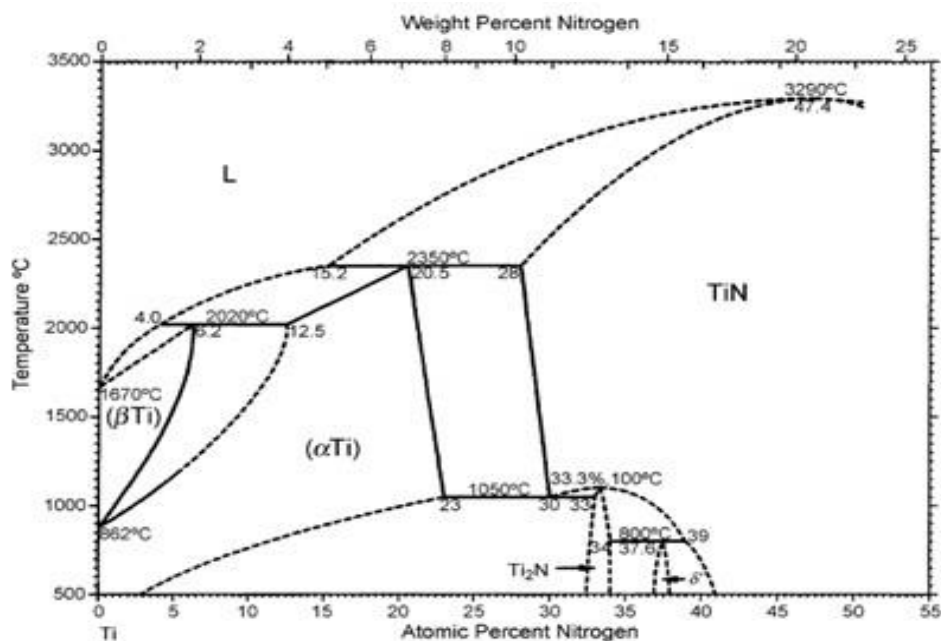
Figure 2-11 Ti-N phase diagram [56]
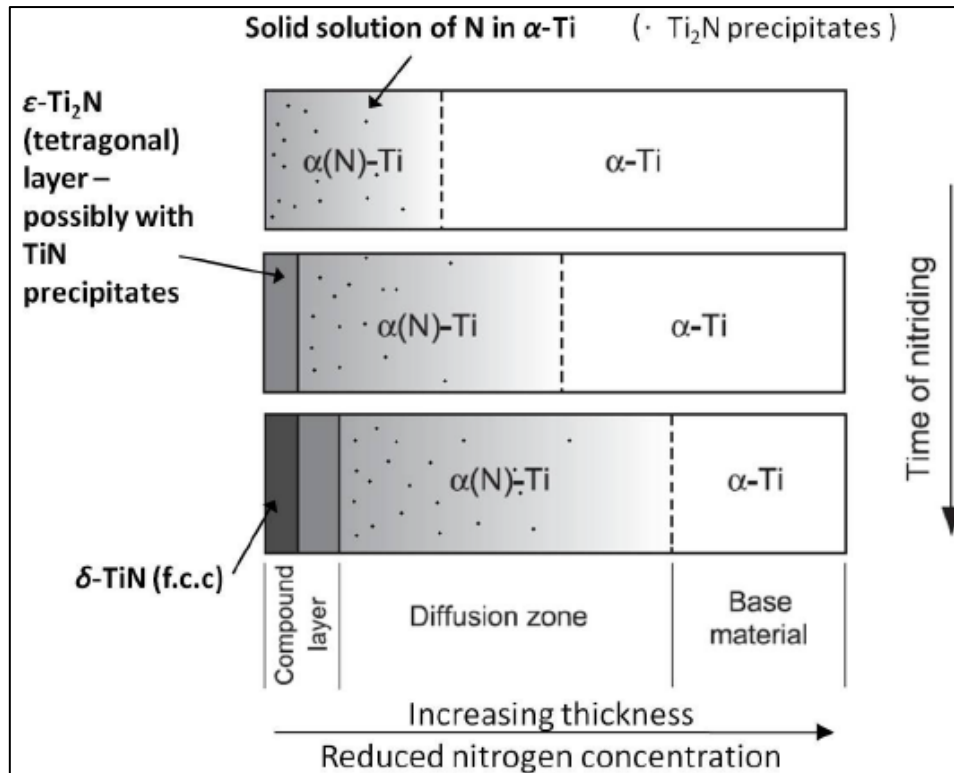
Figure 2-12 Kinetics of formation and growth of nitride surface layers on titanium [74]

The nitriding process for titanium alloys can be different depending on the alloying elements added. Many of the different alloying elements also form nitrides such as V_2N or form some alloy nitride phase with titanium [75]. The alloying elements will affect the α to β transus temperature. Sha et al. [76] reported that the nitriding of titanium alloy is more efficient when applied just below the transus temperature. However, beta titanium alloys tend to have lower transus temperatures and therefore require a lower nitriding temperature. The diffusion rate will be much lower at such lower temperatures, and conventional gas nitriding techniques will be less effective for the beta titanium alloys. Because, the amount of nitrogen which is diffused inside the substrate will be lower (surface diffusion kinetic is low), and it will reduce the hardening effect on the sample (in this condition). Therefore, the selection of both the nitriding technique and the different titanium alloys is very important to maintain the effective results.

The different crystal structures of the α and β phases (in different titanium alloys) result in various nitride structures in both compound layer and nitrogen (interstitial solute solution)

diffusion zone (saturated layer). At any given temperature, the nitrogen diffusion coefficient is different for the α and β phases of titanium. β-Ti is believed to have a more significant diffusion coefficient (by as much as three orders of magnitude), and thus the depth of the diffusion zone may be expected to be more prominent on nitriding.

A comparison of the nitrogen diffusion zone hardness profile of three different types of titanium alloy is seen in Figure 2-13. H represents the hardness value (which can generally be correlated with nitrogen content) while l represents the distance from the substrate surface. The depth and strengthening of the nitrogen-saturated layer of titanium alloys are based on the phase compositions. The morphology of these layers also depends on both the phase composition and the nitriding process temperature. On the other hand, the formation and thickness of nitride compound layers, such as TiN and Ti_2N (see Figure 2-12) are directly associated with the type of titanium alloys. The change of the thickness of the nitride layer (with time) on the α alloys is bigger than β titanium alloys [77].
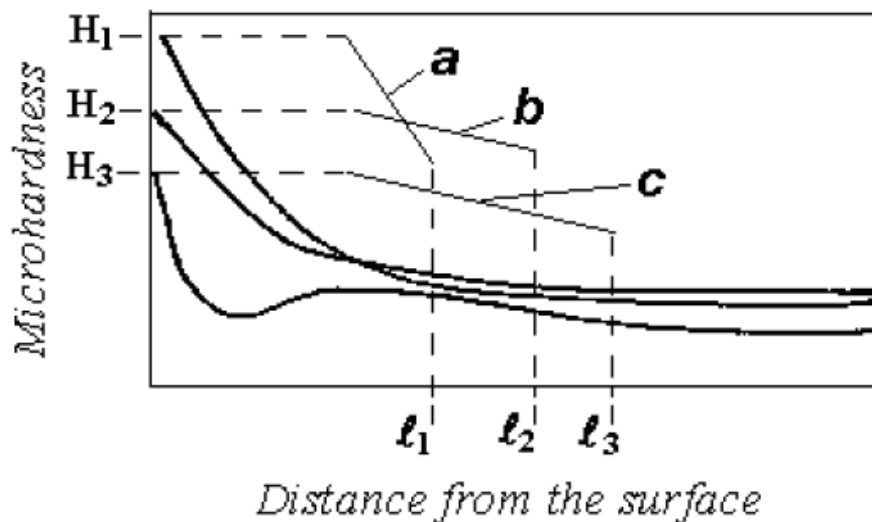
Figure 2-13 Distribution of hardness value after nitriding of α- (a), α+β- (b), β- (c) titanium alloys at (T > T $_{α»β}$) [77]

The formation of the nitride phase on the surface prevents or decreases the rate of the nitrogen diffusion into the substrate because the nitrogen diffusion coefficient of the titanium nitride is

lower than that of the metallic titanium phases. The diffusion coefficient of the nitrogen gas in TiN is 3.76×10^{-12} cm^2/s, for α titanium is 1.29×10^{-10} cm^2/s, for β titanium is 3.92×10^{-8} cm^2/s at 950°C [77]. If there is little or no nitride compound layer on the surface of the titanium, it means that there is no diffusion barrier and that the passage of nitrogen into the titanium alloy substrate will be as high as possible (at the chosen temperature). In this condition, the partial pressure of the nitrogen is a key factor for enhancing the nitriding process. By decreasing the partial pressure of the nitrogen, the formation of the nitride compound layer will be postponed. Figure 2-14 illustrates the effects of partial pressure, temperature and nitrogen flow rate on the structure of the surface layers on titanium alloys. Therefore, the creation of the compound layer will not be instant (or the thickness of the continuous nitride film will be very small). Besides this case, the penetration of the nitrogen will be high, and the depth of the diffusion zone will increase. On the surface, a solid solution of nitrogen in titanium metal (alloy) will form.
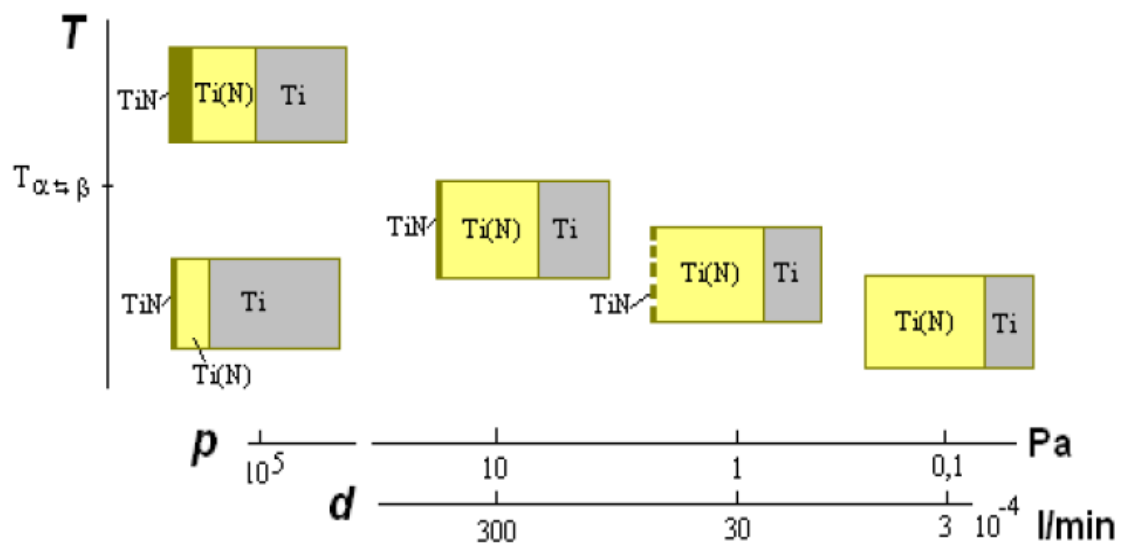
Figure 2-14 Influence of temperature and nitrogen partial pressure on the structure of the surface layer of titanium alloys [77]

Besides its barrier effect on diffusion, a compound layer such as titanium nitride on the surface of the titanium alloys may also cause some failures such as microcracks because of the brittle (and high elastic modulus) structure. Furthermore, the formation of a nitrogen stabilised layer

(α case) [78], which is also brittle and an undesired phase, in turn, leads to a decrease in some properties, such as fracture toughness or ductility. It is important to choose an accurate nitriding parameter to avoid the formation of this phase (particularly during the early stages of nitriding). There are more remedies to increase the nitriding efficiency, such as increasing the sputtering time before plasma nitriding treatment to remove surface the oxide layer and the utilisation of gas mixtures instead of only nitrogen to control the partial pressure of nitrogen [75].

In the light of this literature information above, in this work, a β-Ti alloy PVD coating will be deposited on titanium alloy substrates before plasma nitriding to understand the effects on the nitriding process efficiency. The additional group Vb and VIb elements for this beta titanium alloy will be selected with special attention to the predetermined plasma nitriding temperature (particularly between 500 and 700ºC). As a result, the low hardenability and other issues, such as the poor wear resistance of the beta alloys will be addressed.

2.5   The effect of nitriding process parameters on material properties

Nitriding is a very complicated process where there are a high number of variables that can play a role in the treated materials' final structures and properties. There are several works in the literature which show while different parameters such as process temperature, process time, total gas pressure, nitrogen partial pressure and substrate bias voltage affect the final properties such as surface hardness, surface roughness, the structure of the compound layer, the thickness of the compound layer, etc. The type of the nitriding process is also very important; for example, 24 h conventional gas nitriding process could give a similar result with 4 h triode plasma nitriding. In conclusion, when the variables are high, the possibility of creating different nitriding path is increasing and, because of this issue, it is sometimes difficult to find similar work to compare with this study. The review paper (2017) related to "plasma diffusion

techniques of Ti-6Al-4V alloy" which was written by Xing et al. [79] may be useful to those who are looking for detailed information about plasma nitriding technique and its parameters.

2.5.1 Process Temperature

Nitriding is a thermochemical diffusion process where the process temperature has a significant effect on the resultant properties. The temperature dependence of the diffusivity (D) can be seen as a form of Arrhenius equation [80]:

$$D = D_0 e^{-Q/RT}$$ **Equation 2.1**

where

D_o is a pre-exponential factor (m^2/s)

Q is the activation energy (J)

R is the gas constant (8.31 J/mol*K)

T is temperature (K)

It is mentioned in the literature that ε-Ti$_2$N phase is the dominant phase in the nitriding layer at lower temperatures (500°C-700°C), on the other hand, δ-TiN is the dominant phase in the nitriding layer at higher temperatures [81]–[85]. Besides the type of nitride phase, it was also mentioned that the thickness of the nitrided layer (compound layer thickness and nitrogen diffusion layer thickness) could be increased with temperature [86]–[92]. By linking all these changes on the "near surface" of the titanium and titanium alloys, the increase of the surface hardness was also seen [63], [87], [90], [91], [93]–[97]. Because of the diffusion-controlled nature of the nitriding process, the diffusion is highly activated by the increasing of the temperature, and the formation of the nitride layer and nitrogen saturation are accelerated. As a result, the hardness and the thickness of the diffusion layer are increased [56]. Additionally, the increase of the temperature of the nitriding process can lead to increase of final surface roughness values which can be detrimental for the wear performance of titanium and its alloys [64], [95], [98].

2.5.2 Process Time

Process duration is also one of the more critical parameters which can influence the structure of the nitride layer. It is mentioned in some works that increasing the process duration can allow to change the nitride phase structure from ε-Ti$_2$N to δ-TiN or to increase the intensity of the present peaks (depend on the structure and thickness of the compound layer). Because, the amount of nitrogen on the near surface is increased by the time [81], [85], [99]. The nitrogen concentration from the surface to the inside of the titanium alloy can be increased by time and consequently the hardness values from the surface to the core of the material is increased [100]. The effect of the process time on the thickness of the nitrided layer was reported as the thickness increased linearly with the square root of the process duration [101]. The relationship of the diffusion depth with time can be seen in Equation 2.2.

$$\text{Diffusion depth} \propto \sqrt{D_T . time} \qquad \textbf{Equation 2.2 } [102]$$

It should be noted that the efficiency of the nitriding process can be increased by increasing both time and temperature. The temperature should be selected carefully depending on which titanium alloy is nitrided. There are various studies which reported that the use of high nitriding temperature could affect the bulk mechanical properties (grain growth). It was also reported that the use of the temperature above the alpha to beta transus temperature (above 850°C) could affect the nitriding process negatively [53], [81], [103]. It can be thought that the increase of the duration can sometimes be a better option for the overall nitriding performance.

2.5.3 Total Gas Pressure

The higher total pressure of the conventional plasma nitriding treatments has some problems such as surface contamination or arc formation. The created nitride layer could be very thin although a very long nitriding time was chosen. D.C glow discharge under a triode condition can be used in a low pressure, to reduce the possibility of the worst effects [71]. Triode

configuration achieved with a third thermionic electron source (biased tungsten filament is used in this study) can exhibit higher ionisation levels than the diode configuration [104]–[106]. The effect of the working pressure on the surface microhardness was also reported as the pressure is increased from 10 Pa to 30 Pa (in the plasma ion nitriding process), the surface microhardness decreased from 500 HV to 300 HV for pure titanium which may be related to the formation of the compound layer. It is also reported that the surface microhardness reached very high values (1200 HV) at about 7 Pa and decreased to lower values (500 HV) at 5 Pa and 10 Pa (at higher and lower total pressures). It is related to the optimisation of the glow discharge intensification with pressure [62].

2.5.4 Nitrogen Partial Pressure

In nitriding processes, the reactive gas (nitrogen) is used either as a pure gas or as a mixture with hydrogen and/or argon gases. Argon is an inert gas which should not create any reaction in the system. On the other hand, hydrogen is a reactive gas which could build up some reactions in the treatment environment. It was reported that the β-Ti (H) and δ- TiH$_x$ phases could be expected in the diffusion layer when an N$_2$-H$_2$ gas mix was used [107]. The nitride layer formation is also affected by the condition of gases used in the process. An 80 vol. % N$_2$ – 20 vol. % H$_2$ gas mixture (rather than the use of pure nitrogen) was reported to lead to the preferred formation of TiN phase (rather than the Ti$_2$N phase) in the compound layer. In the same work, it was also mentioned that the compound layer was found thicker for the process which used the gas mixture rather than pure nitrogen [108]. The same group also reported that the surface microhardness was higher for 80 vol. %N$_2$ – 20 vol. %H$_2$ gas mixture conditions than pure nitrogen conditions for the plasma nitriding process of Ti and Ti-6Al-4V substrates [109]. It was also reported that the compound layer was found thicker when using 20 % hydrogen (in the N$_2$-H$_2$ gas mixture) rather than 20 % argon (in the N$_2$-Ar gas mixture) in plasma nitriding process (on Ti-6Al-4V substrate) at 800ºC. It is probably (mainly) due to more

effective oxide surface layer removal when hydrogen is used. Beside the thicker compound layer, the hydrogen absorption while modifying the surface structure was also mentioned, and vacuum annealing under an inert atmosphere was suggested for dehydrogenation [110]. The effect of the nitrogen partial pressure (in N_2-H_2 and N_2-Ar gas mixture comparing with pure nitrogen environment) on the surface nitrogen concentration after the plasma nitriding process was studied in detail. It was reported that the surface nitrogen concentration (measured with Rutherford backscattering spectrometry and nuclear reaction analysis) was varied between 59 and 64 at. % for pure nitrogen gas plasma, 56 and 60.5 at. % for hydrogen-nitrogen plasma, 62.5 and 63.5 at. % for nitrogen-argon plasma. It should be noted that these surface nitrogen values are valid with the other parameters which were used in their study [111]. The surface roughness change depends on the gas mixture as reported by Ali et al. [61], the use of pure nitrogen gas rather than N_2-H_2 gas mixture made the final surface roughness value lower.

2.5.5 Applied Substrate Voltage

The bias voltage is also one of the more important parameters which can influence the thickness and the structure of the nitride layer. Rie et all. [91] mentioned that the thickness of both Ti_2N and TiN compound layer was increased by increasing voltage. The compound layer thickness increased from 0.77 μm to 1.99 μm when the applied voltage was increased from 350V to 650V. It was also found in the same study that the plasma nitrided Ti-6Al-4V substrates showed 951 $HK_{0.05}$ (Knoop Hardness) when it as applied with 350V, on the other hand, the hardness rose up to 2140 $HK_{0.05}$ while applying the same process with 650V substrate bias voltage. In the meantime, the surface roughness values increased from 0.16 μm to 0.29 μm. In another study by Cassar et all. [112], the use of higher substrate negative bias voltage ended up with higher surface hardness. A higher nitrogen concentration on the surface was obtained, and consequently, the XRD peaks of the Ti_2N and TiN ceramic phases were stronger. On the other hand, the more profound nitrogen penetration was found when the substrate negative bias

voltage decreased from 1000V to 200V. It should be noted that the thicker compound layer on the surface and higher hardness values obtained from high voltage process must be balanced with further nitrogen diffusion inside the substrate to improve the load-bearing capacity of the titanium alloy substrates. The applied bias voltage may be selected moderately, or the nitriding process may start with low voltage value, and it can be finalised with higher substrate negative bias voltage [113].

2.6 New attempts to improve nitriding efficiency: The effect of depositing thin α-Ti and β-Ti alloy surface layer coatings on material properties

It was already discussed in Section 2.5 that the conventional plasma nitriding process which is applied at higher temperatures and for longer process times brings about the degradation of the materials properties such as higher surface roughness and grain growth that lowers the core strength of the substrate. These drawbacks can affect the mechanical properties of the materials in a bad way. The temperature and time need to be decreased, to get rid of these problems but, in such cases, it will affect the diffusion kinetics, and it will not be possible to obtain sufficient diffusion depth. Therefore, different approaches need to be found to speed up the nitrogen diffusion rate. The literature suggests some attempts to accelerate the diffusion rate such as applying explosive shock treatment before plasma nitriding [114], [115], applying severe plastic deformation (SPD) treatment before plasma nitriding [116], applying plasma based ion implantation (PBII) technique [117], [118] or using low-pressure plasma nitriding treatment techniques (Triode Plasma Nitriding (TPN) was also used in this study).

Although TPN technique is much more efficient than the conventional nitriding processes, the changing of variables such as temperature, applied voltage, and the addition of different gas mixtures to the plasma environment can change the hardness depth profile, fatigue life, surface roughness, etc. Beta titanium alloys, which often have a relatively large grain size (as well as a smaller packing density value), need more interstitial elements for strengthening (or create a

nitride compound layer on them). A high treatment temperature may be needed to achieve the required level of interstitial element saturation. Under these circumstances, the surface roughness of the substrate will increase unacceptably. According to Cassar et all. [2], the roughness value of a Ti15Mo substrate increases from 0.04 µm to 0.71 µm when it is triode plasma nitrided for 8 hours at 800°C. This roughening effect was suppressed by depositing a thin α-Ti layer before the process of plasma nitriding. In this study, PVD surface pre-modification followed by triode plasma nitriding (i.e., by depositing a thin α-Ti or β-Ti PVD surface layers) before TPN treatment was applied at 700°C on different titanium alloy substrates to improve the nitriding efficiency.

3 EXPERIMENTAL PROCEDURE

3.1 Production Stages

The production stage of the duplex plasma diffusion/coating system for this study includes two main parts. The first part is Ti and Ti-Nb surface layer deposition on Ti-6Al-4V (Ti-64) and Ti-4Al-10V-22Mo (Ti-AVM) substrates. The second part is the triode plasma nitriding process which was applied to uncoated, Ti coated, and Ti-Nb coated titanium alloys.

3.1.1 Ti and Ti-Nb Coatings

3.1.1.1 Substrate Preparation

The two titanium alloy substrates (Ti-64 and Ti-AVM) were selected for this study to show the different nitriding behaviours of different crystal structured titanium alloys. The rectangular Ti-64 coupons (15 mm x 15 mm x 2.5 mm) and Ti-AVM coupons (12 mm x 14 mm x 2.5 mm) were sectioned by using a precise abrasive cutting machine. The samples were firstly mounted in bakelite and grinded by using P120, P400, P800, P1200, P2500 and P4000 SiC abrasive grinding papers (3 minutes each) respectively. Finally, they were polished with 1 μm diamond suspension and 0.06-micron colloidal silica suspension respectively (10 minutes each). The mirror polished titanium alloy (see in Figure 3-1) substrates were removed from the bakelite carefully and cleaned in ultrasonic cleaner using acetone and isopropyl alcohol respectively (15 minutes each) and finally were dried by compressed air. All the substrate coupons have about 0.02 μm mean surface roughness (as measured by surface profilometry) before the deposition process.
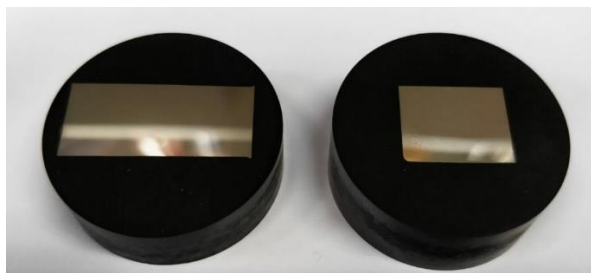
Figure 3-1 Mirror polished Ti-64 (left) and Ti-AVM (right) substrates

3.1.1.2 Deposition Process

An unbalanced magnetron sputtering rig (Nordiko, UK) was used for deposition of pure Ti and Ti-Nb alloy coatings on Ti-64 and Ti-AVM alloy substrate coupons. The substrate holder (300 mm x 130 mm) which was placed in the middle of the chamber is made of stainless steel, and the position of the holder was parallel to the target. Therefore, it was possible to adjust the concentration of the coatings on the substrates (which were clamped on the holder) by changing their positions vertically. A rectangular (380 x 105 mm) pure Ti block target was used for pure titanium coatings. Three pieces (2 x Nb + 1 Ti) and (2 x Ti + 1 Nb) of metallic targets (Figure 3-2) for two different runs (Run 1 and Run 2 respectively) were used for Ti-Nb alloy coatings to adjust the Nb concentration of the films (optimisation runs). After obtaining EDX results from the surface, it was decided to use the Run 2 configuration for the future runs (before nitriding process). The distance between target and substrate was kept at 21 cm. The chamber was pumped down to approximately 2×10^{-5} mbar base pressure. Firstly, a rotary pump was used for initial evacuation until the base pressure is reached to 5×10^{-2} mbar level and then a diffusion pump was activated to get the desired pressure level.
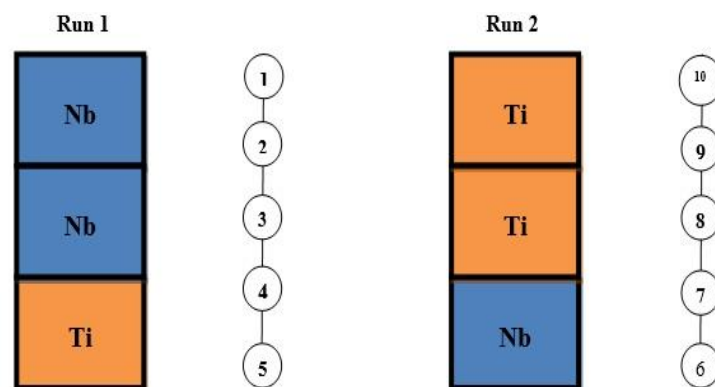
Figure 3-2 Schematic representation of the target configurations for Ti-Nb alloy coatings optimisation

The first stage of the deposition process (after having enough pressure level) was substrate sputter cleaning. Argon gas was introduced into the system with a flow rate of 54 sccm (working pressure was about 3.2×10^{-2} mbar), and the substrate holder was biased to -500 V. The surface of the substrates were etched by (Ar^+) ions for half an hour to get a clean and oxide free substrate surface. The second stage of the deposition process was target sputter cleaning. After finishing substrate sputter cleaning, the negative bias was cut off from the substrate holder, and the argon flow was decreased to 12.5 sccm (working pressure was about 4.8×10^{-3} mbar). The power supply (which is connected to the back of the target) adjusted to the power of 1000 W. The target sputter cleaning process was applied for about 15 minutes to get rid of any contamination on the surface of the target. A rotatable shutter was placed between the substrate holder and target during the target sputter cleaning process, to inhibit any possible contamination (which could come from sputtered target atoms during target sputter cleaning stage) on the clean substrates.

The deposition stage was started directly after finishing the target sputter cleaning process. The same argon flow rate (12.5 sccm; working pressure of 4.8×10^{-3} mbar) was used for the deposition process. The power supplied to the Ti, or Ti-Nb targets was 1000 W, and the substrate holder was biased to -50 V. The rotatable shutter which had been placed between the substrate holder and the target was removed, and the deposition was started. The duration for pure Ti and Ti-Nb alloy coatings were varied according to the desired thickness of the coatings. On the other hand, the different sputter yield values of the Ti and Nb metals affected the duration of the processes to obtain similar coating thickness. During the coating optimisation stage for Ti-Nb coatings (first trials), all the coatings were deposited for 120 minutes. In these trials, the coating's thickness was approximately 2.5 μm. The aim of these trials was understanding the concentration and phase change by different positions of the substrates on the holder. As a result, to produce approximately 1.25 μm thick coatings, 70 and 60 minutes

were found for Ti and Ti-Nb coatings respectively. To see if the relationship of thickness with duration is linear or not, thicker coatings were deposited (280 minutes and 240 minutes) for Ti and Ti-Nb coatings respectively. The thickness of the coatings was approximately 5 μm. These thin (1.25 μm) and thick (5 μm) coatings were used for the later triode plasma nitriding process.

At the end of the process durations, all the power supplies and argon gas supply were shut down. The diffusion pump was also shut down, and about 1 hour later (after cooling of the diffusion pump oil by circulating cold water around it), the chamber was vented, and the samples were collected. There is no additional heating system for this rig so that the temperature of the samples after 1 hour is suitable for collection (it would not cause any oxidation problem when the chamber door opened).

3.1.2   Triode Plasma Nitriding (TPN)

Uncoated, Ti coated, and Ti-Nb coated Ti-64, and Ti-AVM coupons were diffusion treated (triode plasma nitriding) in a modified Tecvac IP70L PVD coating machine by using low-pressure d.c. triode configuration [70]. The uncoated samples (only substrate) prepared by the same technique as the coating deposition stage (sectioning, grinding, and polishing). The uncoated (mirror finished) and coated samples (taken from magnetron sputtering system) were cleaned ultrasonically with acetone and isopropanol and then were dried by compressed air jet. The cleaned samples were mounted (hung with a wire which allows adjusting the distance between the samples and the floor of the chamber) to the sample holder. This distance (200 was chosen mm) is a very important factor which affects the nitriding efficiency.

In this triode plasma nitriding process, the chamber plays the anode role, and the sample holder plays the cathode role. Moreover, a tungsten filament (which is biased during the process and gets very hot) placed on the base of the chamber. It is an additional cathode which emits electrons to the system (and plasma enhancement is procured). Some trials (working distance

to the base of the chamber was more than 300 mm) showed us that the sample position affects the sample's working temperature in the chamber and according to this difference, the nitrogen diffusion rate and formation of the nitride phases are affected significantly.

In the nitriding runs, six samples (uncoated, Ti coated, and Ti-Nb coated Ti-64) and (uncoated, Ti coated, and Ti-Nb coated Ti-AVM) alloy coupons were mounted to the sample holder, and they were treated together. Despite all the precautions being taken, there is still a minimal risk to keep all the parameters constant from run to run. Therefore, extra care was given to sample assembling. Two similar size dummy samples (titanium alloy) were also mounted to the sample holder, and K type thermocouples (which are frequently replaced and calibrated before starting to the nitriding runs) were connected to these dummy samples to check the temperature change during the nitriding process. The temperature control is the primary factor for nitriding process and so that to make sure the temperature similarity of 6 samples in a run, two different dummy samples were placed to two different reasonable (same height with the treated samples) places.

After mounting all six samples and two dummy samples, the chamber door was closed, and the roughing pump was turned on (the evacuation was started). The pumping continued until the pressure level was 5×10^{-2} mbar level. After that, the diffusion pump was activated, and the chamber was pumped down to less than 2×10^{-5} mbar base pressure to make sure any undesirable residual gas (such as oxygen or hydrogen) inside the chamber which was ejected from the system. When the chamber pressure reached a desirable level, the radiant heaters were activated. It took about 45 minutes to reach a temperature of 400°C inside the chamber. While the temperature rises, some change in the base pressure was seen and waited about 15 minutes to stabilise the pressure (again) to 2×10^{-5} mbar level. After the temperature and pressure reached to intended levels, argon gas was introduced into the system with a flow rate 140 ml/min (working pressure of 2×10^{-2} mbar) and meanwhile, the substrate holder (hanged samples also) was biased to -800 V. The argon gas started to ionise (it is very similar to the

magnetron sputtering coating system) and generated the plasma. This was used for substrate sputter cleaning for 15 minutes. In this case, the configuration of the chamber is still in diode condition because the tungsten filament is not activated yet.

The working temperature for the nitriding runs was chosen 700°C for the triode plasma nitriding process in this study. The temperature difference between the one which obtained from radiant heaters (400°C) and the desired working temperature (700°C) caught up by plasma heating stage. The temperature which obtained from radiant heaters could be adjusted maximum 500-550°C, but the heating elements are placed on the wall of the chamber, and this could be not suitable for the nitriding rig. Therefore, the plasma heating (more localised heating onto the samples by gas ion bombardment) was preferred to increase the temperature of the samples to the working condition. After finishing substrates sputter cleaning stage, argon gas flow rate was reduced to a flow rate 80 ml/min (working pressure is 4 x 10^{-3} mbar), and the substrate bias voltage was reduced to -300V. In the same time, the tungsten filament (which is placed in the middle of the chamber base) was biased to -200V. In this case, the configuration of the chamber is the triode condition by adding the hot tungsten filament to the system. The current which is passing through the tungsten wire heats up the filament, and electron emission starts. These energetic electrons intensified the plasma and this strong Ar plasma heated up all samples to the working condition (700°C). This plasma heating stage took about 45 to 60 minutes with higher filament current values.

When the desired working temperature reached, the nitrogen (working gas) was introduced to the system. The ratio of the Ar and N flow rate (partial pressure) was kept constant (70 %N and 30 %Ar). However, to obtain total pressure at the desired level (0.4 Pa= 4 x10^{-3} mbar), the flow rates of the gases were adjusted instantaneously until the total pressure stabilised. When the nitrogen gas was introduced into the system, the plasma nitriding stage started. The duration

of the nitriding process was selected to be 4 hours or 8 hours (4+4) depending on the intended conditions.

Keeping the temperature at 700°C (after nitrogen gas was introduced the chamber) was difficult because (at the same time), to maintain the total pressure constant, the flow rate of the argon gas was reduced, and the strength of the plasma was changed accordingly (plasma bombardment is not enough). In this condition, the substrate temperature could drop to about 650°C rapidly with this sample configuration (the distance between samples and base of the chamber again plays a crucial role). If this temperature drop happens, the initial stage of the nitriding process will take place at lower than intended working temperatures. Some parameters could be altered such as increasing the filament heating or increasing the substrate bias voltage to resolve this problem. In this study, the trial runs showed that, if the amount of current which is passing through the tungsten filament is increased, the sample heating will be better. On the other hand, if the filament bias voltage and current are increased more, it will cause a problem to the tungsten metal by more (argon ions) sputter etching on it, and slow evaporation from its surface will decrease the life of the filament. The surface structure of tungsten filament before and after triode plasma nitriding process at 700°C for 4 hours can be seen in Figure 3-3. The diameter of the tungsten wire 0.75 mm before starting the nitriding process and the diameter was decreased to 0.57 mm (approximately %25 reduction) after 4 hours nitriding process (Figure 3-3 also shows how the dimensions were changed). This reduction can lead to the break of the tungsten wire which a short circuit can happen if this wire contacts with the chamber walls. It means that the run is aborted and therefore the tungsten filament must move on to complete the plasma nitriding process. Because of these reasons, the filament heating was used near to its factory limit, and the substrate bias voltage was increased to -300 V to inhibit temperature drops and maintain the working temperature at 700°C. It is also thought that the

radiant heaters can help to maintain the temperature at the desired levels, but this would be dangerous to the chamber walls and connections.

When the process duration was completed, the cathode bias voltage and filament heating were switched off. Then, the gas supplies were switched off. Finally, the radiant heaters were switched off. The samples were left for furnace cooling in the vacuum environment until their temperatures reached around $150^{\circ}C$ to avoid undesirable oxidation. When the temperature reached less than $150^{\circ}C$, the high vacuum valves were deactivated, and the chamber was vented for collecting the samples.
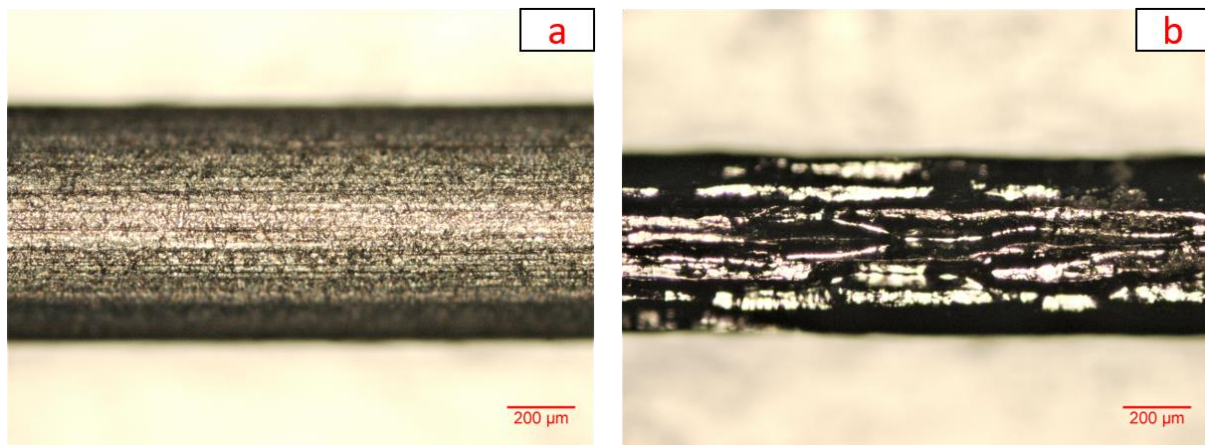
Figure 3-3 The surface morphology of the tungsten (wire) filament (a) before (b) after the nitriding process at $700^{\circ}C$ for 4 hours

3.2   Testing Techniques

3.2.1   X-ray Diffraction (XRD) Analysis

X-rays are a form of electromagnetic radiation that can travel through space and cannot be seen. X-ray diffraction technique is used to identify unknown phase structures of a material or to determine its structural parameters. The wavelengths of the X-rays used in the examination of the materials are comparable to the interatomic distances which in the range from approximately 0.5 Å to 2.5 Å. The diffraction of the X-rays in the crystal structure is explained by the Bragg Law. When the X-rays are directed to the crystal structure, they are scattered by

the parallel planes of the atoms in the crystal system (Figure 3-4). In some directions, scattered X-rays are in the same phase and strengthen each other (constructive interference). A diffracted beam can be defined as a beam consisting of many scattered X-rays superimposed on each other. For constructive interference, the path difference (AB + BC) between the two X-rays must be a whole number multiple of the wavelength. The simplest form of Bragg's law is given by the following formula [119]:

$$2dSin\theta= n\lambda \qquad \text{Equation 3. 1}$$

where, d: interplanar distance, θ: incidence angle, n: whole number multiplier, λ: wavelength.
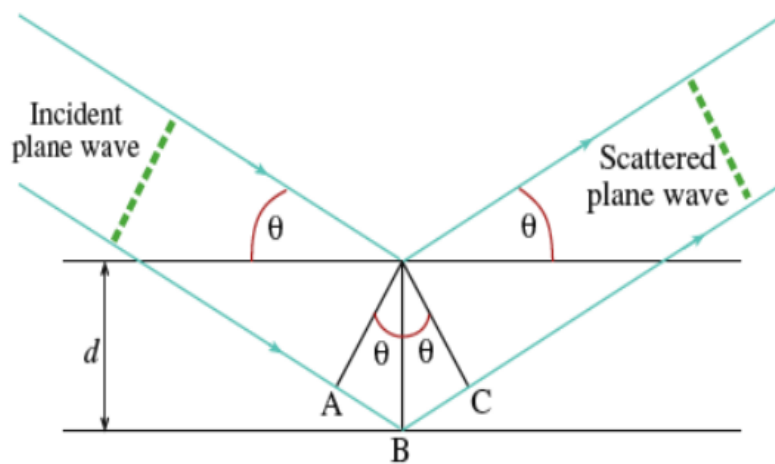
Figure 3-4 Diffraction of an X-ray by a crystal lattice

A diffractometer consists of an X-ray tube (generates X-rays), X-ray detector (measures the intensity of the diffracted beam), a monochromator (arranges the incident beam), and slits (adjusts the beam position and shape). The sample holder is located between the X-ray tube and the X-ray detector. These three parts rotate independently of each other. Once the rotation at the desired angle (2θ) has been completed, the data collected in the detector are transformed into a graph (intensity vs 2θ) and compared to known PDF (Powder Diffraction File) cards to estimate the unknown phases of the sample.

3.2.1.1 Glancing Angle X-ray Diffraction (GAXRD)

The use of conventional methods in XRD analysis of thin films or diffusion-modified surface layers has a disadvantage of producing weak signals from the film. The signal is usually generated mainly from the substrate material because the film thickness is very low. The GAXRD method was used to produce stronger signals from the film structure, and in this case, the penetration depth of X-rays into the material was reduced by keeping the incident angle smaller [120]. The incidence angle of the X-ray beam can be selected between 1° and 10° and, as the angle increases, the X-rays penetrate deeper. The thickness of the film and type of the material will help to select the test angle to be used, and almost all signal can be received (only) from the film with the selection of the appropriate parameters. On the other hand, using the GAXRD method, the intensities of diffracted X-rays are much lower than those of conventional methods.

In this study, the phase structure analysis was carried out by using Siemens D5000 X-ray diffraction machine (Cu Kα, radiation; λ=0.15418 nm) for Ti and Ti-Nb interlayer coating optimisation with a step size of 0.02^o and a step time of 6s in the 20° to 120° 2θ range with 2-degree glancing angle mode. A PANalytical X'Pert[3], X-ray diffraction machine, was used for as-deposited PVD metallic coatings and for nitrided samples with a step size of 0.02^o and a step time of 3s in the 30° to the 80° 2θ range with 2-degree glancing angle mode. Glancing angle mode (2-degree incident angle) was selected for both machines to inhibit the effect of the substrate contribution on diffraction results. The coating thickness was the main factor to consider when selecting the incident angle.

3.2.2 Optical Microscopy (OM)

The light microscope is an optical device that produces an image (which is magnified) of a sample (or specimen) by using visible light and represents this image to the human eye or

imaging instrument (such as computer screen). The optical microscope has two essential parts to create an image: an objective lens and a condenser lens. The objective lens collects light which is coming from the specimen (diffracted light) and creates a magnified image. The condenser lens focuses the light which is coming from the light source (illuminator) onto a specimen (as a small area). These two lenses involve several lens elements, so they are the most expensive parts of the optical microscope (careful attention must be taken while handling). Other components of the optical microscope can be sorted as Ocular (eyepiece), a microscope stage, specimen focusing knob, lamp power adjustment knob, microscope stand, etc. The specimen which is placed on the microscope stage is firstly viewed by the objective lens, and it creates a magnified image of the specimen (real intermediate image). When the human eye looks at the ocular of the microscope, the intermediate image is examined, and the magnified real image is formed on the retina of the eye. Then, the human brain interprets this image (as a magnified virtual image) about 25 cm out from the eye. It is how the image of the specimen is perceived from an optical microscope by the eye [121].

In this study, Nikon Eclipse LV150n optical microscope was used to investigate the surface morphology of the substrates after surface finishing, Ti and Ti-Nb coating deposition and different plasma nitriding processes. It was also used for thickness measurements (from cross-section). The magnification functionality of this microscope can be increased until 1000 times.

3.2.3 Scanning Electron Microscopy (SEM)

Scanning Electron Microscope is a kind of instrument which produces magnified images (with high resolution). It can be used to examine the surface morphology of the specimens (deeply) and to measure the coating thickness (when the coating is very thin). The necessary components of the scanning electron microscope can be sorted as an electron source, lenses, scanning coil, vacuum chamber, and different kind of detectors. The electrons which are produced in an

electron source (can be a thermionic electron gun or field emission gun) are accelerated by a voltage (1-50 kV) and pass over a combination of lenses (first condenser lens, a second condenser lens, and objective lens) and objective apertures. This allows obtaining a focused beam of electrons (with a 2-10 nm diameter) which are directed on the specimen surface [122]. The sample is placed on a stage (which is adjustable in three dimensions) inside the chamber, and it is evacuated by using one or two pumps depending on the required level of vacuum pressure. A scan coil (above the objective lens) is used for adjusting the electron beam position. This scan (deflection) coil scans the electron beam (probe) over the specimen surface. The magnification can be provided by reducing the current on the scan coil [123]. This beam scanning process obtains some information from a specific area by interacting with the sample. When the electrons interact with the sample, secondary electrons, backscattered electrons and different kinds of X-rays are produced. All these products are obtained from different depths from the surface of the samples. The electron beam which directed to sample surface penetrates the sample (to a few microns depth), and the depth of the travel relates to the adjusted electron acceleration voltage and the density of the material. Then, the released products are picked up by different detectors, and they are converted to an image (which is projected on the computer screen). The resolution of the image is affected by some factors such as electron spot size, type of material, the position of the sample inside the chamber, the working distance, and accelerating voltage. For example, a resolution of 1.5 nm can be obtained at 30 kV (applied accelerating voltage), on the other hand, the resolution can be dropped to 7 nm at 1kV [124].

In this study, a Philips XL 30 scanning electron microscope (field emission gun) was used to investigate the cross-sectional surface morphology of the substrates after Ti and Ti-Nb coating deposition and different plasma nitriding processes. It was operated at 10 kV, and the samples were placed at a working distance of 5 to 10 mm for taking SEM micrograph.

3.2.4 Energy Dispersive X-ray (EDX) Spectrometer

Energy Dispersive X-ray analysis is an analytical method that is used for determining the elemental composition of the material. The essential components of the EDX analysis can be sorted as the excitation source (electron beam excitation in scanning electron microscope), the X-ray detector (convert X-ray intensity to mV signals), the processor (measure the signals) and the analyser (a data collection computer). As mentioned in Section 3.2.3, while the interaction of directed electron beam with the sample surface, the incident electron beam ejects an electron (by exciting it) from the inner shell of the sample by creating a hole where the electron was located. Then, an electron from an outer shell fills the vacant site, and the energy difference between the outer shell (higher energy) and inner shell (lower energy) is released as an X-ray of characteristic energy [125]. The emitted X-ray from the sample is measured by an energy dispersive spectrometer which is an attachment of the Scanning Electron Microscope. Due to the energy of the X-rays are characteristic (specific energy for each element), this method allows the elemental compositional analysis of the materials. When an EDX spectrum (seen in Figure 3-5) is analysed, it can be easily seen that corresponding peaks of each element are standing at different peak energy level.
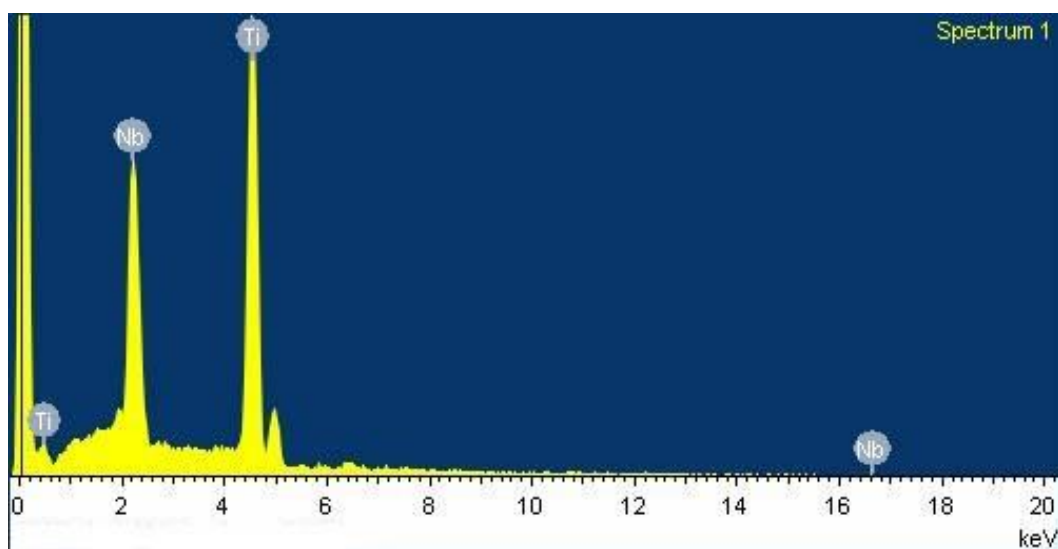
Figure 3-5 An example of EDX spectrum for a Ti-Nb coating

The intensity of these peaks helps to measure the content of the element in an alloy or compound. While the electron (from outer shell) fills the hole, the released energy could be transferred to another electron (Auger electron) which is ejected instead of being released as X-ray. Because of this reason, the EDX method is more practical for the heavy element (higher atomic number) because the probability of characteristic X-ray emission for heavy elements is high [126]. For light elements, it is difficult to determine composition accurately when the content of the element is low. The accuracy of this technique is imposed by different factors which the most important one is the low energy peak overlap due to the limited energy resolution of this method [127]. For example, the Kα peak of nitrogen (low energy peak which is close to the 0 keV) and the Lα peak of Ti are very close to each other, and the peaks can overlap. Therefore, it would be challenging to identify the chemical composition of Ti$_2$N or TiN compound layer if their thicknesses are low.

In this study, energy-dispersive X-ray spectroscopy which is attached to a Philips XL 30 scanning electron microscope was used for chemical composition analysis of the Ti alloy substrates after Ti and Ti-Nb coating deposition and different plasma nitriding processes. The microscope was operated at 10 to 20 kV (depending on the material), and the samples were placed at a working distance of 5 mm for EDX analysis. The chemical composition of treated and untreated samples was calculated using INCA (Oxford Instruments) software. High purity cobalt sample is used for calibration to get reliable results.

3.2.5 Nanoindentation Testing

The intention of the nanoindentation test is to determine hardness (H), and elastic modulus (E) of the coatings and diffusion treated samples by using load-displacement curve measurements. The well-known indentation hardness techniques (such as Vickers hardness test) are applied by creating residual plastic traces (as a function of applied load) and the area of these traces

are measured by optical microscopy to calculate hardness values of the samples. Beside

hardness measurements, the nanoindentation method allows measuring the elastic constant (i.e.

Young modulus) which could not be obtained by conventional hardness testing methods. On

the other hand, in a nanoindentation test, it is difficult to measure the size of the imprints

(hundreds of nm) by any optical devices [128]. The working principle of nanoindentation

testing can be clarified as: firstly, the diamond tip is compressed onto the material which results

in elastic and plastic deformation. Then, when the tip reaches the maximum load (usually in

mN levels), it can be held at the maximum force which allows measuring any creep in the

material. The holding and dwell time are customizable parameters for different materials. At

the end of the process, the tip is unloaded, and this provides some elastic recovery. For each

indentation, a load-displacement curve (Figure 3-6) is constructed, and the mechanical

properties are calculated from this curve by using some calculation methods [129], [130].
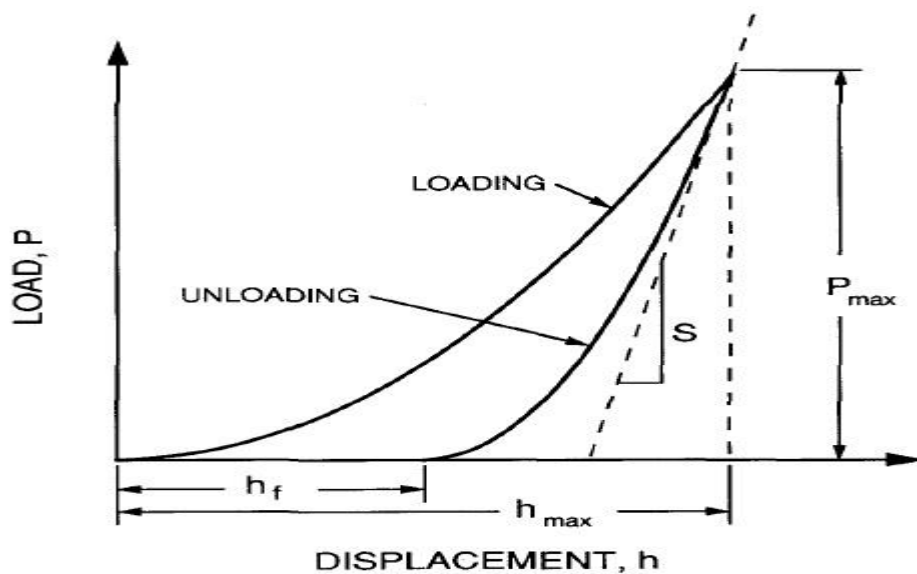
Figure 3-6 A load-displacement curve for nanoindentation test [129]

The load-displacement curve has some quantities such as P_{max}: the maximum load, h_{max}: the indenter displacement at maximum load, h_f: the final depth after unloading, S: the unloading stiffness. The initial slope S of the unloading curve (change rate of the load and depth) allows the elastic modulus (E) of the material to be measured. The displacement (h) under the applied load (P) should be smaller than one-tenth of the coating thickness to reduce substrate contribution on the mechanical properties of the surface layers [131].

In this study, a Hysitron Triboscope ® nano-indenter with Berkovich, a three-sided pyramidal diamond tip (see Figure 3-7), was used for mechanical property measurements. The hardness measurements (which were applied from the surface of the coated samples) were done by using a matrix of 4 x 4 indents. In each hardness test, the total number of indents was therefore 16, and every run was repeated twice to get more reliable data set (by obtaining 32 indents). The load (2 mN) was chosen for the Ti-Nb coatings' surface hardness measurements in considerations of the thickness and roughness of the coatings. The indentation depth (about 100-150 nm) was limited to 3-5% of coating thickness to eliminate substrate contributions. The load was 5 mN for the diffusion treated samples' surface hardness measurements because the surface roughness value of the samples was increasing after the nitriding process and the lower loads would give incorrect results.
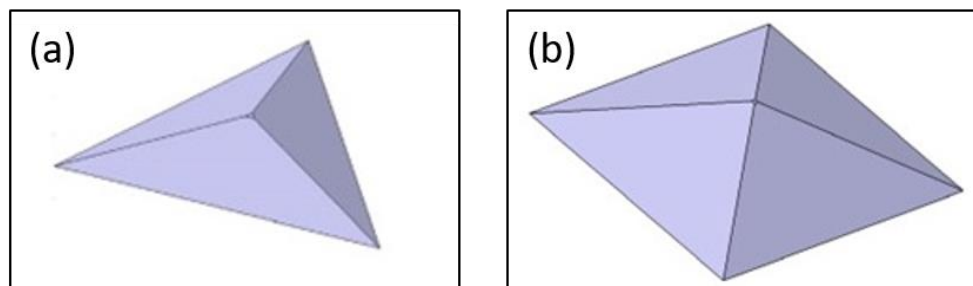
Figure 3-7 Indenters geometry for (a) Berkovich and (b) Vickers hardness tests (reproduced from Ref. [132])

To decide the best load values (it is very important for nanoindentation hardness tests to inhibit substrate contributions on hardness values), varying loads (i.e. from 1 mN to 10 mN) were applied to each sample before applying 32 indentations. This trial runs help to analyse the relationship between indentation depths and hardness values for different loads. On the other hand, the cross-sectional hardness profile experiments were done by using a 5mN load, at least 110 indentations were taken from each diffusion treated sample (cross-sectional). The hardness template was prepared as a matrix of 5 x 11 which the hardness profile (from the surface to the substrate) could be composed by indenting 11 points (5 repeats) from the cross-section (Figure 3-8). Each test was also repeated twice to get a total number of 110 indents to get more reliable data set. The distance between the two indents was about 5 μm. Therefore, the hardness values (up to 60 μm away from the surface of the sample) could be measured. This allowed to understand the amount of N diffusion from the surface to the inside of the substrates.
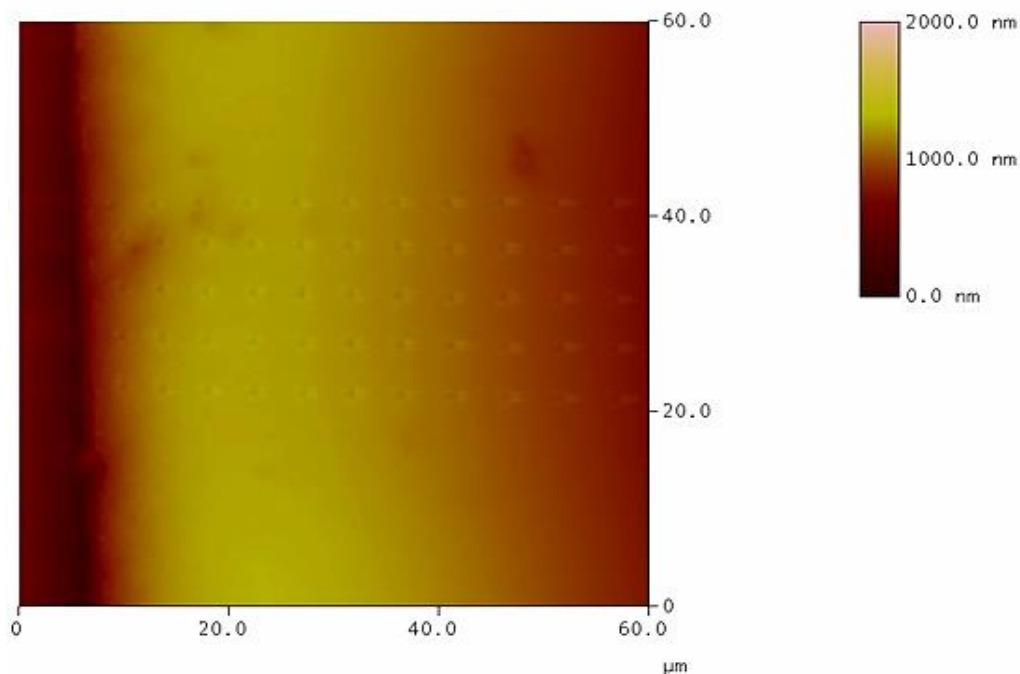
Figure 3-8 AFM image is showing 55 indents on the cross-section of a diffusion treated sample. (Left to right direction indicates surface to the substrate direction

3.2.6 Knoop Hardness Testing

Knoop hardness technique is applied by pressing a diamond indenter onto the samples which form a trace. The length of the trace is measured by optical microscopy (which is performed in the same machine) to calculate the hardness values of the samples. The shape of the Knoop hardness indenter (see in Figure 3-9-a) is a rhombic base pyramid. The longitudinal angle is 172.5^o, and the transverse angle is 130°. A projected area is calculated by using the longer diagonal (d_1). The hardness value is calculated by dividing the applied force to the projected area. The necessary formulations and detailed calculations can be found in ASTM E384-11 [133]. The Knoop hardness test can be suitable for very hard and brittle materials (Vickers hardness test may induce cracks on the indentation) and thin (narrow) samples which the Vickers hardness (the indentation geometry can be seen in Figure 3-9-b) indentation could be too large. The advantages of this method (rather than using Vickers hardness) is the less damaging of the sample surface. If the same force is applied, the indentations for the Knoop hardness would be shallower [134].
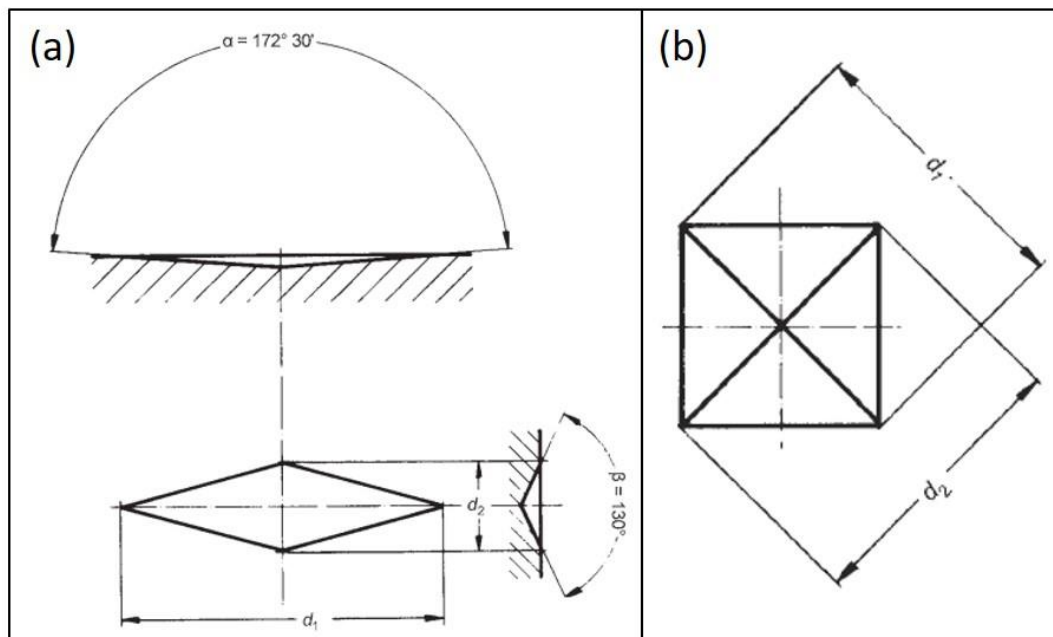
Figure 3-9 Indenters geometry for (a) Knoop and (b) Vickers hardness tests [134]

In this study, Knoop microhardness measurements were carried out by using a Struers Durascan hardness tester for the nitrided uncoated Ti-64 and Ti-AVM substrates (at 500°C and 600°C). The 10 gf of load was applied about 20s (dwell time) for all samples. At least 5 indentations were performed on the top of each sample to obtain an average value. The load was selected to reduce the risk of substrate contribution. Knoop hardness test method was not used for the samples (pre-coated or uncoated) which were treated at a higher temperature. This is due to the thin nature of the coatings could lead to more substrate contribution after deformation and for the samples which has a higher surface roughness value (treated at higher temperatures) could reduce the clarity of the trace on the surface while measuring the length of the diagonal

3.2.7 Micro-Abrasion Testing

Micro-abrasion is a suitable wear test technique for bulk samples (polymers, metals, ceramics), coatings (thin or thick) and duplex treated samples which provides information about the wear resistance [135]–[140]. The knowledge of abrasive wear resistance of the samples will help users while selecting proper coatings or diffusion treatments for their application. Besides the wear resistance properties, this method allows inspecting the quality of the coatings by checking if any cracks or pores present in the coating structure. Moreover, the adhesion between the coating and substrate can be observed during the experiment. It is better to apply this test on flat samples (not require any complex equipment). The advantage of this method is the test can be applied on a very small sample test area (a few millimetres square) [141]. The test is applied by a ball which is pressed against the sample. The speed of the ball and the applied load are kept constant during the test. While the ball is rotating, a slurry (containing water and SiC abrasive particles) is fed on to the ball, and the contact of the ball and sample surface kept wet during the experiment (sedimentation of the abrasive particles is undesirable). The position of the ball, sample and weight can be seen in Figure 3-10. A hemispherical crater

is created at the end of the experiment. A series of tests are applied by increasing the number of revolutions to obtain deeper craters. The depth and size of these craters are measured by using surface profilometry or optical microscopy, and the wear coefficient of the samples are calculated. The dominant wear mode (two body or three body abrasions [142]) can be obtained by analysing the morphology of the wear scars. Micro-abrasion tests of coatings can be performed as perforating or non-perforating. If only the coating is desired to be examined (related to wear rate performance), the non-perforating test is used. On the other hand, the perforating test is used to detect the thickness of the coatings and the wear rate for the coating and substrate together. More detailed information can be found in the BS ISO 26424 [143].

In this study, micro-abrasion tests were applied by using a Plint TE-66 micro abrasion test rig (Figure 3-10). The abrasive slurry was prepared by using SiC particles (F1200, ~3–4 μm particle size) and distilled water. The concentration of the slurry was 80 g/100 ml for all experiments. A 25 mm diameter (SAE52100 bearing steel) preconditioned ball was used. The rotation of the ball was adjusted at a tangential velocity of 0.1 ms^{-1} which equals about 80 rpm. The time of the experiments were decided by the number of ball revolutions (25, 50, 100, 200, 400), and the applied load was selected as 0.1 N. The wear coefficient (κ) of the untreated substrates (for comparison purpose), only nitrided substrates, only coated substrates and duplex treated (coated and nitrided) substrates were calculated by using the equation below.

$$K = \frac{V}{SN} = \frac{\pi b^4}{64RSN}$$
<div align="right">**Equation 3.2** [144]</div>

where

V is the total wear scar volume

S is the abrading distance

N is the normal load

b is the crater diameter

R is the radius of the ball.
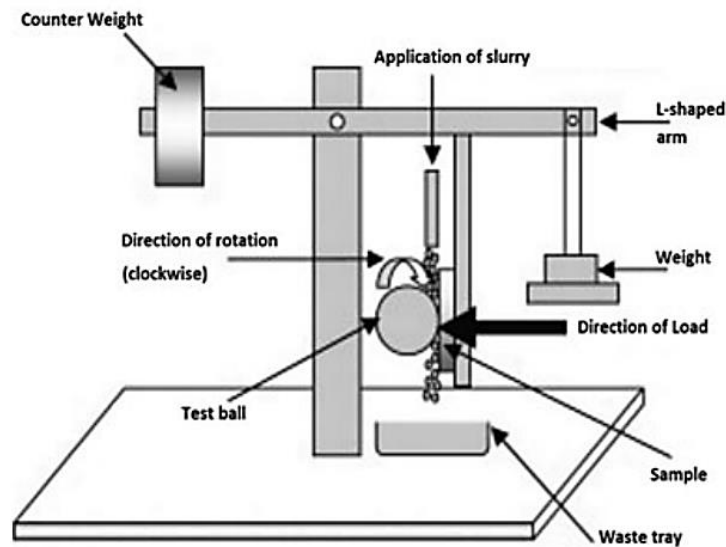
Figure 3-10 The schematic representation of the Plint TE-66 Micro Abrasion Test Rig [145]

3.2.8 Surface Profilometry

The surface topography of the coated and diffusion treated samples are analysed by using surface profilometer. This device has a stylus which scans the surface of the samples and gives two-dimension traces to analyse the surface roughness of the samples or wear rate measurements after any wear tests which create wear scars. The connected computer (and software) records all surface irregularities, and a profile is created by combining the magnitude of these irregularities. The stylus is usually made from diamond and connected to a motorised arm which travels on the surface of the material with constant speed. The speed of the arm can be customised by changing the total travel distance and total travel time. The resolution of the profiles can be adjusted by changing these parameters [146].

In this study, a Veeco Dektak 150 stylus profilometer (with 12.5 μm radius diamond tip) was used to obtain surface roughness values. The tip was forced with a load of 3 mg. Six scans (randomly placed) were performed on each sample, and an average R_a value was calculated for all samples. The scan length was kept at 1mm, and scan duration was set to 120 seconds.

4 Production and Characterisation of PVD Ti-based Coatings

This chapter includes the composition, phase structure, hardness, and elastic modulus analysis of the substrate materials, α-Ti and β-Ti alloy coatings (whereby pure Ti and Ti-Nb coatings were deposited before the nitriding process) with the aim to increase the N diffusion efficiency of Ti alloy substrates.

4.1 Substrate Materials

Two different titanium alloy substrates with, respectively, mainly alpha and mainly beta phase composition (Ti-6Al-4V and Ti-4Al-10V-22Mo) were selected for this study. Some initial coatings (trial runs) were also deposited on M2 steel coupons; these were used for coatings composition optimisations. The Nb-dependent phase composition of Ti-Nb coatings was also examined by using M2 steel substrates. The variety of the substrates provided convenience while selecting glancing angle degree for XRD measurement (to get rid of substrate contribution). When a substrate is coated with a coating which both have similar phases (such as Ti-Nb coating and the Ti-4Al-10V-22Mo substrate which both have a mainly BCC structure), it could be confusing while separating the XRD peaks of coating and substrate.

4.1.1 Ti-6Al-4V (Ti-64)

Ti-64 is a well-known titanium alloy stands in the class of alpha-beta Ti alloys. The XRD diffraction pattern for the Ti-64 alloy used in this study is shown in Figure 4-1. It can be seen from the XRD peaks that this alloy has two different phases (α and β) which are HCP and BCC respectively. This alloy composes two phases because of containing alpha and beta stabiliser elements (which Al is an alpha stabiliser, and V is a beta stabiliser). The elemental composition of the Ti-64 alloy (obtained by EDX analysis) can be seen in Table 4-1. The hardness and elastic modulus values for Ti-64 alloy (obtained by nanoindentation) can be seen in Table 4-2.

Table 4-1 The elemental composition of Ti-64 alloy substrate

Ti-64	Ti	Al	V
Weight %	89.4 ± 0.2	6.7 ± 0.2	3.9 ± 0.2
Atomic %	85.2 ± 0.2	11.3 ± 0.3	3.5 ± 0.2
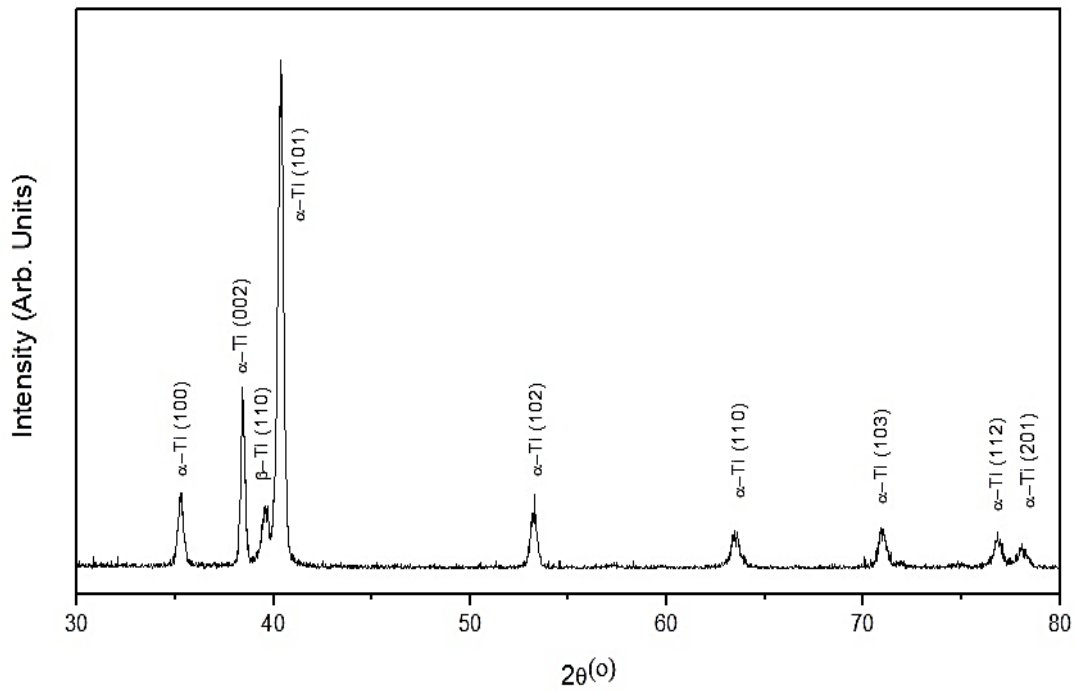
Figure 4-1 Theta-2theta diffraction patterns for Ti-64 alloy

Table 4-2 Nanoindentation hardness and elastic modulus results for substrates

Substrate Name	Hardness (GPa)	Elastic Modulus (GPa)
Ti-64	5.0 ± 0.2	136.4 ± 3.3
Ti-AVM	4.7 ± 0.3	123.3 ± 1.2
M2 steel	8.8 ± 0.5	188.5 ± 5.5

4.1.2 Ti-Al-V-Mo (Ti-AVM)

Ti-AVM alloy stands in the class of metastable beta Ti alloys which includes only beta phase (BCC). The XRD diffraction pattern for the Ti-AVM alloy (used in this study) is given in Figure 4-2. The (slightly high) amount of molybdenum and vanadium elements inside the alloy composition (which are beta stabilisers for Ti) makes the phase of this alloy cubic. The elemental composition of the Ti-AVM alloy (obtained by EDX analysis) can be seen in Table 4-3. The hardness and elastic modulus values for Ti-AVM alloy (obtained by nanoindentation) can be seen in Table 4-2. As a beta type of Ti alloy which its crystal structure is cubic, it showed lower elastic modulus than α + β type of Ti alloys [147].
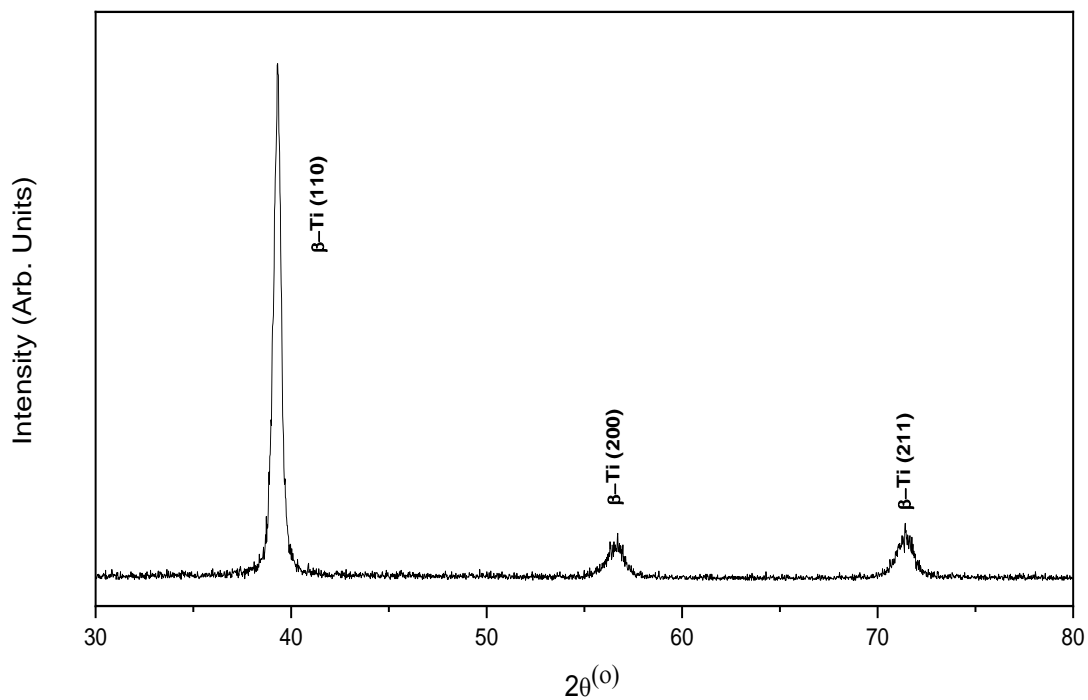
Figure 4-2 Theta-2theta diffraction patterns for Ti-AVM alloy

Table 4-3 The elemental composition of Ti-AVM alloy (substrate only)

Ti-AVM	Ti	Al	V	Mo
Weight %	63.8 ± 0.3	3.9 ± 0.1	9.8 ± 0.2	22.5 ± 0.5
Atomic %	69.9 ± 0.2	7.6 ± 0.2	10.1 ± 0.3	12.4 ± 0.3

4.1.3 M2 Tool Steel

Initial coatings (trial runs) were deposited on M2 tool steel coupons which and were used for coating composition optimisations. The XRD diffraction pattern for the M2 steel (used in this study) is shown in Figure 4-3. The diffraction pattern of the M2 steel (uncoated) shows two groups of peaks coming from the steel matrix and from the dispersed carbides, respectively [148]. In fact, this substrate was not used for the nitriding process; it was only used as a substrate material for Ti-Nb surface coating development. Therefore, the phase structure of the M2 steel will be helpful if any unknown peak appears in the XRD patterns of Ti-Nb coatings (to see if there is any substrate contribution). And also, the phase dependence of the coatings on the substrate crystal structure was also examined by depositing Ti-Nb coatings on M2 steel substrates. The elemental composition of the M2 steel (obtained by EDX analysis) can be seen in Table 4-4. The hardness and elastic modulus values for M2 steel (obtained by nanoindentation) can be seen in Table 4-2. The relatively high hardness value (comparing to Ti alloy substrates) of M2 steel substrate will also give some idea while measuring the nano-hardness of the Ti-Nb coatings (to see if any substrate contribution).
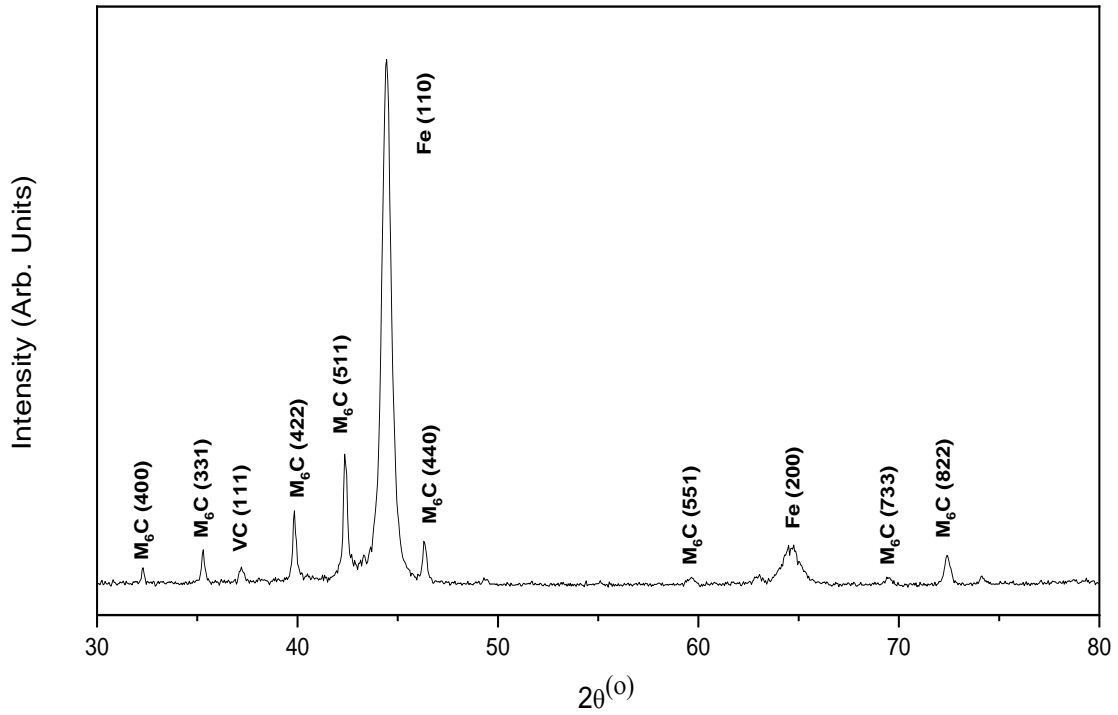
Figure 4-3 Theta-2theta diffraction patterns for M2 tool steel

Table 4-4 The elemental composition of M2 tool steel substrate

M2 steel	Fe	Cr	Mo	W	V	Mn	Ni
Weight %	81.9 ± 0.3	4.0 ± 0.1	4.3 ± 0.2	7.6 ± 0.2	1.4 ± 0.1	0.5 ± 0.1	0.3 ± 0.1
Atomic %	87.7 ± 0.3	4.6 ± 0.1	2.7 ± 0.2	2.5 ± 0.2	1.7 ± 0.1	0.5 ± 0.1	0.3 ± 0.1

4.2   PVD Surface Coating Deposition

4.2.1   Ti Coatings

The pure Ti surface layer which was deposited before nitriding was produced with a single piece Ti target. There was no need to do any coating optimisation (related to the concentration of the coating) by arranging the substrates' position on the substrate holder because all coatings were expected to be pure on the substrate holder. The Ti target and the target holder (substrates placed on it) is shown in Figure 4-4. The small substrate indicates Ti-AVM alloy and the bigger ones show Ti-64 alloy substrates. It is also seen in Figure 4-4 that substrates were placed in the transverse direction to see the homogeneity of the process. Because of the configuration of the target and substrate holder (they are standing face to face, 21 cm distance between them), all positions on this rectangular area (where the substrate are sitting on it) were suitable to deposit pure Ti coatings. The power supplied to the Ti target was 1000 W, and the substrate holder was biased to -50 V.
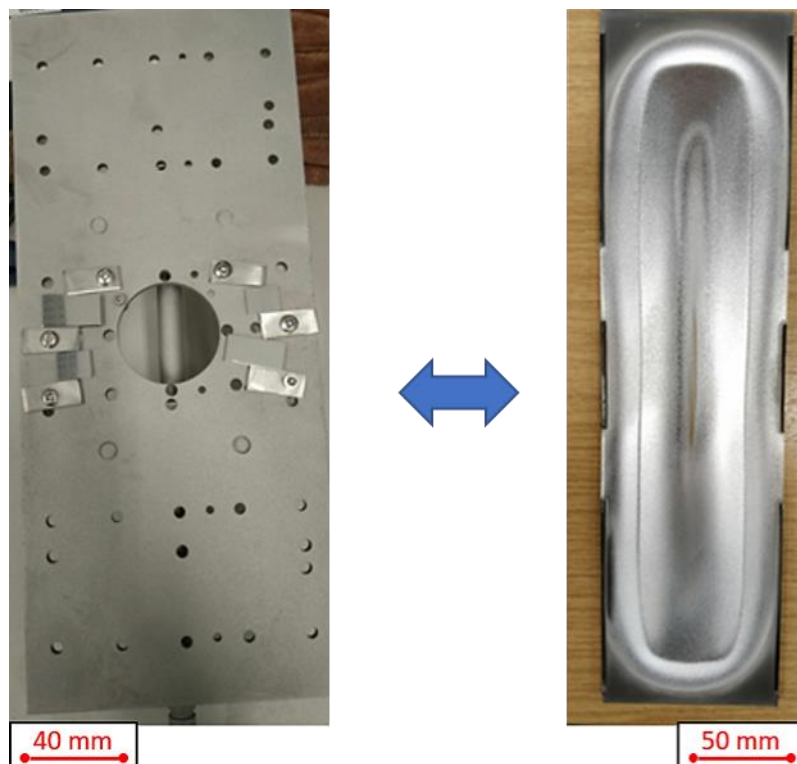
Figure 4-4 The substrate holder (showing the position of the Ti-64 and Ti-AVM alloy substrates) for pure Ti coatings and one whole piece of Ti target

63

The XRD diffraction pattern for Ti coatings on Ti-64 and Ti-AVM alloys are shown in Figure 4-5. It can be seen that the coatings include only one phase in which all the XRD peaks were HCP structure (pure α-Ti). The XRD analysis for this coating was performed by glancing angle mode (2-degree) to eliminate substrate peaks. The X-ray penetration depth calculated by AbsorbDX software (which uses the density and composition of the material while determining the X-ray penetration depth) suggested that the X-rays would penetrate Ti coatings by about 0.9 μm at 2-degrees glancing angle. The thickness of the Ti coating was 1.25 μm (for these XRD patterns), and therefore any effect from the substrate was not expected on XRD peaks, and this was confirmed by the XRD patterns (seen in Figure 4-5)
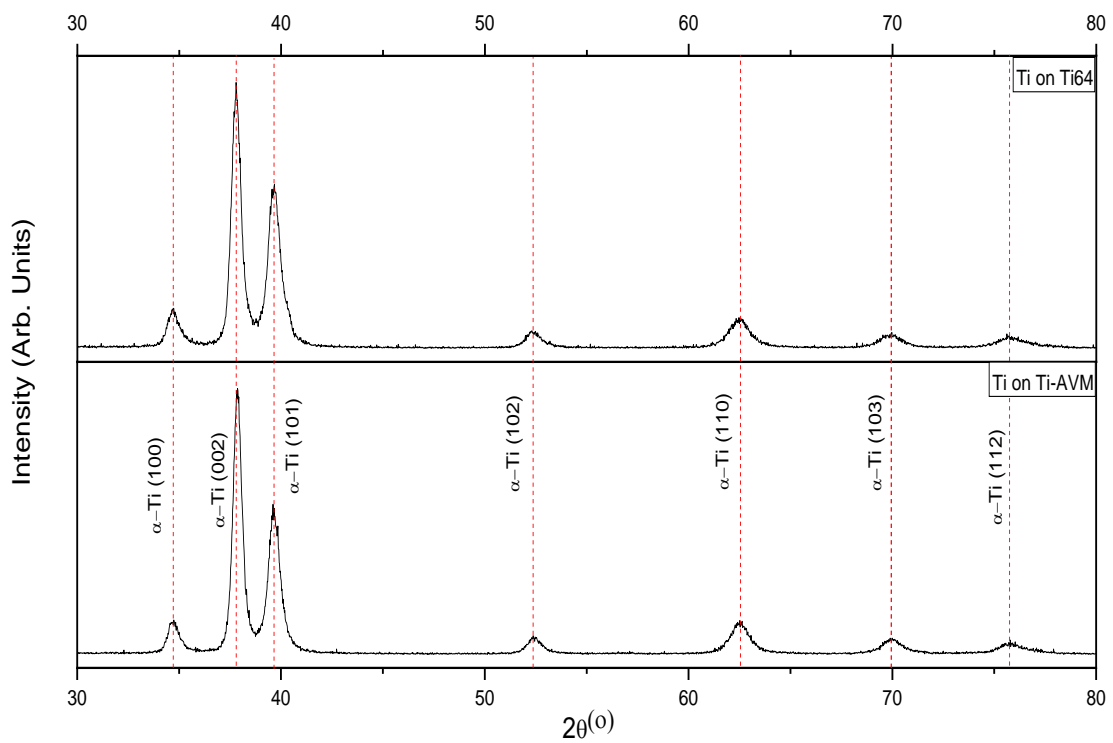
Figure 4-5 GAXRD (2º angle of incidence) diffraction patterns for Ti surface layer coatings on Ti-64 and Ti-AVM substrates

4.2.2 Ti-Nb coatings

4.2.2.1 Optimization of Nb concentration by changing target configuration for Ti-Nb coatings (Set Nb1)

The pure Ti (surface layer) coating deposition process was easy to apply because only one kind of metal target was used. On the other hand, the binary Ti-Nb alloy surface coatings required compositional optimisation. This coating optimisation set which consists of 2 runs was entitled as S-Nb1. The two runs (each run had five M2 tool steel substrates) with different substrate and target positions (as explained in Figure 3-2) yielded ten different Ti-Nb concentrations. Run 1 included (Nb-Nb-Ti) target configuration and run 2 included (Ti-Ti-Nb) target configuration. The working distance between the substrate holder and the target was 21cm. The power supplied to the Ti-Nb target as1000 W, and the substrate holder was biased to -50 V. The elemental composition of the Ti-Nb coatings (obtained EDX analysis) for S-Nb1 can be seen in Table 4-5. The target configuration in run 2 was selected after optimisation work to produce the Ti-Nb surface coatings because it was planned to produce Ti alloy coatings which have Nb concentrations in the range of 20 to 50 at. %. The schematic representation (with target and substrate configurations) of run 2 can be seen in Figure 4-6.

Table 4-5 The elemental composition results of the Ti-Nb coatings in S-Nb1

Set No	Run No	Sample No	Ti (at. %)	Nb (at. %)
S-Nb1	1	A1	11.7 ± 0.2	88.3 ± 0.2
		A2	12.8 ± 0.2	87.2 ± 0.2
		A3	19.0 ± 0.2	81.0 ± 0.2
		A4	25.9 ± 0.1	74.1 ± 0.1
		A5	35.3 ± 0.1	64.7 ± 0.1
	2	A6	46.6 ± 0.1	53.4 ± 0.1
		A7	54.3 ± 0.2	45.7 ± 0.2
		A8	60.7 ± 0.1	39.3 ± 0.1
		A9	74.3 ± 0.1	25.7 ± 0.1
		A10	81.9 ± 0.2	18.1 ± 0.2
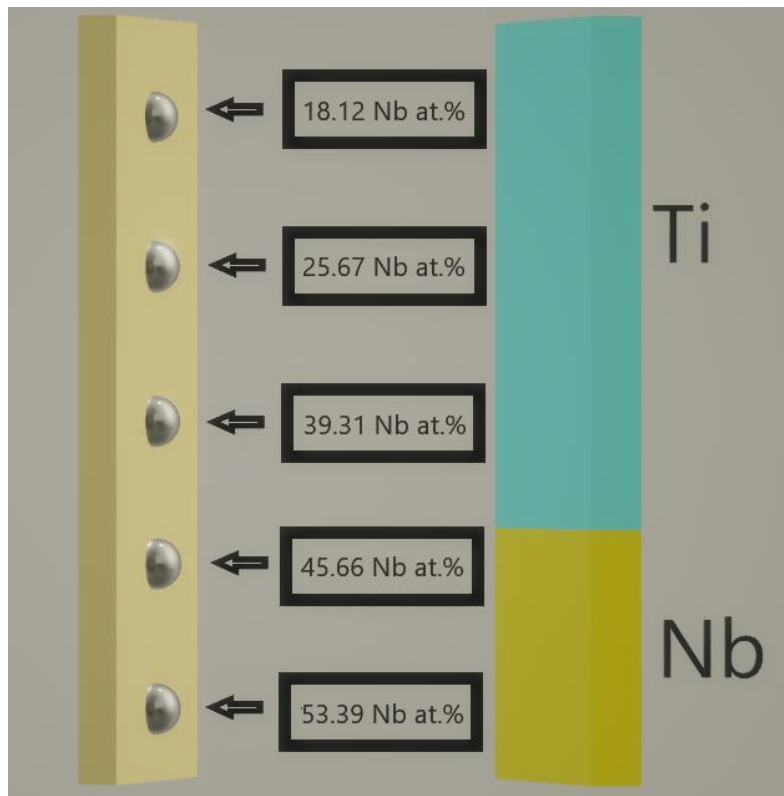
Figure 4-6 Schematic representation of the Run 2 in S-Nb1 with Nb atomic percentages.

The XRD diffraction pattern for Ti-Nb coatings in Run 2 (A6-A10) on M2 tool steel substrates was given in Figure 4-7. These five coating (the lowest Nb concentration is 18.1 at. %) showed cubic structure (BCC) as their principal peak is (110). The second and third peaks (200) and (211) were started to become apparent with Sample A9 which has 25.7 at. % Nb. Because the intensity of each coating's first peaks (110) is much higher than the other peaks, it is difficult to see how the other peaks are developing with the increase of Nb concentration inside the Ti-Nb alloys. The XRD diffraction patterns were enlarged (from 50° to 100°) to analyse growing of small peaks clearly. It is seen in Figure 4-8 that the fourth and fifth peaks of β-Ti were started to develop from Sample A8 which has approximately 40 at. % Nb. Considering the results of the optimisation runs, a coating composition between sample 8 and sample 9 could be a good candidate for a Ti-Nb surface layer deposited before the nitriding. It was also reported in the literature that the phase of Ti-Nb coatings was %100 β (cubic) with 34 at. % Nb concentration [9].
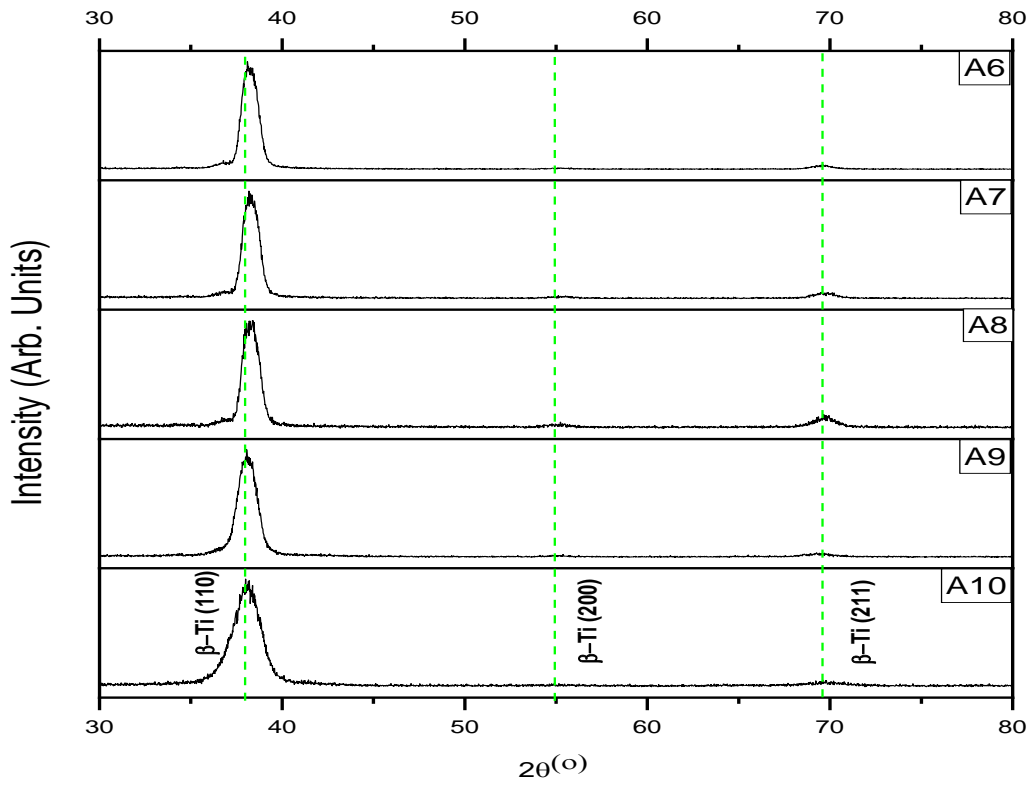
Figure 4-7 GAXRD (2º angle of incidence) diffraction patterns for Ti-Nb surface layer coatings on M2 tool steel substrate for Run 2 in S-Nb1
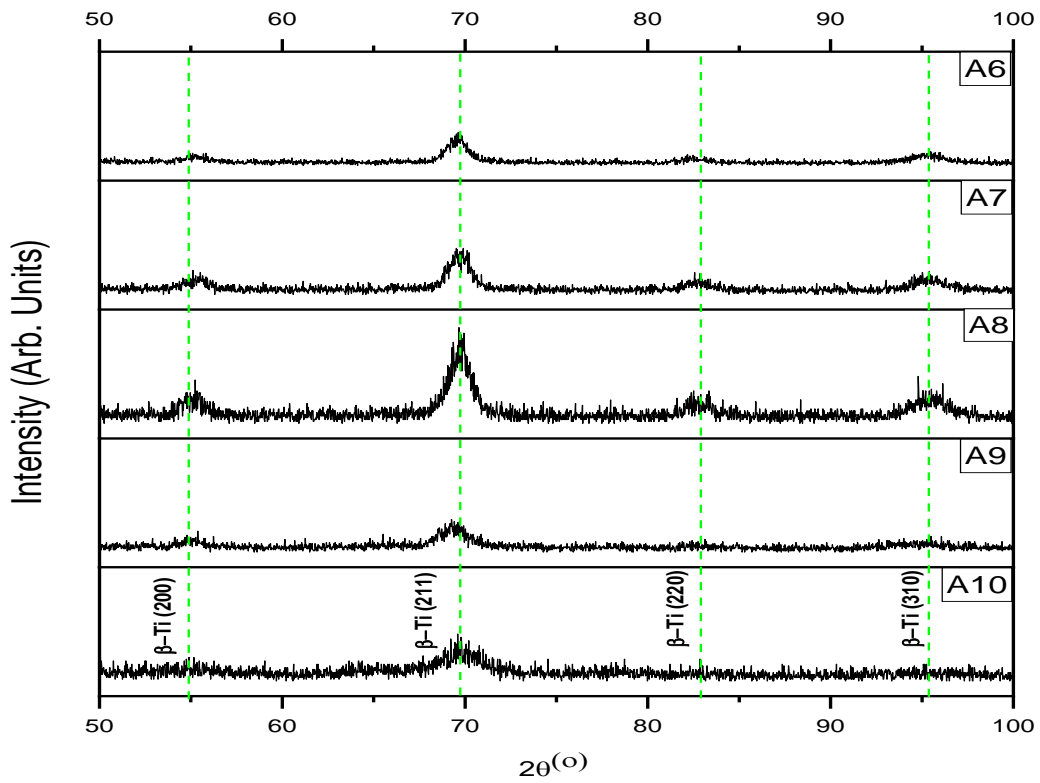
Figure 4-8 GAXRD (2º angle of incidence) diffraction patterns for Ti-Nb surface layer coatings on M2 tool steel substrate for Run 2 in S-Nb1 (small peaks from 50º to 100º)

The nanoindentation hardness and elastic modulus values are given in Table 4-6. It was observed from the values that, with increasing Nb content, the coating hardness values also increased by the effect of solid solution (structural hardening) due to the addition of Nb to Ti. [149].

Table 4-6 Nanoindentation hardness and elastic modulus results for Ti-Nb coatings in S-Nb1

Set No	Run No	Sample No	Hardness (GPa)	Elastic Modulus (GPa)
S-Nb1	2	A6	6.2 ± 0.4	$128.5 + 4.7$
		A7	5.9 ± 0.3	122.1 ± 3.1
		A8	5.8 ± 0.3	119.2 ± 3.5
		A9	5.4 ± 0.3	105.1 ± 4.3
		A10	5.1 ± 0.2	102.6 ± 2.8

4.2.2.2 Determining the effect of substrate types on the phase structure of Ti-Nb coatings (Set Nb2)

The first set of Ti-Nb coatings was deposited on only M2 tool steel substrates; on the other hand, the second Ti-Nb coating set was applied on three different substrates. Because the main aim of this study is to improve the nitriding behaviour of various titanium alloys (with different crystal structures), two titanium alloy substrates were also included in this set. The effect of substrate type on β stabilisation of Ti-Nb coatings was investigated with this set, and the repeatability of the coating runs was also compared with the first set. This set of coatings was entitled as S-Nb2 which has two runs (Run 3 and Run 4). The process parameters kept same with previous runs. Run 3 was performed on Ti-64 and M2 tool steel substrates; in total six samples (three circular M2 steel, three rectangular Ti-64 samples) were placed on the substrate holder (see Figure 4-9). The elemental composition of the Ti-Nb coatings (obtained by EDX analysis) for Run 3 in the S-Nb2 set can be seen in Table 4-7. The P1, P2 and P3 are used to show the positions of the samples from top to bottom.

Table 4-7 The elemental composition results of the Ti-Nb coatings for Run 3 in S-Nb2

Set No	Run No	Sample No	Ti (at. %)	Nb (at. %)
S-Nb2	3	Ti-64-P1	83.1	16.9
		Ti-64-P2	74.5	25.5
		Ti-64-P3	59.4	40.6
		M2-P1	83.6	16.4
		M2-P2	74.2	25.8
		M2-P3	57.5	42.4
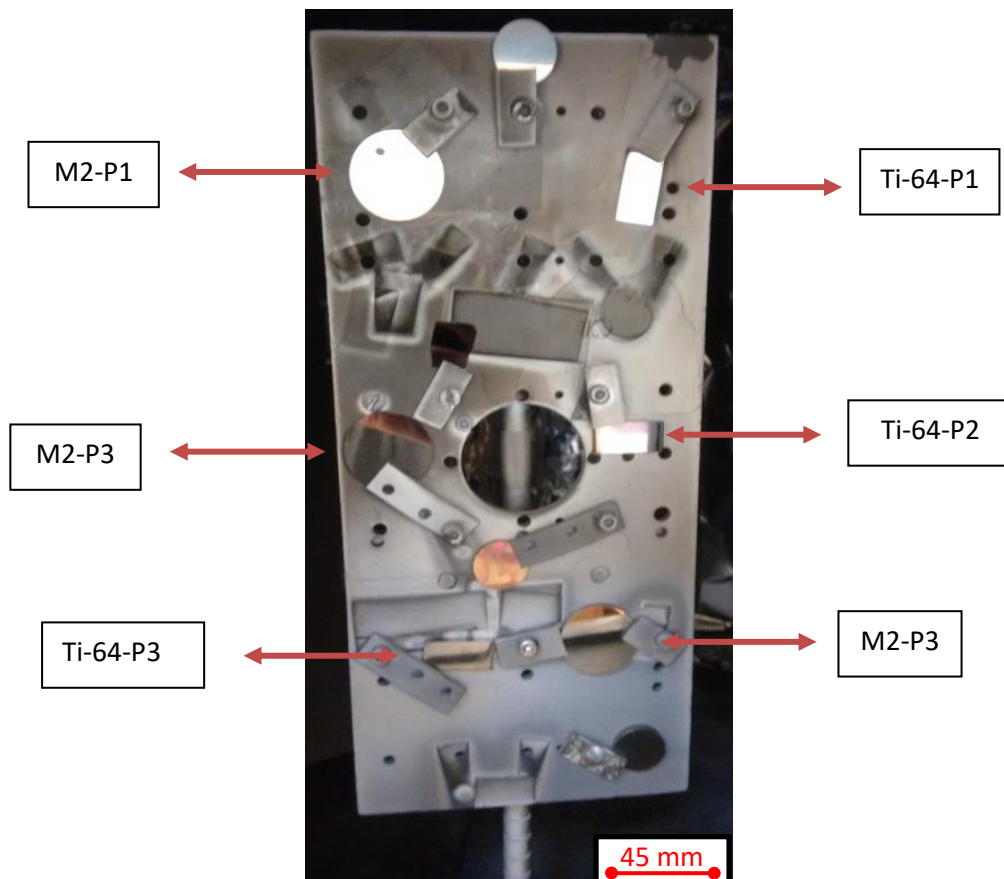
Figure 4-9 The substrate holder (showing the position of the substrates) for Run 3 in S-Nb2

It is seen from Table 4-7 that the parallel samples (i.e. Ti-64_P1 and M2-P1) are showing very similar concentrations because they were placed so their centres would sit on the same alignment in the vertical direction of the substrate holder. This situation will be understood better at Run 4 in S-Nb2. The XRD diffraction patterns for Ti-Nb coatings on M2 steel and Ti-

64 substrates are shown in Figure 4-10 and Figure 4-11 respectively for Run 3 in S-Nb2. A minimum Nb concentration, of around 16.5 at. % was obtained for Ti-Nb coating on M2 steel and Ti-64 substrates. The phase structure of the Ti-Nb coatings deposited on M2 steel substrates showed a similar (cubic) structure to the coatings in the Run 2. On the other hand, the Ti-Nb coating which was deposited on Ti-64 substrates included α phase peaks in the upper position (P1). It was thought that the substrate's predominantly HCP crystal structure could suppress the BCC crystal structure of the Nb-modified Ti coatings. It was also reported previously in the literature that the types and positions of the phases for Ti-Nb coatings would be different if they are deposited on different substrates such as pure Ti, α+β Ti alloy, β-Ti alloy and stainless steel [150]. (It was also mentioned that the mechanical properties of the coatings could be affected by the type of the underlying substrates.)
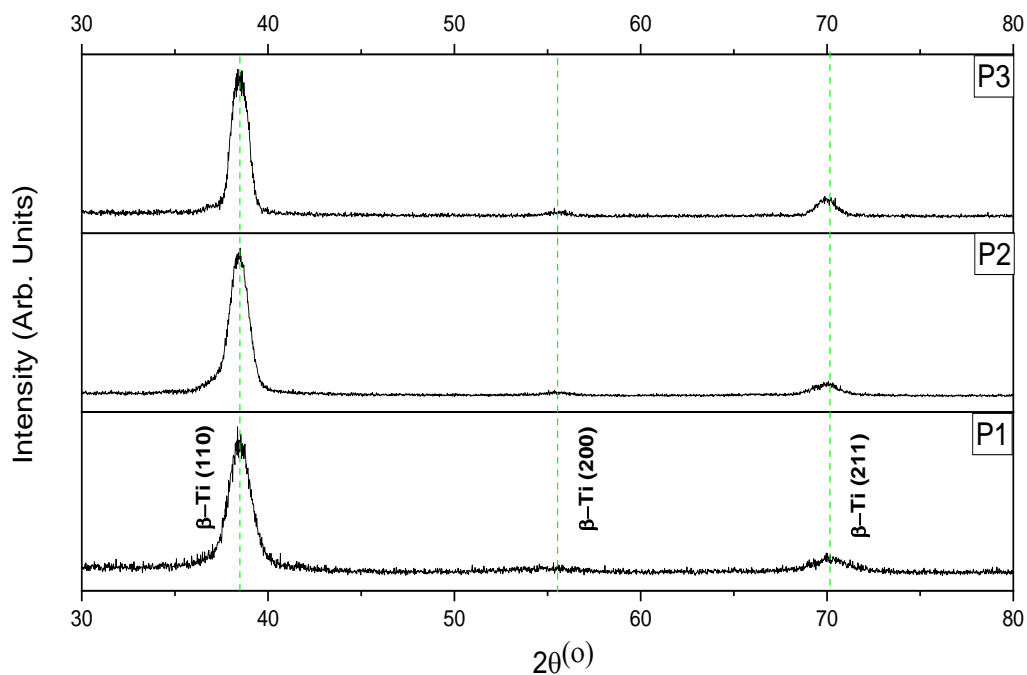
Figure 4-10 GAXRD (2º angle of incidence) diffraction patterns for Ti-Nb surface layer coatings on M2 tool steel substrates for Run 3 in S-Nb2
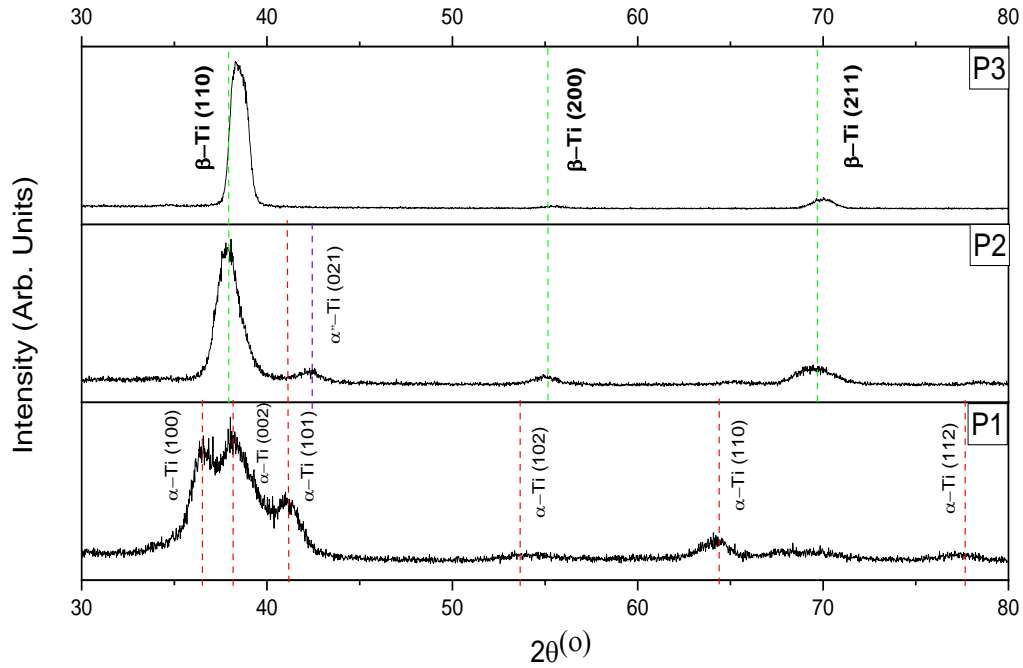
Figure 4-11 GAXRD (2º angle of incidence) diffraction patterns for Ti-Nb surface layer coatings on Ti-64 substrates for Run 3 in S-Nb2

It can be seen in Figure 4-11 that when the concentration of Nb is increased, the phase structure tends towards a BCC structure. However, in the P2 (about 25 at. % Nb), an extra peak is seen in the XRD pattern at 42.5º. When the Nb is introduced into the Ti system, it may be in the tendency to remove the α-Ti (100) and α-Ti (101) peaks and transform the α-Ti (002) into α″-Ti (111) martensite, and β-Ti (110) depends on the amount of Nb in the system. The Ti-Nb coatings in this study were examined with glancing angle XRD, and so it resulted in broader peaks. In the XRD patterns, the peaks (especially beta and martensitic phases) are very close to each other, and it would be very difficult to distinguish all the peaks with the result of glancing angle XRD (due to overlapping of the peaks). However, the α″-Ti (021) peak which stands about 42.5º (it is far enough from the major peaks) will be helpful to understand if any martensite phase is found or not. There are various studies in the literature which show the effect of Nb on the phase structure of bulk Ti-Nb alloy production. Chang et al. [151] reported that the Ti-Nb alloy which includes 20 Nb at.% showed mixed α″ and β phase; on the other hand, the Ti-Nb alloy which includes 30 Nb at.% showed fully β phase. Ahmed et al. [152]

reported that the martensite phase was found in Ti-Nb alloy system up to 23.4 at. % Nb, and that increasing Nb concentration lead to retention of the β phase. Moffat et al. [153] reported that the martensite phase (α″) was found in Ti-Nb alloys which contained 20-25 at. % Nb. It should be noted that this complex metallurgy of Ti alloys is also affected by the temperature of the process and the quenching rate of the molten alloys. Our aim in this study is to find a proper Nb concentration for Ti-Nb surface layer coatings which allows pure β phase structure to avoid any effects of the other phases on nitrogen diffusion efficiency.

Beside these bulk Ti-Nb works, some studies can also be found in the literature which relate to Ti-Nb coatings. Achache et al. [9] found that the phase structure of sputtered Ti-Nb coatings is a mix of α and β Ti phases, and there is no sign of an α″ martensitic phase. Gonzales et al. [149], [154] showed that the phase structure of sputtered Ti-Nb coatings is fully beta phase from 15 at. %. Nb. Stary et al. [150] deposited (using sputtering technique) Ti-Nb coatings (which contain about 25 at. % Nb) on various substrates. The XRD patterns of the Ti-Nb coatings deposited on Ti-6Al-4V substrate showed martensite phase peaks, but interestingly they did not mention it in their results. However, at least, it can be an example of the martensite phase surviving in Ti-Nb coatings containing up to 25 at. % Nb. Photiou et al. [155] reported that sputtered Ti-Nb alloy coatings containing 15 at. % Nb showed the martensitic phase (α″), which is fully converted to β above 20 at. % Nb. All these examples related to Ti-Nb alloy coatings show that there is a possibility for formation of martensite phase in the range of 15 and 30 at. % Nb. It should be noted that (as in bulk Ti-Nb production) there can also be different parameters which affect the phase structure (and consequently the formation of martensite phase) for the Ti-Nb coatings such as process temperature, substrate type, substrate bias voltage. It was also reported that the kinetic energy (of the sputtering system) could provide enough momentum for β stabilisation at lower temperatures compared with the bulk Ti-Nb alloy production which contains a similar Nb concentration [155].

The next coating run (for S-Nb2 set) was performed by including also the Ti-AVM alloy substrates, and this run was entitled as Run 4. In this run, twenty-one substrates were placed on the substrate holder, and seven different Ti-Nb coating compositions (for different vertical positions) were expected. The substrates were placed as Ti-AVM is on the left, Ti-64 in the middle and M2 steel on the right for all vertical positions. The arrangement of the substrates can be seen in Figure 4-12 from position 1 to position 7. The elemental composition of the Ti-Nb coatings (obtained by EDX analysis) for Run 4 in the S-Nb2 set can be seen in Table 4-8. The substrates which stand in the same horizontal levels were showing again very similar compositional values (as seen in previous runs).
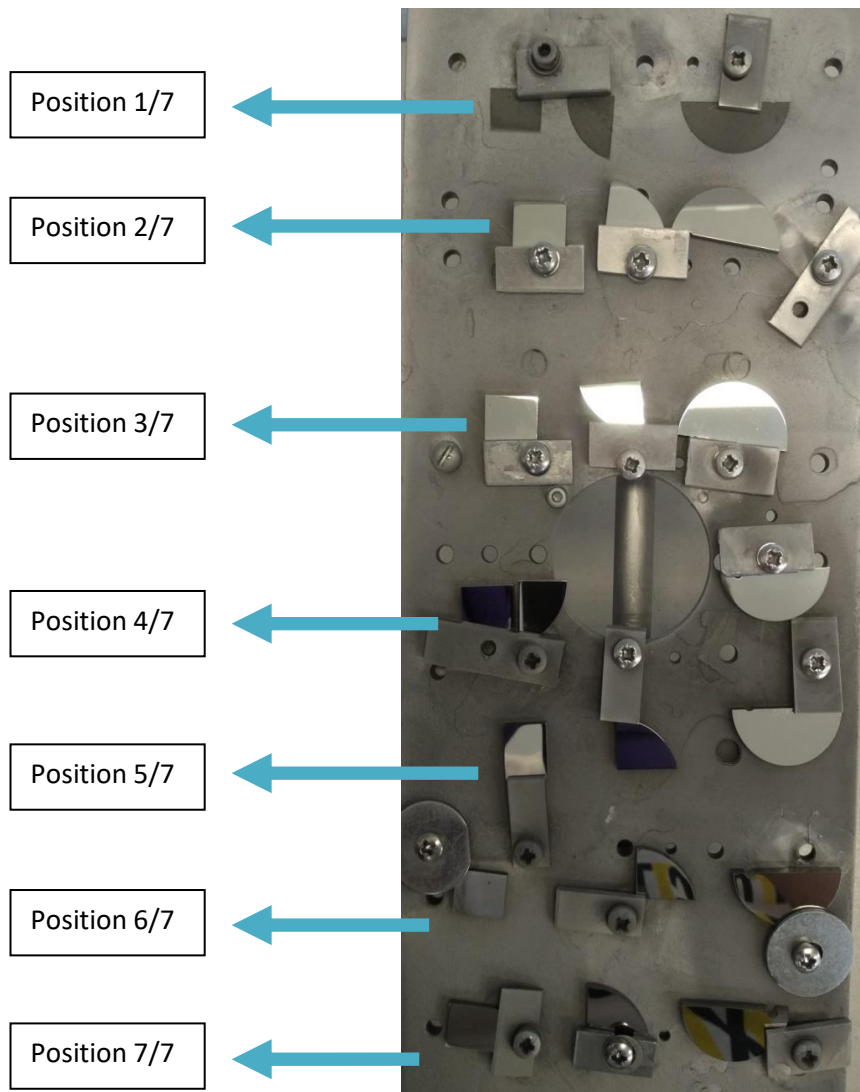
Figure 4-12 The substrate holder (showing the position of the substrates) for Run 4 in S-Nb2

It was understood that there is no concentration change in horizontal levels (in the same positions) and the results look repeatable for this coating configurations. The significance of this finding would not be so critical for a pure Ti coating because every place on the substrate holder should give the same chemical composition. On the other hand, it was very important while depositing alloy coatings such as Ti-Nb. When the concentration is decided (i.e. 40 Nb % at.), the user of the coating rig would know where the substrates must be placed in vertically, and more than one substrate can be placed in horizontally. It will allow producing more than one coating in one run if needed. The power was supplied to only one magnetron/target system, and the target was placed as pieces (such as 2 Ti + 1 Nb), so in this condition, the concentration of the coatings was controlled by moving the substrate positions horizontally.

Table 4-8 The elemental composition results of the Ti-Nb coatings on Ti-64, Ti-AVM and M2 steel substrates for Run 4 in S-Nb2

Set No	Run No	Substrate Position	Ti-64		Ti-AVM		M2 steel	
			Ti (at %)	Nb (at %)	Ti (at %)	Nb (at %)	Ti (at %)	Nb (at %)
S-Nb2	4	1/7	81.7	18.3	81.2	18.8	79.9	20.1
		2/7	78.9	21.1	78.6	21.4	77.9	22.1
		3/7	72.7	27.3	73.5	26.5	73.7	26.3
		4/7	64.9	35.1	64.7	35.3	65.2	34.8
		5/7	59.2	40.8	59.4	40.6	58	42
		6/7	52.8	47.2	51.3	48.7	52.6	47.4
		7/7	46	54	45.3	54.7	43.5	56.5

On the other hand, the coating deposition process could have been achieved by using two different magnetron/target systems where the power to each target could be supplied separately [9], [154]. In this configuration, the amount of power applied to each target would decide the composition of the coatings. It can be applied a constant power to one of the targets, and a varying amount of power can be applied to the second target. It would reveal one more parameter to control, and more energy would be consumed. Rather than its economic benefits, the control of the concentration of the coatings would be very sensitive, and there is a possibility to contaminate both targets. On the other hand, the split (alloy) target model (which is used in this study) will allow getting different concentrations in one coating run. For example, to produce all the coatings (which are seen in Figure 4-12), at least seven different runs (by changing the amount of power to be applied to both targets) would be needed if the co-sputtering model (with two magnetron/target systems) were used. Therefore, it can be easily said that to try new alloy compositions is easy with "split target model". It must be noted that this argument is valid for alloy coatings which include two or three different elements. If it is desired to use more than three different metals in the alloy coatings, the co-sputtering model should be used.

The XRD diffraction patterns for Ti-Nb coatings on Ti-64, Ti-AVM and M2 steel substrates (for the first three positions) are seen in Figure 4-13, Figure 4-14 and Figure 4-15 respectively for Run 4 in S-Nb2. The Nb concentrations for the coatings (in the same horizontal level) are almost the same (as can be seen in Table 4-8). The Ti-Nb coatings in the third position (3/7) on all kind of substrates were most beta-stabilised compared to other positions (1/7 and 2/7). The coating which deposited on all three substrates on position 1/7 and 2/7 showed a mix of $\beta + \alpha''$ phases. The reason for this phase difference is the Nb concentration of the Ti-Nb surface layer coatings. If the Ti-Nb coating deposited on Ti-64 substrate (P1) in Run 3 is compared with the

75

three Ti-Nb coatings deposited on M2 steel substrate (1/7), (2/7) and (3/7) in Run 4, it can be

seen how the phase constitution changes with Nb concentration.
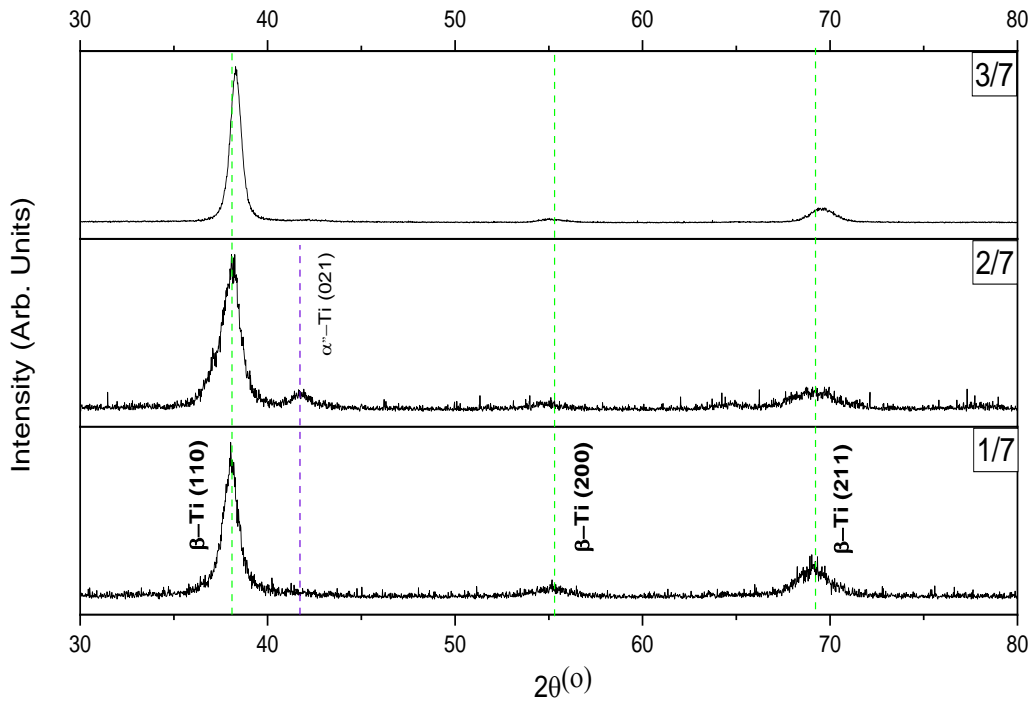
Figure 4-13 GAXRD (2º angle of incidence) diffraction patterns for Ti-Nb surface layer coatings on Ti-64 substrates for Run 4 in S-Nb2
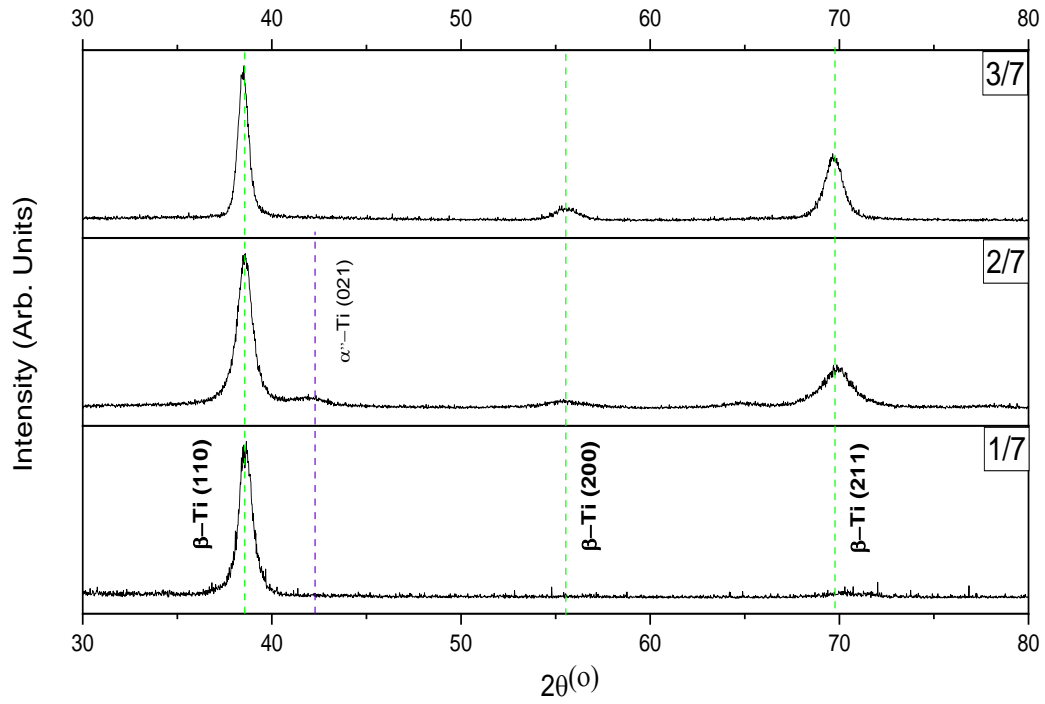
Figure 4-14 GAXRD (2º angle of incidence) diffraction patterns for Ti-Nb surface layer coatings on Ti-AVM substrates for Run 4 in S-Nb2
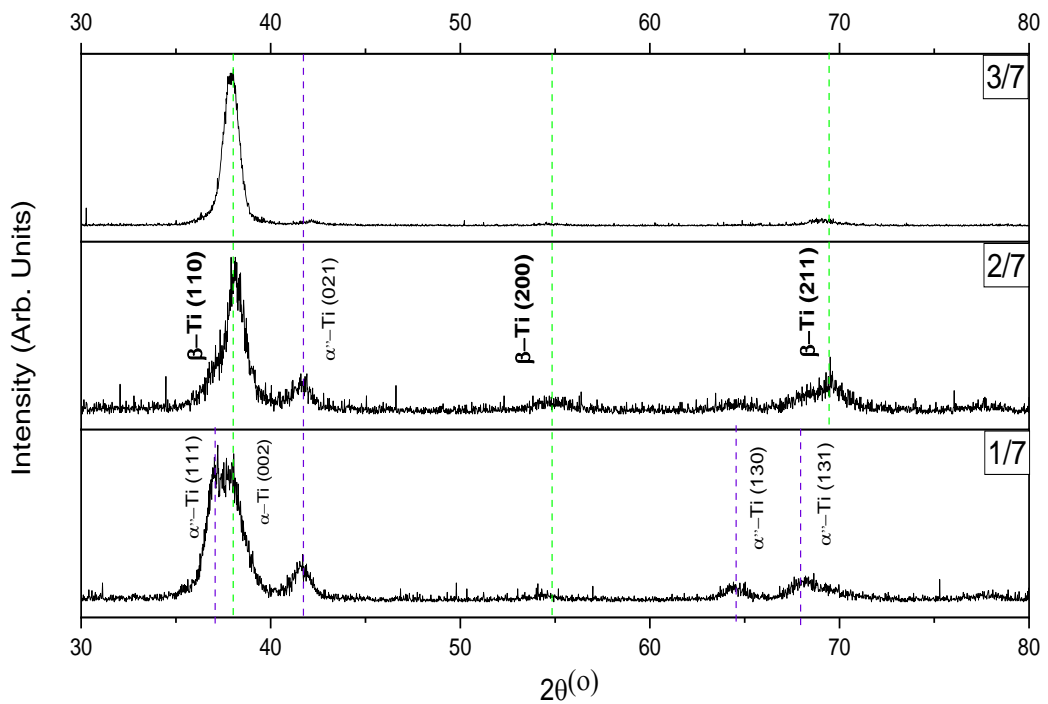

Figure 4-15 GAXRD (2º angle of incidence) diffraction patterns for Ti-Nb surface layer coatings on M2 steel substrates for Run 4 in S-Nb2

The phases were changed from α to a mix of β + α″, and then the α″ phase was eliminated by changing the Nb concentration from 16 at % to 26 at. %. Moreover, the (strong) martensite phase in the Ti-Nb coating deposited on M2 steel (1/7) rather than the Ti-64 and Ti-AVM substrates may be related to the uncoated crystal structure of the M2 steel substrate. As mentioned in section 4.1.3, the XRD pattern of the M2 steel (see in Figure 4-3) has two sets of peaks, of which one set is related to the steel matrix, and the other one to the dispersed carbide phases [156]. The complex crystal structure of the substrate may lead to postponing the beta stabilisation to higher Nb amounts, where it is seen in position (3/7) that the crystal phase is nearly cubic.

It was also realised that the intensity of the β-Ti (110) peak for the Ti-Nb coating deposited on M2 steel substrate is relatively lower than the same peaks for Ti-Nb coatings deposited on other substrates. And also, the XRD patterns are noisier for the Ti-Nb coatings (clearly for the position 1/7 and 2/7) which deposited on M2 steel substrate. It may be related to the smaller grain size and/or less preferred texture of the Ti-Nb coatings. Moreover, the Ti-Nb coatings may wish to stay in α phase or to form martensite phase depend on the Nb concentration. Because it was seen that the coatings have more than 26 at. % Nb started to show clear XRD results (for M2 steel substrate as well) by showing cubic phase formation. The XRD patterns of the Ti-Nb coatings which stand in position (4/7) or below (see Figure 4-12) were not given because all the coatings showed a fully β-stabilised structure with their Nb concentration of 35 at. % or above (see Table 4-8).

4.2.2.3 Improvement of coating uniformity across the whole substrate surface for Ti-Nb coatings (Set Nb3)

EDX analyses were performed on the Ti-Nb coated substrates from at least five different points. The first measurement was done from the centre (0,0) of the sample, and the other four measurements were taken as a distance 3 mm away (in x and y directions) from the origin point. In other words, the coordinates of the other 4 points can be written as (0, 3), (0, -3), (3, 0) and (-3, 0). If any mismatch was seen on the results, the number of repeats were increased or could be repeated, to get similar concentration on the whole surface of the substrates. While doing EDX analyses for run 4 in S-Nb2, it was found that one of the samples (Position 2/7 for Ti-AVM substrate which stands in the left column in Figure 4-12) was constrained. A detailed EDX analysis (twenty-four measurements) was performed on it. The EDX map for sample 2/7 can be seen in Figure 4-16 (each side of the small squares is 1mm long).
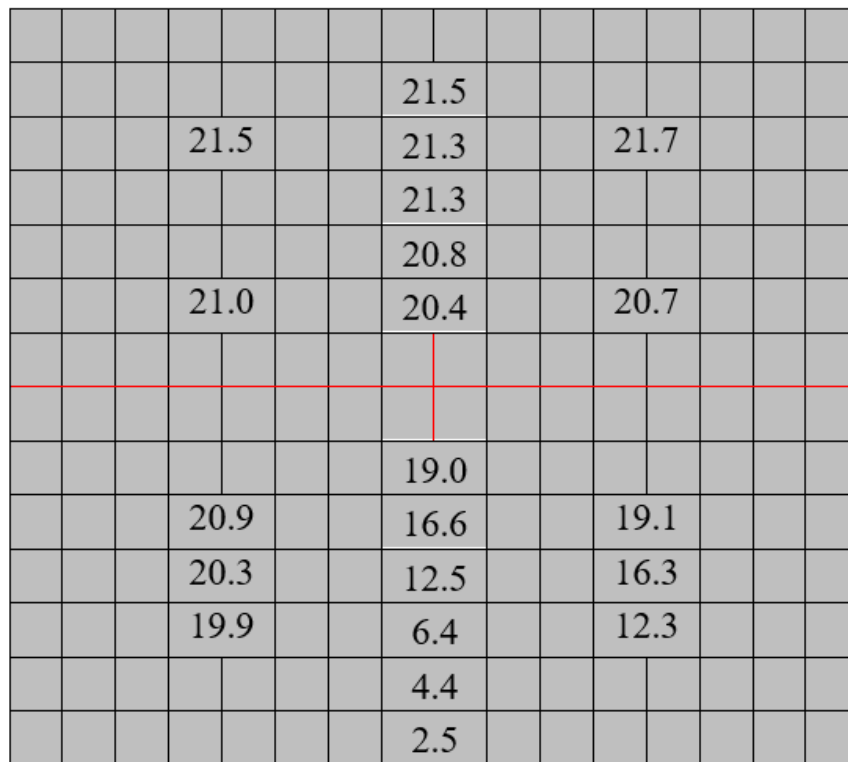
Figure 4-16 EDX composition map of Nb for the Ti-Nb coating on Ti-AVM substrates at position 2/7 in Run 4

The EDX map was drawn on a graph paper which includes squares (each side is 1mm long), and the point of junction of two red lines on the paper represents the centre of the samples which can be shown as (0, 0). The red zigzag line (on the EDX maps) is showing the edge of the material which is assembled to the substrate holder with a metallic washer and screw. The numbers on the graph paper are showing the amount of Nb (in % at.) for each point. It can be seen in Figure 4-16 that the Nb concentration is rapidly decreased from the centre of the sample to (-y) direction. The most important matter is that the surface Nb concentration should be homogeneous at every point on the surface such that the local crystal structure of the coatings is not changing.

A new run was prepared (Run 5) with a new configuration to understand why this concentration is changing. The Run 5 was done with a new thick metallic cover which was placed directly onto the second magnetron (as explained previous section, only one magnetron/target system was biased) to inhibit if there is any magnetic effect on the plasma. The second magnetron (which was not biased) stands at 90° to the other magnetron (which was biased) and therefore the magnetic field in front of the sputter target could be distorted by the second magnetron. The arrangement of the substrates is seen in Figure 4-17 from position 0 to position 3. The position of the substrates in Run 5 was exactly the same with Run 4 in S-Nb2. For example, the 2/7 in Run 4 and 2/3 in Run 5 should have very similar Nb concentration. The elemental composition of the Ti-Nb coatings (obtained by EDX analysis) for Run 5 in the S-Nb3 set are shown in Table 4-9.
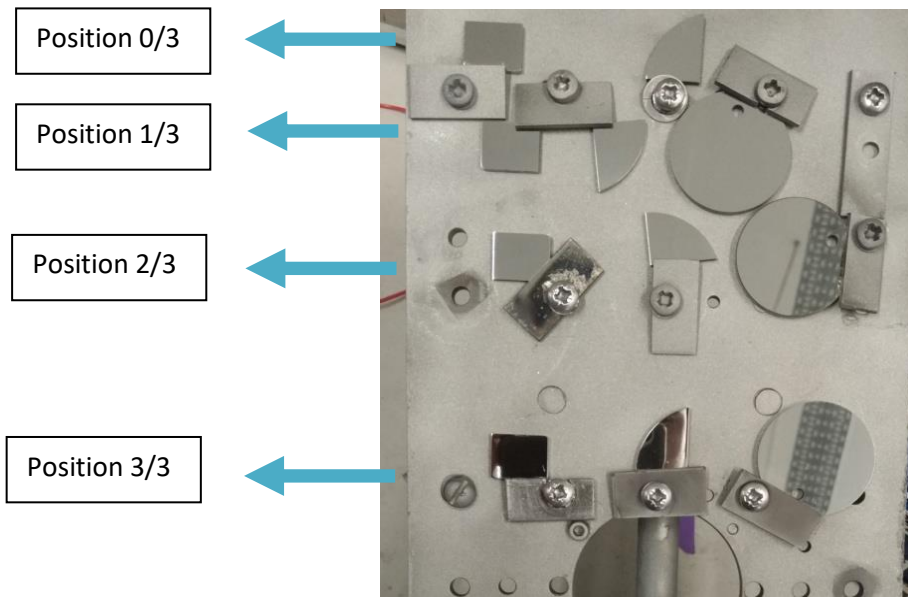
Figure 4-17 The substrate holder (showing the position of the substrates) for Run 5 in S-Nb3

Table 4-9 The elemental composition results of the Ti-Nb coatings for Run 5 in S-Nb3

Substrate	Ti-AVM		S-Ti-64	
Position	Ti (at%)	Nb (at%)	Ti (at%)	Nb (at%)
0/3	83.0	17.0	83.3	16.7
1/3	80.4	19.6	80.6	19.4
2/3	78.8	21.2	78.8	21.2
3/3	74.4	25.6	74.7	25.3

It can be seen from Table 4-9 that the average Nb concentrations of the Ti-Nb coatings are very similar with the previous runs which shows the repeatability of this coating systems is very good. The detailed EDX analysis was performed for the sample on the position 2/3 (Ti-AVM substrates) the EDX map of which can be seen in Figure 4-18. The homogeneity of the Nb concentration of this coating looks very stable.
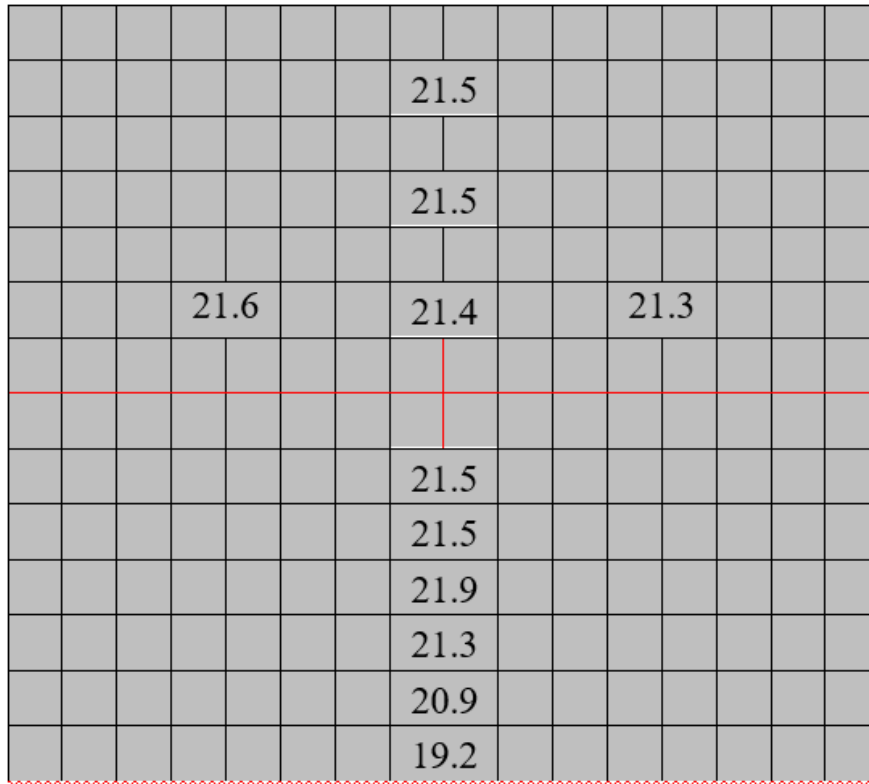
Figure 4-18 EDX composition map of Nb for the Ti-Nb coating on Ti-AVM substrates at position 2/3 in Run 5

To understand the effect of shielding (magnetically) the unused magnetron on the homogeneity of the coating, the EDX map technique was also applied for position 1/3 and 3/3 (for Ti-AVM substrate). The maps can be seen in Figure 4-19 and Figure 4-20 respectively. It was understood from the EDX map (for position 3/3) that the concentration of Nb is again decreasing, but it is happening in a smaller area than the Sample 2/7 in Run 4 (see Figure 4-16). It was concluded that the position of the washer and the height of the head of the screws could also be critical to getting a uniform coating. If the washer sits on the bottom edge of the substrates, the area near the washer showed less Nb concentration, but while the second magnetron was covered, this non-uniform area was tightened. If the washer sits on the upper edge of the substrates (like position 1/3), there is no change seen in the concentration of Nb. The reason why the coating for position 2/3 is uniform is that it is affected by the direction of the washer which was standing not straight. The size of the substrates is also important with the small substrates affected more than the bigger substrates.

82
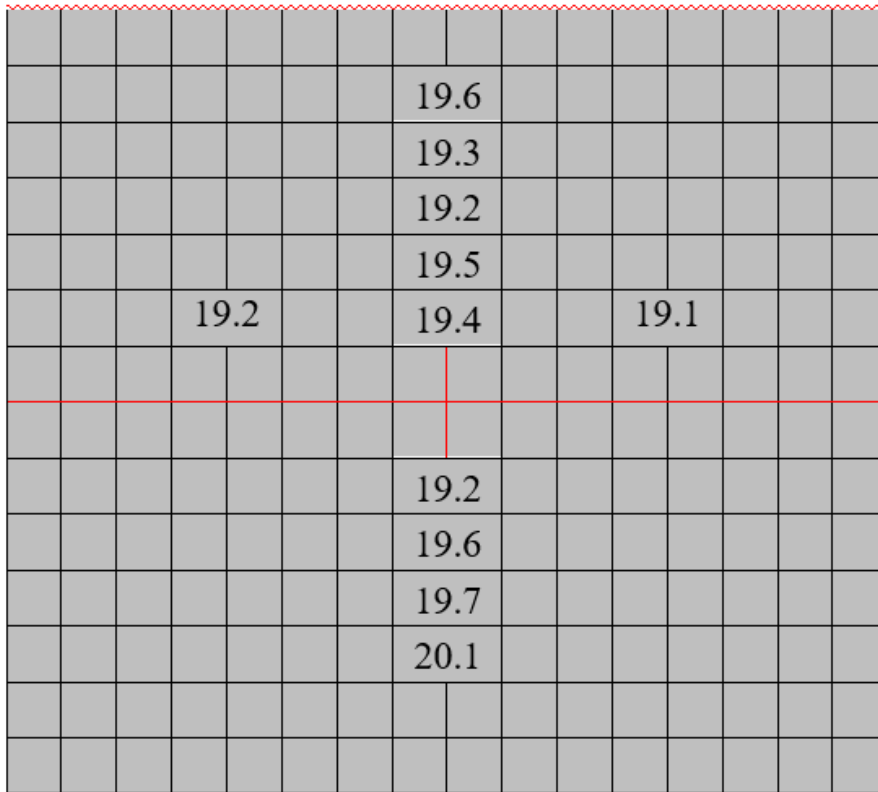
Figure 4-19 EDX composition map of Nb for the Ti-Nb coating on Ti-AVM substrates at position 1/3 in Run 5
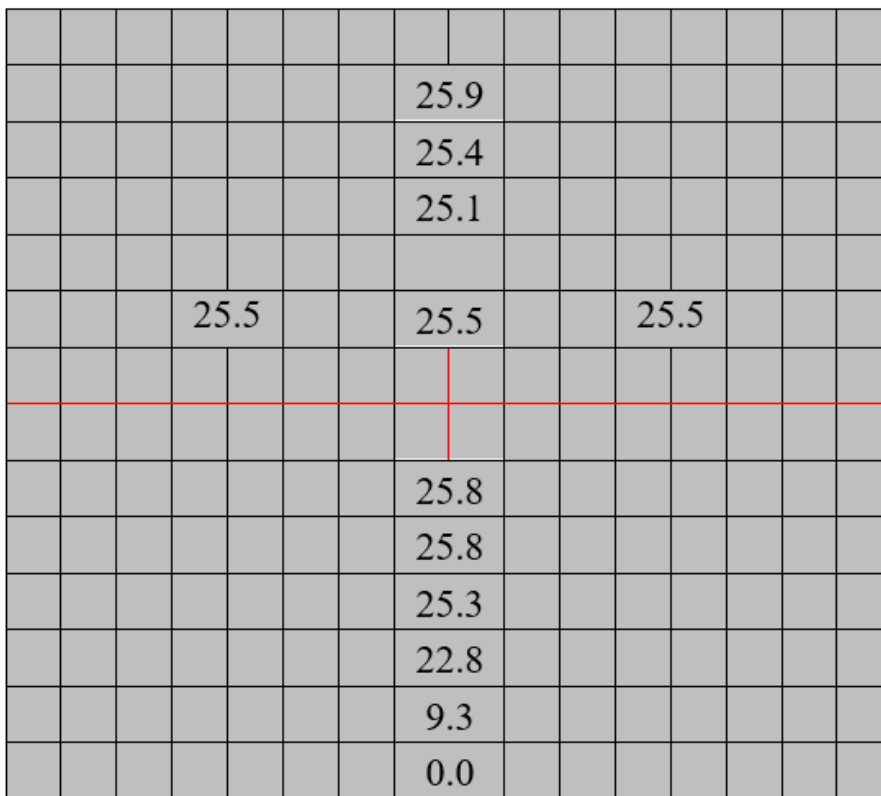
Figure 4-20 EDX composition map of Nb for the Ti-Nb coating on Ti-AVM substrates at position 3/3 in Run 5

These runs were all for coating optimisation to produce high quality/uniform coatings prior to the nitriding process. Therefore, the "clean" coatings were decided to deposit by using at least two washers. The washers would not sit on the surface of the substrates. They would touch the side of the substrate and squeeze it, to prevent falling during deposition (as can be seen in Figure 4-21).

Figure 4-21 The position of the washers and substrates for "clean" coatings

4.2.2.4 Understanding the effect of the working distance on the concentration and thickness of Ti-Nb coatings (Set Nb4)

The Ti-Nb coating optimisation was completed with five different runs in total, but the understanding of concentration limit (minimum and maximum Nb concentration) of this configuration was still missing. One extra run was planned to figure out the concentration limit. In this run, the working distance (between the substrate holder and target) was changed. In previous runs, the working distance was 21 cm which is the maximum adjustable distance for this chamber. The working distance was adjusted to 15 cm which is the minimum working distance for this chamber. The power supplied to the Ti-Nb split target was 1000 W, and the substrate holder was biased to -50 V. This set of coatings was entitled as S-Nb4 which has one run (Run 6). This run included six different sample positions vertically from 1/6 to 6/6 (the arrangement of the substrates is seen in Figure 4-22). In our split target model, when the

substrate which is closer to the Nb part of the target, it should contain more Nb than previous runs. The elemental composition of the Ti-Nb coatings (done by EDX analysis) for Run 6 in the S-Nb4 set can be seen in Table 4-10.
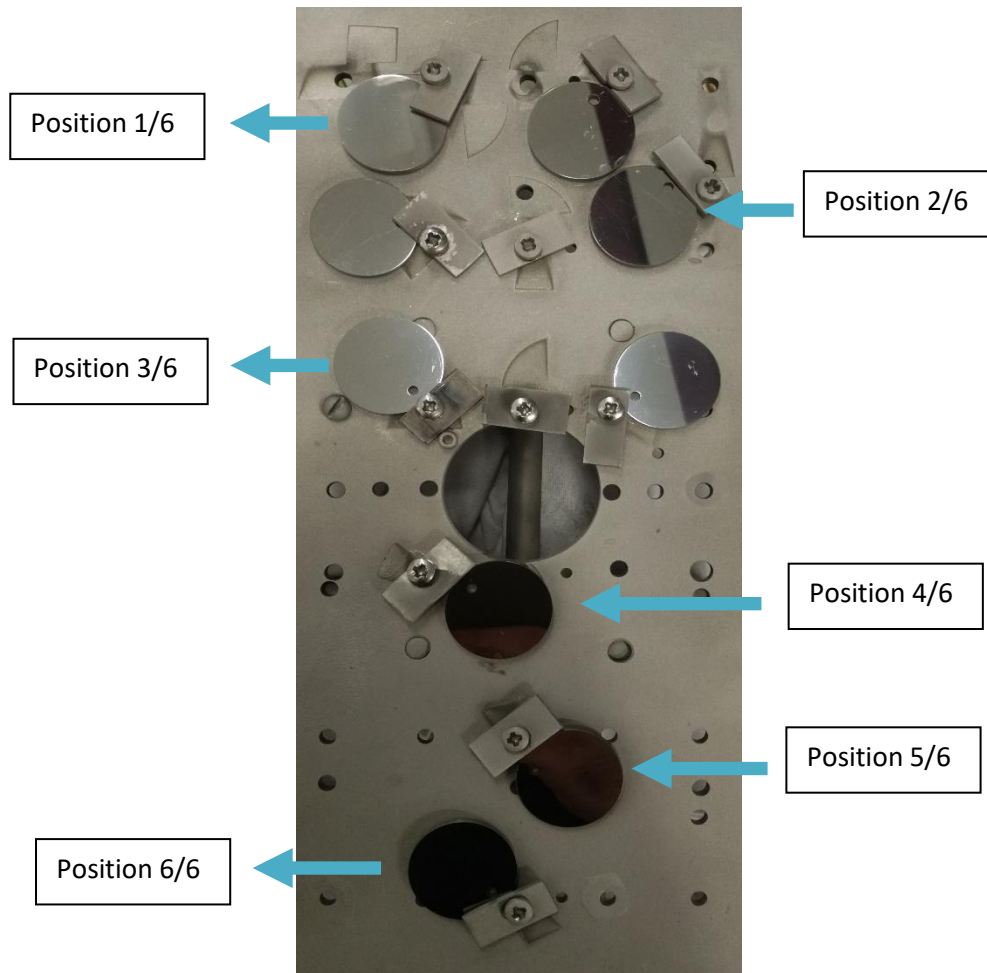
Figure 4-22 The substrate holder (showing the position of the substrates) for Run 6 in S-Nb4

As seen in Table 4-10, the Nb concentrations for position 1, 2 and 3 were too close to each other. The minimum Nb concentration is smaller than the previous runs (compared to position 1/6 in this run and the sample which stands on place 1/7 in run 4) although the substrates were tried to place in the similar alignment (vertical direction). On the other hand, the sample which has the highest Nb concentration (position 6/6) in Run 6 has more Nb than the sample which stands in place 7/7 in run 4. Therefore, it can be said that the minimum and maximum limit could be controlled by adjusting the working distance.

Table 4-10 The elemental composition results of the Ti-Nb coatings for Run 6 in S-Nb4

Set No	Run No	Sample No	Ti (at. %)	Nb (at. %)
S-Nb4	6	1/6	88.7	11.3
		2/6	86.0	14.0
		3/6	81.8	18.2
		4/6	67.2	32.8
		5/6	49.9	50.1
		6/6	39.6	60.4

Sample 4 was sitting in the middle of the substrate holder, so it is not affected so much by the working distance because the amount of Nb in the middle of the substrate holder will remain nearly same (the average position). It can be concluded that the Nb concentration of the substrates was separated into two sides (low and high Nb concentration).

The second thought was how the thickness is changed by decreasing the working distance of the deposition process while keeping the other parameters constant. The literature is suggesting that when the working distance is decreased, the deposition rate could be significantly increased in planar magnetron sputter deposition system [157]. Therefore, this argument was also investigated by measuring the thickness of the coatings. The thickness of the Ti-Nb coating which stands on place 4/6 of run 6 (in which the working distance was 15cm) was compared with the coating which stands at the same coordinates on the substrate holder (but the working distance was 21cm). The Ti-Nb coating deposited with 15 cm working distance was found to be 1.30 times thicker than the other. It can, therefore, be said that the deposition rate increased by about 30 % when decreasing the working distance from 21cm to 15 cm (these two distance

values are the minimum and maximum distances for the substrate holder configuration used in this study).

4.2.2.5   Deposition of the "clean" coatings before nitriding process (Set Nb5)

Following the optimisation study, it was decided to deposit a set of "clean" Ti-Nb coatings. This set of coatings was entitled to S-Nb5 which has only one run (Run 7). The target position in run 2 in S-Nb1 was used for this set to produce Ti-Nb surface layer coatings. The Ti-Nb alloy coatings (by planning 2Ti/1Nb atomic ratio) were deposited on Ti alloy substrates before applying triode plasma nitriding process. The arrangement of the substrates can be seen in Figure 4-23. The working distance between the substrate holder and the target was 21cm. The power supplied to the Ti-Nb target was 1000 W, and the substrate holder was biased to -50 V. The elemental composition of the Ti-Nb coatings (done by EDX analysis) for Run 7 in the S-Nb5 set can be seen in Table 4-11.
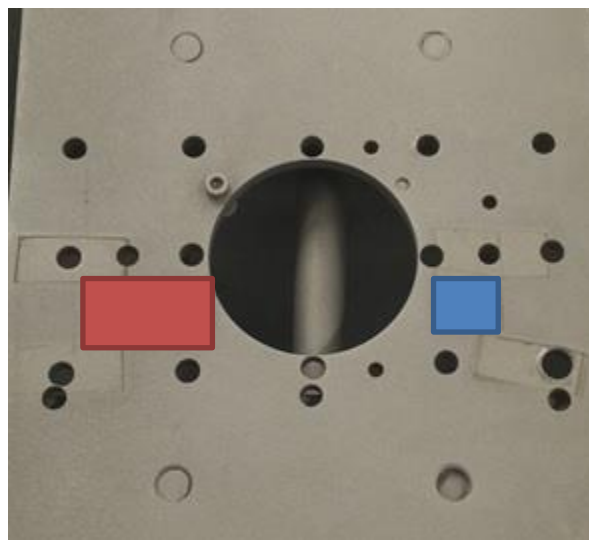
Figure 4-23 The substrate holder (showing the position of the substrates) for Run 7 in S-Nb5

The exact position of the substrate (red indicated Ti-64 and blue indicates Ti-AVM substrates in Figure 4-23) resulted in approximately 33 at. % Nb. The XRD diffraction pattern for "clean" Ti-Nb coatings in Run 7 for Ti-64 and Ti-AVM substrates is shown in Figure 4-24. It can be

seen from the XRD patterns that both coatings have a cubic structure. A fracture cross-section

SEM image of the Ti-Nb alloy coating (32.9 at. % Nb) is shown in Figure 4-25. It is seen that

the coating has a columnar and dense structure.

Table 4-11 The elemental composition results of the Ti-Nb coatings for Run 7 in S-Nb5

Set No	Run No	Substrate	Ti (at. %)	Nb (at. %)
S-Nb5	7	Ti-64	67.1	32.9
		Ti-AVM	67.2	32.8
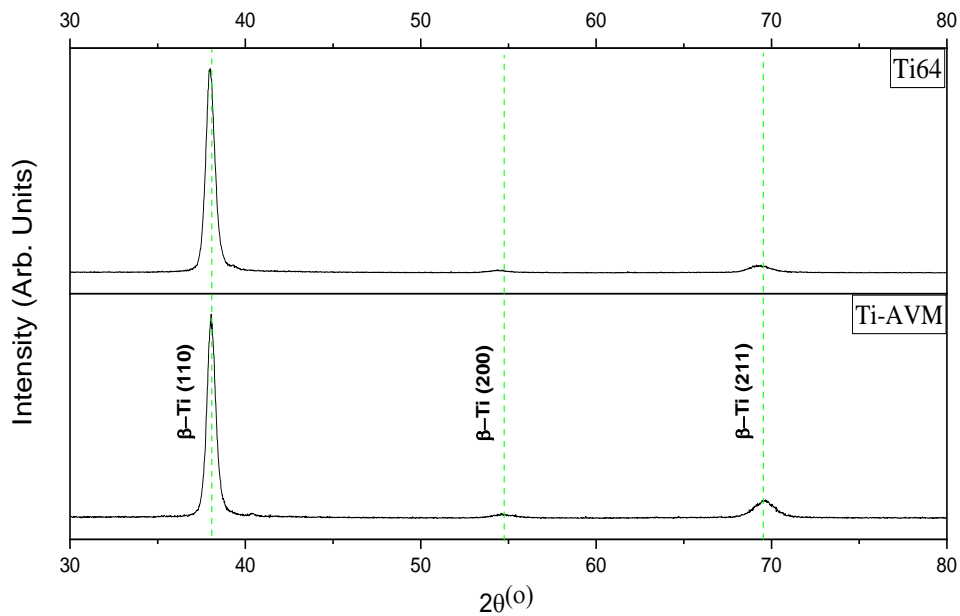
Figure 4-24 GAXRD (2º angle of incidence) diffraction patterns for "clean" Ti-Nb surface layer coatings on Ti-64 and Ti-AVM substrates for Run 7 in S-Nb5
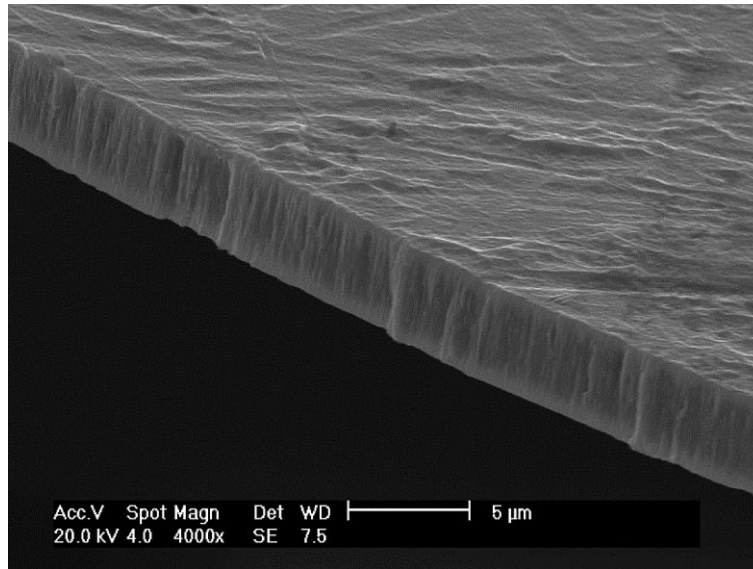
Figure 4-25 SEM fracture cross-section of "clean" Ti-Nb coating

4.2.3 Optimisation of the thickness of the Ti and Ti-Nb surface layer coatings

Ti and Ti-Nb coatings were deposited with 21 cm working distance between the substrate holder and the target. The power supplied to the Ti, or Ti-Nb target was 1000 W, and the substrate holder was biased to -50 V. The thickness of the coatings for these parameters can be seen in Table 4-12. The thickness measurement of the coatings was done in SEM after sectioning, mounting, grinding and polishing of the coated samples. The cross-section SEM images for Ti, and Ti-Nb alloy (32.9 at. % Nb) coatings are shown in Figure 4-26. It is seen in Table 4-12 that the thickness of the coatings is increasing linearly with time.

Table 4-12 The thickness of the Ti and Ti-Nb coatings for 1,2 and 4h deposition time

Type of Coating	Duration	Thickness (µm)
Ti	1 h	1.15 ± 0.03 µm
Ti	2 h	2.29 ± 0.05 µm
Ti	4 h	4.55 ± 0.11 µm
Ti-Nb	1 h	1.23 ± 0.02 µm
Ti-Nb	2 h	2.45 ± 0.05 µm
Ti-Nb	4 h	4.95 ± 0.10 µm

89

Although the deposition time is similar, the thicknesses of Ti and Ti-Nb coatings are different. The reason for this is the different sputter yields of the Ti and Nb elements in magnetron sputtering system. The ratio of sputter yield value for Nb to Ti metal is approximately 115/100 (estimated from [158], [159]). In this study, the target configuration for the Ti-Nb coating is 2Ti/1Nb. From this point of view, the sputter yield ratio of Ti-Nb coating system to Ti coating system should be 105/100. If the thickness of the Ti coating for 1 h deposition is 1.15 μm, the thickness of Ti-Nb coating should be 1.21 μm for this study. The measured thickness of Ti-Nb coatings (1.23 μm) was found to be approximately 1.65 % bigger than the calculated thickness value (1.21 μm).
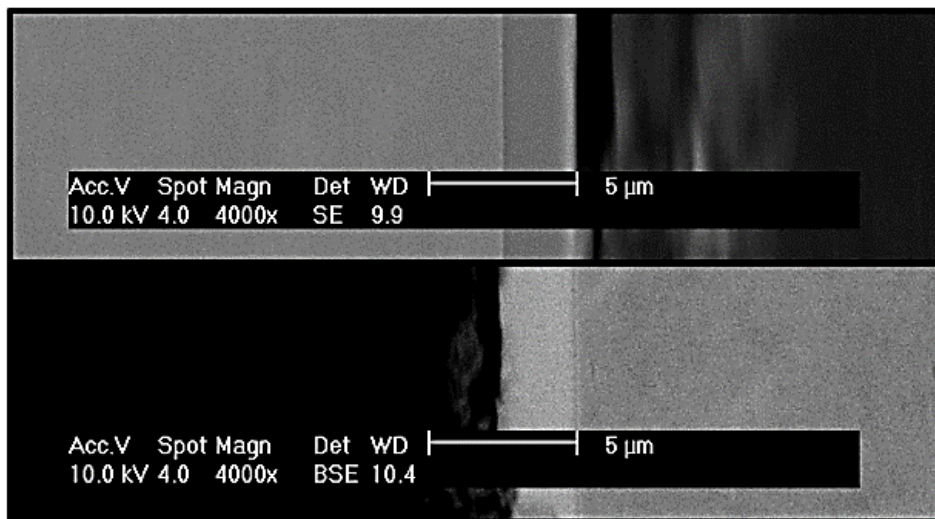
Figure 4-26 SEM cross-section images for Ti and Ti-Nb coatings for 2h deposition time (upper image shows Ti coating, lower image shows Ti-Nb coating)

4.2.4 Ti-Nb-N coatings

PVD Ti-Nb-N coatings were deposited on M2 steel and Ti-64 substrates (in the same run), to analyse the structure of the hard-ceramic coatings and to compare with plasma nitrided Ti-Nb coated Ti alloy substrates. The plasma nitriding process is a diffusion process which was applied on (previously Ti-Nb coated) Ti alloy substrates, and the amount of nitrogen decreases from the surface to the bulk. On the other hand, the PVD Ti-Nb-N ceramic coatings were produced by adding nitrogen gas to the Ti-Nb coating environment, and the nitrogen concentration inside the coating was kept same from the surface to bulk. All the process parameters, as well as the substrate positions on the substrate holder (see Figure 4-9), were kept similar with the Run 3 in Set Nb2. The only difference was adding nitrogen which was introduced into the system with a flow rate of 10 sccm.

At first sight, the surface colouration for Ti-Nb-N coatings showed that the golden appearance is lowering (changing from yellow to greyish) from P1 to P3 (see Figure 4-27). The change of the golden colour tone suggested us that the composition of the coatings are changing (TiN coatings show yellow colour [160], [161]) from P1 to P3. The difference between the P1 and P3 is related to the different amount of Nb inside the coatings. The elemental composition of the Ti-Nb-N coatings (obtained by EDX analysis) can be seen in Table 4-13. Because of the substrate positions (from P1 to P3), the amount of Nb inside the Ti-Nb-N coatings increased from top to bottom on the substrate holder. The similar trend was seen (Table 4-7) for Ti-Nb metallic coatings in the Run 3 in S-Nb2. The nitrogen concentration was observed similar (around 50 at. %) for all the coatings.
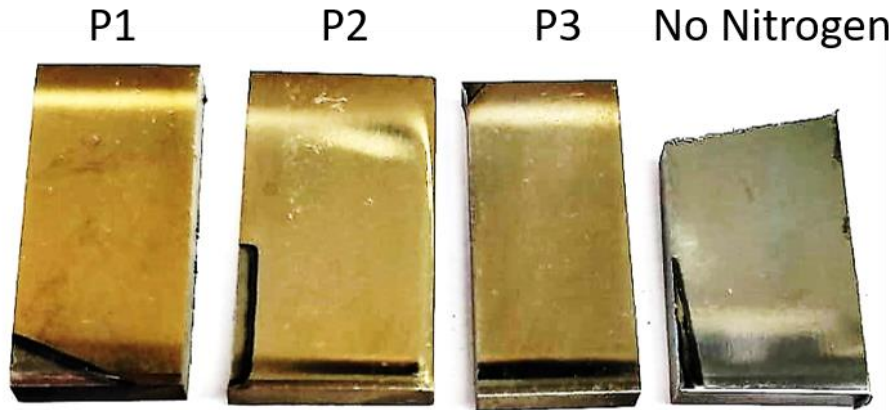
Figure 4-27 Ti-Nb-N and Ti-Nb coatings deposited on Ti-64 substrate showing different surface colouration

Table 4-13 The elemental composition results of the Ti-Nb-N coatings

Sample No	Ti (at. %)	Nb (at. %)	N (at. %)
N-Ti-64-P1	37.4	9.4	53.2
N-Ti-64-P2	32.2	15.4	52.4
N-Ti-64-P3	26.6	24.7	48.7
N-M2-P1	38.1	8.9	53
N-M2-P2	32.5	15.1	52.4
N-M2-P3	26.1	24.2	49.7

The Ti-Nb-N coatings deposited on M2 steel substrates were also showed the same characteristics as the coatings deposited on Ti-64 substrates. Therefore, it will only be given the results of coatings deposited on Ti-64 substrates (after this point) to not fall into repetition. The metallic Ti-Nb coatings had shown some substrate dependence on phase structure, on the other hand, the ceramic Ti-Nb-N coatings (with nearly 50 % at N) did not show any substrate dependence (at least for this run). It may be related to the allotropic modification effect of the "metallic" Ti coatings. The XRD diffraction patterns for Ti-Nb-N coatings (for the three positions) on Ti-64 substrate can be seen in Figure 4-28. At first sight, the XRD patterns suggest us that the coatings included only one phase (there is no substrate contribution) and this phase looks like a cubic (NaCl prototype) ceramic phase. The peak positions (from P1 to P3) were

observed to shift to lower angles. The reason for this the different amount of Nb concentrations inside the Ti-Nb-N coatings. It can be also seen in the Figure 4-28 that the pink peak which belongs to the TiN phase (ICDD file #01-087-0627), the blue peak which belongs to NbN phase (ICDD file #03-065-5063) and the orange peak which belongs to $NbTiN_2$ phase (ICDD file #01-077-2990) explain how peaks shift to lower angles. Beside (111) peaks, the same shifting trend was also seen for the other peaks as well. As a summary of EDX and XRD results, the Ti-Nb-N coatings (for three different positions) have a similar phase (with different concentrations).
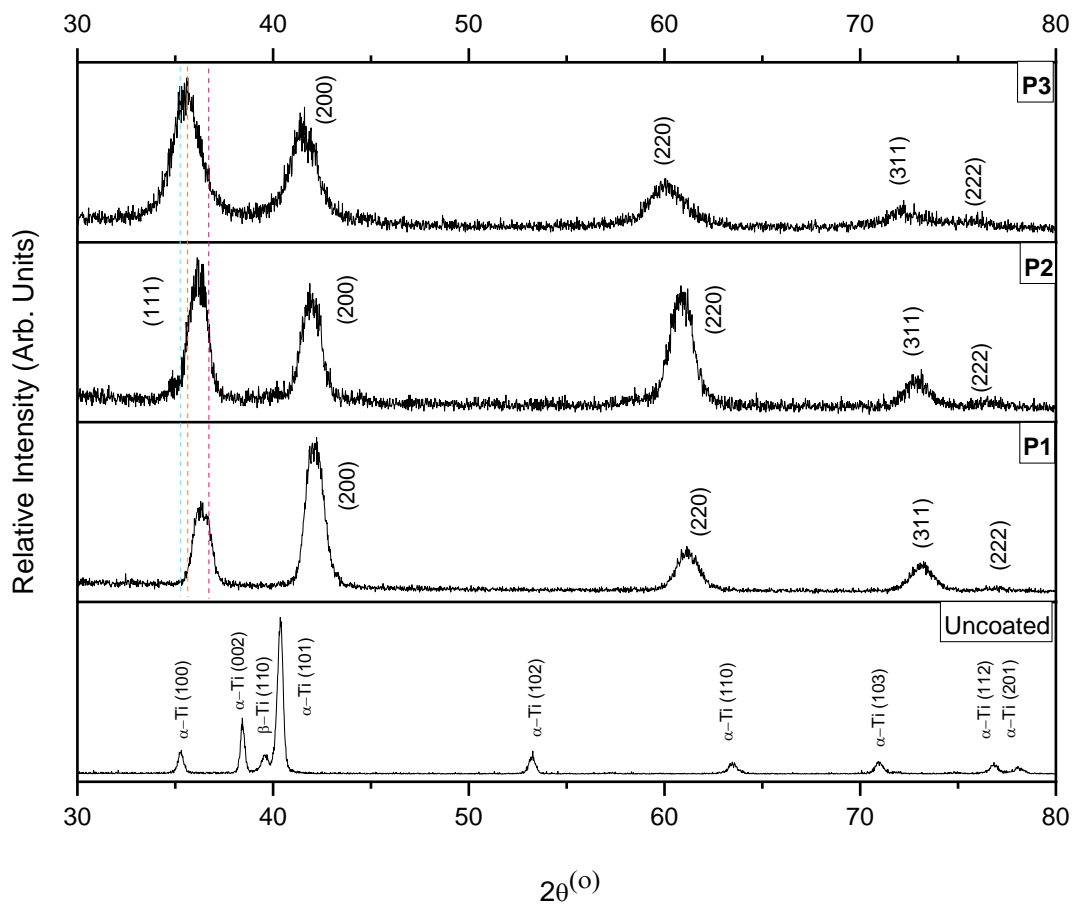
Figure 4-28 GAXRD (2º angle of incidence) diffraction patterns for Ti-Nb-N coatings on Ti-64 substrates

Table 4-14 Nanoindentation hardness and elastic modulus results for Ti-Nb-N coatings

Sample No	Hardness (GPa)	Elastic Modulus (GPa)
P1	23.1	243.9
P2	22.6	220.2
P3	21.9	201.2

The different amount of Nb inside the Ti-Nb-N coatings led to being having different hardness and elastic modulus values. It can be seen in Table 4-14 that the hardness and elastic modulus values for Ti-Nb-N coatings are decreasing by increasing Nb concentration. In the literature, the hardness and elastic modulus values for TiN coatings were reported higher than the results found for Ti-Nb-N coatings (in this study) [162]–[164]. It should be noted that these values can vary with the process parameters such as negative bias voltage, nitrogen partial pressure etc. The H and E values which found in this study allow to keep the hardness to elastic modulus ratio for the Ti-Nb-N coatings higher (which were found to be 0.095, 0.102 and 0.109 from P1 to P3, respectively). Having H/E values (≥ 0.1) could provide outstanding properties under various tribological tests and can be used as relatively tough and protective ceramic coatings [165].

4.2.5 Ti-Staballoy® coatings

Ti-Staballoy PVD coatings which were produced (similar to Ti-Nb surface coatings) by replacing the one piece of Nb target with one piece of staballoy target. Staballoy target includes mainly Fe, Mn, Cr and Ni metals which can be classified as a beta stabiliser for Ti alloys. The aim for producing this coating was to compare with Ti-Nb coating (related to the nitrogen diffusion efficiency) by depositing as a surface coating on Ti alloy substrates. The substrates positions and the target configurations can be seen in Figure 4-29. The substrate which was placed the top was named as Ti_Stab_1, and the bottom one was named as Ti_Stab_4. All coatings have different concentrations considering their positions from the staballoy target. The EDX results for the Ti-Staballoy surface layer coatings can be seen in Table 4-15.
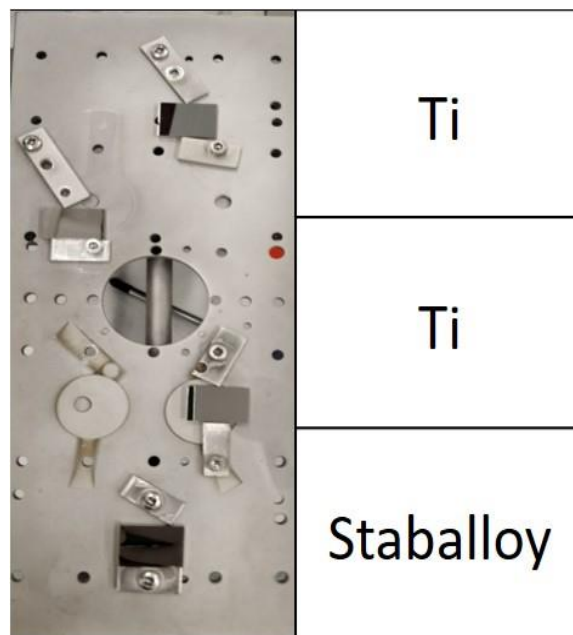
Figure 4-29 The substrate and target positions for the PVD Ti-Staballoy surface layer coatings

The additional elements were found to increase from top to the bottom. The previous Ti alloy coatings were produced with pure metallic targets so the effect of the additional element can easily be recognised. On the other hand, the staballoy provided 4 different additional elements to the Ti-Staballoy surface coatings. The XRD diffraction patterns for Ti-Staballoy coatings (for all four positions) are seen in Figure 4-30.

Table 4-15 The elemental composition results of the Ti-Stab alloy surface layer coatings

Samples	Concentrations (at %)				
	Ti	Fe	Mn	Cr	Ni
Ti_Stab_1	70.2	18.8	5.4	5.4	0.2
Ti_Stab_2	62.4	23.5	7.0	6.7	0.4
Ti_Stab_3	43.4	34.4	11.8	10.0	0.4
Ti_Stab_4	33.4	41.0	13.3	11.8	0.5
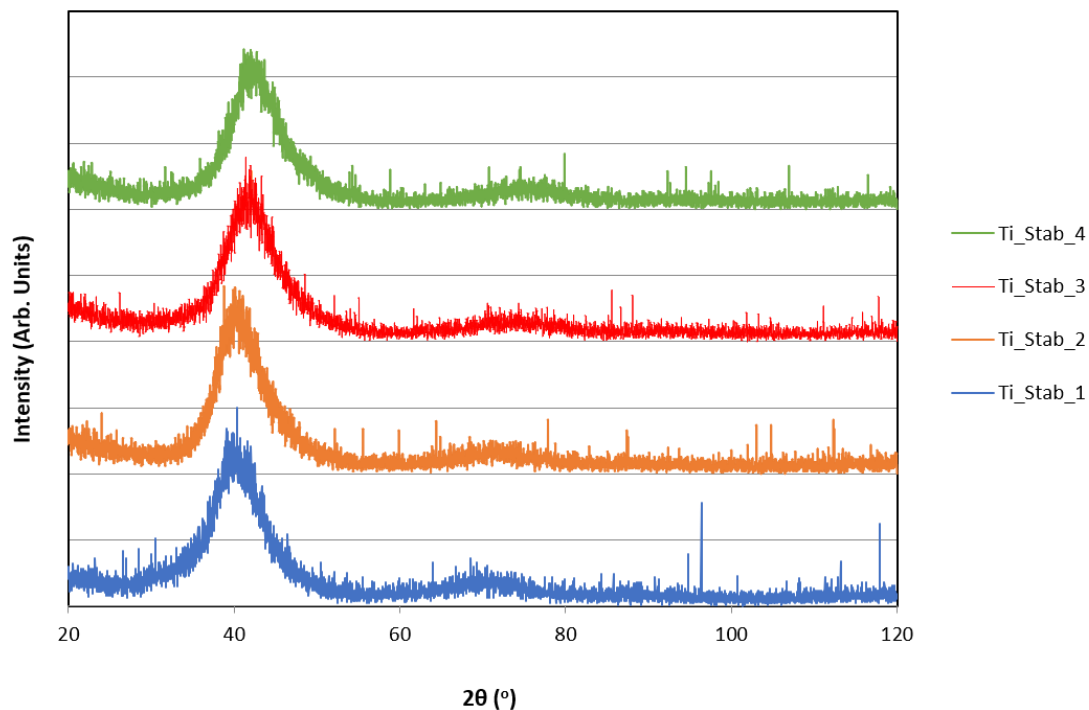
Figure 4-30 GAXRD (2º angle of incidence) diffraction patterns of the Ti-Staballoy coatings

The trend of the XRD patterns was found similar for all positions. The only one big and broadened peak was shifted to higher angles by increasing the concentration of additional elements from position 1 to 4. The phase structure was predicted (by applying a simulation work) as nanocrystalline particles were embedded inside an amorphous matrix. XRD pattern simulation was performed using the ICDD database and 'SIeve+' tool of the 'PDF-4+' fitting software [166].

The simulated XRD patterns for β-Ti (for 0.5, 0.75 and 1 nm crystallite sizes) can be seen in Figure 4-31. The XRD patterns of four Ti_Staballoy coatings showed only two peaks which one of them is placing around 40° and the other one is placing 70°. It can be seen from the simulated β-Ti XRD profiles that the peak (placing around 55°) is almost disappearing when the crystallite size is decreasing from 0.75nm to 0.5nm. This trend of the XRD profiles suggested that the crystallite size of the Ti_Staballoy coatings is less than 0.75nm.
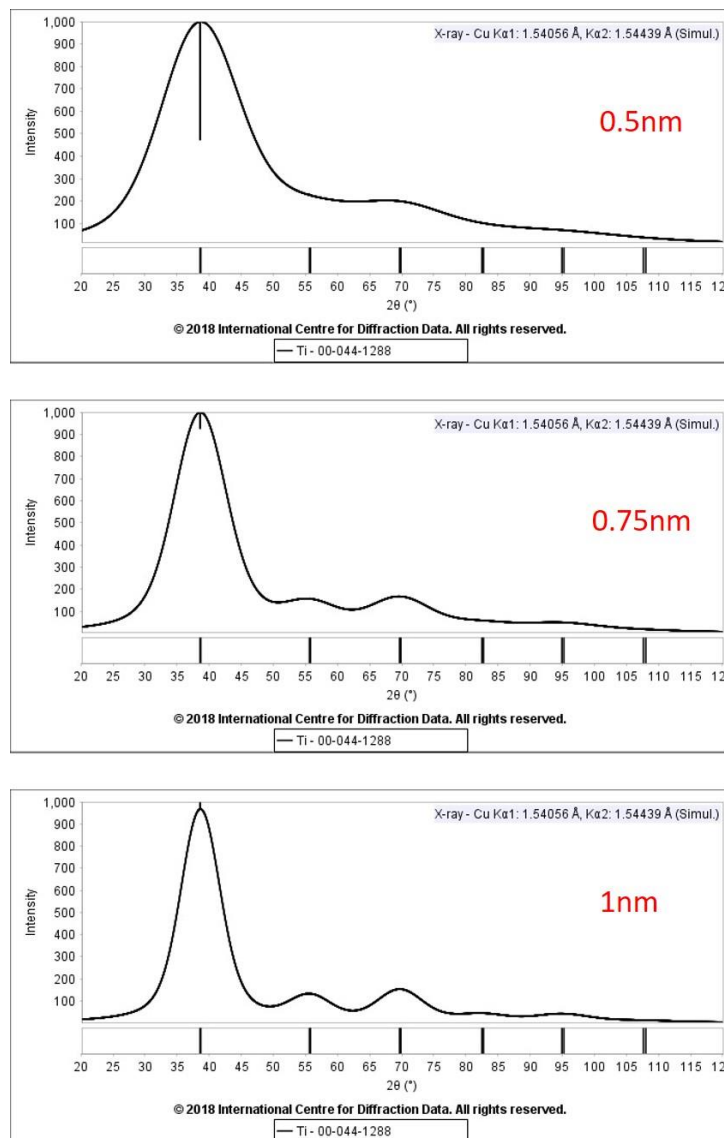
Figure 4-31 Simulated XRD profiles for β-Ti for 0.5, 0.75 and 1 nm crystallite sizes

The XRD patterns of the Ti_Staballoy coatings was also compared with the simulated XRD patterns of $Ti_{0.8}Fe_{0.2}$ phase (see Figure 4-32) to see the effect of the additional elements on the simulated XRD profiles. The trend (while decreasing the crystallite size) was found similar with the simulated XRD profiles of the β-Ti. The peaks of the simulated XRD patterns of $Ti_{0.8}Fe_{0.2}$ phase are placing at higher degrees compared to β-Ti peaks which is related to the addition of Fe. Moreover, the peaks of $Ti_{0.8}Fe_{0.2}$ phase have higher intensity values than the peaks of the β-Ti phase. The simulated XRD profile of $Ti_{0.8}Fe_{0.2}$ phase (for 0.5nm crystallite size) fits well with the XRD pattern of the Ti_Stab_1 coating (blue profile in Figure 4-30).
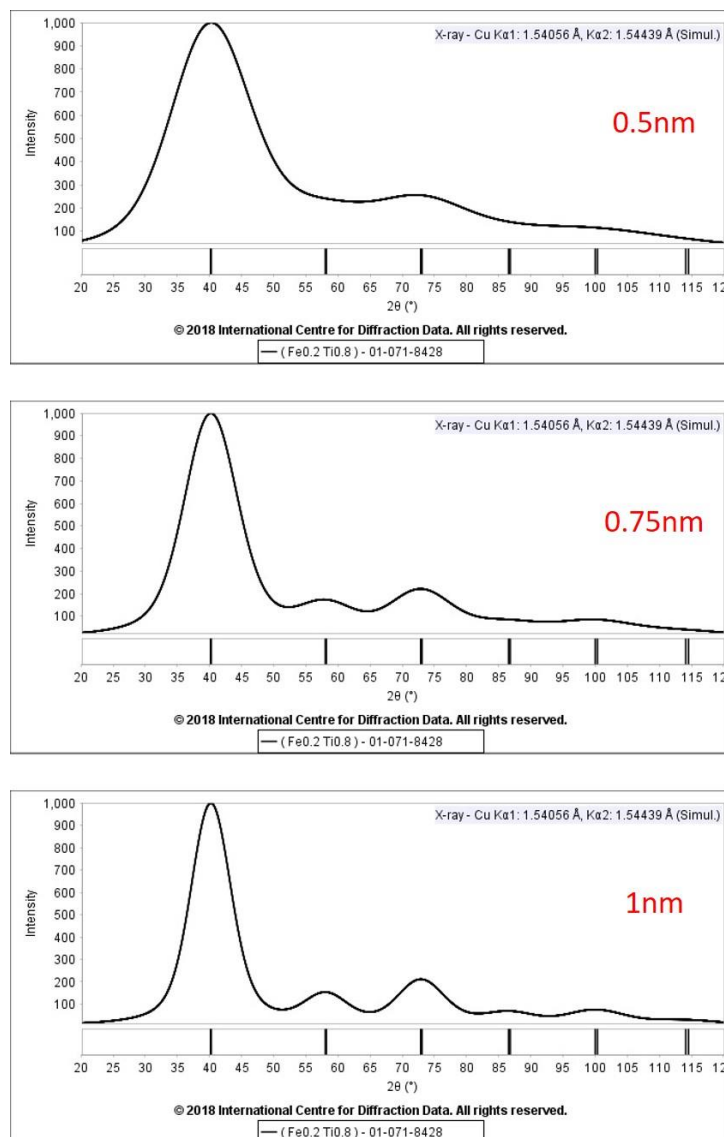
Figure 4-32 Simulated XRD profiles for $Ti_{0.8}Fe_{0.2}$ for 0.5, 0.75 and 1 nm crystallite sizes

The increase of the additional elements also affected the mechanical properties of the coatings. The nanoindentation hardness and elastic modulus of the coatings can be seen in Table 4-16. The hardness and elastic modulus values were approximately doubled by increasing the amount of additional elements position 1 to 4.

Table 4-16 Surface nanoindentation hardness data for Ti-Staballoy coatings

Samples	Hardness (GPa)	Elastic Modulus (GPa)
Ti_Stab_1	6.6	94.6
Ti_Stab_2	7.7	129.3
Ti_Stab_3	11.2	143.7
Ti_Stab_4	12.3	167.1

As being amorphous-like coating and having relatively better mechanical properties, the nitrogen diffusion efficiency of the Ti alloy substrate (after depositing Ti-Staballoy coatings on them) is a curious subject. Moreover, the increased final surface hardness with an increased load-bearing capacity of the substrate (after plasma nitriding process) could be an important candidate for the wear resistant applications.

4.3 Summary

The pure Ti and Ti-Nb (alloy) surface layer coatings were deposited on M2 steel (optimisation purpose), Ti-64 and Ti-AVM substrates before triode plasma nitriding with the aim to improve the nitrogen diffusion efficiency. For comparison purposes, PVD Ti-Nb-N and Ti-Staballoy coatings were also produced. The following key points can be drawn:

- The β-Ti (Ti-Nb) surface layers required compositional optimisation work before producing the desired coatings for triode plasma nitriding. The first set of Ti-Nb coatings (S-Nb1), which were deposited on M2 steel substrates, included ten different coatings with Nb concentrations of 18.1 to 88.3 at. %.

- The effect of substrate type on the phase structure (β stability) of Ti-Nb coatings was analysed by depositing the coatings on different substrates such as M2 steel, Ti-64 and Ti-AVM in Set Nb2. It was determined that the β phase stability of the Ti-Nb coatings for lower Nb concentrations (about 16 at. %) could be affected by the type of substrate.

- Besides the stability of the β phase, the intensity and position of the XRD peaks can be attributed not only to the Nb concentrations in the coating but also to the type of substrate.

- The formation of the martensitic Ti phase (α″) was also observed depending on the Nb concentration in Ti-Nb coatings. This undesired phase started to form about 20 at. % Nb and disappear for the Ti-Nb coatings which contain Nb more than 26 at. %.

- The concentration uniformity of the Ti-Nb coatings on the whole substrate surface is also an important key point for this study. If any concentration inhomogeneity is seen on the surface which can cause the formation of a different crystal structured grains (locally), it could affect the nitrogen diffusion efficiency (results) after plasma nitriding process). To inhibit this, the size of the substrates was chosen relatively small. However, there is some mismatch seen for the Nb concentration on the surface of some

Ti-Nb coatings, and the Set Nb3 was prepared to solve this problem. It was found that to cover the second (unbiased) magnetron with a thick metallic shield (to reduce the effect of extra magnetic field) and to place the washers and screw properly (to not cover the substrate surface unnecessarily) will improve the Nb concentration homogeneity of the Ti-Nb coatings.

- The minimum and maximum Nb concentration limit were figured out by changing the working distance from 21 cm to 15 cm in the Set Nb4 by keeping the other parameters like other runs. The minimum Nb concentration limit was decreased from approximately 18 at. % to 11 at. % and the maximum Nb concentration limit was increased from approximately 54 at. % to 60 at. %.

- The changing working distance values did not give the only benefit for expanding the Nb concentration range but also is provided to deposit thicker coatings while keeping other parameters constant (such as time and bias voltage). The Ti-Nb coating which deposited with a 15 cm working distance found %30 thicker than the coating which deposited with a 21 cm working distance while keeping the coordinates of both coatings same on the substrate holder.

- After getting the useful information from optimisation sets, to produce "clean" coatings, a new set was established (S-Nb5). It was decided to produce the coatings with a 2Ti/1Nb atomic ratio before plasma nitriding process. The exact position of the substrates on the substrate holder was predicted, and the coatings were deposited successfully (with 33 at. % Nb). It was found that the coating has a columnar and dense structure with almost fully β structure.

- The Ti and Ti-Nb coatings had different coating thickness while they were produced with similar process duration. The thickness optimisation runs showed that the Ti coating has a deposition rate of 1.15μm/h and the Ti-Nb coating has a deposition rate

of 1.12 μm/h. The increase of the coating thickness was found to be almost linear with process time. The reason for this difference is related to the different sputter yield of the Ti and Nb metals (of which approximately 115Nb/100Ti). The importance of the thickness optimisation run is to find the proper process duration for PVD Ti and Ti-Nb coatings to produce equal thick coatings before nitriding process.

- The hard (~ 22-23 GPa) Ti-Nb-N ceramic coatings were produced in the same PVD rig system by adding nitrogen gas to the chamber while producing the usual Ti-Nb alloy coatings. The aim of this run to determine the behaviour of nitrogen gas with Ti and Nb metal. It would give a chance to compare with plasma nitrided (previously Ti-Nb coated) Ti alloy substrates.

- As a further approach, Ti-Staballoy coatings were deposited on steel substrates (for initial optimisation work). Fe, Cr and Mn were the main alloying elements which allowed a wide range of mechanical properties for these coatings). Moreover, it is expected that these alloying elements allowed the phase structure of the Ti-Staballoy coatings to be nanocrystalline and therefore the nitrogen diffusion efficiency into this coating can be a curious subject.

5 Triode Plasma Nitriding (TPN) on Uncoated, Ti coated, and Ti-Nb coated Titanium Alloy Substrates

The initial trials for the TPN process were applied at 500°C (TPN500) for 2, 4, 6 and 8 hours on uncoated Ti-64 and uncoated Ti-AVM substrates. Following these trials, a new TPN treatment set was designed to analyse the effect of treatment temperature on TPN performance. In this set, the TPN process was applied at 600°C (TPN600) on uncoated Ti-64 and Ti-AVM substrates. The literature suggested that the performance of triode plasma nitriding on titanium alloys can be increased by increasing temperature (as a diffusion process) and the efficiency of the process is expected to be better at 700°C. Therefore, the triode plasma nitriding process at 700°C (TPN700) for 4 hours was applied to uncoated, Ti coated, and Ti-Nb coated Ti-64 and Ti-AVM substrates. The temperature for the TPN700 process is the highest value that could be achieved (for the TPN equipment used in this study) because of the technical condition of the equipment, so it was not possible to try more than 700°C. A TPN700 treatment was also applied for 8 hours on uncoated, Ti coated, and Ti-Nb coated Ti-64 and Ti-AVM substrates to see the effect of nitriding duration on treatment properties. Apart from the time and temperature, all other parameters were kept constant. The substrate bias voltage was -300 V, the ratio of the Ar and N flow rate (partial pressure) was (%70 N and %30 Ar), and the total working pressure was (0.4 Pa= 4 x10^{-3} mbar). All these parameters were selected with the aim of obtaining deep hardened case (to increase the load-bearing capacity of the substrate) before creating any nitride compound layer on the substrate surface because the nitride compound layer is known to block further nitrogen uptake at the titanium alloy surface [12], [167]. The phase structures were analysed by XRD, and if any nitride layer was found, the cross-sections of the samples were analysed by SEM. The nitrogen diffusion inside the substrates was explored by nanoindentation test (from the cross-section of the treated samples) to analyse changes in hardness from the surface to bulk.

5.1   Experimental Design

Before starting the TPN processing, variables such as the type of substrate, type of surface layer coating which was deposited before TPN, process time and process temperature, were carefully considered to minimise the number of the samples which would need to be characterised. The variables for all the TPN treatments are presented in Table 5-1.

Table 5-1 The variables for TPN processing

Substrates	Coatings	Temperatures	Time
Ti-64	Uncoated	500 (^{o}C)	2 (h)
Ti-AVM	Ti	600 (^{o}C)	4 (h)
	Ti-Nb	700 (^{o}C)	6 (h)
			8 (h)

If all variables are changed one by one, the possible total number of samples should be 72 Although the other parameters (such as substrates substrate bias voltage, nitrogen partial pressure or total gas pressure) are constant for all TPN runs, the sample size (72) is still high. Some of them were eliminated (by considering the initial results) to reduce the number of samples. The TPN treatments performed at 700°C were repeated for the coated samples which have different coating thicknesses. In the repeat runs, uncoated substrates were also placed in the chamber to confirm the reproducibility of the TPN process such that comparisons could be reliably drawn from sample batch to batch.

The process temperature for TPN treatment is one of the most important parameters, which affects the nitrogen diffusion kinetics, substrate bulk mechanical properties and crystal structure (if for example the alpha to beta transformation temperature is exceeded). Therefore, the process temperature should be selected carefully. Various temperatures were used in previous nitriding studies. Muraleedharan et al. [62] applied plasma nitriding at 480ºC, Fouquet et al. [81] applied between 500ºC and 900ºC, Borisyuk et al. [97] applied between 500ºC and 900ºC, Avelar-Batista et al. [71] applied between 600ºC and 800ºC, Fernandes et al. [168] applied at 600ºC and 700ºC, Wilson et al. [169] applied at 650ºC and 700ºC, Galliano et al. [95] applied at 700ºC and 900ºC, Fossati et al. [170] applied at 700ºC and 900ºC. The minimum temperature for nitriding processes was 500ºC for this study.

5.2   Triode Plasma Nitriding at 500ºC (TPN500)

The initial nitriding trials were applied on uncoated Ti-64 and Ti-AVM alloys (i.e. substrate only) at 500ºC. These runs were beneficial for understanding the basis of the nitriding process and equipment. Before starting the TPN process, four Ti-64 and four Ti-AVM alloy substrates were placed in the nitriding chamber, and one of each sample was collected every 2 hours. By this means, 2, 4, 6 and 8 hours nitrided samples were produced in four 2-hour run.

5.2.1   X-ray Phase Analysis

The XRD diffraction patterns for nitrided Ti-64 and Ti-AVM substrates are seen in Figure 5-1 and Figure 5-3 respectively. It can be seen in Figure 5-1 that there is no evidence of any nitride compound layer formed on the substrates, although the nitriding process was applied for 8 hours. It can be indicated from Figure 5-1 that the first β peak (around 40º) in Ti-64 starts to disappear after 2 hours of nitriding and the second β peak (around 58º) disappears after 8-hour nitriding process, indicating that the nitrogen is diffusing inwards in sufficient quantity to cause α-stabilisation of any retained β-phase in the Ti-64 alloy.
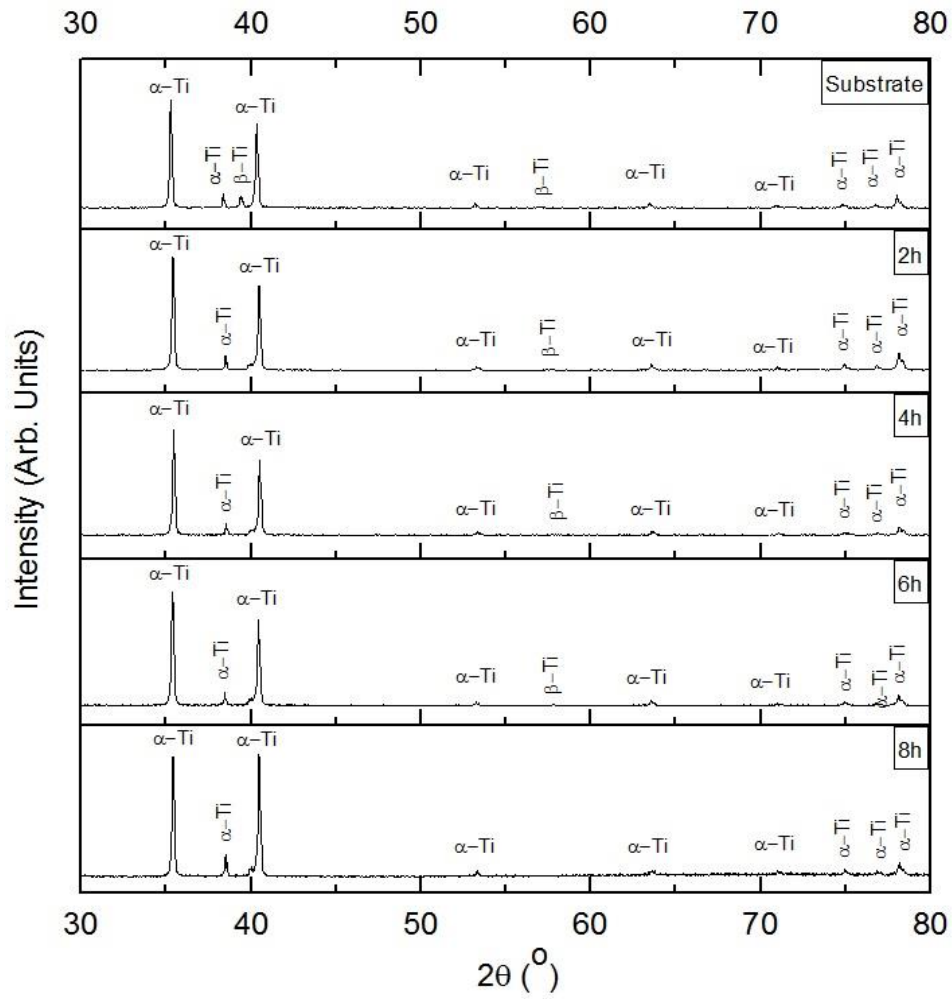
Figure 5-1 Theta-2theta diffraction patterns for untreated and nitrided Ti-64 at 500ºC
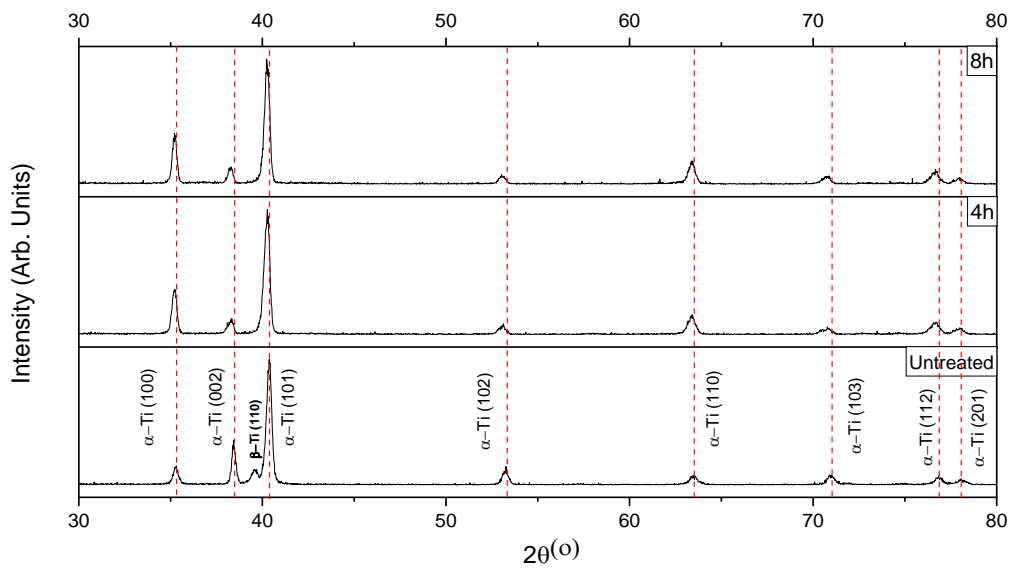
Figure 5-2 GAXRD (2º angle of incidence) diffraction patterns of Ti-64 treated at 500ºC for 4 and 8 hours
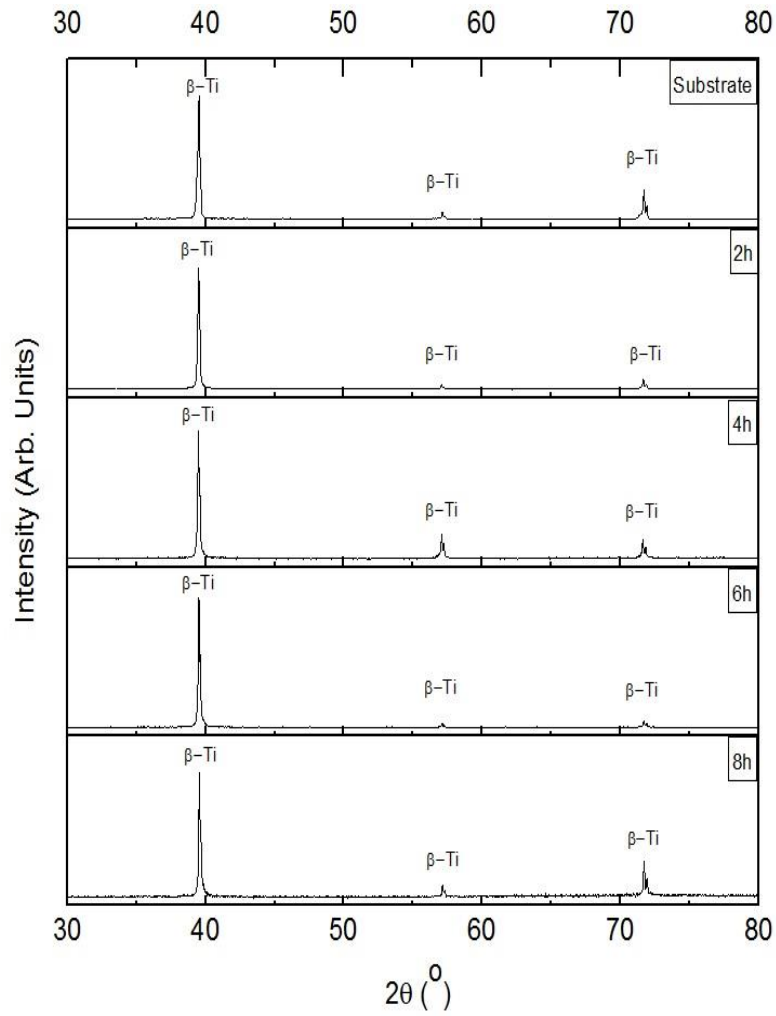
Figure 5-3 Theta-2theta diffraction patterns for untreated and nitrided Ti-AVM at 500ºC
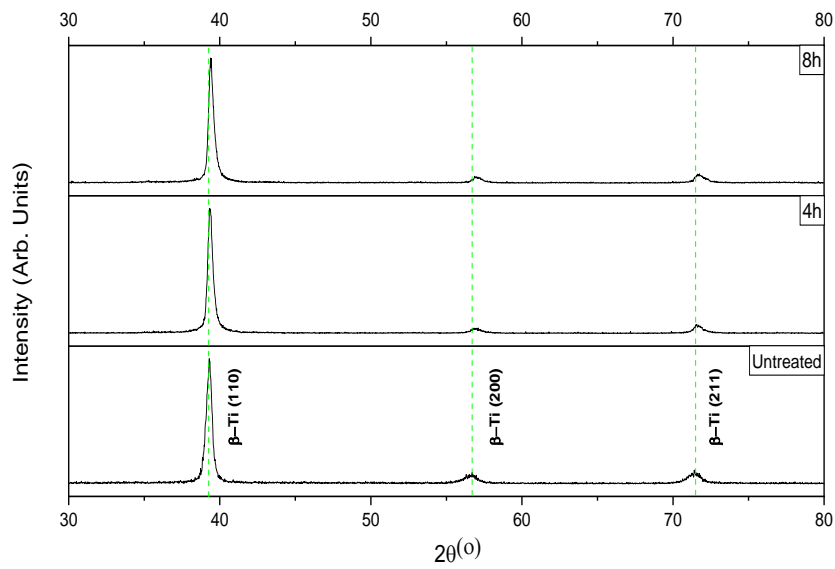
Figure 5-4 GAXRD (2º angle of incidence) diffraction patterns of the Ti-AVM treated at 500ºC for 4 and 8 hours

The α stabilisation effect of the nitrogen was allowed disappearance of the β phase on the surface of the Ti-64 alloy substrate. On the other hand, no change can be seen in Figure 5-3 for Ti-AVM alloy. As a fully β Ti alloy with its high Mo content, the phase structure remained the same after nitriding at 500°C, suggesting that the local concentration of interstitial nitrogen was insufficient to promote α-stabilisation in this alloy. To better analyse the surface of both substrates, a glancing angle XRD test was also performed. The GAXRD patterns for Ti-64 and Ti-AVM alloys which were nitrided 4 and 8 hours (more detailed characterisation was only performed on the samples which were treated for 4 and 8 hours) can be seen in Figure 5-2 and Figure 5-4 respectively. It is also seen from the glancing angle (2 degrees) XRD result that there is again no evidence related to any formation of a titanium nitride compound layer or any α peaks for Ti-AVM substrates. It is known that the glancing angle mode of the XRD scans a less deep region from the surface. GAXRD of Ti-64 also showed that the β peaks disappeared entirely at the near surface region.

The only change after TPN500 process was observed for Ti-64 (α+β alloy) substrates, in which the β peaks disappeared with time, and the α peaks were shifted to the lower angles. It can be understood that nitrogen atoms are dissolved interstitially inside the α-Ti lattice and do not reach a sufficient amount to create a compound layer (or a nanometrically thin compound layer is created which could not be detected by glancing angle XRD). The only observed change for the Ti-AVM alloy substrate was that the major peaks of the β-Ti shifted slightly to higher angles after TPN500 process.

5.2.2 Surface Hardness Measurements

To understand if any change in the surface hardness (to which interstitial solid solution of nitrogen inside titanium alloy can lead [95], [171]–[173]), a series of nanoindentation tests were applied. The surface nanoindentation hardness data for uncoated Ti-64 and Ti-AVM substrate after nitriding at 500°C for 4 and 8 hours can be seen in Table 5-2.

Table 5-2 Surface nanoindentation hardness data for uncoated Ti-64 and Ti-AVM substrate nitrided at 500ºC for 4 and 8 hours

Sample	Temperature (ºC)	Duration (h)	Surface Hardness (GPa)
Untreated Ti-64	-	-	5.0
Uncoated Ti-64	500	4	7.2
Uncoated Ti-64	500	8	7.6
Untreated Ti-AVM	-	-	4.7
Uncoated Ti-AVM	500	4	6.8
Uncoated Ti-AVM	500	8	7.2

It is observed that the surface hardness values for both substrates were significantly increased by the nitriding process and the values also increased with nitriding time. It may be related to the amount of nitrogen (which diffused from the surface) was increased by time. The EDX data (taken from the surface) of both substrates did not show any nitrogen. It can be caused by the low amount of nitrogen which cannot be detected by EDX technique. Cassar et al. [2] showed that the β Ti alloys are difficult to harden by nitriding (even at 700ºC). It is also seen in this study that Ti-AVM alloy has lower hardness value than Ti-64 alloy substrate after TPN500 process. A better comparison will be made in Section 5.4 (for higher temperatures). When the hardness data of nitrided samples (for 4 hours at 500ºC) is compared with the untreated substrate, the hardness increase was seen to be about 45% for both alloy substrates. It can also be seen from the Table 5-2 that when the nitriding time was doubled, the change in hardness is limited. When the hardness data compared to two different nitriding durations (4 hours and 8 hours), it only provided extra 7 % increase of the hardness of both substrates. The reason for this limited effect of increasing nitriding duration on hardness may be related to the low

nitriding temperature (500ºC). Because of the diffusion-controlled nature of the nitriding process, the diffusion is highly efficient by the increasing of the temperature. The increase of the process duration may not affect the surface hardness significantly at lower temperatures. It could be that there is not such a significant hardness increase with time, but the treated layer becomes deeper, so the substrates' contribution to the hardness value could be less.

5.2.3 Surface Topography

The surface roughness was also measured for the nitrided samples at 500ºC and no differences were seen for all substrates. Because of the low temperature of the process, no nitride compound layer formation, the surface structure did not change. By taking advantage of this smooth surface after the nitriding process, the Knoop hardness test was also applied to see the hardness behaviour of the substrate more deeply. The literature also mentioned that, because of the nature of the rough surface, reading the length of the indents is challenging [81], [174]. The results will be given in Section 5.3 as a comparison with the nitriding process at 600ºC.

5.3 Triode Plasma Nitriding at 600ºC (TPN600)

The efficiency of nitrogen diffusion inside any metal (alloy) can be increased by increasing the temperature. Nitrogen diffusion coefficient data for α and β-Ti and alloying elements (beta stabilisers) can be seen in the literature [10], [175]–[183]. All these references include diffusion equations which show the dependence of nitrogen diffusion on temperature. To see the effect of the temperature on nitrogen diffusion inside the Ti-64 and Ti-AVM alloy substrates, a new set of TPN process was prepared. All other parameters kept constant with the TPN500 process, and the temperature was increased to 600ºC. To try to avoid the creation of a nitride compound

layer (which blocks the further nitrogen diffusion inside titanium alloys), the temperature of the process was increased by only 100°C.

5.3.1 X-ray Phase Analysis

The XRD diffraction patterns for Ti-64 and Ti-AVM substrates nitrided for 4 hours can be seen in Figure 5-5 and Figure 5-6. The beta peak of the Ti-64 substrate disappeared (same as in TPN500 experiments) after 4-hour TPN600 process. The alpha stabilisation effect of nitrogen may be the effect for this change. The α peaks were shifted to the lower angles, which may indicate a nitrogen interstitial solid solution in the α-Ti lattice. The theta-two theta type of experiment showed some evidence related to Ti_2N peaks, but the intensities of these peaks were rather low, and they could be recognised from the zoomed version of the X-ray patterns (see Figure 5-5). This evidence showed that (although the experiment was done for 4 hours) there is enough nitrogen concentration on the surface. However, the weak peaks suggested that this phase is a nanometrically thin surface layer or that fine Ti_2N precipitates are formed randomly in the substrate near surface. The alpha stabilisation effect of nitrogen can be perceived clearly for Ti-AVM alloy substrate. It is seen in Figure 5-6 that the intensity of the major β-Ti (110) peak is much bigger than the other peaks and thus, a zoomed version of the XRD diffraction patterns of Ti-AVM alloy substrate is inserted into the same figure, to see the phase changes more clearly (see Figure 5-6). 4 or 5 new peaks were formed after TPN600 process which these peaks belong to the α phase of Ti metal. On top of that, the major peaks of the β-Ti shifted to higher angles after the nitriding process. The nitrogen which is diffused from the surface caused

alpha stabilisation and peak shifting. There is no evidence of nitride compound layer formation on the Ti-AVM alloy substrate after 4-hour TPN600 process.
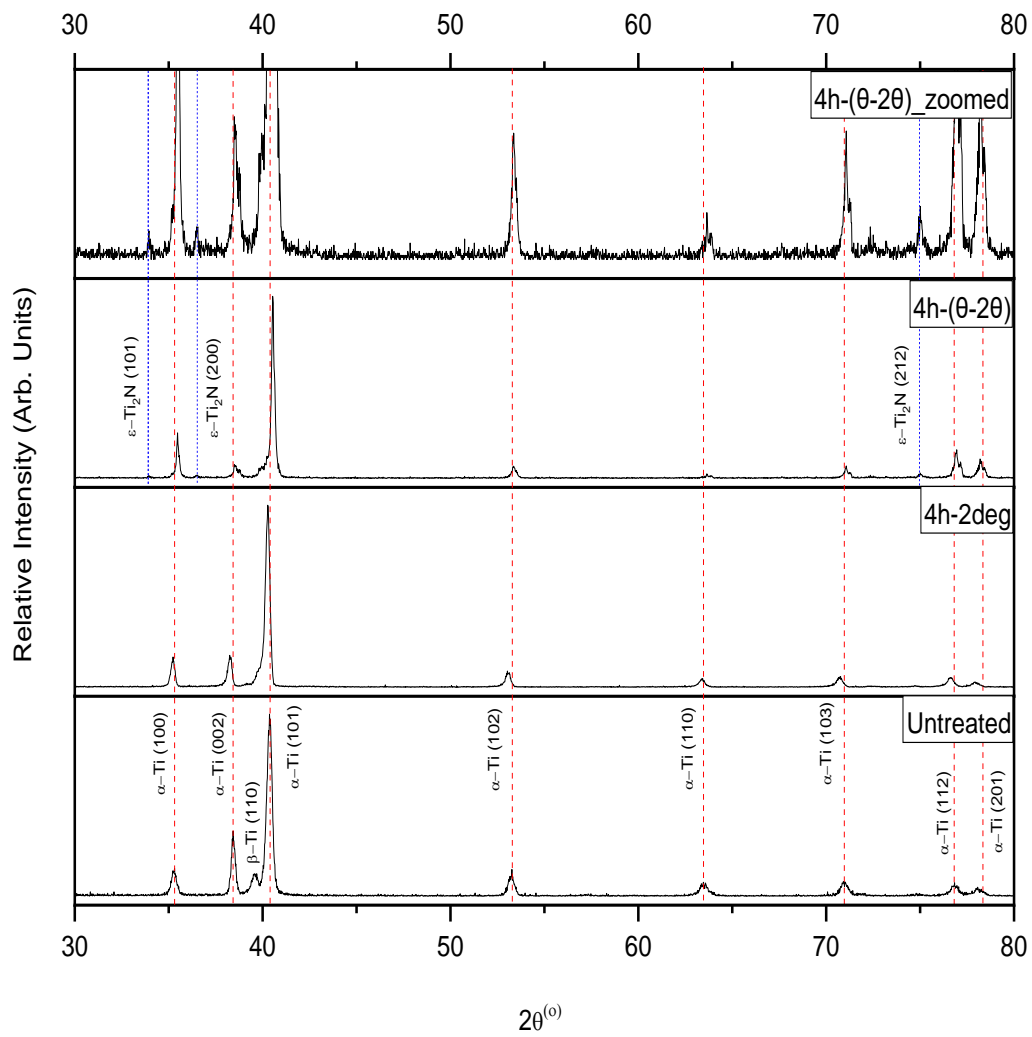
Figure 5-5 GAXRD (2º angle of incidence) and Theta-2theta diffraction patterns of the uncoated Ti-64 substrate treated at 600ºC for 4 hours (also includes θ-2θ peaks as zoomed)

Figure 5-6 GAXRD (2° angle of incidence) diffraction patterns of the uncoated Ti-AVM substrate treated at 600°C for 4 hours (also includes 4h peaks as zoomed)

5.3.2 Surface Hardness Measurements

The surface nanoindentation hardness data for uncoated Ti-64 and Ti-AVM substrates after nitriding at 600°C for 4 hours is shown in Table 5-3. It can be easily seen from the nanoindentation hardness data that increasing the treatment temperature from 500°C to 600°C affected the hardness values positively. When the hardness data (for 4-hour nitriding time) compared to two different temperatures (500°C and 600°C), the increase was seen about 25 % for Ti-64 and 20 % for Ti-AVM alloy substrate. The hardening effect is maintained only by interstitial incorporation of nitrogen (as there is no evidence of titanium nitride at the substrate surface) in the Ti lattice [71], [168], [173].

Table 5-3 Surface nanoindentation hardness data for uncoated Ti-64 and Ti-AVM substrates nitrided at 600°C for 4 hours

Sample	Temperature (°C)	Duration (h)	Surface Hardness (GPa)
Untreated Ti-64	-	-	5.0
Uncoated Ti-64	600	4	8.7
Untreated Ti-AVM	-	-	4.7
Uncoated Ti-AVM	600	4	8.4

Knoop hardness tests were also applied to investigate the hardening response of the substrates more deeply. The depth which can be read for the nanoindentation test is about one to two hundred microns. The minimum Knoop test load is 10gf (HK 0.01) which the magnitude of the force is almost 100 times larger than the force which the nanoindenter applied. However, the indenter geometry and reading methods are entirely different, the penetration depth of the Knoop hardness test would not be expected to be 100 times bigger than the nanoindentation depth. In general, the depth of the indentation for Knoop test is about 1/30 of the major diagonal length, and the depth of the indentation of the Vickers test is about 1/7 of the diagonal length [184]. From this argument, the sensitivity of the Knoop test (compared to the Vickers test) can easily be seen. The depth of the indentation for HK $_{0.01}$ is expected less than 0.5 μm, and the substrate contribution to these results may be higher than the contribution of nanoindentation tests.

Table 5-4 Surface Knoop hardness data for uncoated Ti-64 and Ti-AVM substrates nitrided at 500 and 600°C for 4 and 8 hours

Sample	Temperature (°C)	Duration (h)	Surface Hardness (HK$_{0.01}$)
Untreated Ti-64	-	-	471
Uncoated Ti-64	500	4	549
Uncoated Ti-64	500	8	606
Uncoated Ti-64	600	4	616
Untreated Ti-AVM	-	-	460
Uncoated Ti-AVM	500	4	539
Uncoated Ti-AVM	500	8	601
Uncoated Ti-AVM	600	4	611

The results showed that there is some change in surface hardness although the process temperature is very low (500°C). It was also mentioned in the literature [64], [84] that the surface hardness increases with increasing temperature (from 500°C to 600°C). Process duration also has a positive effect on hardness at the same temperature. It can be observed that the process at 600°C for 4h gives similar hardness values to the process at 500°C for 8h. All of this could simply be due to increase in layer thickness and different substrate contributions to measured hardness.

All Knoop hardness results yielded lower values than for the nanoindentation data, but the untreated substrates are very similar with nano-hardness results. There is no effect of the nitrogen on untreated substrates and the only influence on the hardness results can be a thin surface oxide layer or the compressive stresses coming from the grinding and polishing

process. Therefore, the hardness results are almost the same for these two techniques. All these discussions are suggesting that the Knoop hardness results are reliable and the reason for the different hardness values is the penetration depth of the indenters. Bars et al. [173] have mentioned that the solid solution of α-Ti and nitrogen gives an increase of the hardness of about 92 HV per increase of 1 at. % N until 9 at. % N (which was done by the Vickers microhardness test with a 100 g load). This is suggesting that the Ti-64 and Ti-AVM substrates have only 3-4 at. % N after the nitriding process at 500 and 600°C. The ability of the EDX technique is not enough to capture these low amounts of nitrogen, and thus other techniques should be used to verify the amount of nitrogen near the surface.

5.4 Triode Plasma Nitriding at 700°C (TPN700)

After having tried TPN500 and TPN600, it was seen that the hardness values were improved by alpha stabilisation (nitrogen diffusion inside the material), but no compound layer was seen on the treated substrate surface. It was already discussed in Section 2.5 that nitride compound layer formation could be promoted by increasing the substrate bias voltage at 600°C, but it would be detrimental to surface finish, and the rapid formation of a nitride layer will suppress further nitrogen inward diffusion. A new set of TPN process samples was prepared at 700°C to see the effect of the temperature on nitrogen diffusion inside the Ti-64 and Ti-AVM alloy substrates. This set of TPN parameters was applied to uncoated, Ti coated, and Ti-Nb coated substrates for 4 and 8 hours. This temperature would be the maximum temperature which the triode plasma nitriding process could be applied to not experience any unfavourable effect on bulk properties [53], [81]. After the nitriding process, it was realised that the thickness of the (previously coated) surface layer coatings was decreased. It was probably happening because of argon and nitrogen gas sputtering on the coated substrates. Thicker surface layers (5 μm) were therefore deposited on the titanium alloy substrates before TPN treatment, to analyse "the sputter off effect" (it will be discussed later). The near-surface EDX results after TPN700

process for uncoated, Ti coated (1.25 μm), and Ti-Nb coated (1.25 μm), Ti-64 and Ti-AVM substrates (for 4 hr process duration) are seen in Table 5-5.

5.4.1   X-ray Diffraction Phase and EDX Analysis

Firstly, the most immediate deduction from EDX results is that the atomic percentage of nitrogen on the surfaces is nearly the same for all samples. However, despite having similar nitrogen concentration on their surfaces, the XRD results (see Figure 5-7 and Figure 5-8) showed that (after 4 hours nitriding) nitrogen creates Ti_2N nitride phase on uncoated Ti-64 substrates. Interestingly, the cubic (β) phase (inside Ti-64 substrates) did not disappear (which was expected from the stabilisation effect of nitrogen), but β phase is still available for uncoated Ti-64 substrates (but significantly shifted to the higher angles), and the intensity of this phase decreased from Ti coated to Ti-Nb coated substrates. The reason for these different intensity values of the β-Ti phases may be related to the formation of nitride compound layer or the diffusion of the additional elements (such as V) to the near surface (more detailed analysis can be found in Section 5.5.1.1). On the other hand, there is no evidence of nitride phase on the surface of uncoated Ti-AVM substrates due to the different crystal structure of beta titanium alloys, nitriding behaviours are different (much difficult to reach critical concentration for Ti_2N formation, i.e. 33at% N required) [76].

Table 5-5 Near surface EDX results of the samples nitrided at 700ºC for 4 hours.

Sample No	Details	Ti (at. %)	Al (at. %)	V (at. %)	Nb (at. %)	Mo (at. %)	N (at. %)
*	Ti-64 Substrate (untreated)	85.2	11.3	3.5	-	-	-
1	TPN700, 4h, Uncoated Ti-64	72.9	12.9	2.1	-	-	12.1
2	TPN700, 4h, Ti-coated Ti-64	73.5	11.7	1.9	-	-	12.9
3	TPN700, 4h, Ti-Nb coated Ti-64	74.8	11.1	1.3	0.0	-	12.8
*	Ti-AVM Substrate (untreated)	69.9	7.6	10.1	-	12.4	-
4	TPN700, 4h, uncoated Ti-AVM	61.3	6.4	8.6	-	11.2	12.6
5	TPN700,4h, Ti-coated Ti-AVM	61.4	6.4	8.9	-	11.1	12.2
6	TPN700, 4h, Ti-Nb coated Ti-AVM	61.7	6.5	8.7	0.0	11.4	11.7

The peak shifts can be seen for uncoated Ti-AVM alloy because nitrogen diffuses inside the substrates and alpha stabilisation started (the formation of α-Ti peaks can be seen in Figure 5-8) because of the incorporation of nitrogen in the Ti lattice.

Secondly, the Ti-Nb coated substrates (Sample 3 and Sample 6) show that the niobium concentration is zero after the TPN700 process. It can be explained by the nature of the plasma nitriding process that "sputtered off" the 1.25μm thick coating after 4 hours of nitriding at 700°C. It suggests that a thicker PVD coating layer should be used for this nitriding process.
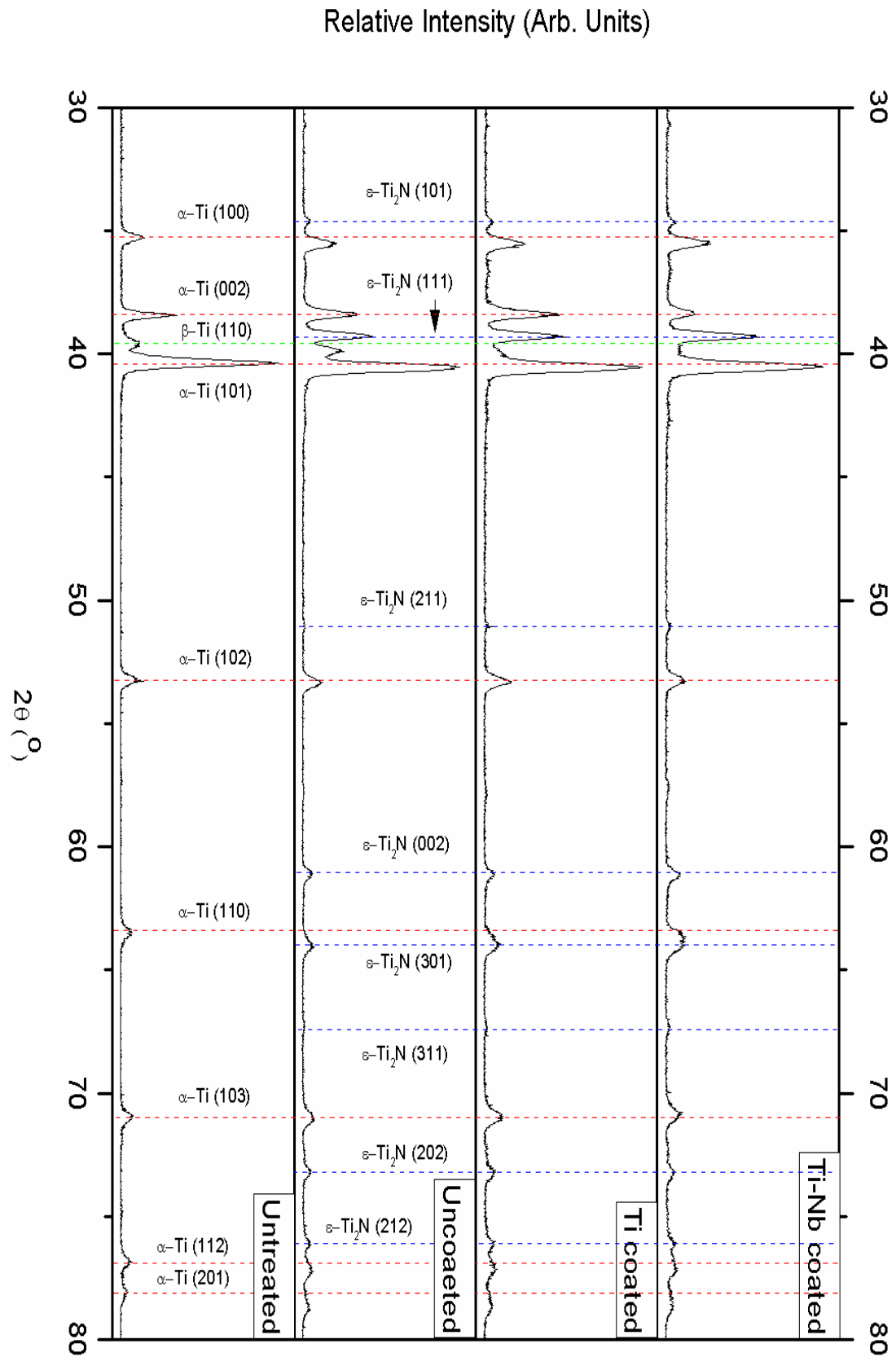
Figure 5-7 GAXRD (2º angle of incidence) diffraction patterns of untreated (substrate only) and nitrided Ti-64 substrates at 700ºC for 4 hours
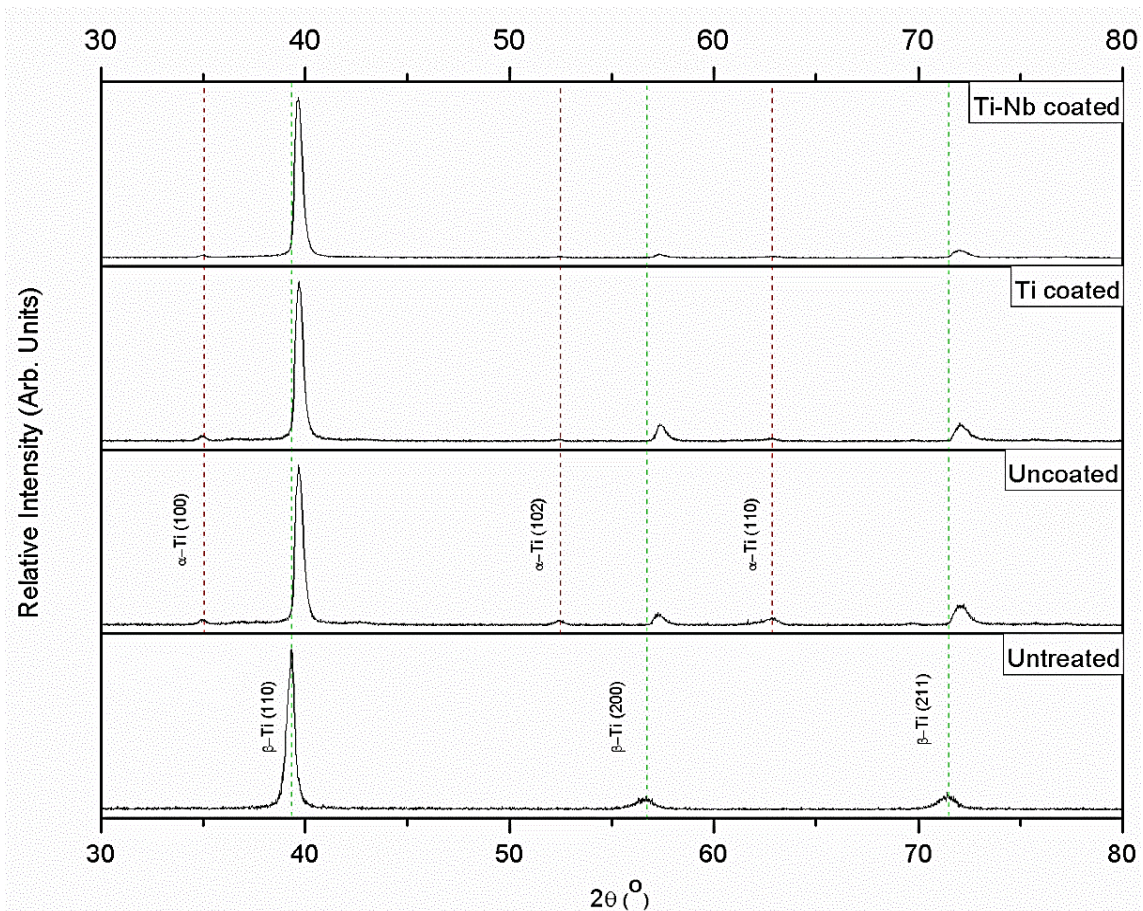
Figure 5-8 GAXRD (2º angle of incidence) diffraction patterns of untreated (substrate only) and nitrided Ti-AVM substrates at 700ºC for 4 hours

It is also expected that the Ti coatings on substrates (Sample 2 and Sample 5) were sputtered off after plasma nitriding. It is easy to say (from the EDX data) that the Ti-Nb coating was sputtered off because both substrates do not have Nb inside which prevents any complexity or misunderstanding. In this study, usage of different kinds of substrates and surface layer coatings which have different crystal structures and hence different XRD peaks provides convenience while comparing the results. However, for the pure Ti surface layer, it sometimes could be difficult to interpret unambiguously (at first sight) the EDX results because the substrates are also Ti-based. To understand what did happen to Ti coated substrates after TPN700 process (sputtered off or not), there are some different ways: The most consistent way is taking cross-section images of the samples by SEM to see if any coating is left or not. The other way: it can be understood from the XRD results. It is seen in Figure 5-7 that the Ti-Nb

coated Ti-64 substrate shows similar XRD pattern with the uncoated Ti-64 substrate after TPN700 process for 4hr. This shows that the Ti-Nb surface layer coating (1.25 μm thick) could not survive until the end of the process. It was sputtered off by argon and nitrogen completely (or left about a few nm thick) and resulted in the same structure of an uncoated substrate. If there were still Ti-Nb coating left, it could give some strong XRD peaks belonging to cubic (beta) structure. The same thought is valid for Ti coating which was deposited on Ti-AVM substrate. It is seen in Figure 5-8 that the Ti coated Ti-AVM substrate shows a similar XRD pattern to the uncoated Ti-AVM substrate after TPN700 process for 4hr. If there were still Ti coating left, it could give some strong XRD peaks belonging to hexagonal (alpha) structure. This suggests that the choice of thickness of the PVD surface layers which are deposited before the nitriding process is critical to obtain better efficiency over the duration of the treatment. A different way to understand the behaviour of the surface layer coatings after the nitriding process is by checking the concentration of alloying elements (such as Al, V, Mo) which is seen in EDX results from the surface (especially for Ti-AVM substrates). If all of them are approximately similar to the uncoated ones, it could be expected that the PVD surface layer has been sputtered off. Due to the limited depth resolution of EDX, If there is a remaining coating on the surface, the alloying elements of the substrates could be counted less (substrate contribution to the EDX result will be less) compared to uncoated substrates.

Thirdly, the Al and V concentrations were found to be different for uncoated and coated Ti-64 substrates (Samples 1,2 and 3) after the nitriding treatment. The concentrations for these additional elements are decreasing from uncoated (Sample 1) to Ti-Nb coated (Sample 3). On the other hand, these same additional elements do not show any difference after nitriding of Ti-AVM substrates (neither uncoated nor Ti or Ti-Nb coated). Ti-AVM alloy substrates do not show any nitride layer evidence from their XRD spectrums. Therefore, the reason for variance of alloying elements may be related to the thickness of the Ti_2N nitride layer which is formed

on Ti-64 substrates after TPN700 process. Moreover, the concentrations of alloying elements (Al and V) in Ti-64 substrates after TPN700 process for 4h showed that the Al diffused from the matrix to the nitrogen-rich area (near surface) and the Vanadium decrease its concentration near nitrided layer. Although, the Ti_2N phase formed on the uncoated Ti-64 substrate, the Al concentration was found higher (see Table 5-5) than the untreated sample (substrate only). The different distribution of these alloying elements (compared to the untreated condition) can be related to the particular affinity of these elements with nitrogen [185].

5.4.2 Surface Morphology and Topography

Figure 5-9 shows the surface roughness data after nitriding of untreated, Ti coated, and Ti-Nb coated Ti-64 and Ti-AVM substrates. It is concluded from the results that the uncoated substrates were found rougher than Ti and Ti-Nb coated substrates after TPN treatment. This means that the PVD pre-coatings helped to keep the roughness of the substrate low. The surface SEM images (Figure 5-10) show that the conical features [186] of the surface are deeper for the uncoated Ti-64 substrate than Ti and Ti-Nb coated Ti-64 substrates after the nitriding. The coarse texture of the uncoated Ti-64 substrate can be based on the effect of sputter etching during the nitriding process and the formation of conical asperities (bringing about a 'peak and valley' structure) during the plasma diffusion treatment [84], [187]. The PVD layers (with dense nanocolumnar structure) protected the surface of the substrates until they are sputtered off completely by the TPN plasma bombardment. After the surface layer disappeared, it was expected that the surface of the coated substrates would behave as uncoated one (which has the highest surface roughness). Therefore, it can be said that the increase in the surface roughness of the coated substrates was postponed by depositing a PVD metallic layer before nitriding, even if the thickness of the surface layer was not enough to survive the entire nitriding process duration. Depositing a surface layer which lasts at least until the end of the nitriding treatment will keep the resultant surface roughness values at minimum. The ''sputter-off'' rate of the Ti

and Ti-Nb surface coatings will be calculated and discussed later while talking about thicker surface layer coatings (in Section 5.5).
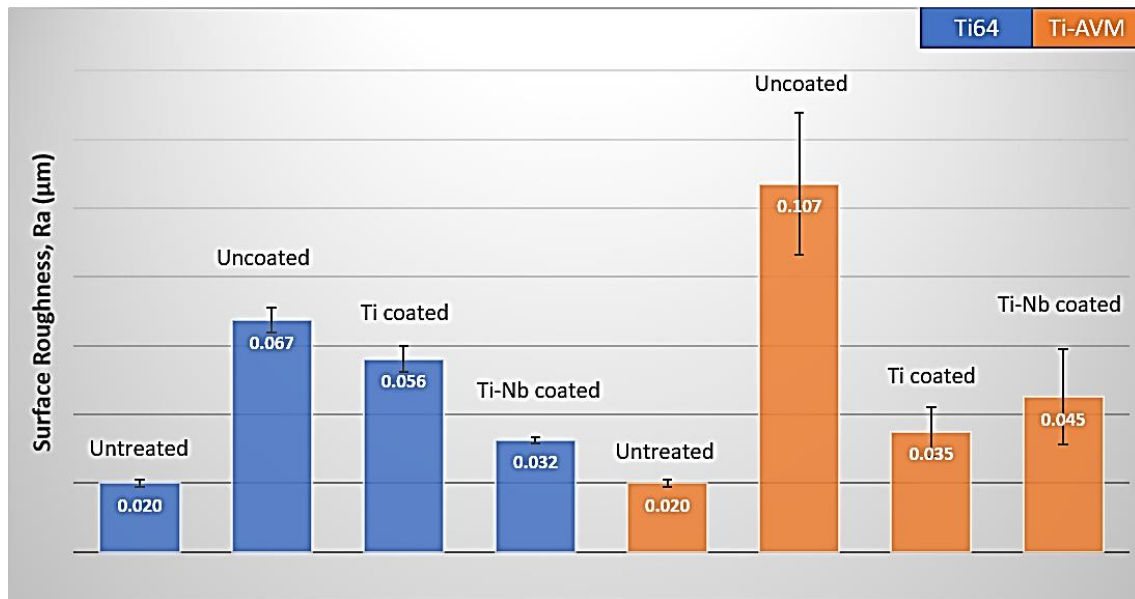
Figure 5-9 Surface roughness data for uncoated, Ti- coated and Ti-Nb coated Ti-64 and Ti-AVM substrates TPN-treated at 700ºC for 4 hours

The uncoated Ti-AVM was found to be significantly rougher than uncoated Ti-64 substrates after 4 hours of nitriding process at 700ºC. This can be explained by the diffusion anisotropy in the cubic structure (β phase) exhibiting a large grain size (with different crystallographic orientations to the surface) [3]. It can be verified with the SEM images and optical microscopy images (from the surface of the Ti-64 and Ti-AVM substrates) in Figure 5-10 and Figure 5-11 respectively. The bigger error bars (which the roughness results for Ti-AVM substrates exhibit) can be attributed to the same effect because the scans were done over 1mm length (approximately 10 grains) and the results can be affected by the different nitriding behaviours of each grain. It can be seen in Figure 5-10 (d) that the two grains (which stands two sides of the grain boundary) have a different plasma etched topography. It seems the grain which stands to the right was affected more by the nitriding and the surface features of this grain are more conical than the other grain. The difference (between two neighbouring grains) can also be

monitored easily in the profilometer (from 2D profiles across the surface) which causes higher

roughness value (Ra: 0.107 μm for the uncoated Ti-AVM substrate after 4h treatment).
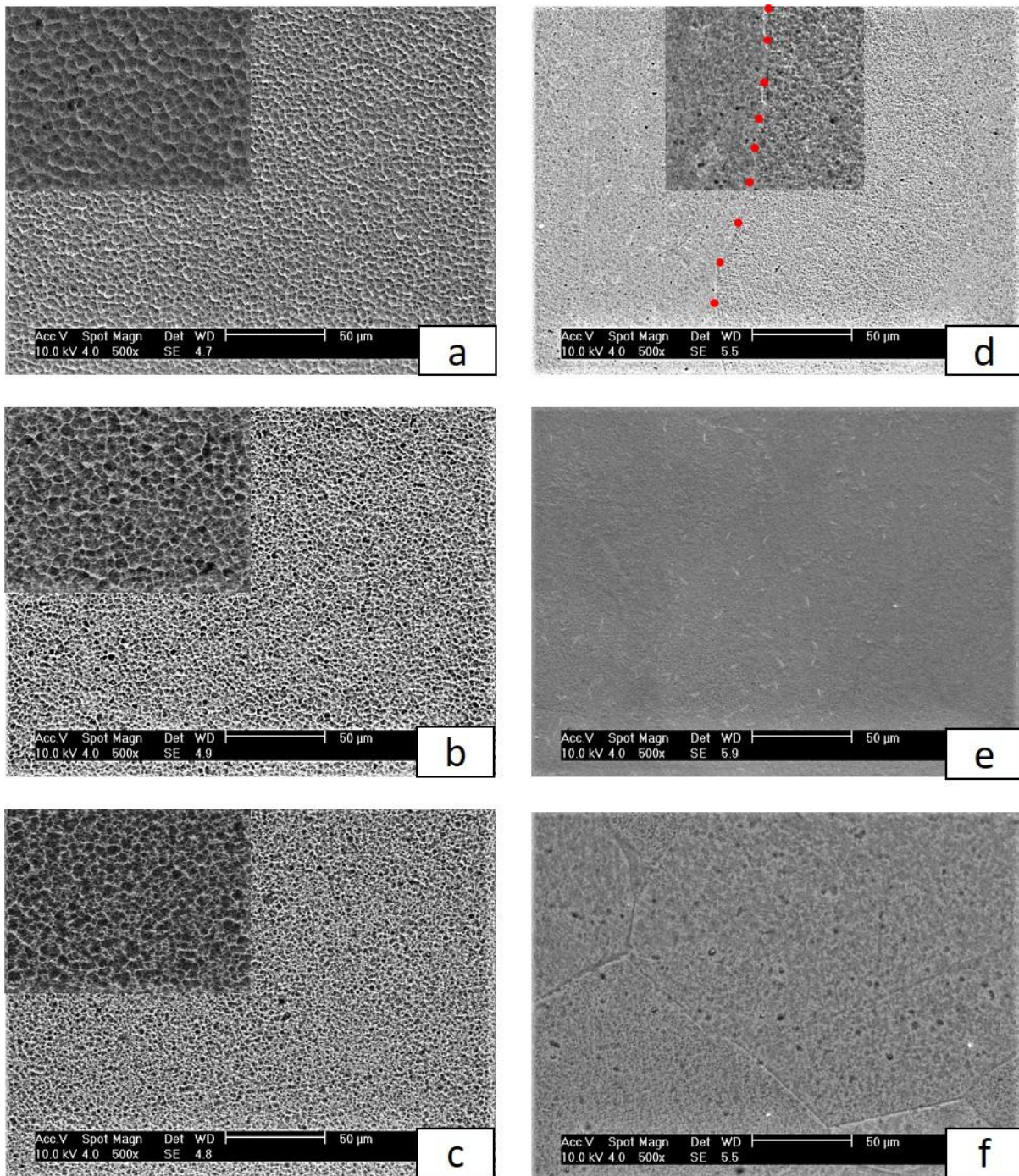
Figure 5-10 SEM images of the surface topography of samples treated at 700ºC for 4 hours. (a) uncoated Ti-64 (top-left quarter of the image magnified 5 times) (b) Ti coated Ti-64 (top-left quarter of the image magnified 5 times) (c) Ti-Nb coated Ti-64 (top-left quarter of the image magnified 5 times) (d) uncoated Ti-AVM (top of the image magnified, and the grain boundary indicated) (e) Ti coated and (f) Ti-Nb coated Ti-AVM
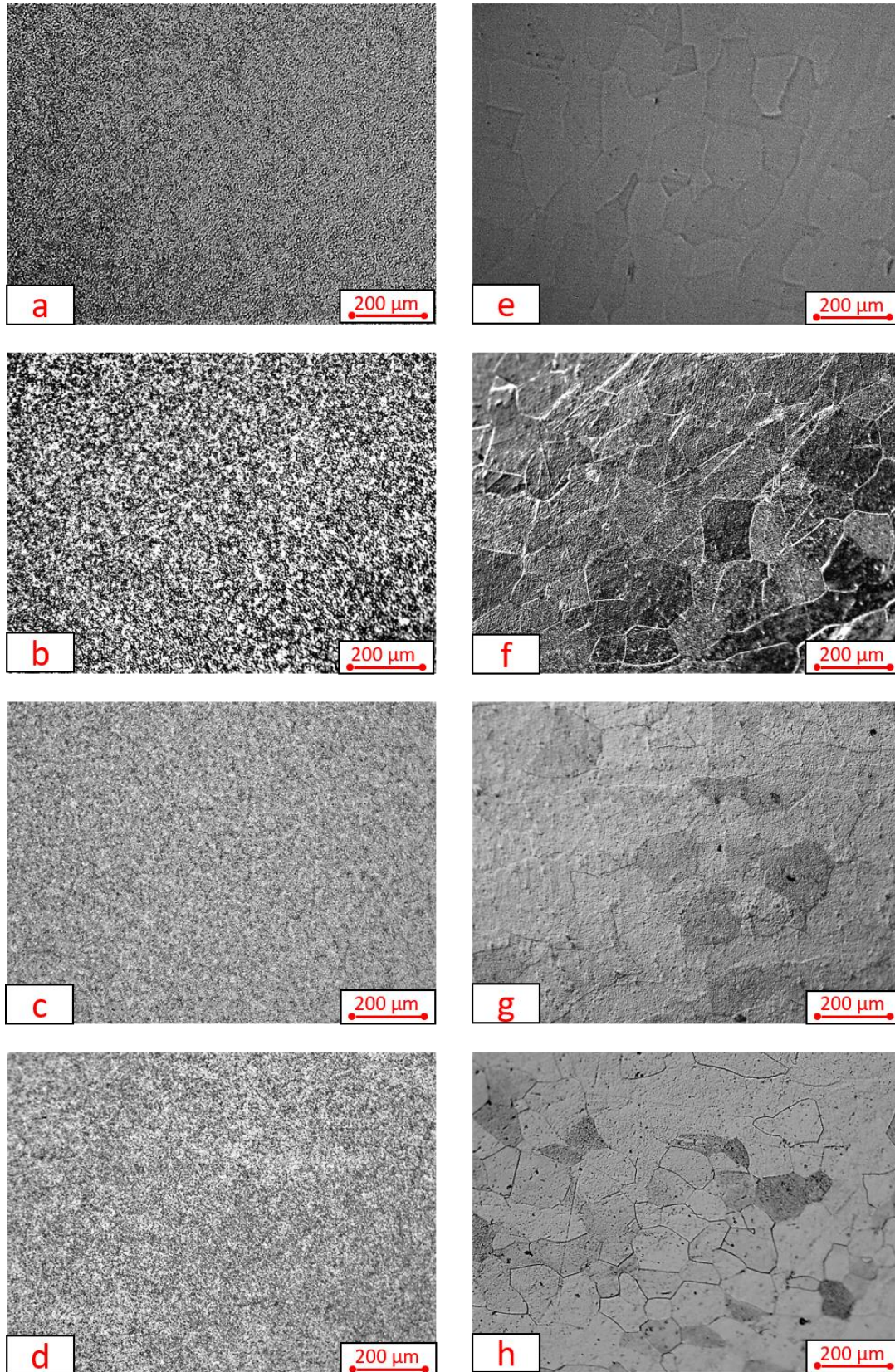
Figure 5-11 Optical microscopy images of the surface topography of samples treated at 700ºC for 4 hours. (a) untreated Ti-64 (b) uncoated Ti-64 (c) Ti coated Ti-64 (d) Ti-Nb coated Ti-64 (e) untreated Ti-AVM (f) uncoated Ti-AVM (g) Ti coated and (h) Ti-Nb coated Ti-AVM

125

It is also interesting that there is some difference between the roughness data for coated Ti-64 and Ti-AVM substrates after 4 hours nitriding at 700°C. The surface roughness of the Ti-Nb coated Ti-64 substrate is less than the Ti coated Ti-64 substrate. On the other hand, the roughness of the Ti coated Ti-AVM sample is less than the Ti-Nb coated Ti-AVM substrate. This can be seen in the surface SEM images (Figure 5-10) where the Ti-Nb coated Ti-64 substrate looks smoother than the Ti coated Ti-64 substrate. The error bars for the Ti and Ti-Nb coated Ti-AVM (related to the large grain size of Ti-AVM substrate) makes it difficult to compare the roughness results. However, the coated Ti-64 coupons showed that the different changes in the roughness values could be related to the "sputter off" rate of the different surface coatings. (These rates are calculated in Section 5.5). The different surface roughness values for Ti and Ti-Nb coated Ti-64 substrates were also verified with AFM three dimensional topographic maps which can be seen in Figure 5-12. On the first appearance, the three images show how the surface morphology is going from rough (conical) to smoother features (hemispherical). The AFM 3D maps were deduced (with Nanoscope software) from AFM images which were taken for an area of 50 μm x 50 μm.

The different sampling areas for AFM and profilometer techniques can result in different surface roughness values. The surface compound layer growth is not always uniform, and this can yield different values in each scan (particularly for AFM). Therefore, the average values of surface roughness tests are given. However, it can be proved with AFM results that the effect of Ti-Nb PVD coatings deposited before nitriding on surface roughness is superior to pure Ti coatings. The 50 μm length may be fine for the Ti-64 alloys because the small grain size allows lots of grains to be sampled and it is possible to get a meaningful average from them. On the other hand, for the Ti-AVM alloy, there can be a mistake in applying the AFM technique. In this fine scale measurement, it can scan only one or two grains for Ti-AVM alloy because of

the larger grain size. Therefore, it needs to be scan over more than one grain to reduce the risk of differently oriented grains biasing measurement for beta alloys [2].
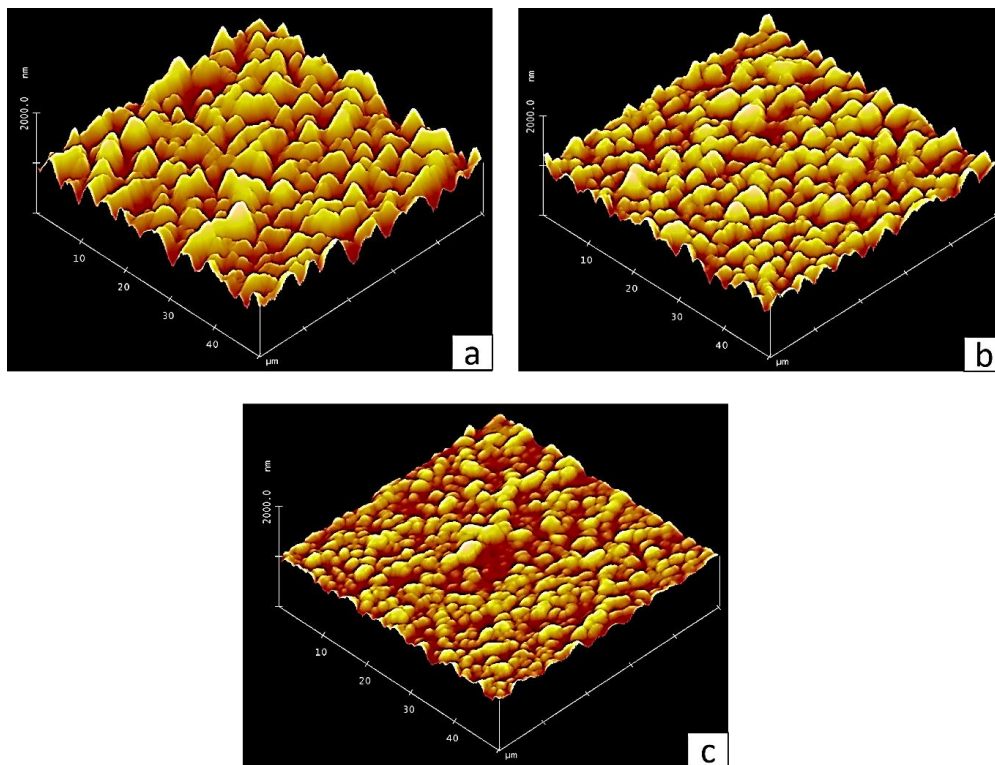
Figure 5-12 AFM 3D topographic maps of (a) uncoated, (b) Ti-coated, (c) Ti-Nb coated Ti-64 substrates TPN-treated at 700ºC for 4h

The 2D scan profile for uncoated Ti-AVM alloy can be seen in Figure 5-13. The total number of grains which was scanned is less than 10, and the heights of the hills or valleys are changing very sharply (every two hundred microns). However, the plain part of these asperities could show lower surface roughness values (in itself). The risk of the AFM (for this case) is the probability of scanning an area which is less rough because the sampling range of the AFM indenter is much smaller than the profilometer technique. Therefore, to not fall into error, large-scale methods (such as profilometer) would be beneficial for nitrided Ti-AVM alloys.
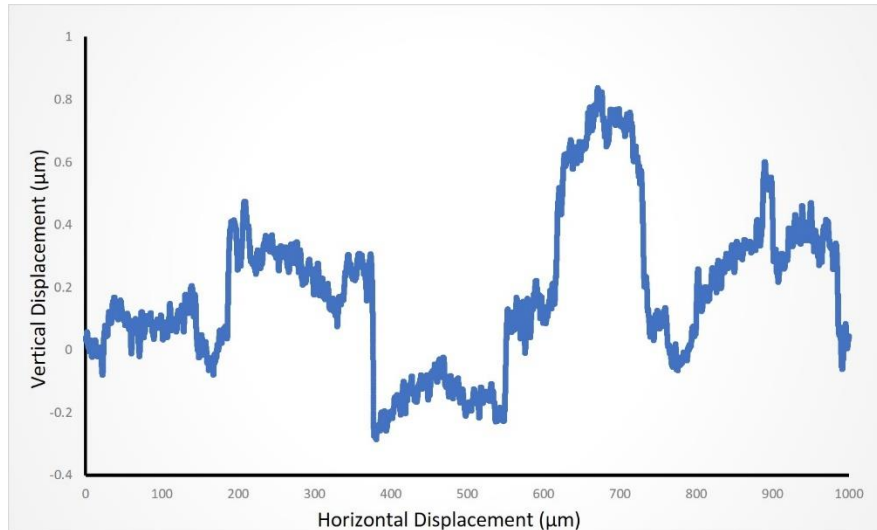
Figure 5-13 2D scan profile across the nitrided surface of the uncoated Ti-AVM sample

5.4.3 Cross-sectional Morphology

SEM cross-sectional images were taken for all six substrates which can be seen in Figure 5-14. The compound layer which formed after the nitriding process for uncoated Ti-64 is approximately 850 nm thick, for Ti coated Ti-64 it is about 650 nm thick and for Ti-Nb coated Ti-64 it is about 1100 nm thick. It was already discussed with the XRD patterns (Figure 5-7) that all these layers are composed of Ti_2N. There is no evidence related to TiN or other alloying element's nitride phases (such as V_2N) or any intermetallic phases (such as Ti_3Al, $Ti_{0.80}V_{0.20}$) which the literature mentioned about the surface phase structure of Ti alloys (mostly for Ti-64) after nitriding process [62], [85], [92], [93], [97], [103], [107], [188]–[190]. It was already mentioned in Section 2.5 that the different parameters used for the nitriding treatments would bring various final products. Therefore, it was always tried to find some works (done with similar process parameters with this study) to compare the results and demonstrate the beneficial effects of PVD surface layers deposited before the nitriding. However, there is one more variable (rather than the process parameters) for this study which is the different type of substrate. The Ti-AVM substrate (with a fully β phase structure) has very different final features than the Ti-64 substrate. It was already verified with XRD patterns (Figure 5-8) that Ti-AVM substrates did not show any evidence related to compound layer formation after nitriding.

128
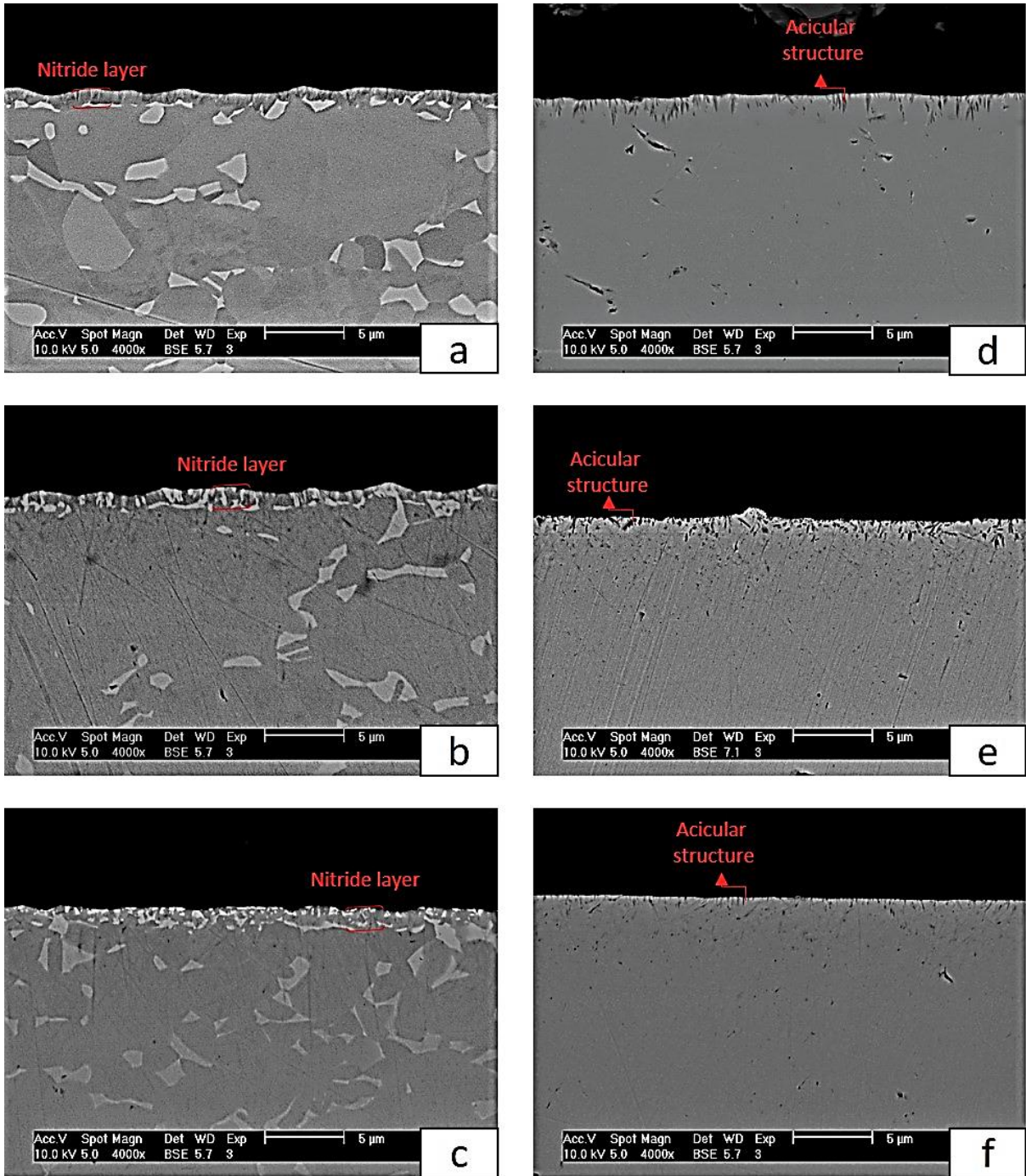
Figure 5-14 SEM cross-sectional images of the samples treated at 700ºC for 4 hours. (a) uncoated Ti-64 (b) Ti coated Ti-64 (c) Ti-Nb coated Ti-64 (d) uncoated Ti-AVM (e) Ti coated and (f) Ti-Nb coated Ti-AVM

The alpha stabilisation (some alpha peaks appeared) and observation of the peak shifts referred to nitrogen dissolved in the beta titanium phase. The diffusion treated cross-sectional images for Ti-AVM alloy (seen in Figure 5-14 d, e, f) showed nitrogen stabilised layers (α phase

formation) which has acicular (needle-like) feature [2]. Although the near surface EDX results (after TPN700 process for 4h) showed about 12 at. % N (Table 5-5) for both type of substrates, the final structures/morphologies were very different from each other. It appears that this amount of nitrogen would not be enough to create a nitride compound layer on the surface of the Ti-AVM alloy. The Ti-N binary equilibrium phase diagram (Figure 2-11) is unable to clarify the amount of N which dissolves in β Ti (for pure Ti), without creating a nitride compound layer, because no β-Ti can be found at 700°C. The ternary (Ti-Mo-N and Ti-Al-N) phase diagrams were drawn (calculated in the ThermoCalc software) to have an idea (estimation) about the phase structures at 700°C. The isothermal sections (the concentration of the elements is given in atomic %) can be seen in Figure 5-15 and Figure 5-16. There is normally more than one additional element present in each alloy, but the software is only capable of describing (maximum) three-element systems. Therefore, the Ti-64 and Ti-AVM alloys were estimated as Ti-Al and Ti-Mo alloys respectively to see the different effects of α and β stabilisers on the phase structures. The effect of other elements in respect to α or β stabilisation was added or extracted by making simple calculations (from Table 4-1 and Table 4-3) in consideration of "Mo equivalent formula" [191]. The estimated (at. %) of Mo and Al elements were marked with blue arrows on ternary phase diagrams. Both phase diagrams have an area which shown (A-B-Ti) triangle. These small areas show where N dissolves only in Ti (no Ti_2N or TiN compound layer). The stable phases of these areas are HCP and BCC+HCP for Ti-64 and Ti-AVM alloys, respectively. It is seen from the diagrams that the maximum solubility of nitrogen at 700°C (without forming a compound layer) is about 10 at. % and 16 at. % for these (marked) Ti-64 and Ti-AVM alloys, respectively. The A-B lines are the boundaries for the formation of Ti_2N phase. It is easily seen from the direction of the A-B lines that the increased amount of Mo allows dissolving more nitrogen. On the other hand, when the amount of Al is increased, the solubility of nitrogen is decreased. From this point of view, the absence of the Ti_2N phase may

be explained for uncoated Ti-AVM alloy, despite the amount of dissolved nitrogen being similar to the Ti-64 alloy (i.e. reaching 12-13 at % N in both after 4hr TPN treatment at 700°C).
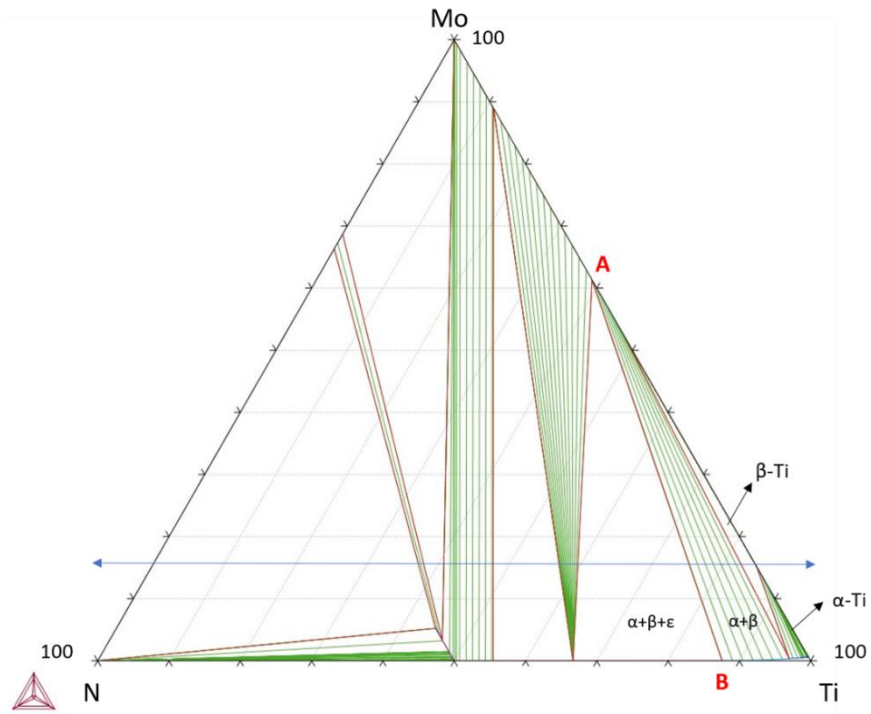
Figure 5-15 Calculated isothermal phase diagram of the ternary Ti-Mo-N system at 700°C
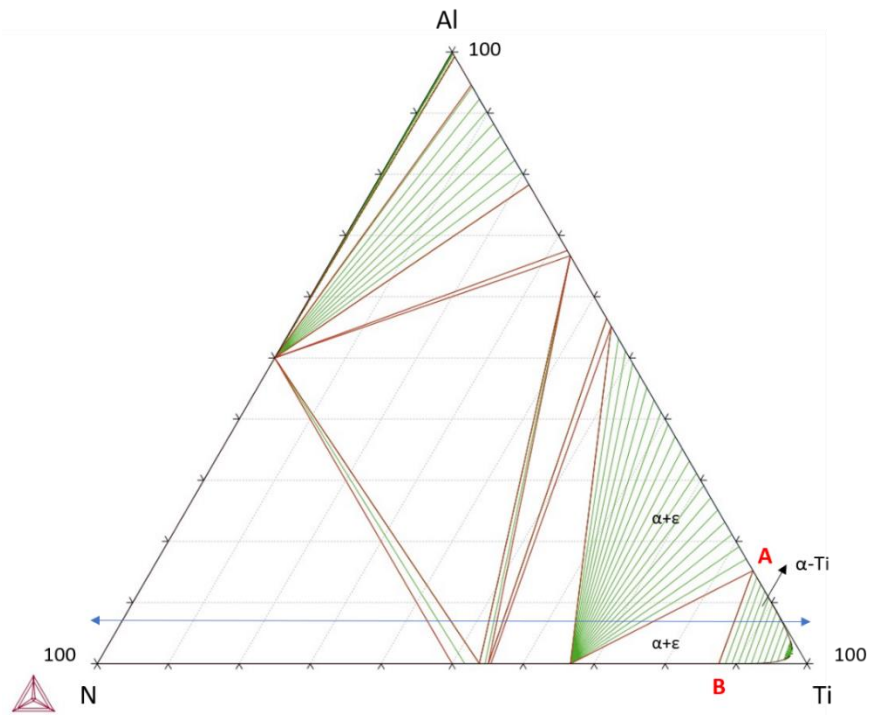
Figure 5-16 Calculated isothermal phase diagram of the ternary Ti-Al-N system at 700°C

The literature contains little or no data on plasma nitriding of beta titanium alloys compared to Ti-64 or any (α+β) Ti alloys. Gordin et al. [192], [193] applied gas nitriding (at 1200°C and 1400°C) to metastable-beta Ti94Mo6, Ti92Mo8 and Ti84Mo16 alloys to increase the surface hardness by achieving hard TiN surface layer. They also used the knowledge of Ti-Mo-N (tentative) ternary phase diagram [194] which was drawn for 1147 °C. Mohan et al. [96], [195] applied plasma nitriding (at 800°C and 850°C) to β-21S and Ti-15V-3Cr-3Al-3Sn alloys to increase the corrosion and biocompatibility properties. They have also tried 600°C and 700°C nitriding, but they only mentioned hardness properties (there is no information related to low-temperature nitriding phase characteristics). It is apparent from their data that there is a very big jump in hardness from 700°C to 800°C; suggesting that the compound layer formation started at 800°C; a similar trend is also shown by Cassar et al. [2]. Akahori et al. [196] applied gas nitriding (750°C to 950°C) on Ti-Nb-Ta-Zr (TNTZ) alloy to increase the wear resistance. All works performed above 800°C showed Ti_2N or TiN compound layers (depending on the nitriding technique and process parameters). In our study, inhibition of the negative effect of the nitride layer (blocks the inward diffusion) on the nitrogen diffusion efficiency was tried. Therefore, the process temperature was kept to a maximum 700°C to see if the surface coatings provide any benefits on nitrogen diffusion efficiency.

5.4.4 Surface and Cross-sectional Hardness Measurement

The results attained from cross-sectional nanoindentation measurements are shown in Figure 5-17 and Figure 5-18 for Ti-64 and Ti-AVM substrates treated at 700°C for 4h. The indentations were applied about 2μm away (see the indentation traces for all samples in Figure 5-19) from the surfaces to avoid any damage from the indenter slipping. Figure 3-8 shows an example of the AFM image (after finishing 1 nanoindentation set) having 55 indents on the cross-section of a treated sample. Eleven indents in a row are lying from 2μm to approximately 57 μm depth, and the hardness values on this row showed the diffusion zone hardenability.

There are 5 columns in one nanoindentation set, but 2 repeats were done on each sample, so 110 indentations were taken in total. Thus, an average of 10 hardness values (at the same treatment depth) were taken to get reliable results for all samples. The cross-section hardness results for Ti-64 substrates show that the hardening effect under the surface is higher for Ti-Nb coated sample (until about 10 μm depth). The hardness values for all samples show a similar trend and nearly the same with the untreated condition after 10 μm depth. The fluctuation of each line can be explained by the nature of the nanoindentation test mechanism. Smoother results can be obtained by doing more repeats (ten repeats for each point has about 0.3-0.4 GPa deviations). The hardening effect for Ti-Nb coated Ti-64 substrate can be explained by the higher diffusion rate of nitrogen (in the beta phase coating) than in the substrates. Nitrogen can diffuse to the substrate faster and allows higher nitrogen concentration near the surface. Ti-AVM substrates indicate that the hardening effect under the surface (until about 10 μm depth) is higher for the Ti coated sample. It is shown (in Figure 5-18) that the uncoated Ti-AVM substrates show similar hardness trend with untreated samples. It has been discussed before that 4 hours of nitriding at 700°C is not enough for the Ti-AVM alloy to harden the surface. The Ti-Nb coated sample is also not showing significant hardening effect because the coating and substrates have same structures (β phase). The hardening effect for Ti coated Ti-AVM substrate can be explained with a lower diffusion rate of nitrogen (in the alpha phase coating) than in the substrates. This allows inward diffusion of interstitial nitrogen to be slowed down (compared to their diffusion rate in the β phase substrate), and they can, therefore, generate a significant hardening effect by increasing their concentration in near surface.

Figure 5-20 shows the surface hardness results for the uncoated and coated Ti alloy substrates. The values are higher than the cross-section hardness data, and the hardening effect was seen for both Ti alloys. It can be explained by these results that the thickness of the nitride layer is less than 2 μm which can also be easily seen in Figure 5-14. The effect of Ti-Nb coating on Ti-

64 substrates and less responsive behaviour of Ti-AVM to nitriding at this experimental condition can be observed again from surface hardness results.
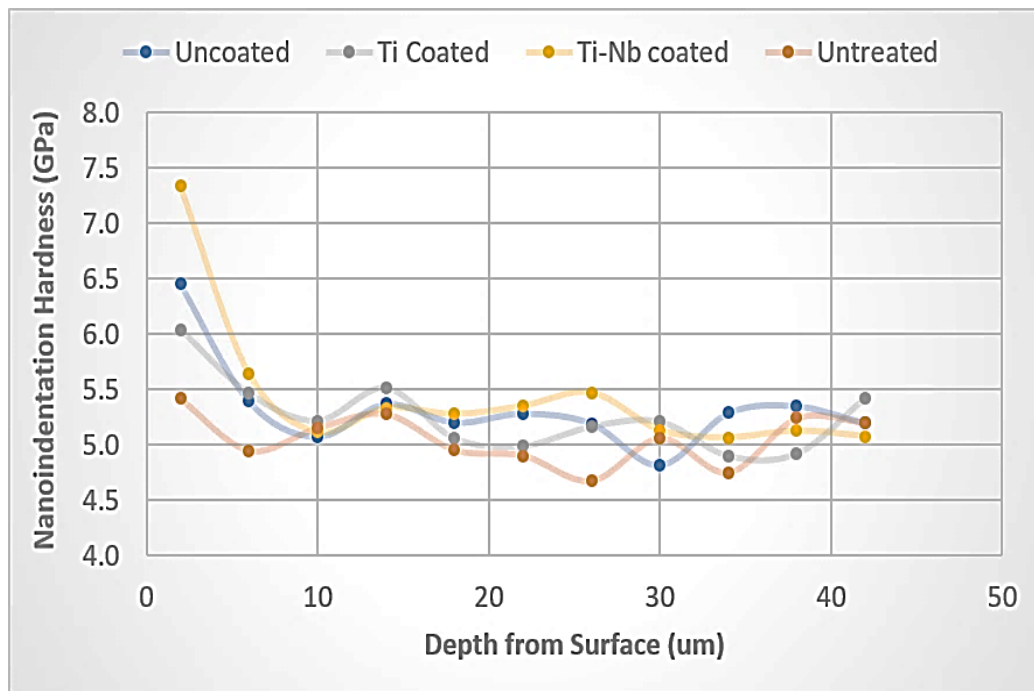
Figure 5-17 Cross-Sectional Nanoindentation data for Ti-64 substrates treated at 700ºC for 4h. (Each point is an average of 10 indentations)
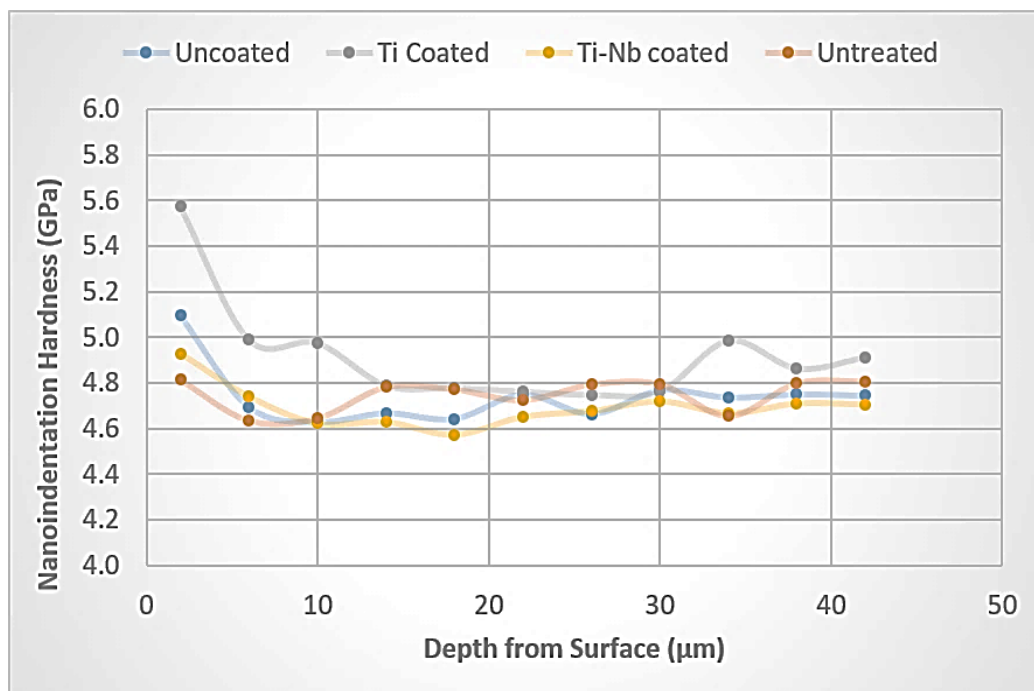
Figure 5-18 Cross-Sectional Nanoindentation data for Ti-AVM substrates treated at 700ºC for 4h. (Each point is an average of 10 indentations)
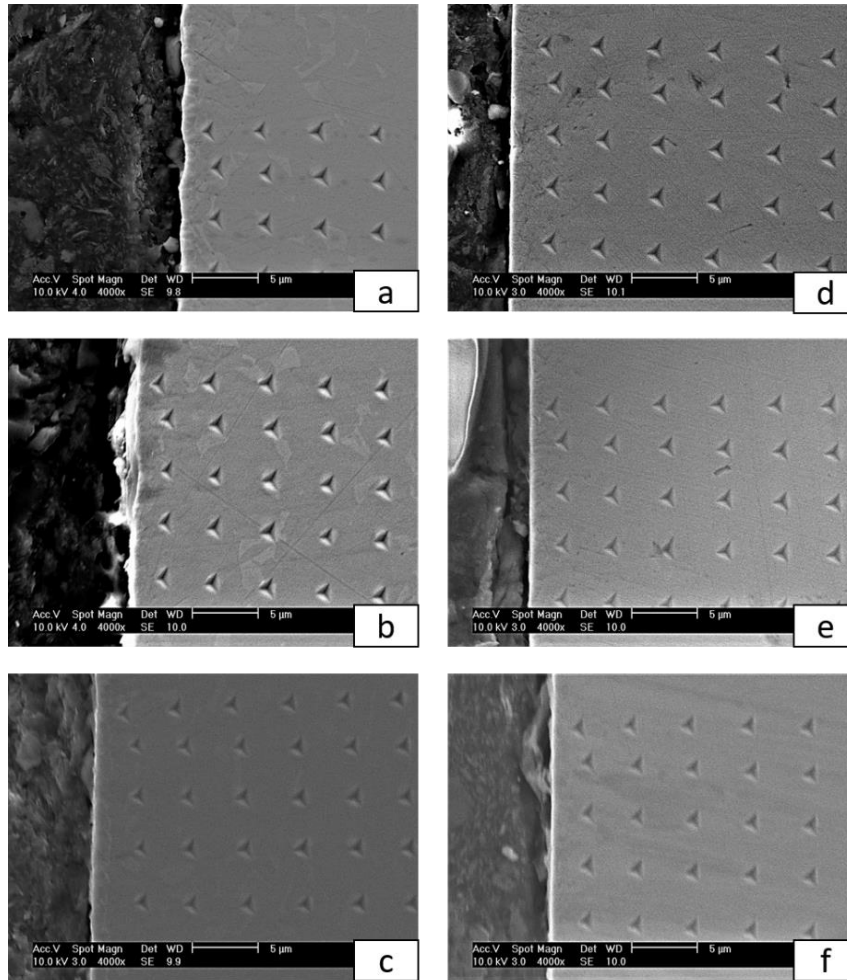
Figure 5-19 SEM cross-sectional images of the samples treated at 700ºC for 4 hours showing the nanoindentation traces. (a) uncoated Ti-64 (b) Ti coated Ti-64 (c) Ti-Nb coated Ti-64 (d) uncoated Ti-AVM (e) Ti coated and (f) Ti-Nb coated Ti-AVM
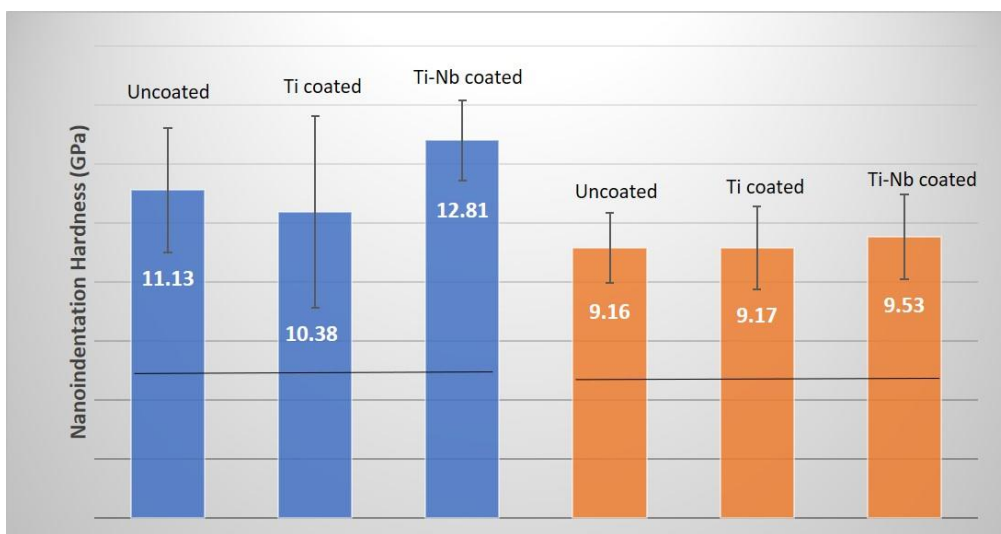
Figure 5-20 Surface nanoindentation hardness data for Ti-64 and Ti-AVM substrates treated at 700ºC for 4h

5.5   TPN700 process for thicker surface layer coated Ti alloy substrates

The thickness of the coatings was increased from 1.25 μm to (approximately) 5 μm to analyse the behaviour of the Ti and Ti-Nb surface layer coatings (by allowing them to survive until the end of the process) after nitriding. In the meantime, the nitriding duration was increased up to 8 hours at 700ºC. The 8h nitriding process was applied by dividing the process into two runs (4h+4h) to inhibit any problems related to over-heating of the chamber walls and failure of the hot tungsten wire filament used to intensify the plasma. This was also beneficial because before starting the first 4h run, two ''control sample'' Ti-AVM substrates (which were Ti and Ti-Nb coated) were also placed in the chamber and were collected before starting the second 4h run. In this way, it was possible to analyse the residual coating thickness after 4h nitriding process for the thicker (5 μm) coatings. On the other hand, this set of nitriding treatment provided information related to the uncoated substrate nitriding behaviour for 8h (i.e. the effect of the process duration on nitriding efficiency and surface roughing could also be understood). All other parameters were kept constant, and only the process duration was doubled.

5.5.1   EDX and X-ray Diffraction Phase Analysis

The near-surface EDX results after TPN700 treatment for uncoated, Ti coated, and Ti-Nb coated Ti-64 and Ti-AVM substrates (for 8 hours of treatment duration) are seen in Table 5-6. At first glance, the amount of nitrogen at the surface of the uncoated and coated substrates showed a measurable increase after 8 hours of nitriding, compared to 4hours at 700ºC (see the EDX result for 4h nitriding process in Table 5-5). Increasing the time of the nitriding process allowed more nitrogen to diffuse on the surface. The nitrogen concentration values for all samples treated for 4 hours were almost equal. After 8 hours nitriding process, the nitriding behaviour of the surface coating layers (Ti or Ti-Nb) was seen differently than with titanium alloy substrates. It can be deduced from the differences in the nitrogen concentration between the coated and uncoated substrates after 8-hour nitriding process. It was also different from the

4 hours nitriding treatment because the surface coatings survived until the end of the nitriding process due to their selected higher thickness.

Table 5-6 Near surface EDX results of the samples nitrided at 700ºC for 8 hours.

Sample No	Details	Ti (at. %)	Al (at. %)	V (at. %)	Nb (at. %)	Mo (at. %)	N (at. %)
*	Ti-64 Substrate (untreated)	85.1	11.4	3.5	-	-	-
7	TPN700, 8h, Uncoated Ti-64	62.8	8.4	2.9	-	-	25.9
8	TPN700, 8h, Ti-coated Ti-64	61.5	7.0	1.6	-	-	29.9
9	TPN700, 8h, Ti-Nb coated Ti-64	39.3	1.6	1.8	26.4	-	30.9
*	Ti-AVM Substrate (untreated)	69.9	7.6	10.1	-	12.4	-
10	TPN700, 8h, uncoated Ti-AVM	62.7	6.0	5.5	-	10.1	15.7
11	TPN700,8h, Ti-coated Ti-AVM	42.8	3.0	5.5	-	6.4	33.3
12	TPN700, 8h, Ti-Nb coated Ti-AVM	38.5	1.9	3.0	23.4	1.6	31.6

The fastest way to understand if any coating remains or sputters off entirely after nitriding process is to check the Nb concentrations for Ti-Nb coated substrates because there is no Nb present in either Ti-64 or Ti-AVM alloy substrates. It can be seen from Table 5-6 that both Ti-Nb coated Ti-64, and Ti-AVM substrates have Nb on their surfaces at about 24-26 at. %. (It

should be noted that the optical microscopy images from the surface and the SEM cross-sectional images can also be used to prove the availability of the Ti and Ti-Nb coatings on the surface after 8 hours nitriding process.)

The XRD diffraction patterns for nitrided (uncoated and coated) Ti-64 and Ti-AVM substrates for 8 hours at 700°C can be seen in Figure 5-21 and Figure 5-22. The nitrogen concentrations of the Ti and Ti-Nb coated substrates are changing between 30-33 at. % after 8 hours nitriding process. It can be seen from the XRD patterns that there are some signs of Ti_2N phase (precipitation) for the Ti and Ti-Nb coated Ti-64 and Ti-AVM substrates. However, it can be said that these are minor phases in which the substrate peaks were seen with more powerful intensities (although this XRD characterisation was made with 2° glancing angle mode). The XRD patterns show the availability of nitride phases on the surface but the weakness of these nitride phases (in the XRD patterns) can be explained that the nitride layer could be very thin (nanometre levels) or these phases are not continuous as a compound layer. They can be in precipitation form within the coating structure.

The other finding from the EDX results is a different behaviour of the uncoated Ti-64 and Ti-AVM substrates after the 8 hours nitriding treatment. The nitrogen concentration for the Ti-64 substrate was found to be about 26 at. %, which is almost double that obtained from 4 hours of nitriding treatment (Table 5-5). The XRD pattern for the uncoated Ti-64 substrate (Figure 5-21) is almost identical to that obtained after 4 hours of nitriding treatment (Figure 5-7).
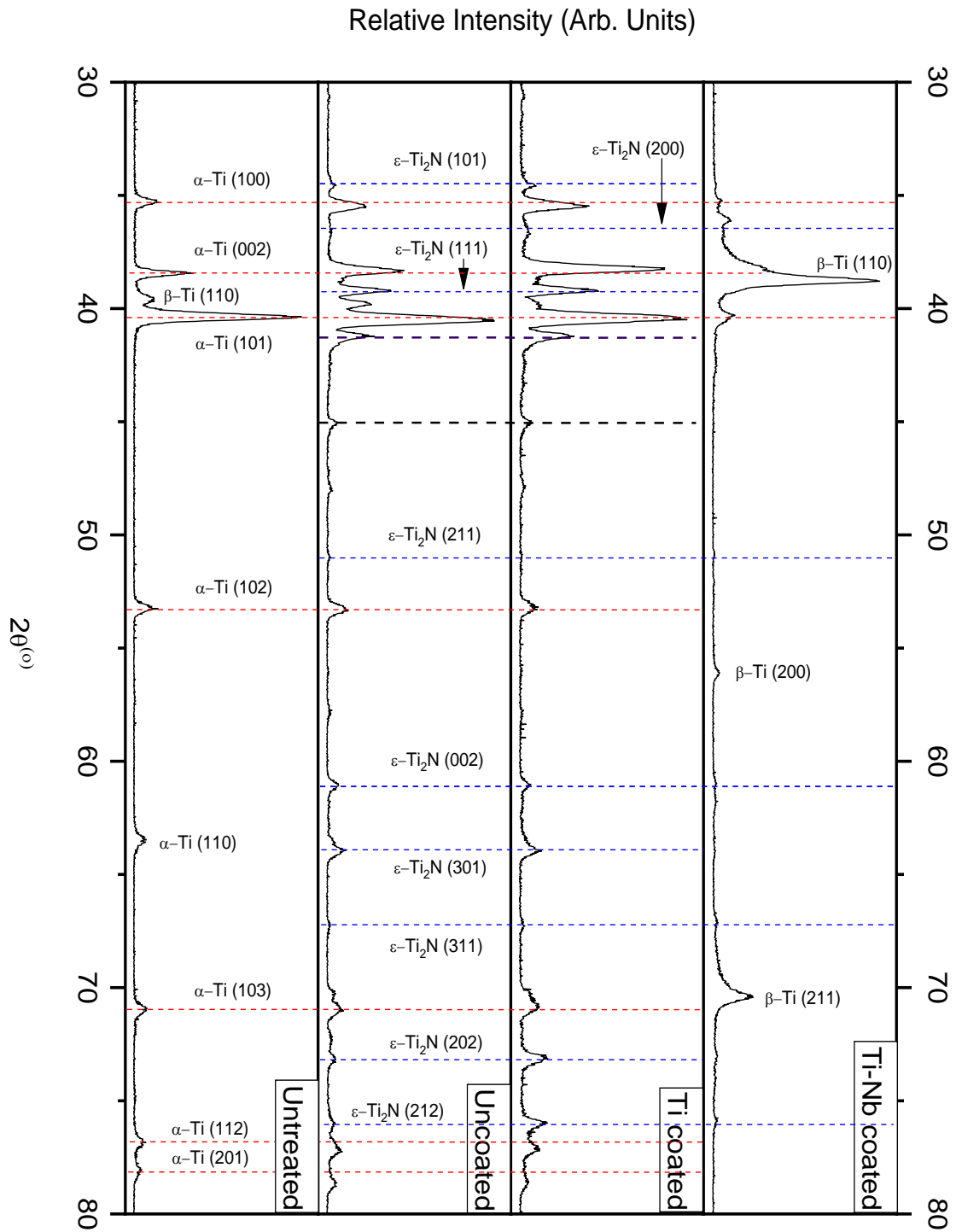
Figure 5-21 GAXRD (2o angle of incidence) diffraction patterns of untreated (substrate only) and nitrided Ti-64 substrates at 700°C for 8 hours

There is no TiN phase seen in the patterns. It can be understood that the temperature of the process is not enough to create a TiN phase on the surface (while the other parameters kept same). The only difference between the two XRD patterns is that there are some extra peaks

(at about 41.5°, 45° and 48°) after 8 hours of nitriding. The XRD match analyses (and in the light of previous studies by Morgiel et al. [103]) suggest that these peaks belong to martensitic Ti and Ti-Al intermetallic phases. All possible phases for the uncoated Ti-64 substrate after 8-hour nitriding were analysed and can be found in Figure 5-23. It is very interesting that the formation of both α''-Ti and Ti-Al intermetallic phases were seen only for Ti-coated substrates and uncoated Ti-64 substrates. This suggests that the presence of Ti atoms (as HCP form) on the surface of the samples (together with the nitrogen diffusion inside the substrates) are leading to the mobilisation of the Al atoms (and also resulting with the grains which included more V than it should be). On the other hand, these phenomena were not seen for Ti-Nb coated substrates or uncoated Ti-AVM alloy.
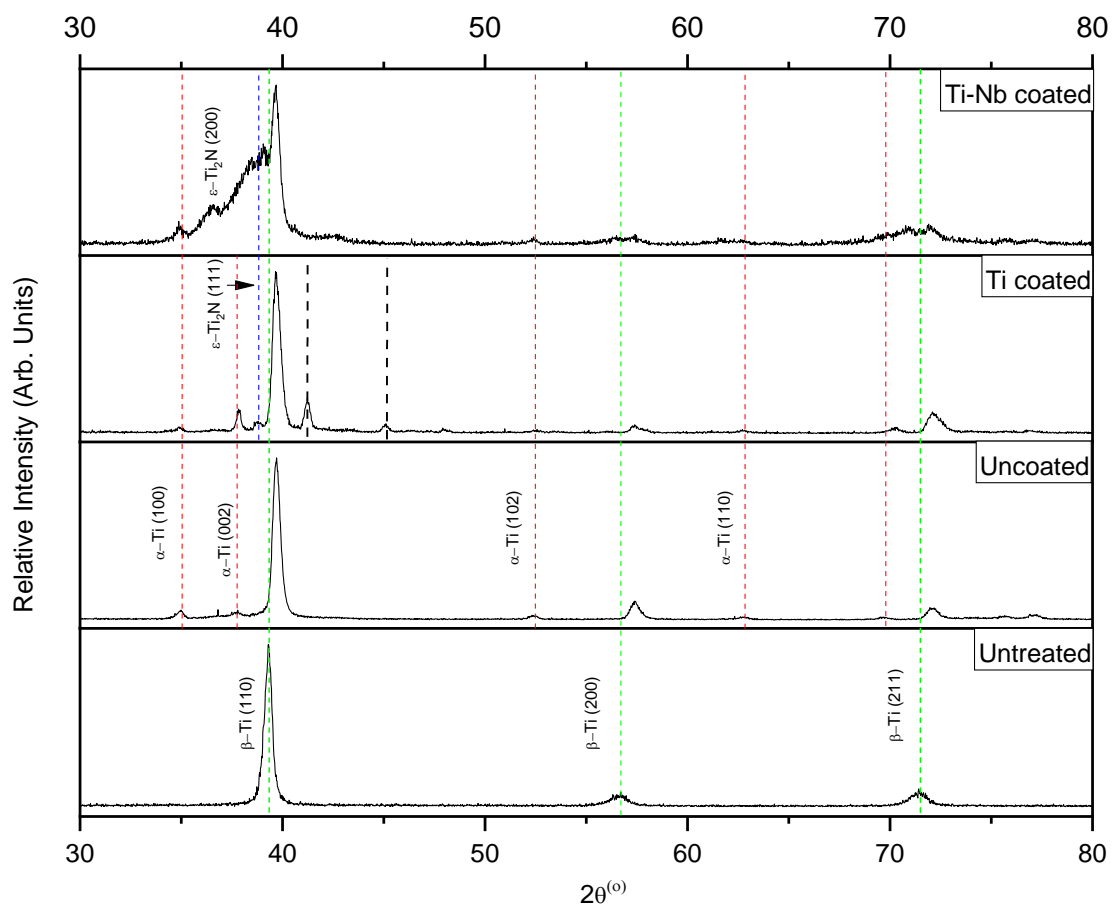
Figure 5-22 GAXRD (2° angle of incidence) diffraction patterns of untreated (substrate only) and nitrided Ti-AVM substrates at 700°C for 8 hours

140
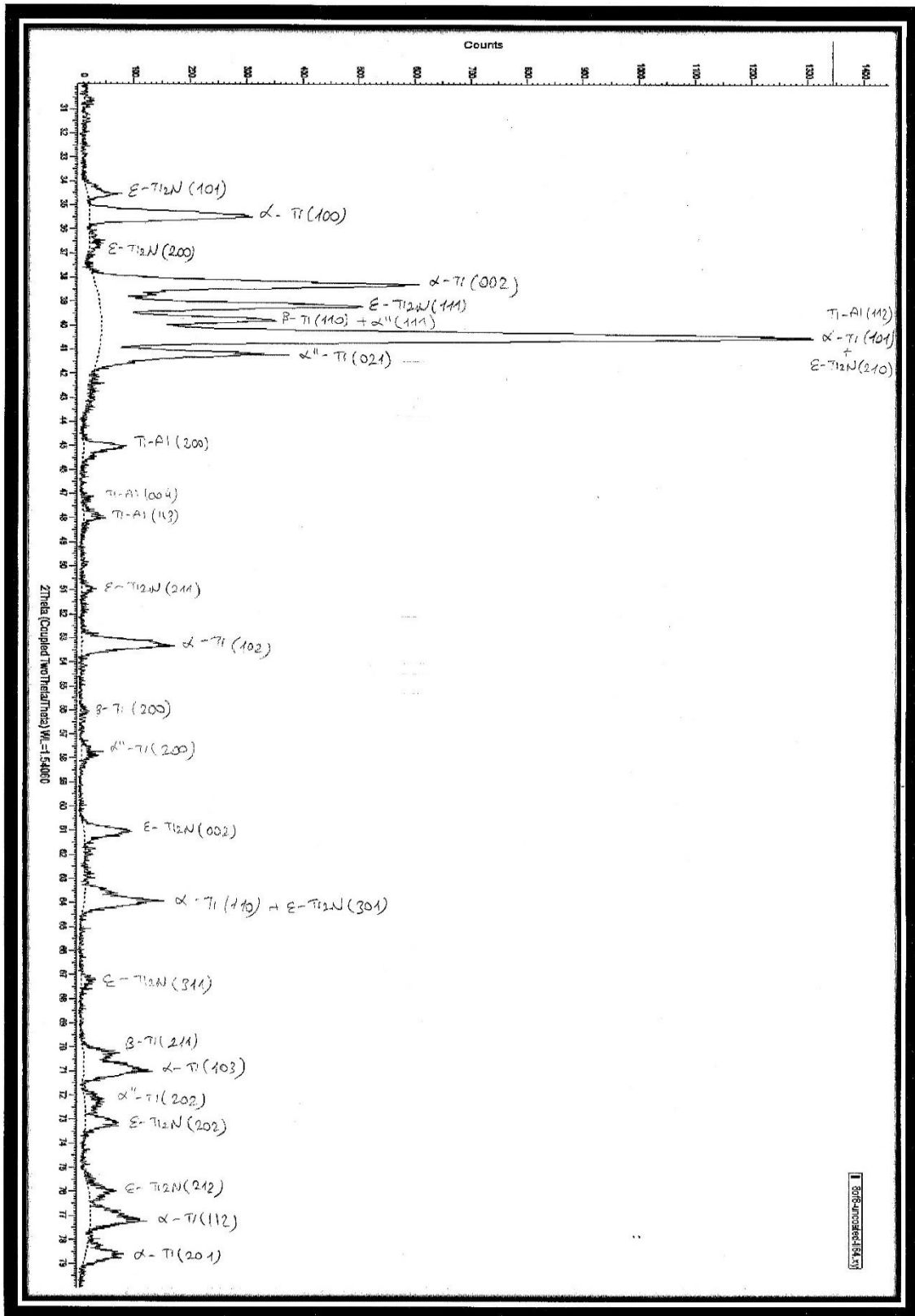
Figure 5-23 GAXRD (2º angle of incidence) diffraction pattern of uncoated Ti-64 substrate nitrided at 700ºC for 8 hours

The uncoated Ti-AVM substrate showed only minor differences in nitrogen concentration on the surface after 8 hours of TPN treatment. The nitrogen concentration was about 12 at. % after 4 hours, and the concentration rose only slightly to about 16 at. % after 8 hours of treatment. The XRD patterns for the uncoated Ti-AVM substrate (Figure 5-22) however showed stronger alpha peaks, with the other peaks similar to the XRD pattern obtained after 4 hours nitriding (Figure 5-8). There is no sign of any nitride phases such as Ti_2N. The nitrogen concentration at the surface is lower than expected although the duration of the process is doubled. The reason for this can be explained by the nitrogen diffusion coefficient of the β-Ti which (as discussed earlier) is reported to be as much as 3 orders of magnitude higher than in α-Ti. The higher diffusion coefficient value allows the interstitial nitrogen inside the β titanium alloy to disperse more quickly and accordingly it is difficult to accumulate nitrogen near the surface at a level sufficient to provide a significant hardening effect. There is an exciting point that the EDX results and XRD patterns for the uncoated Ti-AVM substrate after 8 hours nitriding treatment show very good agreement with the Ti-Mo-N ternary phase diagram prediction (Figure 5-15). The Thermocalc estimation made for Ti-Mo alloys at 700°C suggested that N can be dissolved at a maximum of 16 at. % without creating nitride phases. The EDX value for nitrogen is 15.7 at. %. Moreover, there is no sign of any nitride phases. In conclusion, it can be understood that the nitriding of β titanium alloy is difficult (in the context of generating a useful hardening effect) different process parameters are needed to get better nitriding efficiency. An increase in process duration alone may not be enough to create significant interstitial hardening and/or nitride phases on the surface. This known (suspected) property of β titanium alloys was one of the starting points of this study because there is a need to develop surface deposition of PVD metallic coatings before the nitriding process to produce effective thermochemical hardening process.

5.5.1.1 XRD Analysis at Different X-ray Penetration Depths

The Glancing angle mode of the XRD technique allows adjusting the depth of X-ray penetration by changing the incident angle of the X-rays. All samples were (until this stage) examined with 2° angle of incidence. The aim of selecting a lower glancing angle was to determine the crystal structure of the PVD metallic surface coatings before nitriding and to analyse any nitride compound layer formation after the nitriding. Any substrate contributions were inhibited by selecting the 2° angle of incidence, but despite all efforts, the substrate peaks were presented on the XRD diffraction patterns (especially after the nitriding treatments). The reason for this (firstly) is the thickness of the deposited coatings or formation of a nitride layer. Ti or Ti-Nb surface layer coatings did not show any problems because the thickness of these coatings was always higher than the possible X-ray penetration depth. However, after nitriding treatment, it was observed that the remaining coatings were not uniform, and the edge of the samples behave as uncoated because of the "plasma edge effect" especially at 700°C (will be discussed in Section 5.5.3). These phenomena increase the probability of having substrate peak in the XRD pattern although the 2° angle of incidence was used.

A new set of XRD experiments was established to analyse the desired interval of the XRD patterns (i.e. between 30-50°) from 2 to 10° angle of incidence, and thus the phase dependence could be detected by increasing the depth of penetration. The X-ray penetration was calculated (by using the AbsorbDX software) to give an idea related to the angle of incidence. The penetration depth was found from 0.8 to 3.3 µm for pure Ti metal from 2 to 10° angle of incidence (for the Cu Ka1 line and intermediate 2θ values of 40°). The depth of the penetration calculation for Nb metal showed a depth range from 0.6 to 2.4 µm. This range was calculated for an uncoated Ti-64 substrate from 0.9 to 3.6 µm from 2 to 10° angle of incidence. All these values showed that a set of comparable measurements could be performed (from near the surface) by using the 2-10° angle of incidence range while the X-ray penetration depth

calculation for the θ-2θ type of XRD measurement (not glancing angle mode) showed approximately 5 μm. The XRD patterns were placed together in DIFFRAC.EVA software.

The Figure 5-24 shows the GAXRD diffraction patterns (2° to 10° angle of incidence) of the uncoated Ti-64 substrate with TPN700 treatment applied for 8 hours. The XRD patterns can be followed by the given colours. The black line which belongs to the 2° angle of incidence showed lowest intensities for α-Ti phase, and it did not show any β-Ti peaks. The reason for this because the surface of the Ti-64 substrate is (almost) completely modified after 8-hour TPN700 treatment. On the other hand, the Ti_2N peak is the highest peak for the 2° angle of incidence (the red line which belongs to the 4° angle of incidence showed a similar trend for Ti_2N). Moreover, the intensity of the Ti_2N peak is decreasing from 2° to 10° angle of incidence. The martensitic Ti (α") phase is also lowest for the 2° angle of incidence (the pink line which belongs to the 10° angle of incidence showed a similar trend for α"-Ti). And the intensity of the α"-Ti peak is decreasing from 2° to 10° angle of incidence. The β-Ti increases its intensity from 4° to 10° angle of incidence. The Ti-Al phase has the lowest intensity for the 2° angle of incidence (the pink line which belongs to the 10° angle of incidence showed a similar trend for Ti-Al phase). All these findings (the positions and intensities of the peaks depend on the different depth profiles) showed that the major phase of the surface of the uncoated Ti-64 substrate (after 8 hours TPN700 treatment) is a Ti_2N phase. After this level, the α-Ti and β-Ti phases are coming to light with 4° angle of incidence, and the phase structure has also started to decompose to α"-Ti and Ti-Al phases. It is obvious that, besides the Ti_2N phase, the α"-Ti and Ti-Al lose their intensities in the 10° angle of incidence line which shows that these phases are located between the surface Ti_2N phase and the core of the substrate. As a conclusion, the expected phase structure of the uncoated Ti-64 after 8-hour TPN700 treatment contains sub-layers which the predicted model can be seen in Figure 5-25. It should also be mentioned that

the penetration depth of the X-rays does not increase linearly with increasing the angle of incidence from 2° to 10°.
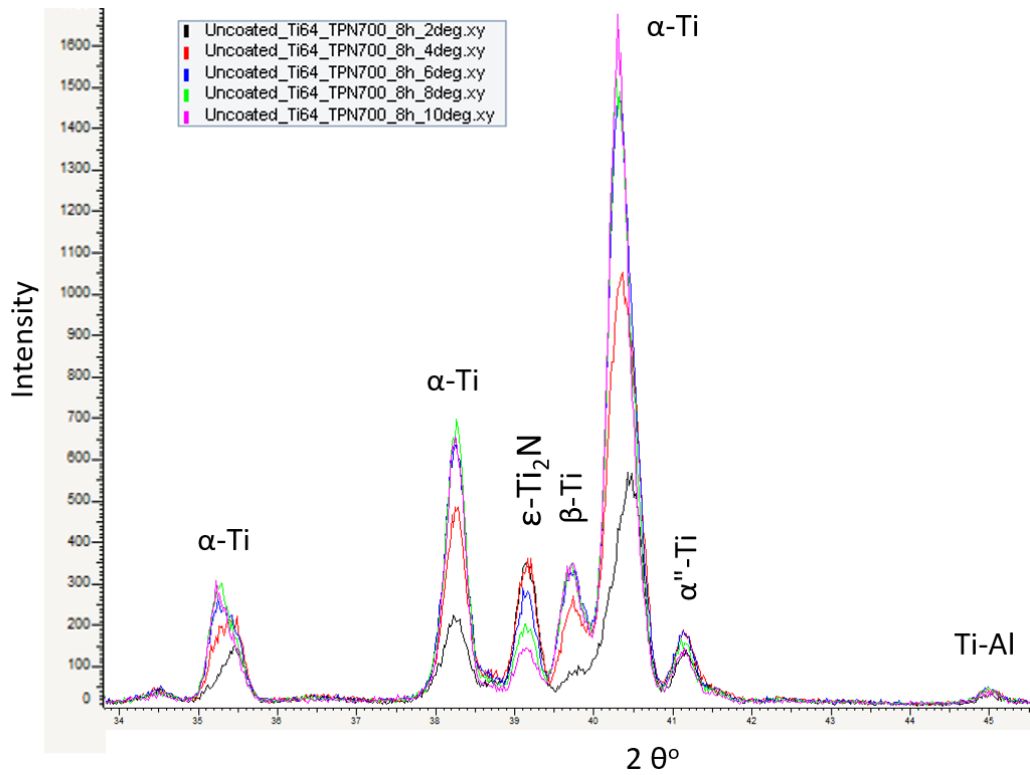
Figure 5-24 GAXRD (2° to 10° angle of incidence) diffraction patterns of uncoated Ti-64 substrate nitrided at 700ºC for 8 hours
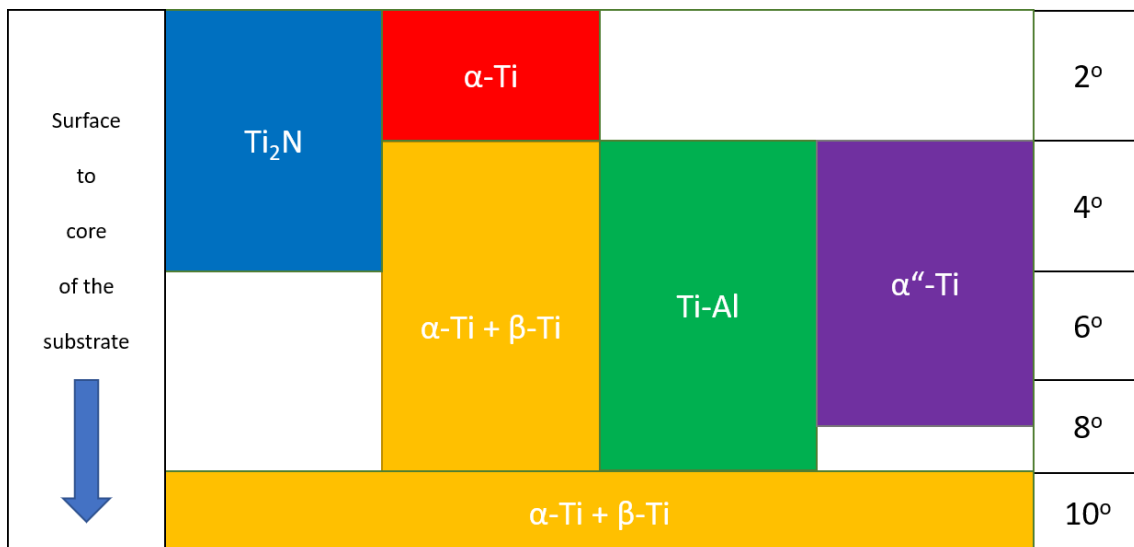
Figure 5-25 The estimated phase positions (based on the different glancing angle X-ray penetration depth) in uncoated Ti-64 substrate nitrided at 700ºC for 8 hours

The disappearance of the β-Ti phase was determined from the GAXRD patterns which were performed by using the 2° angle of incidence for the uncoated Ti-64 substrates which TPN500 and TPN600 treated for various durations. The θ-2θ XRD method (in which the X-rays penetrate approximately 5 μm depth) also proved that the beta peaks are not available or almost gone depending on the type of treatments (compared to the untreated substrate). These findings suggest to us that the 8-hour TPN700 samples could be analysed by using the θ-2θ XRD method from 30° to 50° to see all available phases. This will reduce the risk of remaining coating thickness which could be higher than the penetration depth of the 2° angle of incidence mode. The results of the θ-2θ XRD pattern (see Figure 5-26) showed only the α-Ti peaks as a major phase, and the other phases were seen very weak or not seen depend on the amount and position of the phases (such as Ti-Al phase). No extra phase appeared with θ-2θ XRD method for the Ti-64 substrate.
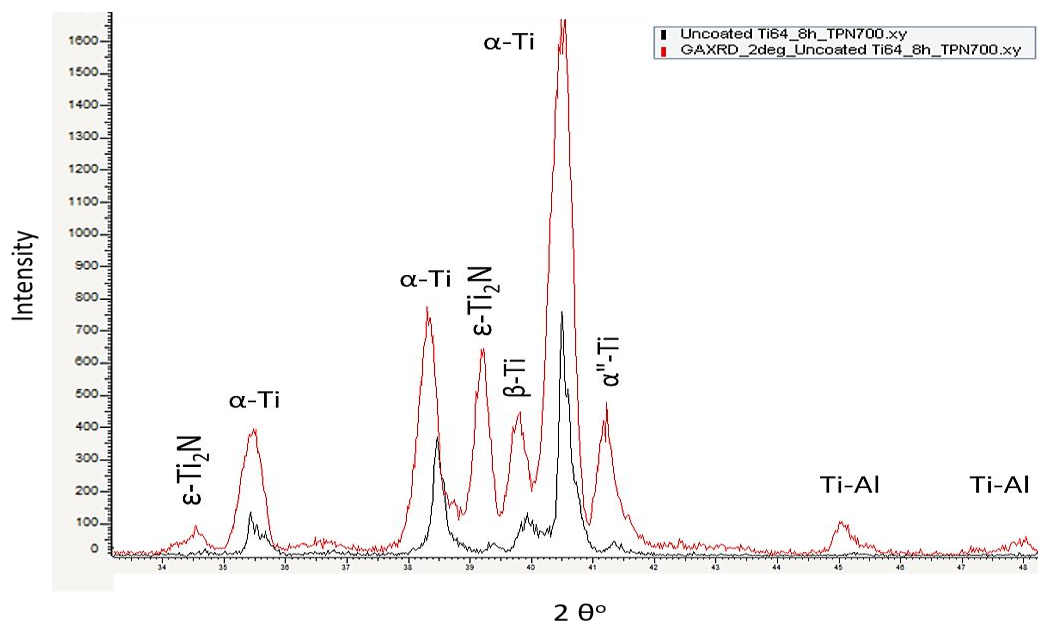
Figure 5-26 GAXRD (2° angle of incidence) and Theta-2theta (black) diffraction patterns of the uncoated Ti-64 substrate treated at 700°C for 8 hours

The θ-2θ XRD pattern for Ti coated Ti-64 did not show the Ti_2N and Ti-Al phases, suggesting that the amount of this phase is very small compared to the measured XRD volume. The Ti-Nb coated Ti-64 substrate (which did not show α"-Ti and Ti-Al phase in its GAXRD result)

which the remaining coating is about 1.95 μm (see Table 5-7) after 8-hour TPN700 treatment showed only α-Ti (substrate peaks) and β-Ti (coating peaks). There is no extra peak observed.

The uncoated Ti-AVM substrate θ-2θ XRD patterns appeared similarly with an untreated Ti-AVM substrate XRD pattern. The α-Ti peaks (formed by the effect of nitrogen) was not seen. The Ti-coated Ti-AVM substrates showed a very similar trend to the Ti-coated Ti-64 substrate after nitriding, in which the intensity of α"-Ti phase decreased and disappeared the Ti_2N and Ti-Al phases. The GAXRD pattern of the Ti-Nb coated Ti-AVM substrate showed no α"-Ti and Ti-Al phase in this sample. In the θ-2θ XRD pattern of the Ti-Nb coated Ti-AVM substrate, two different β-Ti phases (with different peak positions) could be seen which belonged to substrate and coating respectively.

The θ-2θ XRD patterns also showed some difference between the peak positions. It can also be seen in Figure 5-26 that the same peak (i.e. α-Ti (002)) which belongs to GAXRD pattern is placed on the lower angle than the θ-2θ XRD pattern. The reason for this difference is related to the concentration of nitrogen inside the Ti grains which stand near the surface is high. It is allowing the α-Ti peaks to shift to the lower angle. On the other hand, the α-Ti peaks for the θ-2θ XRD pattern are mostly coming from the core of the substrate in which the amount of nitrogen is lower than the surface.

5.5.2 The surface and cross-sectional morphology

Beside the Nb concentration seen by EDX on the surface of Ti-Nb coated Ti-64 and Ti-AVM substrates (which suggested that the Ti-Nb PVD surface layer remained after 8 hours of nitriding treatment), the optical microscopy images from the surface of treated samples and the SEM cross-sectional images were also helpful to prove the continued presence of not only the Ti-Nb but also the pure-Ti surface layer coatings. The optical microscopy images of the surface topography of samples treated at 700ºC for 8 hours can be seen in Figure 5-27. The significant

change in the surface morphology can be seen in Ti coated (g), and Ti-Nb coated (h) Ti-AVM substrates if they are compared with the images after 4 hours nitriding process (in Figure 5-11). The images for Ti coated (g) and Ti-Nb coated (h) samples after 4 hours nitriding process (Figure 5-11) showed a similar morphology with the uncoated substrates (f). On the other hand, the Ti coated (g) and Ti-Nb coated (h) samples after 8 hours nitriding process did not show a similar morphology with the uncoated substrates (f). Their microstructures looked like a nitrided uncoated Ti-64 substrate's microstructure (small grained). This supports the fact that both Ti and Ti-Nb 5 µm thick coatings survived after 8 hours nitriding process. If all the coatings would sputter off, the microstructure will be shown as the underlying substrate microstructure as seen in Figure 5-11 for the 1.25 µm thin coatings.
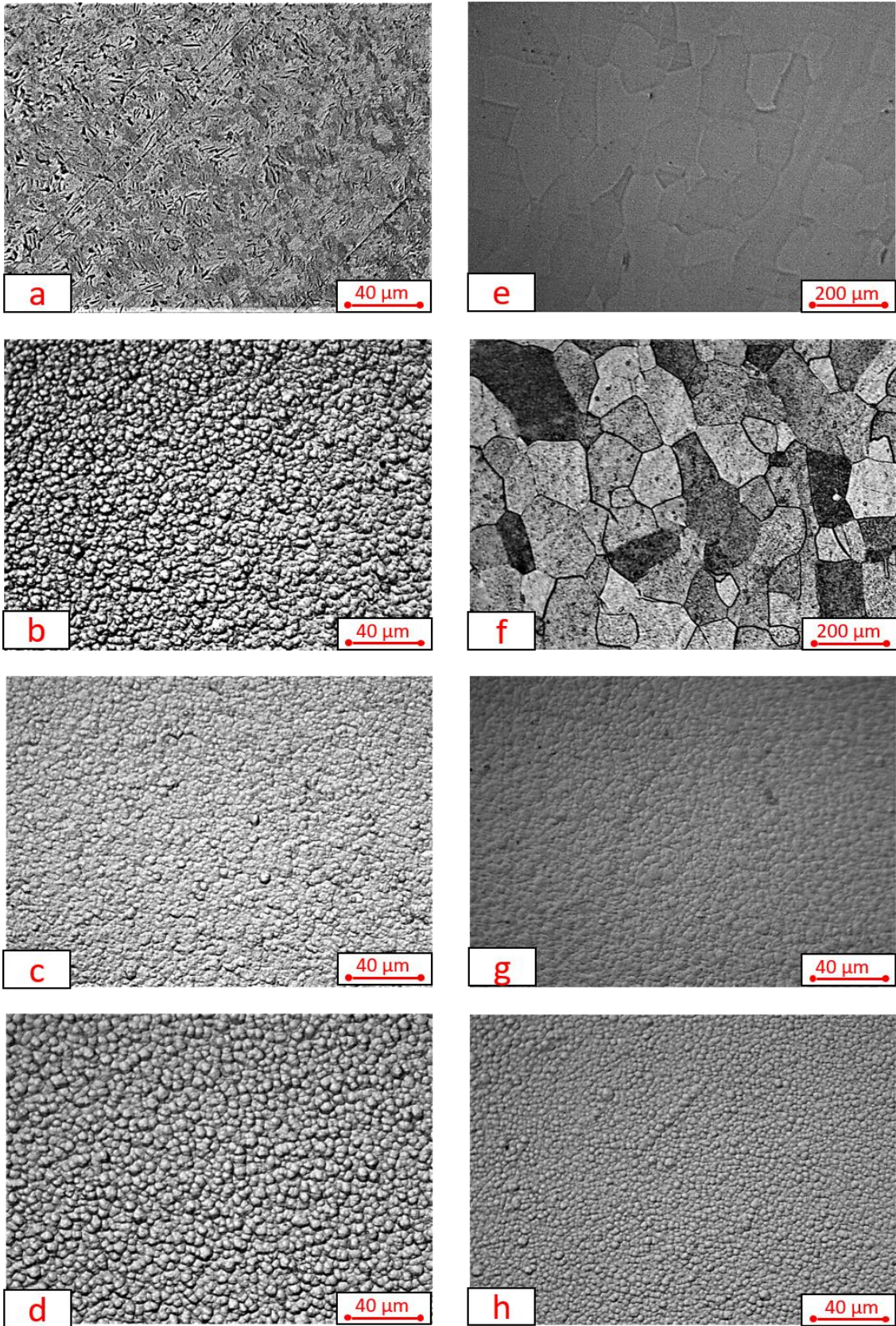
Figure 5-27 Optical microscopy images of the surface topography of samples treated at 700ºC for 8 hours. (a) untreated Ti-64 (b) uncoated Ti-64 (c) Ti coated Ti-64 (d) Ti-Nb coated Ti-64 (e) untreated Ti-AVM (f) uncoated Ti-AVM (g) Ti coated and (h) Ti-Nb coated Ti-AVM

The SEM cross-sectional images of samples nitrided at 700ºC for 8 hours can be seen in Figure 5-28. The BSE mode of the SEM technique showed the different contrasted areas which are very significant for Ti-Nb coatings on Ti-64 substrates because of the higher atomic number of Nb atoms. On the other hand, the contrast difference can be seen for Ti coatings on Ti-AVM substrates because of the Mo atoms inside the substrates which have a higher atomic number than Ti atoms. The atoms which have higher atomic number show a the brighter image in BSE mode [197]. The compound layer which formed after 8 hours nitriding process for the uncoated Ti-64 substrate is approximately 1.50 μm thick, which followed by a bright layer containing vanadium-rich grains. The compound layer was about 0.85 μm thick after nitriding for 4 hours. By the effect of the process duration, the thickness of the compound layer was increased. Moreover, it is still not a rigid compound layer which can be seen in Figure 5-28 (a), that the nitride grains were grown from the surface as a columnar structure. The behaviour of the uncoated Ti-AVM substrate after 8 hours nitriding process was very similar to after 4 hours process. The XRD patterns did not show any sign related to ceramic nitride phase. A modified zone which contains nitrogen stabilised α phase with acicular (needle-like) feature was seen (again) near the surface of the Ti-AVM substrate. The thickness of this structure increased 1.20 μm to 1.50 μm by increasing the time from 4h to 8h which also shows more alpha stabilisation happened by increasing process duration.
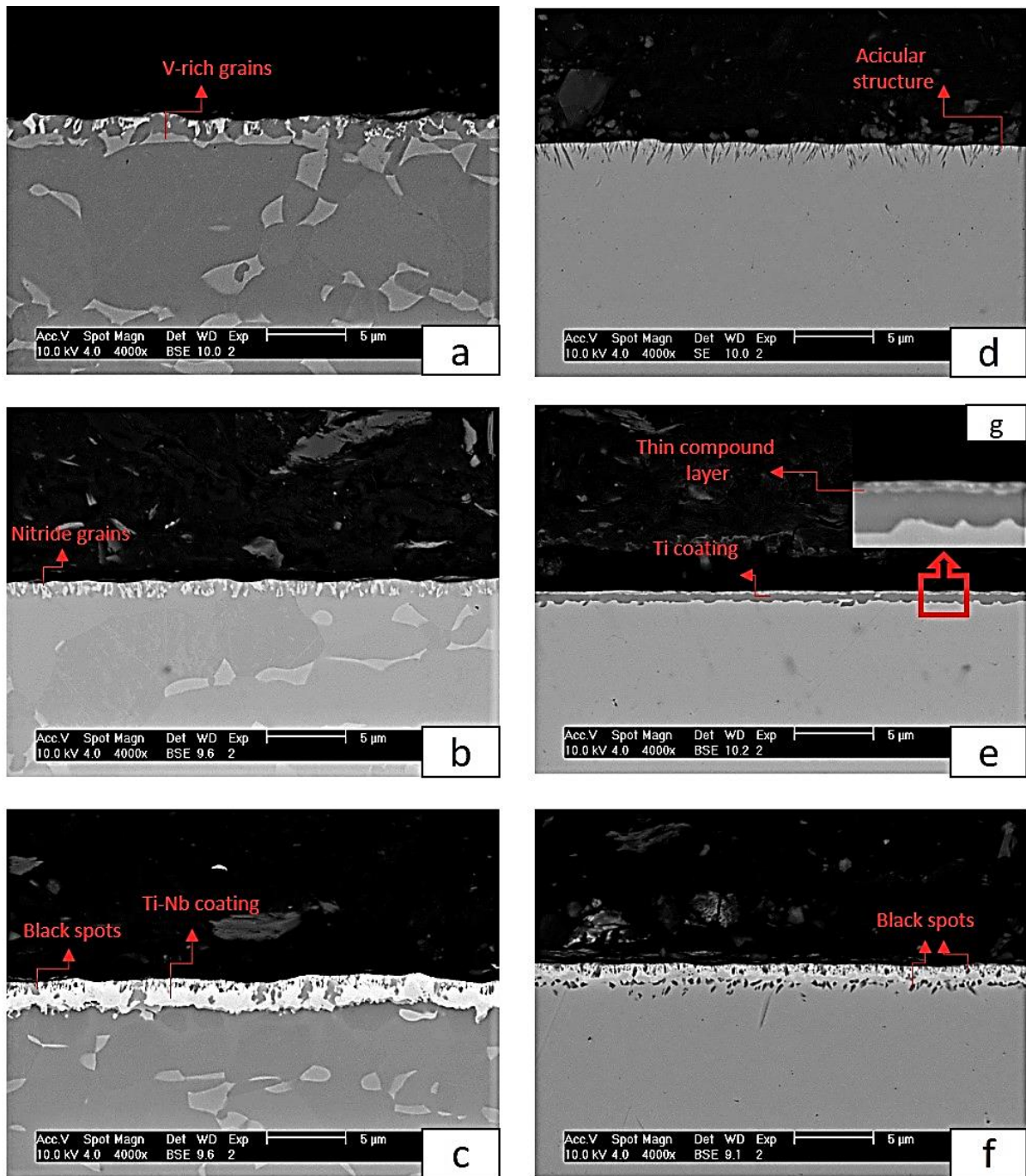
Figure 5-28 SEM cross-sectional images of the samples treated at 700ºC for 8 hours.
(a) uncoated Ti-64 (b) Ti coated Ti-64 (c) Ti-Nb coated Ti-64 (d) uncoated Ti-AVM (e) Ti coated and (f) Ti-Nb coated (g) zoomed Ti coated Ti-AVM

The Ti-coated Ti-AVM substrate showed different final nitride morphology than the Ti coated Ti-64 substrate. It is seen clearly from the cross-section SEM image in Figure 5-28 (e) that the Ti coating still remains and its maximum thickness is about 0.85 μm. XRD results also showed 2 different peaks of Ti_2N phase for the Ti-64 substrate on the other hand only one and small

Ti$_2$N peak was seen for Ti-AVM substrate. It was previously seen that the nitride grains were formed in the coating structure. In this case, nitride phase formed as a thin compound structure which can be seen in Figure 5-28 (g). The reason for these two different nitride structures (for Ti coated Ti-64 and Ti-AVM) must be related to the type of the substrate because all other process parameters were the same (performed in the same chamber/run).

The position of the samples inside the nitriding chamber can be seen in Figure 5-29. The three groups of the sample (on the right) are the Ti coated, Ti-Nb coated and uncoated Ti alloy samples respectively. The piece of Ti metal in the middle is connected to the thermocouple. The three samples (on the left) are control samples and second thermocouple. The identically coated samples (i.e. Ti coated Ti-64 and Ti coated Ti-AVM) were hanged back to back. The paired samples were wrapped tightly with steel wire (from their upper part by opening notches), so it can be given a grant to contact the samples with each other. In this circumstance, the temperature of these substrates must be same (at least for the couples). The samples in each pair would act as one piece of sample, and so the current density on both substrate's surface should be same which would affect the nitriding performance. As a result, the different nitrogen diffusion rates of these two different substrates (the higher nitrogen diffusion was expected for Ti-AVM substrate) would affect the nitriding behaviour of the Ti coatings (on them) because two different nitriding phenomena (for coating and substrate) were taken place in the same time.
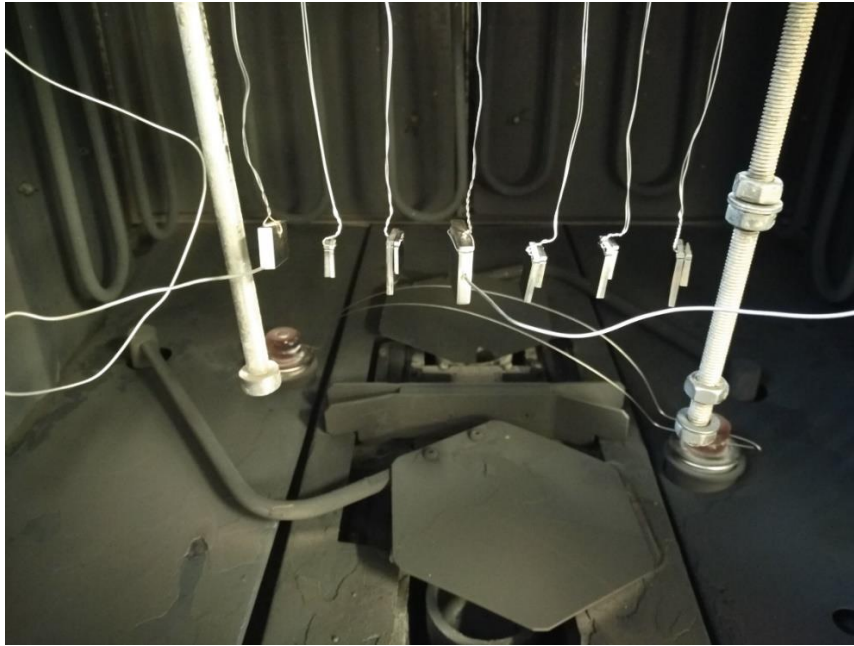
Figure 5-29 The sample positions inside the nitriding chamber

The structure of the remaining Ti-Nb coatings on the Ti-64 and Ti-AVM looks similar. The black spots (acicular structure) on the coatings (see in Figure 5-28 c and f) shows the nitride grains which was also proved with XRD examinations (see in Figure 5-21 and Figure 5-22). The same spots were seen both on coating and substrate for Ti-Nb coated Ti-AVM substrate (same as uncoated Ti-AVM). It is showing the alpha stabilisation near the coating substrate boundary. For the Ti coated Ti-AVM substrate, the spots formation (on the substrate) is found less than the spots formed for Ti-Nb coated Ti-AVM substrates after 8-hour nitriding process (the comparison of Figure 5-28 e and f). Therefore, it can be said that the effect of the faster nitrogen diffusion in Ti-Nb coating leads to the more alpha stabilisation for Ti-Nb coated Ti-AVM than the Ti coated one.

5.5.3 The Analysis of the Remaining Surface Coating Layer Thickness after Nitriding Process

The scenario for the Ti and Ti-Nb coated substrates are a little different due to the deposited surface layer coatings which were thicker than the previous run. The starting Ti surface layer coating thickness before 8 hours nitriding process was 4.85 μm. (It was planned to deposit 5 μm but the 3 % error for thickness estimation is fairly normal for the coatings produced by plasma coating technologies). The "maximum" 1.40 μm Ti coating left on Ti-64 sample after 8 hours nitriding process was measured. The remaining thickness values for all samples can be seen in Table 5-7.

Table 5-7 The thickness of the remaining surface layer coatings after the nitriding process

Sample	Temperature (°C)	Duration (h)	Coating Thickness (μm)		Thickness reduction (%)
			Before Nitriding	After Nitriding	
Ti coated Ti-64	700	8	4.80	1.40	71
Ti-Nb coated Ti-64	700	8	5.05	1.95	61
Ti coated Ti-AVM	700	4	4.80	3.35	30
Ti coated Ti-AVM	700	8	4.80	0.85	82
Ti-Nb coated Ti-AVM	700	4	5.05	3.00	40
Ti-Nb coated Ti-AVM	700	8	5.05	1.50	71

It was expressed as "maximum" for the remaining surface coating layer's thickness because the remaining thickness was not uniform. The highest thickness was seen in the middle of the substrates, and the thickness was observed to decrease from the middle of the samples to both

edges. This phenomenon can be termed as the "plasma edge effect". This effect is most powerful on edges and corners and decreases its effect towards to the centre of the substrates. The plasma edge effect can be seen clearly in Figure 5-30. Due to the bigger grain size of the Ti-AVM substrate underlying Ti coating, it was given as an example. The blue arrow shows the direction from the edge to the centre of the substrate. It can be seen three different morphologies in the image that the first are (between a and b) is most affected part of the sample which the coating sputters off entirely. The grains can be seen misty in the area (between b and c) that this tells there is still coating left, but the thickness is lower than the area between (point c) and the centre of the sample because the grains cannot be seen from (point c).
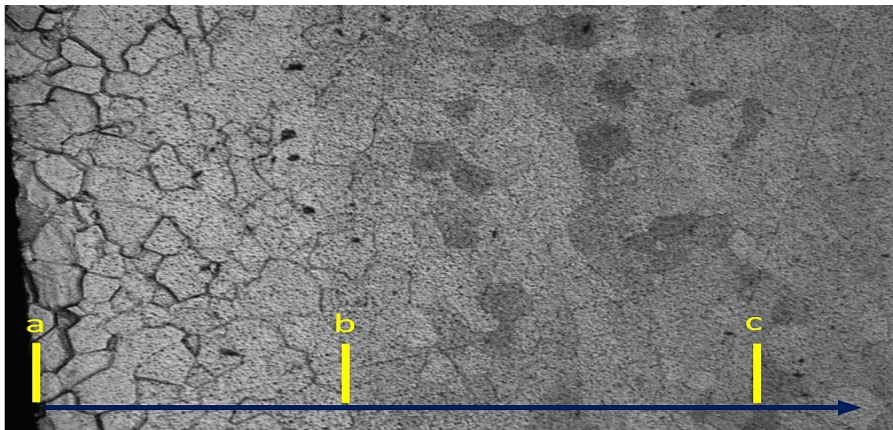
Figure 5-30 Optical microscopy images of the surface topography of Ti coated Ti-AVM substrate after 8 hours nitriding process at 700ºC showing the plasma edge effect

Due to this effect, the coatings which remain after 8 hours nitriding process were found to be non-uniform. To analyse this, the remaining coating thickness was measured from one side to the other (at 1 mm intervals). The remaining coating thickness distribution of Ti-Nb coating deposited on the Ti-64 substrate can be seen in Figure 5-31. The "dome shape" trend shown in the figure explains the significant plasma edge effect. (Here Ti-Nb coating is given as an example because of its higher remaining coating thickness rather than Ti coating deposited on the Ti-64 substrate and the easy application of thickness measurement in SEM examination due to its good contrast between the coating and the substrate).
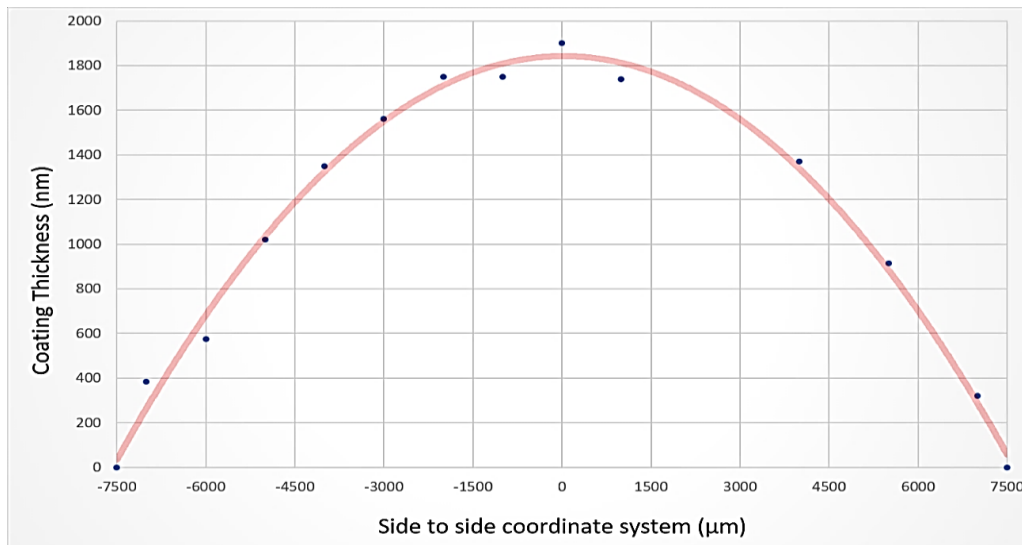
Figure 5-31 The coating thickness distribution of the remaining Ti-Nb surface layer coating (on Ti-64 substrate) after 8h nitriding process at 700ºC

There is also a difference in the rate of change of coating thickness of the Ti surface coating between the two substrates after 8 hours nitriding (see Table 5-7). Although the initial thicknesses of the Ti surface coatings were the same (4.80 µm), the final thicknesses were found different for Ti-64 and Ti-AVM substrates. If the nitriding performance of these two different substrates is believed equal, the differences may be attributed to the resputtering of nitrogen (or nitride grains) at the surface of Ti coated Ti-64 is slower than the Ti coated Ti-AVM (which these phases found different structure). This could be because nitrogen cannot diffuse inward so quickly in Ti-64.

The diffusion phenomena of the additional elements (rather than interstitial nitrogen) was also seen inside the Ti-64 substrate. Some movement of the Al and V atoms in the uncoated Ti-64 substrate after 8 hours nitriding process was observed (a randomly taken EDX map can be seen in Figure 5-32). This map also proves how a bright layer (vanadium-rich) follows the surface nitrogen-rich area. In some grains, the V concentration was seen at about 15-16 at. %. The deficiency of Al in this vanadium-rich area may cause formation a different phase such as martensite Ti phase. The grains in Fig 5.24 (a) and (b) are strongly etched and show a plate-

like structure. These plates may be related to α'' Ti (martensite). The movement of Al towards to the sample surface may be the reason for the formation of Ti-Al intermetallic phase.
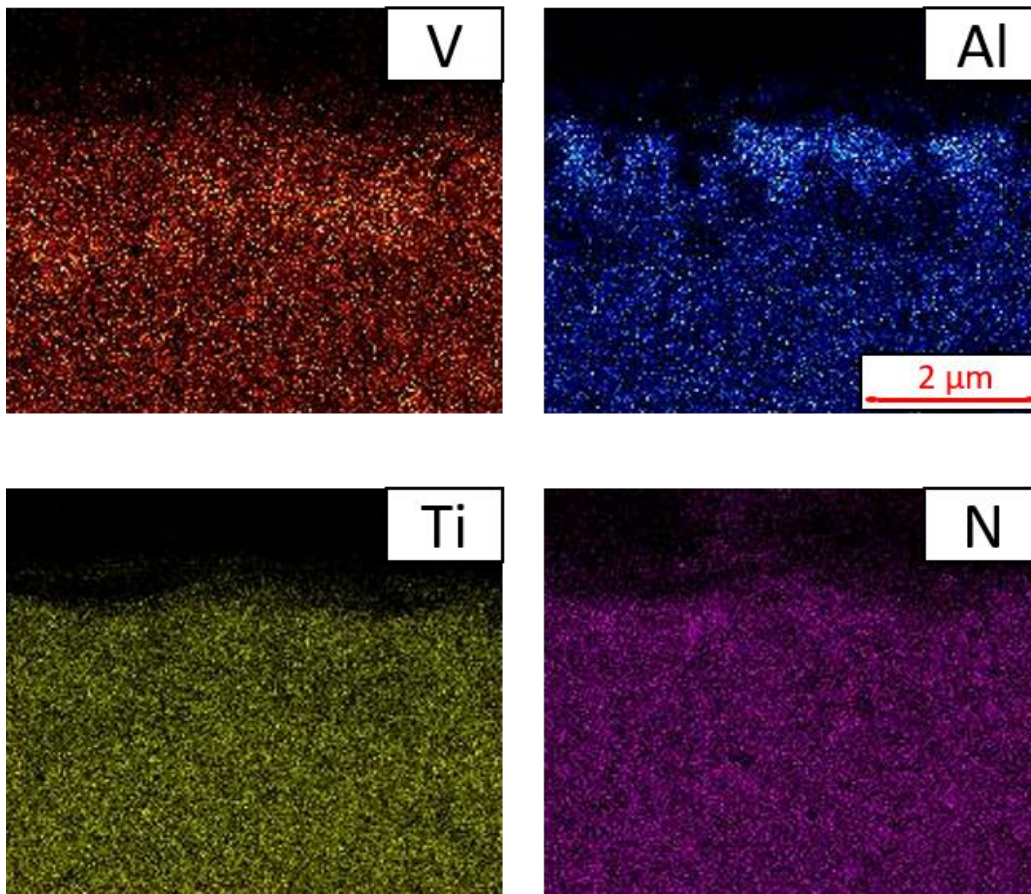
Figure 5-32 The EDX map taken from the cross-section of the uncoated Ti-64 treated at 700ºC for 8 hours (The dark black shows the carbon mounting material)

The contrast differences between some grains (see Figure 5-28) suggest that there are some concentration changes between those grains inside the substrate. These movements suggested that surface coating elements could also diffuse inside the substrate. A couple of EDX analyses were performed from various points (near the surface) from the cross-section of the Ti-Nb coated Ti-64 substrate (TPN treated for 4 hours). This sample is very critical for this study because there is no Nb inside the substrate and the thin (1.25 µm) coating was sputter removed (the surface EDX results show no Nb after 4 hours nitriding process). To see any Nb diffused inside the substrate, some EDX measurements were taken from the grains near to the sample surface. It was observed (from cross-sectional EDX analyse) that the bright grains (which were

the β-Ti grains) include about 2-6 at. % Nb. This finding shows that the PVD surface layer elements are also diffusing inside the substrate. As a result, the 11 % difference between the remaining Ti thickness for different substrates (see Table 5-7) could be related the diffusivity of Ti in the two different crystal structured titanium alloys. The Ti-Nb coated Ti-64, and Ti-AVM substrates also have a different final thickness which can be seen in Table 5-7. The change rate is about 10 % more for Ti-AVM substrate, and these bidirectional changes could be expected for Ti-Nb coated Ti-64 and Ti-AVM substrates. In this case, the Ti and Nb diffusivity (together) inside the two different titanium alloys may lead to this difference.

The nitriding process done here is also a vacuum heat treatment process which leads to diffusion of the elements (temperature and time-dependent process). Therefore, the temperature for all samples should be kept the same. The samples were placed (see in Figure 5-29) very close to each other (with 4 cm intervals) to obtain the similar effect from the plasma heating stage after 400°C (all temperature change was watched with two thermocouples and logged). The temperature change can be sensitive because the process is applied at a relatively high temperature (700°C). On the other hand, the comparison of different surface coatings on the same type of substrate would give some valuable information. For example, the thickness reduction of the Ti coating is 10 % more than for the Ti-Nb coating (both deposited on Ti-64), and 11 % more for Ti coated Ti-AVM substrate (seen in Table 5-7). Because of the sputter yield of the Nb atom is higher than Ti atom (previously discussed in section 4.2.3), the Ti-Nb coating was expected to sputter off more than Ti coatings in same process conditions. However, it does not happen as expected and one of the reasons for this could be the different diffusion rate of the coatings inside the substrates. The slower diffusion rate of Nb atoms [198], [199] (compared to Ti atoms) inside the titanium alloys can lead to this difference. Another reason for this may be related to the changing sputter yield mechanism during nitriding. When the process is starting, the surface layer coatings are metallic, but they are changing their structures

with the diffusion of the nitrogen. The interaction of the Nb with nitrogen may affect the sputter yield of the Ti-Nb coating by decreasing its expected rate (the rate of nitride formation for each coating is different). And, finally, this will affect the remaining coating thickness.

5.5.4 The Surface Hardness Measurement

The 8-hour nitriding process applied to thicker surface layer coatings showed different surface hardness results because of the nitriding behaviour of the remaining coating (the nitriding behaviour of the underlying substrate can affect the hardness results). Thus, the nitriding performance of the coating/substrate pairs were analysed together to clarify the results. The surface hardness data for the uncoated and coated Ti alloy substrates treated at 700ºC for 8 hours can be seen in Figure 5-33.
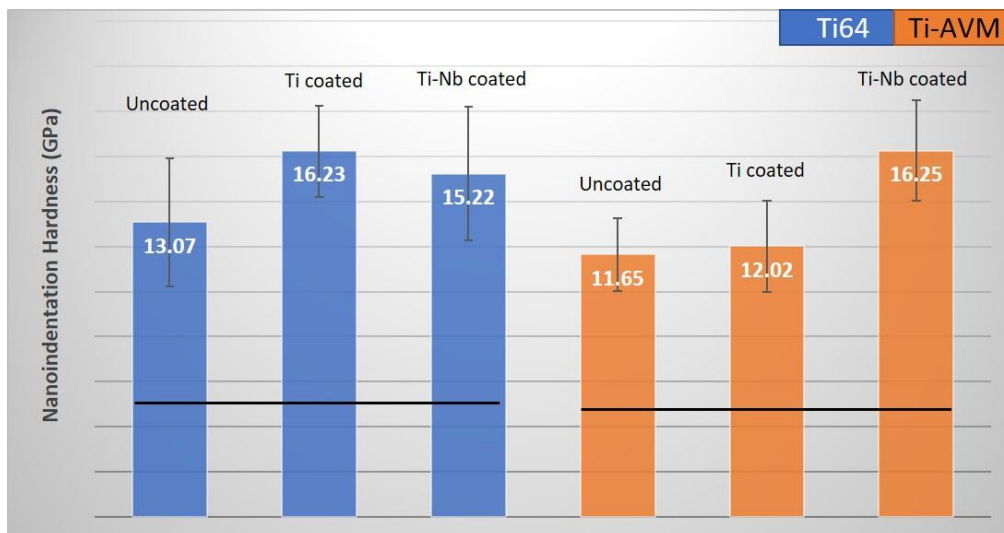
Figure 5-33 Near-Surface nanoindentation hardness data for Ti-64 and Ti-AVM substrates treated at 700ºC for 8-hours

The positive effect of the process duration on the surface hardness values is clearly seen for uncoated Ti-64 and Ti-AVM substrates (compared to 4-hour TPN700 treatment, see Figure 5-20). The increase in nitrogen concentration on the surface and the increased the thickness of the nitrided zone may be the reasons for increasing hardness. On the other hand, the hardness values for the Ti and Ti-Nb coated substrates are higher than for the uncoated ones after TPN

treatment. This is related to the remaining coating on the surface; i.e. the nitriding performance of the surface coating affected the final surface hardness values. It was previously shown that the Ti coatings (deposited on two different Ti alloy substrates) have different nitride structures and this affected the surface hardness results. The formation of the nitride grains inside the Ti coating for the Ti coated Ti-64 substrate (see Figure 5-28 b) ended up with a significantly higher hardness than the Ti coated Ti-AVM substrate which has a very thin compound layer. The lower hardness value for the Ti coated Ti-AVM substrate (although the surface EDX result showed about 33 at. % N) could be related to the weaker load support from the underlying substrate diffusion zone. It should be noted that the surface layer coating thickness (before nitriding process) should be selected by considering the type of substrate and other process parameters. The Ti-Nb coated Ti-AVM substrate showed also higher hardness values. The reason for this is the effect of nitride formation and better nitrogen diffusion into the substrate.

Figure 5-34 shows the surface roughness data after 8 hours nitriding of untreated, Ti coated, and Ti-Nb coated Ti-64 and Ti-AVM substrates. It was concluded from these data that uncoated substrates were invariably found to be rougher than Ti and Ti-Nb coated substrates after plasma nitriding (a similar trend which was seen after 4-hour TPN700 treatment). The positive effect of the surface layer coating on the final surface roughness after the nitriding process was again observed. The greatest reduction in surface roughening was seen for the coated Ti-AVM substrates (as expected) and both types of surface coatings did their job well by keeping the final surface roughness values lower. The Ti-Nb coated Ti-AVM substrate showed a slightly higher surface roughness value than the Ti coated Ti-AVM substrate, but the small difference can be neglected since the error bars overlap (i.e. the difference is not statistically significant). Overall, the coated Ti-AVM substrates showed less surface roughness values than the coated Ti-64 substrates. The fine, nanocolumnar and highly textured morphology of the coatings provides the reduction in roughness by sputtered off very uniformly.

On the other hand, Ti-Nb coating did not give any positive effect on surface roughness for Ti-64 substrate which was also verified with AFM three dimensional topographic maps (it can be seen in Figure 5-35). It was also seen in Figure 5-27 (b) and (d) that the surface topography of the Ti-Nb coated Ti-64 is very similar to uncoated Ti-64 after 8 hours nitriding process. The reason may be related to the higher process duration (8-hour) which leads to the formation of nitride grains (they are not as much as uncoated Ti-64, but the grains are coarser than uncoated Ti-64) on the top of the coating. Moreover, the adding of the better nitriding behaviour of the Ti-64 substrates compared to Ti-AVM substrate (nitride phase is the major reason for increasing the surface roughness) made this sample the roughest (compared to other coated samples). The nitride forming occurs more readily for both coatings on Ti-64 substrate since the substrate blocks inward diffusion of nitrogen compared to Ti-AVM substrate.
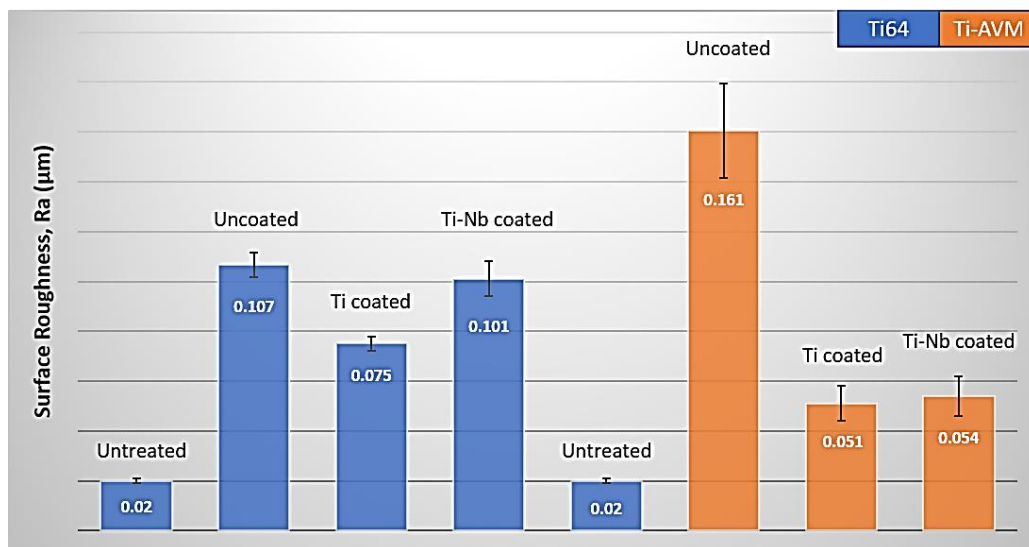
Figure 5-34 Surface roughness data for uncoated, Ti-coated and Ti-Nb coated Ti-64 and Ti-AVM substrates treated at 700ºC for 8 hours
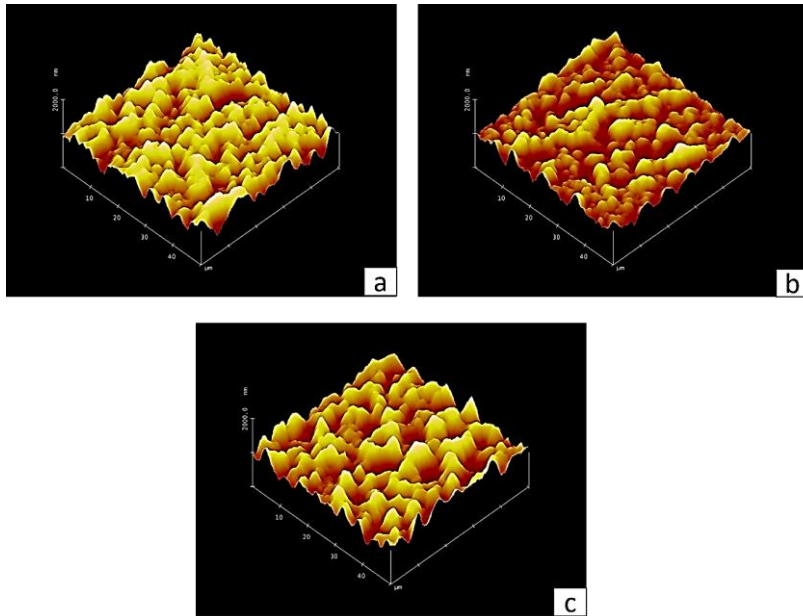
Figure 5-35 AFM 3D topographic maps of (a) uncoated, (b) Ti-coated, (c) Ti-Nb coated Ti-64 substrates treated at 700ºC for 8 hours

5.6 Summary

The uncoated Ti-64 and Ti-AVM substrates were plasma nitrided at various treatment temperature (500-700ºC) and durations (2-8 hours) to determine the better nitriding parameters. For titanium alloys, the 700ºC treatment was decided to be a better candidate to obtain considerable nitrogen diffusion. The surface layer coatings were deposited with different thickness depending on the treatment time. The following key points from this chapter can be drawn:

- TPN500 treatments resulted in no nitride compound layer formation (although it was applied for 8 hours) for both uncoated Ti-64 and Ti-AVM substrates. The β peaks disappeared by the treatment time for uncoated Ti-64 substrate. XRD peak shifting was determined for the uncoated Ti-AVM alloy by nitriding at 500ºC.

- The surface hardness change was observed after TPN500 treatments for both uncoated alloys. It is about 45 % hardness increase after 4-hour nitriding treatment. The increase of the treatment duration from 4 to 8 hours did not affect the surface hardness values further. The only 7 % hardness change was determined.

- TPN600 treatments showed some nitride phase peaks after the 4-hour treatment with some peak shifting for the uncoated Ti-64 alloy. This showed the increase of nitrogen concentration on the surface. On the other hand, besides the peak shifting, the formation of the α phase (α stabilisation) was also observed for uncoated Ti-AVM.

- The hardening effect of the TPN600 treatment on uncoated Ti-64 and Ti-AVM substrate was observed much stronger than TPN500 treatment. About 20 % hardness increase was observed when the 4-hour treatments were compared for 500 and 600ºC.

- The smooth surface finishing of the TPN500 and TPN600 treated samples allowed the Knoop hardness test to be applied although the penetration depth of the Knoop hardness test is bigger than the nanoindentation test, about 15 % hardness increase was seen for

TPN 500 treatment for 4 hours. The Knoop hardness values for TPN500 (8 hours) and TPN600 (4 hours) showed almost similar results which are about 30 % increase in surface hardness.

- TPN700 treatments (4 hours) showed significant changes for uncoated, Ti coated, and Ti-Nb coated Ti-64 substrates. Ti-AVM substrates demonstrated the same behaviour as seen in TPN600 treatment which is only peak shifting and formation of α phases. The EDX results (from the surface) showed about 12 at. % N for all samples.

- The "sputtering off" effect was observed for the Ti and Ti-Nb surface layer (1.25 μm thick) coated substrates after 4-hour TPN700 treatment. It may be one of the most valuable findings for this study because it directly affects the resultant performance of the samples. The EDX results showed zero Nb concentration after 4-hour plasma nitriding treatment which can be evidence for the disappearance of Ti-Nb coatings from the surface during plasma nitriding treatment.

- Although, the Ti_2N phase formed on the uncoated Ti-64 substrate after 4-hour TPN700 treatment, the EDX showed higher Al concentration for uncoated (treated) sample than the untreated substrate (12.9 at. % Al to 11.3 at. % Al). This can be explained the Al diffusion from inner side of the substrate to the surface direction during the nitriding treatment.

- The final surface roughness after TPN700 (4-hour) treatment seen significantly lower for previously Ti and Ti-Nb surface layer coated Ti alloys compared to uncoated Ti alloy substrates. The surface roughness value for Ti-Nb coated Ti-64 substrate found % 52 less than the uncoated Ti-64 substrate. The similar improvement was seen for Ti coated Ti-AVM substrate with a %67 decrease while comparing with the uncoated substrate.

- The different effect of Ti and Ti-Nb surface layer coatings on surface roughness results for the Ti-64 and Ti-AVM substrates was detected. The different "sputter off rate" of these surface layer coatings lead to this contrast because it is thought that the long-lasting surface layer coatings will provide more benefit to the substrates regarding final surface roughness.

- The cross-sectional SEM analysis also confirmed the nitride layer formation for Ti-64 substrates and the absence of nitride layer formation for the Ti-AVM alloy substrates. The different nitriding behaviours of the Ti alloys were tried to clarify by ternary phase diagrams. The amount of Mo can increase the amount of nitrogen solubility in β-Ti alloys. On the contrary, the amount of Al can decrease the solubility of nitrogen in α-Ti alloys.

- The cross-sectional hardness test showed that the hardening effect for Ti-Nb coated Ti-64 substrate is higher than other Ti-64 substrates which are related to the higher diffusion rate of nitrogen (in the β phase coating). Nitrogen can diffuse to the substrate faster and allows higher nitrogen concentration (thicker hardened zone) under the surface. On the other hand, the hardening effect for Ti coated Ti-AVM substrate is higher than other Ti-AVM substrates. It can be explained with a lower diffusion rate of nitrogen (in the alpha phase coating) allowing the slowdown of the of the nitrogen interstitials, and they can build up a hardening effect by increasing their concentration in near-surface rather than spreading inside the Ti alloy substrate.

- TPN700 treatments (8 hours) showed that the nitrogen concentration on the surfaces for all samples was increased. However, the behaviour of the nitrogen was seen to be different for uncoated and coated substrates because the thickness of the Ti and Ti-Nb surface layer coatings was selected as about 5 μm which allowed to survive until at the end of the process. The EDX results for Nb concentrations showed about 25 at. % which

also proved the presence of Ti-Nb surface layer coatings after 8-hour nitriding treatment.

- Ti and Ti-Nb surface layer coated Ti alloy substrates showed about 30-33 at. % N on their surfaces and all these four samples showed Ti_2N phase in their XRD diffraction patterns. The uncoated Ti-64 substrate was also showed Ti_2N phase by increasing its nitrogen concentration to about 26 at. %. The compound layer for Ti-64 substrates increased its thickness (0.85 to 1.50 μm). The uncoated Ti-AVM substrate remained stable (only peak shifting and α stabilisation). The increase of nitrogen concentration (compared to 4-hour treatment) on the surface was very limited which is only about 3 at. %. It is showing how difficult to accumulate nitrogen interstitials on the surface of β Ti-AVM alloys.

- The uncoated Ti-64 substrate, Ti coated Ti-64 substrate, and Ti coated Ti-AVM substrate showed extra peaks (after 8-hour TPN700 treatment) which belong to the Ti-Al intermetallic phase and α" martensitic phase. The X-ray analyses from the different depth of the samples showed that the uncoated Ti-64 substrate showed a layer-like structure which the upper part composed of thin Ti_2N phase and the Ti-Al and α"-Ti phases are following the ceramic nitride phase. The Ti-Al phase was expected to placed closer to the surface than the α"-Ti phase considering the diffusion of Al atoms. The mixture of the α-Ti and β-Ti phases were placed at the bottom of this layered structure. Moreover, the Ti-Al and α"-Ti phase were not appeared in the XRD patterns (neither GAXRD nor θ-2θ XRD method) of the uncoated Ti-AVM substrate, Ti-Nb coated Ti-64 and Ti-AVM substrates. It could be related to the nitrogen diffusion rate (faster for β Ti coating and alloy substrate) which can be an effect of the movement of the other additional element inside the Ti alloy substrates.

- The optical images (after 8-hour TPN700 treatment) from the surface of the Ti and Ti-Nb coated Ti-AVM substrates showed very different morphology than the samples which 4-hour TPN700 treated. This proves the Ti coating also survived until the end of the process. If all the coating would sputter off, the surface morphology will be shown as a coarse-grained structure which seen after 4-hour TPN700 treatment.

- The different nitriding behaviour for the remaining Ti coatings on the different substrates was determined from the cross-sectional SEM images. The nitride morphology of the Ti coated Ti-64 sample (after 8-hour TPN700 treatment) was found almost similar to the uncoated candidate. On the other hand, a very thin nitride layer was formed for the Ti coated Ti-AVM substrate and the remaining Ti protected its structure. This different nitriding behaviour of Ti surface layer coatings may be related to the different nitriding behaviour of the underlying substrate.

- The nitriding behaviour of the underlying Ti-AVM substrates showed different nitriding behaviour for Ti and Ti-Nb coated candidates. It showed significantly more alpha stabilisation near the coating substrate boundary for Ti-Nb coatings. It can be said that the effect of the faster nitrogen diffusion in Ti-Nb coatings caused more alpha stabilisation than the Ti coated one.

- The remaining surface layer coating thicknesses were not found uniform. The highest value was seen in the middle of the samples, and the thickness started to decrease towards to the edges (dome shape trend was observed) of the samples because of the "plasma edge effect". This effect was not clear for the 4-hour TPN700 treatment because there is no coating left at the end of the process.

- The "sputter off rate" for the surface layer coatings found for Ti coated Ti-64 is 71 %, Ti-Nb coated Ti-64 is 61 %, Ti coated Ti-AVM is 82 %, and Ti-Nb coated Ti-AVM is 71 %. All these results showed that both surface layer coatings survived more while

they were coated on Ti-64 substrates. The Ti-Nb surface layer coating survived more for both substrates while comparing with Ti coated candidates.

- The additional element for Ti-64 samples were also proved by drawing an EDX map from surface to the bulk. There is not only nitrogen interstitial diffusion but also Ti, Nb, Al and V substitutional diffusion mechanism was seen in this study. It is also leading to the formation of the α" phase and Ti-Al intermetallic phase under the nitride layer because of the replacement of the Al and V atoms. The depletion of Al can lead to β-Ti to α" transformation (in some grain 15-16 at. % V concentration was seen). The excess of the Al atoms may lead to the formation of the Ti-Al intermetallic phase.

- The sputter yield value for Ti-Nb coatings was found more than Ti coatings during the deposition process. However, the Ti-Nb coatings were survived more than Ti coatings for both Ti alloy substrates. The reasons can be expressed that the sputter yield rates can be changed because of the structure of the surface layer coatings changing from metallic to ceramic during the nitriding. The interaction of the nitrogen with Ti and Nb (together) could be decreased the sputter off rate of the Ti-Nb surface layer coatings.

- The surface hardness was determined higher for all the samples which treated 8-hour at 700°C. The coated substrates showed different hardness results than the 4-hour treated candidates because the surface layer coatings were still present after 8-hour nitriding treatment. Ti coated Ti-64 substrates showed higher hardness value than the Ti coated Ti-AVM because of the different nitride formation structure of the Ti coatings. On the other hand, the Ti-Nb coated Ti-AVM substrate showed higher hardness value than the Ti-Nb coated Ti-64 substrate. The reason for this may be related to the α stabilised substrate which provides better support to Ti-Nb coating.

- The surface roughness values were also increased for uncoated Ti alloy substrates after 8-hour TPN treatment. The undesired surface roughness values of the uncoated Ti-

AVM substrate were decreased to acceptable rates by the effect of Ti or Ti-Nb surface

layer coatings. Similar improvement was seen for Ti coated Ti-64 substrates.

6 Micro-Abrasion Wear Performance of Coated and Nitrided Samples

6.1 The optimisation of the test parameters

The micro-abrasion test was initially applied on the uncoated and untreated (substrate only) Ti-64 and Ti-AVM samples to optimise the test parameters. The wear coefficient (κ) values were calculated (mentioned in Section 3.2.7) and compared for two different substrates for five different numbers of revolutions of the steel ball. The initial results for the substrates (only one repetition was done for each number of revolution) can be found in Table 6-1.

Table 6-1 Wear scar depth and wear coefficient values of Ti alloy surfaces subjected to the different number of revolutions

No of Revolution	Ti-64 (substrate only)		Ti-AVM (substrate only)	
	Wear scar depth (μm)	Wear coefficient ($\times 10^{-4}$ mm^3/Nm)	Wear scar depth (μm)	Wear coefficient ($\times 10^{-4}$ mm^3/Nm)
25	1.08	8.03	0.82	5.12
50	2.09	10.63	1.65	8.50
100	3.17	10.74	2.8	8.13
200	4.45	10.59	4.14	8.34
400	6.66	10.88	6.2	8.61

The wear coefficient values were seen to be similar (except 25 revolutions). This trend was expected because the substrate (to which the micro-abrasion test was applied) was not treated previously, so the wear coefficient values should not be changed for different depth. The wear scar depth value was changed by increasing the ball revolutions. So, a similar number of revolutions must be chosen to make a comparison between different samples to get more reliable results (especially for nitrided samples).

The lower values for the wear coefficient after 25 revolutions (for both substrates) can be explained by the presence of a work-hardened layer as a result of metallographic preparations and having different wear mechanism at the beginning of the test while the surface of the sample is completely flat and smooth. It was seen that at least 50 revolutions are needed to obtain a reliable comparison between different samples.
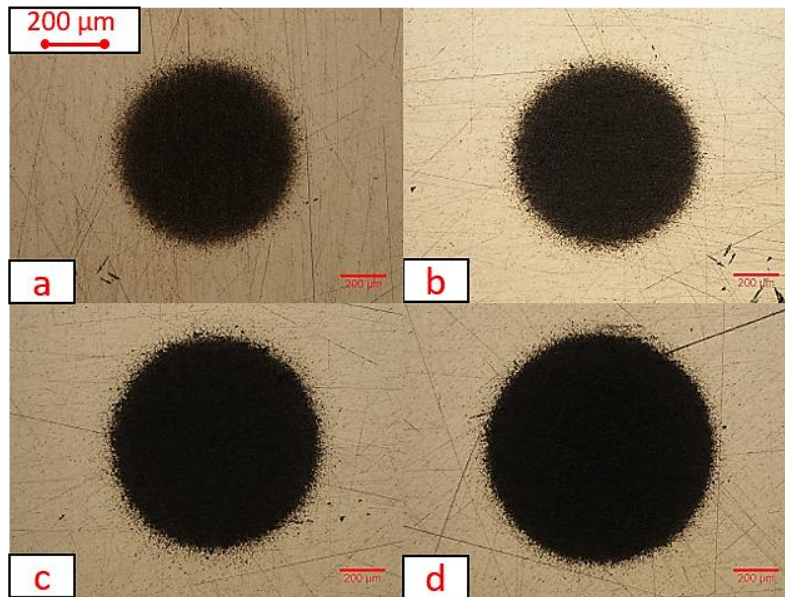
Figure 6-1 Optical microscopy images of the micro-abrasion wear scars for Ti-64 substrate after (a) 25, (b) 50, (c) 100, and (d) 200 ball revolution

Two techniques could be used while measuring the wear scar diameter: Optical microscope or surface profilometer [141]. The optical microscopy images of the micro-abrasion wear scars for Ti-64 substrates can be seen in Figure 6-1 for different ball revolutions. It can be seen the size of the wear scars is generally increased by the effect of increasing ball revolutions. However, the results for 25 and 50 ball revolutions look very similar (which could suggest very critical error while calculating the wear coefficient). The measurements which were taken by surface profilometer allowed the scatter in the scar diameter measurements to be reduced. The 2D profiles of micro-abrasion wear scars for Ti-64 substrates can be seen in Figure 6-2. The accumulation of the abraded particles on the edge of the wear scar circles can be determined

by measuring the scar diameters with a profilometer. It should also be mentioned that the wear coefficient values for 50, 100, 200 and 400 (see Table 6-1) would not be accurate if the scar diameter measurement was made by optical microscopy because all the black region (inside the wear scar region) would not show the real abraded areas.
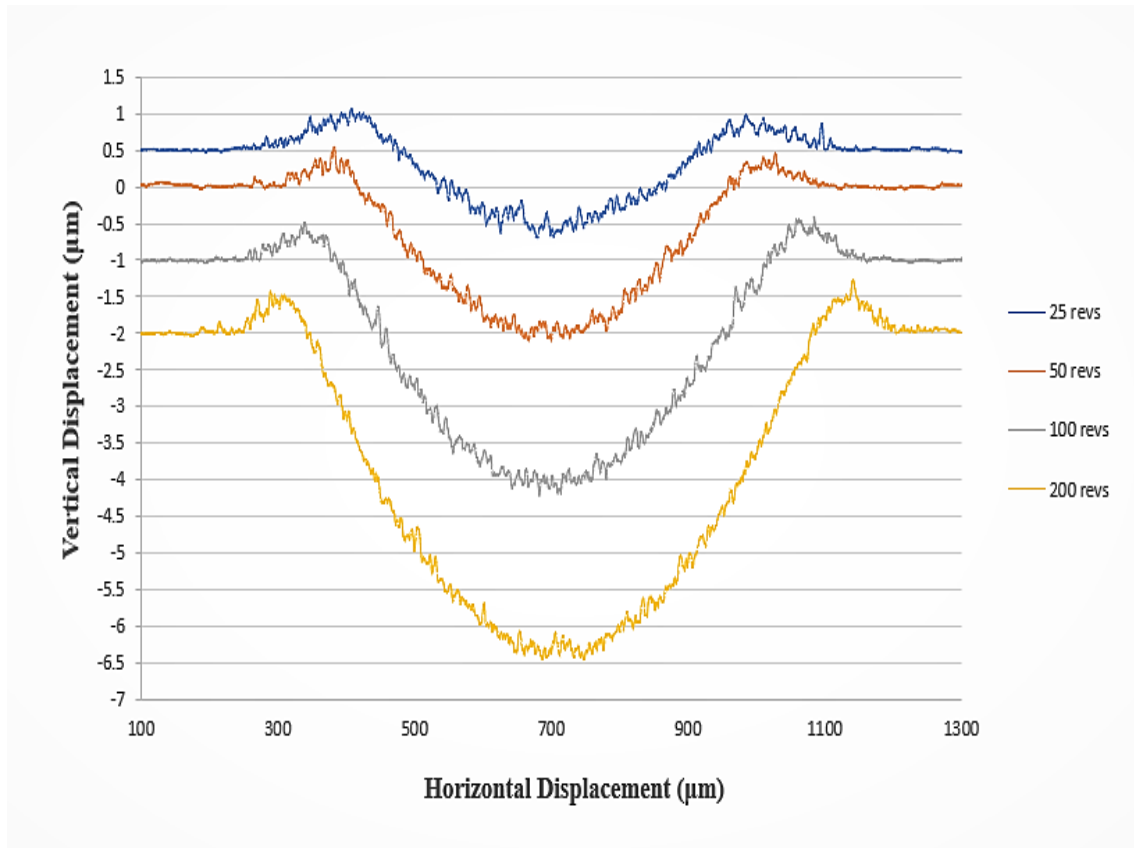
Figure 6-2 2D profiles of micro-abrasion wear scars for an untreated Ti-64 substrate for different ball revolutions

The other parameters such as applied load, volume fraction (V_f) of SiC slurry and the ball speed were chosen to get a three-body (rolling, dimpling) wear mechanism rather than two-body (grooving) and mixed type of wear regime (two-body/three-body). This is important because the crater volume measurement is maintained easily for three-body wear regime. Moreover, the wear volume values should be proportional to the applied load and sliding distance by satisfying the Archard equation (Eq. 3.2). Higher applied load values, lower SiC V_f values and relatively lower ball speeds promote two-body grooving [1], [200], [201]. Therefore, all experiments were applied with a normal load of 0.1N and concentrated SiC slurry including

0.8g particles per ml of water. Keeping the concentration of this super-saturated slurry stable was also tricky because the precipitation of the SiC particles was observed to be very fast (even when experiments were taking place). Separation of the precipitated SiC particles (back to the slurry by using a stick) was almost impossible because there is no time to do this while applying the abrasive wear experiments. In order to keep the concentration of the slurry stable, a small plastic magnetic stirrer bar was dropped into the slurry bottle, and the bottle was placed on a magnetic stirrer (see Figure 6-3). The mixing operation continued during the experimental procedure. It should be noted that besides the optimisation of the parameters, keeping the experimental parameters stable is also important for this wear method because the decreased concentration of SiC slurry would end up with lower wear coefficient results by changing the wear regime.
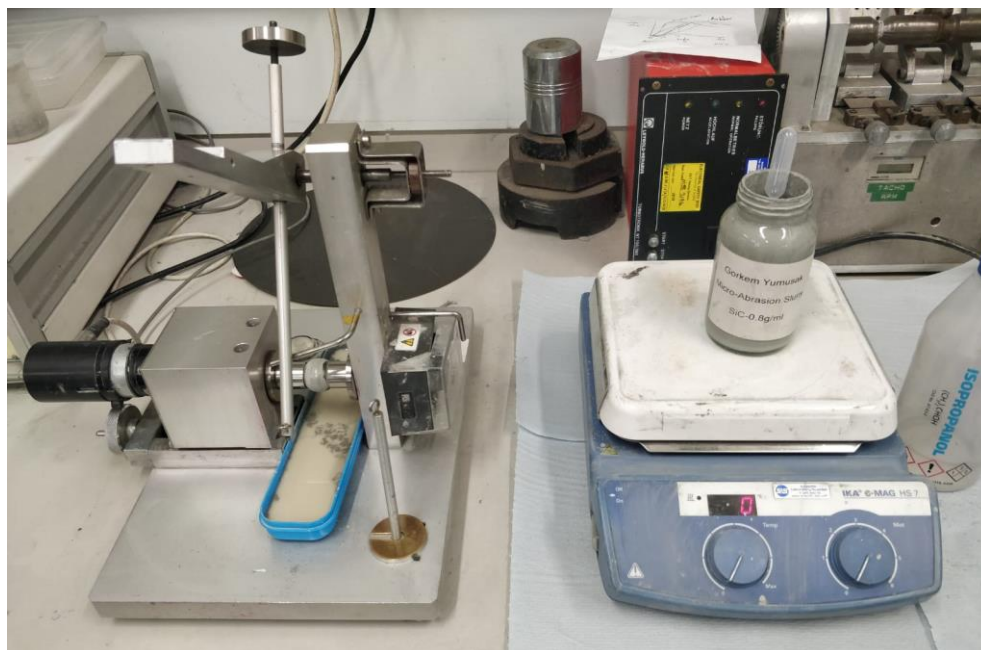
Figure 6-3 The micro-abrasion bench (with the slurry mixing system)

6.2 Ti, Ti-Nb and Ti-Nb-N coatings

The abrasion resistance of the metal (alloy) and ceramic Ti-based coatings was determined by using micro-abrasion technique, of which some examples for this test (applied on Ti-based coatings) can be found in the literature [202]–[206]. The key point of this is to decide the proper number of revolution values because only coatings were desired to be worn out (non-perforating test) and avoide any substrate effects. The effect of Nb addition to the pure Ti coating system and the effect of nitrogen on the Ti-Nb system were determined by comparing Ti, Ti-Nb and Ti-Nb-N PVD coatings. The number of revolutions selected was 50 (by doing several trial micro scale wear tests). In fact, all these PVD coatings were produced for 2 hours deposition time, and they all were expected to have 2-2.5 μm thickness. The trend of having lower wear coefficient data which were found for very low revolution values (see Table 6-1) while doing experimental parameter optimisation for Ti-64 and Ti-AVM substrates were also observed for Ti, Ti-Nb and Ti-Nb-N PVD coatings. An almost 2 times lower wear coefficient was found for 25 revolutions when comparing with 50 revolutions. It is believed to be confusing for the further comparisons, and it was decided to use 50 revolutions for micro-abrasion testing. Moreover, the Ti-Nb-N ceramic coatings which have much higher surface hardness and elastic modulus values (see Table 4-14) yielded a very shallow wear scar (when applied 25 revolutions) while comparing with their equivalent (as respect to their positions on the substrate holder) metallic Ti-Nb coatings (no nitrogen). Some examples of 2D profiles for Ti, Ti-Nb and Ti-Nb-N coatings can be found in Figure 6-4. At first sight, it can be understood that the Ti coating has the biggest scar depth and the Ti-Nb coating (contains 32.9 at. % Nb) showed less scar depth compared to pure Ti coatings. The ceramic Ti-Nb-N coating also showed similar scar topography with metallic coatings, and it is suggested that the abrasive wear modes are similar for all PVD coatings. However, there are some droopy shaped bumps were seen on the 2D profile of Ti-Nb-N coating. It may be related to the generations of hard

coatings debrides during the wear process. They will act as sources of abrasive materials beside SiC in the slurry and may plough into the coating and split (debond) the coating from some points. The elastic mismatch between the hard-ceramic coating and soft Ti-64 substrate could promote the formation of these cracks. The Ti-Nb-N coating did not show any stacked material (a toroidal shaped) which the Ti and Ti-Nb coatings showed. The abraded materials may flow back to the scar during the abrasion process for Ti-Nb-N coatings.
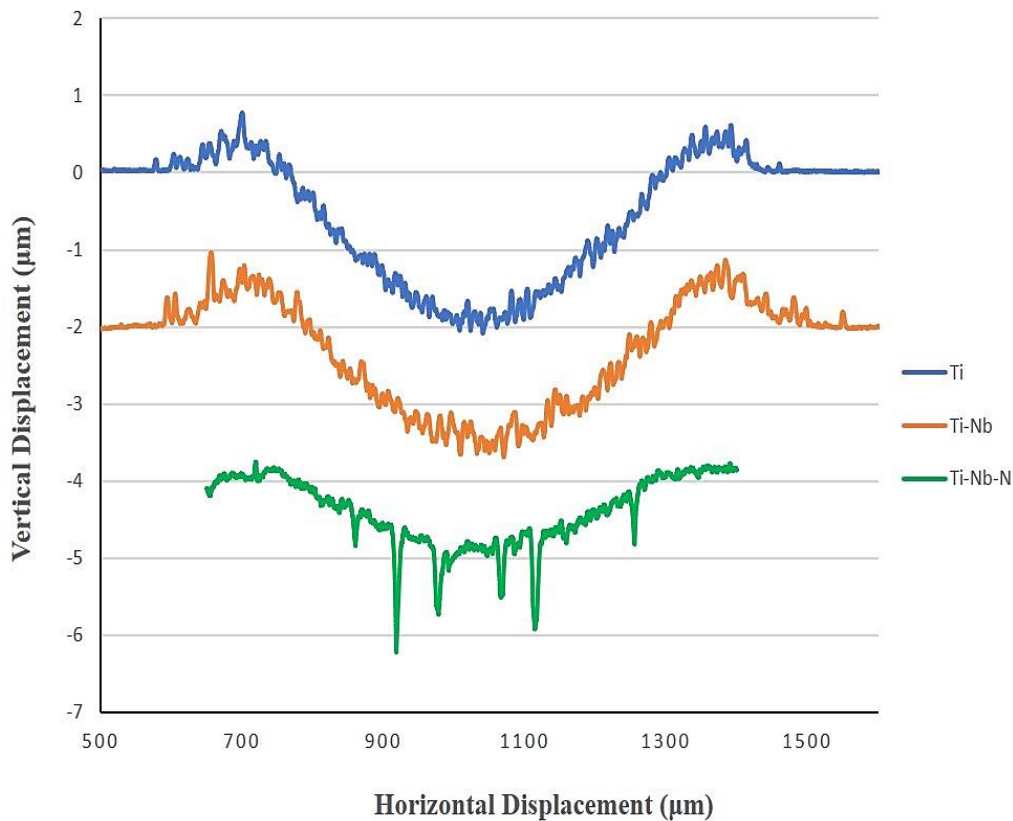
Figure 6-4 2D profiles of micro-abrasion wear scars for Ti (clean), Ti-Nb (clean) and Ti-Nb-N (N-Ti-64-P1) for 50 ball revolutions

The wear coefficient data calculated by surface profilometry for Ti and Ti-Nb coatings can be seen in Table 6-2. The Ti-Nb coatings which were used as surface layer coatings before nitriding process showed approximately 25 % difference by their wear coefficients compared to pure Ti coating. It is because of the Nb alloying which is about 33 at. %. The other Ti-Nb coatings which were produced previously (the necessary information for these coatings can be found in

175

Table 4-7 and Figure 4-11) were also applied micro abrasion test to see the effect of Nb concentration on the wear performance.

Table 6-2 Wear coefficients of Ti and Ti-Nb coatings (deposited on the Ti-64 substrate)

Sample	Nb concentration (at. %)	Wear coefficient ($\times 10^{-4}$ mm^3/Nm)	$\Delta \kappa_c$, % (compared to pure Ti coating)
Ti-coating (clean)	0	9.69	---
Ti-Nb coating (clean)	32.9	7.20	- 25.7
Ti-Nb coating (Ti-64-P1)	16.9	8.81	- 9.08
Ti-Nb coating (Ti-64-P2)	25.4	7.71	- 20.4
Ti-Nb coating (Ti-64-P3)	40.5	7.07	- 27.0

The mean values of the wear coefficients for Ti-Nb coatings showed that the increase of Nb in the coatings enhanced the wear performance. Although, the Ti-Nb coating (Ti-64-P1) contains almost 17 at. % Nb, it showed limited wear enhancement. The behaviour of this coating can be attributed to its phase structure which can be found in Figure 4-11. This coating deposited on the Ti-64 substrate and the β stabilisation was found weaker than other candidates. This phenomenon suggested to us that besides the alloying elements, the phase structure of the coatings could be important regarding abrasive wear resistance. It can be seen for the untreated substrates that the Ti-AVM substrate showed approximately 25 % better abrasive wear resistance than the Ti-64 substrate. It should be noted that the amount of Mo inside the Ti-AVM substrate is also very high to affect the wear performance. Above some critical concentration (depend on the additional elements) the dominant phase is becoming β, and the mechanical properties of the Ti alloys can be improved towards to the additional elements mechanical properties [207].

The wear coefficient values for the Ti-Nb-N coatings can be found in Table 6-3. As a ceramic nitride material; it was expected to have better wear performance compared to metallic Ti and Ti-Nb coatings. The increased surface roughness of these coatings makes the measurement of the scar length difficult. The average wear coefficient values showed that the wear performance of the ceramic Ti-Nb-N coatings decreased with increasing Nb addition. The wear coefficient values are very near to each other, with the maximum difference found to be approximately 10 at. % between (N-Ti-64-P1) and (N-Ti-64-P3) coatings. Therefore, this small difference can be not so critical when considering the desired effect of minimising final surface roughness after treatment (and optimisation of the nitrogen diffusion rate). These wear results were already significantly enhanced compared to Ti and Ti-Nb metallic coatings and not surprising because the mechanical properties of these coatings (see Table 4-14) suggested that high abrasion resistance was likely.

Table 6-3 Wear coefficients of Ti-Nb-N coatings (deposited on the Ti-64 substrate)

Sample	Nb concentration (at. %)	N concentration (at. %)	Wear coefficient ($x10^{-4}$ mm^3/Nm)
Ti-Nb-N coating (N-Ti-64-P1)	8.94	53.03	6.10
Ti-Nb-N coating (N-Ti-64-P2)	15.07	52.38	6.34
Ti-Nb-N coating (N-Ti-64-P3)	24.20	49.69	6.75

The hardness and elastic modulus of the coatings were decreased by the addition of Nb. Although the phase structure of all three coatings was similar (see Figure 4-28), the difference with respect to wear performance may be clarified by the different amounts of Nb inside the coatings. The wear coefficient data also are in a good agreement with the literature work [1] while comparing these coatings with TiN coatings (the wear coefficient was reported to be

6.91×10^{-4} mm^3/Nm for non-perforating micro abrasion tests of TiN coatings deposited on an untreated Ti-64 substrate).

6.2.1 A comparison between perforating and non-perforating tests

Micro-abrasion tests were applied with 100 revolutions on a single-layered Ti-Nb-N coating (N-Ti-64-P2) which was deposited on Ti-64 substrate in order to perforate the coating and reach to the substrate. The κ_c value was calculated using the Hedenqvist method [205] after perforating test and it was compared with the non-perforating (with 50 revolutions) test which was discussed in the previous section. Figure 6-5 shows schematically the contact geometry of the wear scars for only substrate or only coating (non-perforating) and coated substrate (perforating).
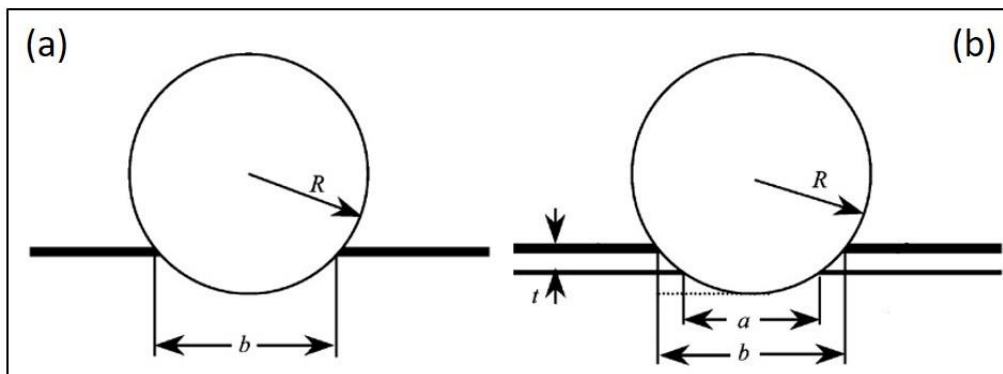
Figure 6-5 The geometry of wear scars formed by micro-abrasion testing (a) in bulk (b) in a coated sample (Reproduced from Ref. [208]

The extended equation (from Eq. 3-2) can be used for the coated substrate which includes the wear coefficient of coating and substrate, and the wear scar volumes of coating and substrate. The wear equation can be written as:

$$SN = \frac{V_c}{\kappa_c} + \frac{V_s}{\kappa_s}$$ **Equation 6.1** [135], [144]

The wear scar volumes (for coating and substrate) can be calculated separately by using the measured a and b values (as can be seen in Figure 6-5) [209]. In order to obtain these values,

178

optical microscopy has to be used because the boundaries are not clear in surface profilometer measurements. As already discussed the measured crater diameters were found to be higher for optical microscopy. To make a valid comparison, the wear coefficient measurement (which was done with surface profilometer) was repeated for the non-perforating test (instead of the value in Table 6-3). The optical microscopy images of the micro-abrasion wear scars for the Ti-Nb-N coated Ti-64 substrate can be seen in Figure 6-6. The black region on the image which belongs to the substrate after perforating test is not perfectly circular. The reason for this prominent shape may be related to the brittle nature of the ceramic coating. Therefore, the wear scar diameter for the substrate (which is necessary to calculate the wear volume) is measured assumptively. First it was tried to measure from the shortest and longest part (and average them), and secondly, the area extracted from the image (by using image analysis software, ImageJ) and the radius is assumed from the total area. Both of the results were found very similar to each other.
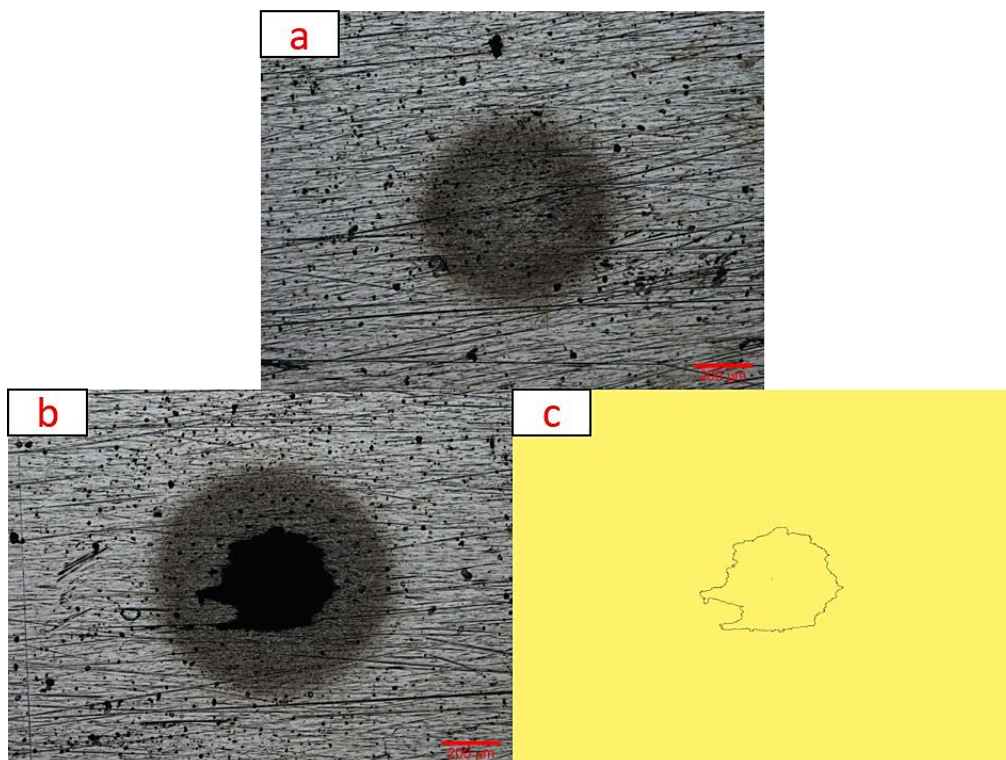
Figure 6-6 Optical microscopy images of the micro-abrasion wear scars for Ti-Nb-N coated Ti-64 substrate after (a) 50, (b) 100 revolutions and (c) extracted area (refers to substrate)

After calculating the wear volumes of the coating and substrate (V_c and V_s), the Hedenqvist approach [205] was used to calculate the κ_c as the value of the κ_s was pre-determined from the untreated substrate (by using the optical image which can be seen in Figure 6-1). The calculated wear coefficients can be found in Table 6-4. It is obvious that booth perforating and non-perforating test results for the Ti-Nb-N coating shows higher resistance to micro-abrasion test when it is compared to the untreated Ti-64 substrate. The κ_c values obtained from two different tests are also making fairly good agreement (about 20 % difference). The reason for this can be relate to: firstly, the formula which is used for the calculating the wear volumes is giving approximate results. The sliding distance seen by the coating is longer than the substrate after perforating. This sliding difference is significant when small numbers of revolutions are used. Secondly, the measured wear diameter for the substrate after perforating test includes some assumptions. Thirdly, the κ_s value used here was obtained from a different micro-abrasion test and any errors may be carried over to the calculation of perforating κ_c value. As a summary, if only the coating wear rate is required, it is better to apply short micro-abrasion tests without any perforation. Therefore, the depth of the wear scar is limited by the coating thickness. By this means, the test and the calculations can be performed quickly, and the results will be less affected by assumptions. Moreover, very low numbers of revolutions (such as 10,15) should be avoided to get more accurate results.

Table 6-4 The perforating and non-perforating specific wear rates of Ti-Nb-N coatings (wear diameters were measured with optical microscopy)

Sample	κ_s (non-perforating) (x10^{-4} mm^3/Nm)	κ_c (non-perforating) (x10^{-4} mm^3/Nm)	κ_c (perforating) (x10^{-4} mm^3/Nm)
Ti-64 (substrate only)	34.57	-	-
Ti-Nb-N coating (N-Ti-64-P2)	-	13.39	16.48

6.3   TPN Samples

The abrasion resistance could be difficult to determine for the diffusion treated (nitrided) samples. The major reason for this is that the boundary between the substrate and the hardened zone or compound layer is not clear. For example, the Ti, Ti-Nb or Ti-Nb-N coatings (their wear performance can be seen in Section 6.2) deposited by magnetron sputtering technique have a clear coating/substrate interface. Also, the structure of the coatings is homogeneous; in other words, it shows the same characteristic at every point through its thickness. In this case, the non-perforating type of the abrasion test could be applied to analyse the exact coating wear rate. On the other hand, diffusion treated samples show very different chemical and mechanical properties from the surface to bulk. Secondly, the different types of samples (although all process parameters were kept constant, except time and temperature), which are Ti coated or Ti-Nb coated before nitriding, each yield different nitride (layer) structure and thickness. Thirdly, depending on the type of the coating and Ti alloy substrate, the nitrogen case depths were also variable. All these findings showed that the wear coefficient of the diffusion treated substrates could be affected by several concurrent factors.

On the other hand, this technique could be a coherent way to grade the efficiency of different diffusion treatments. The nitrogen case depths were estimated from the cross-sectional hardness/depth profile. Moreover, it is proved that the thin Ti or Ti-Nb surface layer coatings (1.25 μm thick) were removed after 4 hours nitriding process at 700°C. Therefore, previously coated samples will also behave as an uncoated material beyond some point in the nitriding treatment cycle. Taking into account all these factors, the diffusion treated samples can be cautiously compared with each other. For this purpose, the number of revolutions was selected as 100, to keep the depth of the penetration of the ball to approximately 3 μm, which is still in the strengthened region for all treatments. Changing the number of revolutions would allow checking any (desired) total depth depend on the structure of the treated samples. The most

important thing is to keep the total number of revolutions the same for all samples to make a reliable comparison.

6.3.1 TPN500

The micro-abrasion wear test was applied to uncoated Ti-64 and Ti-AVM substrates which were nitrided for 4 and 8 hours at 500°C. Because there is no nitride compound layer formed on the surface for these substrates (discussed in Section 5.2), the result of the 100 revolutions were shown only for nitrogen diffusion zone, and the comparison was made with untreated substrate results. The wear coefficient values for the uncoated Ti-64 and Ti-AVM substrates treated at 500°C for 4 and 8 hours can be found in Table 6-5.

Table 6-5 Wear coefficients of uncoated Ti-64 and Ti-AVM surfaces subjected to TPN500 treatments for various process durations

Ti-alloy	Sample	Wear coefficient ($x10^{-4}$ mm^3/Nm)	$\Delta \kappa$, % (compared to the untreated substrate)
Ti-64	Untreated	10.87	---
	Uncoated TPN500-4h	9.66	-11.1
	Uncoated TPN500-8h	9.33	-14.2
Ti-AVM	Untreated	8.13	---
	Uncoated TPN500-4h	7.46	-8.2
	Uncoated TPN500-8h	7.01	-13.7

The wear coefficient was found to be about 11 % less for the uncoated Ti-64 substrate after 4h nitriding process at 500°C. The Ti-AVM substrate which was treated in the same run showed about 8% enhancement in abrasion wear resistance compared to its untreated counterpart.

When the process duration was increased to 8 hours, the wear scar for both substrates was found to be smaller. It means the abrasive wear resistance was improved and about 14 % enhancement was seen for uncoated Ti-64 and Ti-AVM substrates compared to untreated substrates. The more nitrogen (diffusion) inside the Ti alloy substrates may be happened (with extra 4 hours nitriding process) but the measured wear rates after 4 hours and 8 hours nitriding process could be affected by many other factors (not only the effect of saturation of the Ti alloys with nitrogen). The remaining effects from the first 4 hours nitriding process which may be caused by surface finishing before process and ion (argon and nitrogen) bombardment during the process which creates compressive stress. Moreover, the longer nitriding time would have a higher annealing effect which can cause substrate grain growth and affect the bulk mechanical properties.

6.3.2 TPN600

The micro-abrasion wear test was applied to the uncoated Ti-64 and Ti-AVM substrates which were nitrided for 4 hours at 600°C. The disappearance of the β phase and a small Ti_2N nitride phase XRD peak on the surface of the Ti-64 substrate (see Figure 5-5) had proven the cause of an increase in surface hardness by the effect of nitrogen diffusion. On the other hand, the appearance of α peaks (see Figure 5-6) for the Ti-AVM substrate which is related to the strong α-stabilisation effects of interstitial nitrogen, had influenced the increasing of surface hardness. It was also discussed previously that the 4-hour TPN600 treatment gave better enhancement of surface hardness, compared to the 4-hour TPN500 treatment (see Table 5-3 and Table 5-4). The wear coefficient values for the uncoated Ti-64 and Ti-AVM substrates treated at 600°C for 4 hours can be found in Table 6-6. About 20% reduction in wear rate was seen for the uncoated Ti-64 substrate after 4h nitriding process at 600°C, and the Ti-AVM substrate which was treated in the same run was showed about 17% reduction. All these findings are in a good agreement with the improved mechanical properties of uncoated Ti-64 and Ti-AVM substrates

after 4-hour TPN600 treatment. The wear coefficient data after 4-hour TPN600 process was also found better than the 8-hour TPN500 treatment.

Table 6-6 Wear coefficients of uncoated Ti-64 and Ti-AVM surfaces subjected to 4 hours TPN600 treatments

Ti-alloy	Sample	Wear coefficient ($x10^{-4}$ mm^3/Nm)	$\Delta \kappa$, % (compared to the untreated substrate)
Ti-64	Untreated	10.87	---
	Uncoated TPN600-4h	8.75	-19.5
Ti-AVM	Untreated	8.13	---
	Uncoated TPN600-4h	6.77	-16.7

The wear scar depth was found to be about 2.9 μm for Ti-64 and 2.6 μm for Ti-AVM substrates while calculating the wear coefficients for the 4-hour TPN600 treatment. While comparing these values with the untreated samples (see Table 6-1), the difference was found to be about 8.5% and 7% for Ti-64 and Ti-AVM substrates respectively. This may be concluded as: firstly, the nitriding response is better for Ti-64 substrate than Ti-AVM substrate. It may be related to the amount of dissolved nitrogen being higher on the near-surface of the Ti-64 substrate (about 3 μm) which is also the reason for increased hardness. Secondly, the ratio of decrease of the wear scar diameter (and accordingly, the reduction in wear coefficient) is in good agreement with the ratio of decrease in wear scar depth. This shows that the scar geometry has a spherical trend which changing its dimension similarly in all dimensions. It is obeying the 3B wear mechanism and making the results more reliable.

6.3.3 TPN700

The most significant changes were seen after nitriding treatment applied at 700°C. The formation of a nitride compound layer on the surface of the Ti-64 substrate in particular and the presence of a nitrogen-stabilised diffusion zone beneath it (which means a gradual mechanical property transition from surface to bulk) was observed by cross-section nanoindentation hardness tests (see Figure 5-17). This type of surface/cross-section structure for the Ti-64 substrate after 4-hours TPN700 treatment can be beneficial for some applications such as adhesive wear and galling. It is because the improved surface (by changing the chemistry of it) would contact the metal or ceramic surface and a reduced friction coefficient could be obtained. On the other hand, the relatively soft and ductile nature of Ti or Ti-alloys can easily be destroyed while they are contacting with a harder surface. On the other hand, the abrasive wear test (using a slurry containing SiC particles) instead of a dry sliding wear test showed different behaviour for Ti-64 substrates. The wear coefficient values for the uncoated, Ti coated, and Ti-Nb coated Ti-64 substrates treated at 700°C for 4 hours can be found in Table 6-7. The untreated Ti-64 substrate showed some enhancement related to abrasive wear, but it was found about 8% while this enhancement was seen about 19% after 4-hour TPN600 treatment. This suggests that the thin compound layer which is formed on the surface (Ti_2N) may be fractured during the wear test and the newly formed nitride debris can speed up the wear rate. Although the surface hardness values were found better after TPN700 process (see Figure 5-20), the wear performance of the uncoated Ti-64 substrate was found limited after TPN treatment. It also appears that surface hardness alone is not responsible or improved abrasive wear performance but also a gradual change of the mechanical properties from surface to core may be more beneficial.

Table 6-7 Wear coefficients of uncoated, Ti coated, and Ti-Nb coated Ti-64 surfaces subjected to 4 hours TPN700 treatments

Ti-alloy	Sample	Wear coefficient ($\times 10^{-4}$ mm^3/Nm)	$\Delta\,\kappa$, % (compared to the untreated substrate)
Ti-64	Untreated	10.87	---
	Uncoated TPN700-4h	9.97	-8.3
	Ti coated TPN700-4h	9.60	-11.7
	Ti-Nb coated TPN700-4h	9.18	-15.5

The highest surface roughness was found for the uncoated Ti-64 substrate compared to Ti or Ti-Nb coated Ti-64 substrate (see Figure 5-9). The PVD metallic coatings deposited before the nitriding process led to a decrease in the final surface roughness values. The higher surface roughness could end up with higher local contact pressures on the surface while applying the micro abrasion test and this may accelerate the detachment of these nitride asperities. Having lower surface roughness values gave some advantage for the Ti, and Ti-Nb coated Ti-64 substrate based on their wear performance. Moreover, the Ti-Nb coated Ti-64 substrate which showed deeper cross-sectional hardening (see Figure 5-17) by the effect of the higher diffusion rate of nitrogen in the beta phase coating than in the Ti-64 substrate yielded the best wear performance between the Ti-64 substrates. This again shows the importance of a functionally graded change in the mechanical properties with depth after the nitriding process. In the light of all these findings, the higher surface hardness, lower surface roughness and more gradual hardness change from surface to bulk (compared to its uncoated and Ti coated candidates) make the Ti-Nb coated Ti-64 substrate more effective in application areas requiring abrasion resistance.

The response of the Ti-AVM substrates after TPN700 process was completely different from the Ti-64 substrates. The wear coefficient values for the uncoated, Ti coated, and Ti-Nb coated Ti-AVM substrates treated at 700ºC for 4 hours can be found in Table 6-8.

Table 6-8 Wear coefficients of uncoated, Ti coated, and Ti-Nb coated Ti-AVM surfaces subjected to 4 hours TPN700 treatments

Ti-alloy	Sample	Wear coefficient ($\times 10^{-4}$ mm^3/Nm)	$\Delta \kappa$, % (compared to the untreated substrate)
Ti-AVM	Untreated	8.13	---
	Uncoated TPN700-4h	6.11	-24.8
	Ti coated TPN700-4h	5.63	-30.7
	Ti-Nb coated TPN700-4h	5.72	-29.6

On the first appearance, the wear performance of the Ti-AVM substrates was enhanced compared to the TPN500 and TPN600 processes. It means that the wear coefficient of the Ti-AVM substrates decreased after the TPN700 treatment. The uncoated Ti-AVM substrates showed about 25% reduction in wear after 4-hour TPN700 process in which these values were approximately 8% and 17% for 4-hour TPN500 and 4-hour TPN600 process respectively. It should be said (firstly), the surface chemistries of the Ti-AVM substrates did not change a lot (see Figure 5-8), and it was seen that some α-Ti peaks appeared on the surface of the Ti-AVM substrates after 4-hour TPN700 process. The difficulties of the formation of the nitride compound layer on the surface of Ti-AVM substrates was concluded with a lower surface hardness values (see Figure 5-20) after the nitriding treatment. The reason for this because of the relationship between the crystal structure and nitriding behaviour. The final product provides very good abrasive wear performance by not creating a (significant) compound layer on the surface.

It was reported by Cassar et al. [112] that for getting a higher accumulation of nitrogen on the substrate surface after nitriding, a higher cathode bias voltage could be used, but with consequential higher surface roughness. With respect to the applications in which the final product might be used, the process parameters could be changed, or the process can be varied by using different reactive gas mixtures [210], [211].

In our study, more gentle surface roughness results were obtained (see Figure 5-9) related to the chosen process parameters (the position of the samples inside the nitriding chamber is also important). The method of depositing a metallic PVD coating before the nitriding process provided more significant changes on the final properties of the Ti-AVM substrates because the surface roughness of the uncoated Ti-AVM (because of larger grain size) was found to be almost double uncoated Ti-64 substrates (after TPN700 process). The wear coefficient of the Ti and Ti-Nb coated Ti-AVM substrates were found about 5% less compared to the uncoated Ti-AVM substrate after 4-hour TPN700 process. The enhancement of the wear performance of the Ti and Ti-Nb coated Ti-AVM substrates could be related to the reduced surface roughness because the surface morphologies were found similar for all three Ti-AVM substrate conditions. It was previously discussed that the thin (1.25 μm) Ti and Ti-Nb surface layer coatings were sputtered off completely after a 4-hour TPN700 treatment. The 1% difference in wear coefficient was seen between Ti and Ti-Nb coated Ti-AVM substrates, but it is a negligible value compared to the overall enhancement of wear performance. This may be related with the better diffusion hardening response of the Ti coated Ti-AVM substrate (see Figure 5-18).

6.3.3.1 Wear performance after depositing of thicker surface layer coatings

Most of the previous wear experiments were based on the uncoated substrates which were nitrided at various temperatures for different process durations. Although some samples coated

with Ti and Ti-Nb (before the nitriding process), these surface layer coatings did not survive until the nitriding treatment finished. All wear craters (about 3 µm deep) were composed of ceramic nitride layer (depends on the samples and process conditions) and nitrogen diffusion zone. However, thicker surface layer coatings were deposited before the 8-hour TPN700 process in order to see the "sputter off" behaviour of the coatings. Moreover, the remaining coatings with different thickness (see Table 5-7) were also nitrided. Instead of only the nitride layer which formed on the substrate (for uncoated samples), the different nitride layer which belongs to remaining surface layer coating (besides the nitriding of the substrate) could affect the wear performance of the samples. In order to make a good comparison, the wear test parameters were kept the same as the previous tests.

The wear coefficient values for the uncoated, Ti coated, and Ti-Nb coated Ti-64 and Ti-AVM substrates treated at 700°C for 8 hours can be seen in Table 6-9. Increasing the nitriding time to 8 hours enhanced the wear performance of uncoated Ti-64 substrate. The comparison of the wear performance of the uncoated Ti-64 and Ti-AVM substrates (for all nitriding conditions) can be seen in Figure 6-7. The increase of the thickness of the nitride (compound) layer and the more beneficial diffusion zone (with its increased nitrogen concentration) under it may lead to improving the abrasive wear performance of untreated Ti-64 substrate (compared to 4-hour TPN700 process). An approximately 18% reduction in wear (compared to untreated) was also found for the untreated Ti-64 substrate after 8-hour TPN700 process which is better than the wear performance of the Ti and Ti-Nb coated Ti-64 substrates after 4-hour TPN700 process. Therefore, it can be said that the increase of process duration (at relatively higher treatment temperatures) could result in more significant changes compared to lower treatment temperatures (based on wear performance).

Table 6-9 Wear coefficients of uncoated Ti-64 and Ti-AVM surfaces subjected to 8 hours TPN700 treatments

Ti-alloy	Sample	Wear coefficient $(x10^{-4}$ mm^3/Nm)	$\Delta\kappa$, % (compared to the untreated substrate)
Ti-64	Untreated	10.87	---
	Uncoated TPN700-8h	8.90	-18.1
	Ti coated TPN700-8h	8.44	-22.3
	Ti-Nb coated TPN700-8h	8.36	-23.1
Ti-AVM	Untreated	8.13	---
	Uncoated TPN700-8h	4.51	-44.5
	Ti coated TPN700-8h	5.87	-27.7
	Ti-Nb coated TPN700-8h	5.05	-37.9
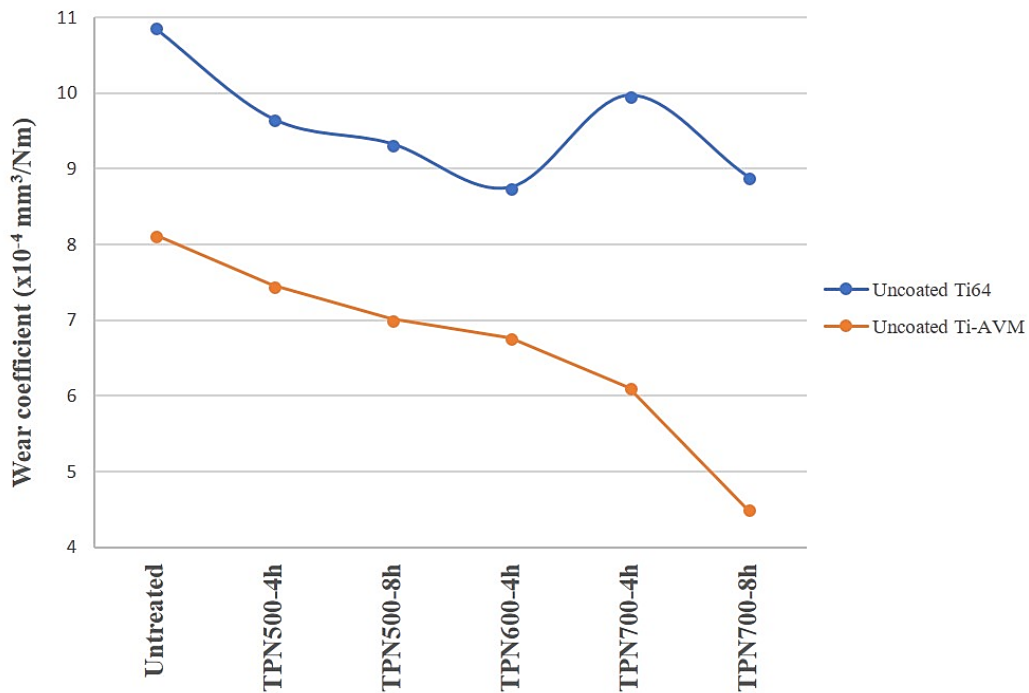
Figure 6-7 The wear coefficient of the uncoated Ti-64 and Ti-AVM substrates (for all nitriding conditions)

On the other hand, the uncoated Ti-AVM substrate showed a similar trend (with previous wear tests) on abrasive wear performance after 8-hour TPN700 process. The increased hardness (see Figure 5-33) depending on the amount of nitrogen on the surface (which was also expected almost maximum nitrogen can be dissolved inside β-Ti phase without forming any ceramic phase) may be the reason to find superior abrasive wear performance for the uncoated Ti-AVM substrate after 8-hour TPN700 process. It can be seen in Figure 6-7 how the uncoated Ti-AVM substrate is improving its nitriding performance by changing the nitriding temperature and time. If the nitriding temperature (which was chosen maximum 700°C) is increased more, the wear mechanism of the Ti-AVM alloy can be different depending on its α to β transus temperature. Moreover, the nitriding time can be increased to see the effect on wear performance but (in this condition) the surface roughness value (the biggest value was found for this sample which was 0.161 μm after 8-hour TPN700 process) could be more detrimental. Cassar et al. [2] reported that Ti-15Mo (which is another example of a metastable β-Ti alloy) has a Ra value which is about 0.34 μm after 4 hours nitriding process at 700°C. This value is almost two times bigger than the value which was found in this study. The increased surface roughness would increase the local contact stresses between the surface and ball. As a result, it would increase the initial increase wear on the surface and moreover the wear coefficient was found more than the untreated sample. They also reported that the previously coated pure Ti on the surface of Ti-15Mo substrate allowed to decrease the final surface roughness and consequently decrease the wear coefficient. The smoother surface which was found in this study did not give any negative effect on the wear performance of the Ti-AVM substrate.

The Ti and Ti-Nb surface layer coated Ti-64 substrates showed better wear performance than the uncoated Ti-64 substrate after 8-hour TPN700 process. The remaining surface layer coatings kept more nitrogen on their surfaces and the gradient hardness change from the surface to the core of the substrates was beneficial in the sense of wear. The EDX results (see Table

5-6) was proof that the surface layer coated substrates have more nitrogen on their surfaces after 8-hour TPN700 process. The surface coatings allowed to have better surface roughness values except for Ti-Nb coatings on a Ti-64 substrate. However, interestingly, the wear coefficient value of the Ti-Nb coated Ti-64 substrate was found less than the Ti coated Ti-64 substrate. It is suggesting that the negative effect of surface roughness on the wear performance was eliminated by the better nitriding efficiency of Ti-Nb coating. It also allowed more nitrogen to diffuse inside the substrate and it made the coating/diffusion system more wear resistant. However, as a result, the Ti coated, and Ti-Nb coated Ti-64 substrates have similar wear performance. This suggests that the thickness of the PVD surface coatings should be selected carefully. If the Ti-Nb coating had chosen 3 μm (rather than 5 μm), the final properties would be maximised.

The effect of the Ti and Ti-Nb PVD metallic coatings which were deposited on Ti-AVM substrate was resulted differently compared to the uncoated Ti-AVM substrate after 8-hour TPN700 process. As discussed earlier, there is no surface layer coating left after 4 hours nitriding process, and there is no nitride layer formed after both 4-hour and 8-hour TPN700 processes. Thus, the abrasive wear performance of the substrates had shown an increasing trend. Thicker coating layers which remained on the surface are also nitrided after 8-hour TPN700 process. Although the surface roughness values (see Figure 5-34) were decreased by the effect of a surface coating, the abrasive wear performance of the Ti and Ti-Nb coated Ti-AVM substrates were worse than the uncoated one. This can be assimilated to the nitrided Ti-64 substrate at 700°C, in which the abrasive wear performance was decreased by the formation of a nitride layer (it was thought to accelerate the wear by the effect of the lower load-bearing capacity of the substrate). It is also found that the Ti-Nb coated Ti-AVM substrate has better wear performance than the Ti coated Ti-AVM substrate after 8-hour TPN700 process. This can be attributed to the higher surface hardness (see Figure 5-33) value of the Ti-Nb coated Ti-AVM

substrate compared to the Ti coated one which has different nitriding behaviour by forming a (too thin) nitride layer on the surface (see Figure 5-28). As a conclusion, the wear performance of the diffusion/coating system strictly depends on the substrates type, surface coating material (and thickness) and the treatment time.

The deposition of metallic PVD coatings (Ti or Ti-Nb) before nitriding process had some influence on wear performance of the titanium alloy substrates depend on process parameters and underlying substrate's crystal structures. Besides the decrease of the wear coefficients of the titanium substrates after TPN process, the aim was here to create better hardened zone (better load bearing capacity) to subsequently deposited PVD hard coatings. Because, the hard PVD ceramic coatings (such as TiN, CrAlN) need good adhesion to the titanium alloy substrate to show beneficial wear performance. It was already shown in Section 6.2 that although the Ti-Nb-N coating (on Ti-64 substrate) has very hard nature (around 23 GPa), the wear performance of this coating was limited because of soft Ti alloy substrate under it which allow to debonding of the ceramic coating easily. A quantitative comparison can be made with the similar works which was applied micro abrasion test after nitriding process or single-layered coating deposition. It should also be noted that the process parameters for both surface engineering methods and wear test methods may affect the final wear performance. On the other hand, to compare the % change of the wear coefficient compared to the untreated substrates will result with a more significant comparison for TPN treated samples. It is seen in Table 6-10 that the TPN process provided better wear performance over untreated samples. The Ti-Nb interlayer coatings (deposited before nitriding process) increased the wear performance. However, the wear performance of the samples which was previously nitrided and subsequently ceramic coated were found superior. In conclusion, to produce a wear resistant titanium alloys, duplex (or triplex) processes are suggested.

Table 6-10 A quantitative comparison of the various materials base on their wear performance

Samples	Wear coefficient (x10^{-4} mm^3/Nm)	
	In this study	References
Untreated Ti-64 (substrate only)	10.87	9.65 [2]
TPN700 (4h) on Ti64	9.97	8.98 [2]
Ti-Nb layer + TPN700 (4h) on Ti64	9.18	-
TPN700 (8h) on Ti64	8.90	-
Ti-Nb layer + TPN700 (8h) on Ti64	8.36	-
Single-layered TiNbN/TiN on Ti64	6.10	6.01[2]
TPN700 (8h) + TiN on Ti64	-	4.87 [2]
Single-layered TiAlSiN on steel	-	6.36 [212]
Single-layered TiB$_2$ on steel	-	6.84 [213]
UNS S32750 stainless steel (substrate only)	-	9.6 [214]

6.4   Summary

The micro-abrasion wear test was used to figure out the wear resistance of single layer Ti, Ti-Nb and Ti-Nb-N coatings, triode plasma nitrided (uncoated, Ti coated, Ti-Nb coated) Ti-64 and Ti-AVM substrates. The wear coefficient of the samples was compared with the untreated sample and the effect of treatment temperature and time on the wear performance was determined. The following key points from this chapter can be drawn:

- The optimisation (and decision) of the parameters was found very critical for this technique. The initial experiments were applied on untreated substrates. 5 different revaluation values were tried (from 25 to 400). The depth of the wear scars was found about from 1 μm to 7 μm.

- It was decided to use 50 revolutions for the single layer coatings to not affect from the substrates. On the other hand, 100 revolutions was used while applying this test to triode plasma nitrided substrates. In order to maintain the concentration of SiC slurry, a magnetic bar and stirrer were used during the experiment. The wear scar measurements were done with a surface profilometer because the optical microscopy measurements were not found stable.

- The wear coefficient of (approximately 2 μm thick) Ti and Ti-Nb coatings were calculated, and the change of the wear coefficient of Ti-Nb coatings compared to Ti coatings was evaluated. The Ti-Nb coating which contains about 17 at. % Nb resulted with 9 % enhancement. When the Nb concentration is increased, the wear performance of the Ti-Nb coatings was improved. It is about 27 % enhancement was found for the Ti-Nb coatings which contain about 40 at. % Nb. The pure Ti and Ti-Nb (33 at. % Nb) coatings which deposited before nitriding treatment showed about 2 μm and 1.75 μm wear scar depths respectively.

- The ceramic Ti-Nb-N coatings showed better wear performance than the metallic Ti and Ti-Nb coatings. The higher surface roughness values made the measurement difficult for these samples. However, it is about 30 % improvement was seen for the Ti-Nb-N coating (compared to Ti-Nb coating). Unlike the metallic Ti-Nb coatings, the increase of Nb concentration in Ti-Nb-N coatings made these coatings less wear resistance. Therefore, while selecting the desired Nb concentration for the pre-deposition process, the Nb and N relationship should be considered.

- The effect of the triode plasma nitriding treatment (which were applied for different time and temperatures) on the wear performance was evaluated for both substrates. Any changes in the physical and mechanical properties of (uncoated, Ti coated, and Ti-Nb coated) Ti-64 and Ti-AVM substrates (after different diffusion treatments) could affect their wear performance. All results were interpreted by considering these changes and compared to each other. The nitride compound layer (if formed after nitriding treatment), the nitrogen diffusion zone, the pre-deposited Ti or Ti-Nb coatings (if remaining after nitriding treatment) were considered as a whole system.

- TPN500 treatment showed very limited wear enhancement which is related to the amount of nitrogen was diffused inside the substrates. The uncoated Ti-64 and Ti-AVM substrates demonstrated about 11 % and 8 % enhancement after 4-hour treatment (compared to the untreated substrate) on their wear performance respectively. The increase of treatment duration to 8 hours resulted in an improvement of wear resistance. However, it is only 3 %, and 5 % (extra) increase was found for uncoated Ti-64 and Ti-AVM substrates respectively. It was already discussed in Section 2.5.2 that the relationship between the nitriding time and the diffusion depth is not linear.

- The uncoated Ti-64 and Ti-AVM substrates showed about % 19 and % 17 improvement on their wear performance after 4-hour TPN600 treatment (compared to the untreated substrate). It can be said that 100ºC increase of the nitriding temperature has a better effect on wear coefficient than the 4 hours increase of the nitriding duration of TPN500 treatment.

- The wear behaviour after TPN700 treatment was found different for different crystal structured Ti-64 and Ti-AVM substrates because of their affinity to the formation of a nitride layer on their surface. The uncoated Ti-64 substrate showed only %8 enhancement after 4-hour TPN700 treatment which was worse than the 4-hour TPN500 treatment. The reason for this low wear performance was attributed to the formation of the compound layer on the surface of the Ti-64 substrate. The pre-deposited Ti and Ti-Nb coatings before nitriding treatment decreased the wear coefficient values which were approximately 12 % and 16 % enhancement seen respectively. It was referred to the decreased surface roughness and increased diffusion performance.

- The uncoated Ti-AVM substrate showed about 25 % enhancement after 4-hour TPN700 treatment. This substrate maintained the increase the wear performance even at 700ºC. It was already discussed that the mechanical properties of the Ti-AVM substrates were enhanced after 4-hour TPN700 treatment without forming any significant compound layer. Therefore, the corruption on the wear performance (at relatively high temperatures) is related to a thin compound layer formation with weak support from the underlying substrate (which seen for uncoated Ti-64 substrate). The Ti and Ti-Nb coatings (no coating was found after the nitriding treatment) which pre-deposited before the nitriding treatment showed about 5 % enhancement. It is

attributed to the decreased surface roughness compared to the untreated Ti-AVM substrate.

- The increase of the treatment duration from 4 hours to 8 hours for TPN700 treatment resulted with better results for uncoated Ti-64 and uncoated Ti-AVM substrates. It is about 18 % and 45 % enhancement were obtained after 8-hour treatment (compared to the untreated substrate) on their wear performance respectively. The uncoated Ti-AVM substrate (still) did not form any compound layer and maintained the increasing trend on its wear performance. Although the uncoated Ti-64 substrate has formed a thicker compound layer after 8-hour TPN700 treatment (compared to 4-hour treatment), the wear performance was improved. It is because of the more rigid structure of the compound layer and the better support which is coming from the underlying substrate.

- The thicker (5 μm) Ti and Ti-Nb surface layer coated Ti-64 substrates showed better wear performance compared to uncoated ones after 8-hour TPN700 treatment. Their benefits were almost similar, and it is attributed to the decreased surface roughness after the nitriding treatment. On the other hand, the wear performance of the Ti and Ti-Nb coated Ti-AVM substrates were found lower than the uncoated one. It is related to the ceramic nitride phase in which the remaining surface layer coatings formed. The substrates which formed a compound layer on their surface showed lower wear performance. The relatively better wear performance of the Ti-Nb coated Ti-AVM substrate (compared to Ti coated one) after 8-hour TPN700 treatment is attributed to the different morphology of their (formed) nitride layers. It is all concluded that the wear performance of the coating/nitriding processes depends on both the type of the substrate and type of pre-coatings (with various thickness).

CONCLUSIONS AND RECOMMENDATIONS FOR FUTURE WORK

Conclusion

This PhD study consisted of two main sets of experiments: the first one was the production of (metallic and ceramic) PVD coatings for different purposes and the second one was the triode plasma nitriding of (uncoated and previously PVD metallic coated) two different Ti alloy substrates (Ti-64 and Ti-AVM). The aim was to use the different nitrogen diffusion behaviours of the PVD metallic Ti (HCP) and Ti-Nb (BCC) surface coatings to improve the nitrogen diffusion efficiency during plasma nitriding. The physical and mechanical properties of the nitrided substrates were examined (as well as their wear performance) and the effects of diffusion treatment temperature, time (and the thickness of the different pre-deposited PVD surface coatings) on nitrogen surface and bulk diffusion kinetics were investigated. The following conclusions can be drawn:

The metallic Ti and Ti-Nb coatings (with Nb concentration of 18 to 88 at. %.) were produced succesfully. In order to obtain almost fully (β) phase Ti-Nb coatings, it was decided to select at around 33 at. % Nb to balance between the phase stability of the Ti-Nb coating and the higher nitrogen diffusion efficiency of 'pure' β-Ti during plasma nitriding.

The hardening effect for Ti-Nb coated Ti-64 substrate was found to be higher than that of other Ti-64 substrates (after 4-hour TPN700 process) which is related to the higher diffusion rate of nitrogen (in the β phase coating). Nitrogen can diffuse to the substrate faster and allows higher nitrogen concentration (thicker hardened zone) under the surface. The hardening effect for Ti coated Ti-AVM substrate was found higher than other Ti-AVM substrates (after 4-hour TPN700 process). It can be explained with a lower diffusion rate of nitrogen (in the alpha phase coating) allowing the slowdown of the nitrogen interstitials, and they can build up a hardening

199

effect by increasing their concentration in the near-surface rather than spreading inside the Ti alloy substrate.

The 1.25 µm thick Ti and Ti-Nb surface coatings (deposited before plasma nitriding) was sputtered off completely after a 4-hour TPN 700 treatment. The sacrifice of the fine-columnar PVD surface coatings led to decrease in final surface roughness of Ti alloy substrates, compared to uncoated equivalents. The post-nitrided surface roughness value for Ti-Nb coated Ti-64 substrate was found to be 52% less than the uncoated Ti-64 substrate-and a similar improvement was seen for the Ti coated Ti-AVM substrate with a 67% decrease (compared to the uncoated substrate). Therefore, it was suggested that the thickness of the surface coatings should be selected by considering nitriding duration (long-lasting surface coatings) to obtain smother surfaces after plasma nitriding.

The uncoated Ti-64 and Ti-AVM substrates showed remarkable wear enhancement (up to 20 %) after TPN500 and TPN600 treatments. However, micro-abrasion wear performance was found to be low for TPN700 treatment (compared to lower temperatures) for the Ti-64 substrate, which can be attributed to formation of the Ti_2N phase. The Ti and Ti-Nb surface coatings provided some benefit, with approximately 12 % and 16 % enhancement (compared to the untreated substrate) seen respectively after the 4-hour TPN700 treatment. On the other hand, the wear performance of the Ti-AVM continued to improve after TPN700 treatment. The Ti and Ti-Nb surface coatings provided approximately 30 % enhancement (compared to the untreated substrate) to the wear performance of Ti-AVM substrates.

Recommendation for Future Work

This work showed that TPN treatment needs to be designed (individually) for different Ti alloy substrates. If the surface coatings are desired to be deposited before plasma nitriding, the material and the thickness of the coatings should be selected carefully. Some recommendations of this work could be addressed to:

- Depositing α-Ti or β-Ti surface coatings inside the same chamber in which the TPN treatment is taking place. Thus, after depositing a surface coating, the TPN treatment can be started directly (all production stages will occur in the same vacuum environment).

- Ti-Staballoy coatings (the phase structure was predicted as nanocrystalline particles were embedded inside an amorphous matrix) with different Fe, Cr and Mn content should be deposited on Ti alloy substrates to analyse the effect on nitrogen diffusion efficiency during TPN treatment. The structure of the Ti-Staballoy coatings needs to be analysed using TEM, to see the effect of the different additional elements on the phase structure (crystallinity) of the coatings.

- The depth of the nitrogen diffusion zone after TPN treatments can be measured more precisely by glow-discharge optical emission spectroscopy (GDOES) to obtain more reliable nitrogen concentration data from the surface to core of the different titanium alloy substrates after TPN treatments.

- TPN studies should be extended by applying at lower temperatures (i.e. 500ºC) after depositing PVD surface coatings. The sputter removal rate is expected to be slow compared to TPN700 treatment, and thus less thick surface coatings can be selected to increase the nitrogen diffusion efficiency for lower treatment temperatures.

- The characterisation of the phase structure of the uncoated and (thicker) Ti and Ti-Nb coated Ti alloy substrates was complex (after 8-hour TPN700 treatment). The findings

from several XRD experiments need to be checked using TEM (especially to determine α'' martensite and Ti-Al intermetallic phase distributions). Most of the pre-existing nitriding work in the literature does not mention these phases because of the possibility of overlapping the XRD peaks (if the duration of the XRD experiment was selected shorter) is very high.

- Other mechanical properties (such as sliding wear, impact and fatigue resistance) of the samples (produced with duplex diffusion/coating system) will be studied with test samples of an appropriate (larger) size than the samples investigated here.

REFERENCES

[1] G. Cassar, S. Banfield, J. C. Avelar-Batista Wilson, J. Housden, A. Matthews, and A. Leyland, "Micro-abrasion wear testing of triode plasma diffusion and duplex treated Ti–6Al–4V alloy," *Wear*, vol. 274, pp. 377–387, 2012.

[2] G. Cassar, A. Matthews, and A. Leyland, "Triode plasma diffusion treatment of titanium alloys," *Surf. Coatings Technol.*, vol. 212, pp. 20–31, 2012.

[3] B. Attard, A. Matthews, A. Leyland, and G. Cassar, "Enhanced surface performance of Ti-6Al-4V alloy using a novel duplex process combining PVD-Al coating and triode plasma oxidation," *Surf. Coatings Technol.*, vol. 257, pp. 154–164, 2014.

[4] Y. Zhang, Y. Cheng, and D. S. Grummon, "The influence of superelastic NiTi interlayers on tribological properties of CrN hard coatings," *Mater. Sci. Eng. A*, vol. 438, pp. 710–713, 2006.

[5] M. J. Park, A. Leyland, and A. Matthews, "Corrosion performance of layered coatings produced by physical vapour deposition," *Surf. Coatings Technol.*, vol. 43–44, pp. 481–492, Dec. 1990.

[6] Q. H. Fan, A. Fernandes, and J. Gracio, "Diamond coating on steel with a titanium interlayer," *Diam. Relat. Mater.*, vol. 7, no. 2–5, pp. 603–606, Feb. 1998.

[7] N. M. Alanazi, A. Leyland, A. L. Yerokhin, and A. Matthews, "Substitution of hexavalent chromate conversion treatment with a plasma electrolytic oxidation process to improve the corrosion properties of ion vapour deposited AlMg coatings," *Surf. Coatings Technol.*, vol. 205, no. 6, pp. 1750–1756, Dec. 2010.

[8] M. J. Donachie, *Titanium: a technical guide*. ASM International, 1988.

[9] S. Achache, S. Lamri, M. Arab Pour Yazdi, A. Billard, M. François, and F. Sanchette, "Ni-free superelastic binary Ti-Nb coatings obtained by DC magnetron co-sputtering," *Surf. Coatings Technol.*, vol. 275, pp. 283–288, 2015.

[10] R. J. Wasilewski and G. L. Kehl, "Diffusion of nitrogen and oxygen in titanium," *J. Inst. Met.*, vol. 83, 1954.

[11] J. P. Bars, E. Etchessahar, and J. Debuigne, "Kinetics, diffusion and morphology of titanium nitriding using high-temperature nitrogen-mechanical and structural-properties of solid Ti-alpha-nitrogen solutions," *J. Less-Common Met.*, vol. 52, no. 1, pp. 51–76, 1977.

[12] N. Kashaev, H. R. Stock, and P. Mayr, "Nitriding of Ti - 6% Al - 4% v alloy in the plasma of an intensified glow discharge," *Met. Sci. Heat Treat.*, vol. 46, no. 7–8, pp. 294–298, Jul. 2004.

[13] C. A. Hampel, "The Encyclopedia of the Chemical Elements," vol. 164, no. 3880. 09-May-1969.

[14] M. Peters and C. Leyens, *Titanium and titanium alloys: fundamentals and applications*. Wiley, 2003.

[15] M. Könönen and J. Kivilahti, "Concise Review Biomaterials & Bioengineering: Fusing

of Dental Ceramics to Titanium," *J. Dent. Res.*, vol. 80, no. 3, pp. 848–854, Mar. 2001.

[16]   C. Yuan, X. Cheng, G. S. Holt, D. Shevchenko, and P. A. Withey, "Investment casting of Ti-46Al-8Nb-1B alloy using moulds with CaO-stabilized zirconia face coat at various mould pre-heat temperatures," *Ceram. Int.*, vol. 41, no. 3, pp. 4129–4139, Apr. 2015.

[17]   Y. G. Zhou, W. D. Zeng, and H. Q. Yu, "An investigation of a new near-beta forging process for titanium alloys and its application in aviation components," *Mater. Sci. Eng. A*, vol. 393, no. 1–2, pp. 204–212, Feb. 2005.

[18]   L. Bolzoni, E. M. Ruiz-Navas, and E. Gordo, "Influence of sintering parameters on the properties of powder metallurgy Ti-3Al-2.5V alloy," *Mater. Charact.*, vol. 84, pp. 48–57, Oct. 2013.

[19]   I. Papadimitriou, C. Utton, and P. Tsakiropoulos, "The impact of Ti and temperature on the stability of Nb5Si3 phases: A first-principles study," *Sci. Technol. Adv. Mater.*, vol. 18, no. 1, pp. 467–479, 2017.

[20]   G. Lütjering and J. C. Williams, *Titanium.* Springer Berlin Heidelberg, 2007.

[21]   C. R. Krenn, D. Roundy, J. W. Morris, and M. L. Cohen, "Ideal strengths of bcc metals," *Mater. Sci. Eng. A*, vol. 319–321, pp. 111–114, Dec. 2001.

[22]   D. H. Buckley, "The metal-to-metal interface and its effect on adhesion and friction," *J. Colloid Interface Sci.*, vol. 58, no. 1, pp. 36–53, Jan. 1977.

[23]   K. Miyoshi, "Adhesion, friction, and wear behavior of clean metal-ceramic couples," in *International Tribology Conference*, 1995.

[24]   K. G. Budinski, "Tribological properties of titanium alloys," *Wear*, vol. 151, no. 2, pp. 203–217, 1991.

[25]   J. Meneve, K. Vercammen, E. Dekempeneer, and J. Smeets, "Thin tribological coatings: magic or design?," *Surf. Coatings Technol.*, vol. 94–95, pp. 476–482, Oct. 1997.

[26]   A. Matthews and A. Leyland, "Hybrid techniques in surface engineering," *Surf. Coatings Technol.*, vol. 71, no. 2, pp. 88–92, Mar. 1995.

[27]   A. P. Hale, "Preparation and evaluation of epitaxial silicon films prepared by vacuum evaporation," *Vacuum*, vol. 13, no. 3, pp. 93–100, 1963.

[28]   A. Kuroyanagi, "Properties of aluminum-doped ZnO thin films grown by electron beam evaporation," *Jpn. J. Appl. Phys.*, vol. 28, no. 2R, p. 219, 1989.

[29]   I. Ames, F. M. d'Heurle, and R. E. Horstmann, "Reduction of electromigration in aluminum films by copper doping," *IBM J. Res. Dev.*, vol. 14, no. 4, pp. 461–463, 1970.

[30]   P. R. Willmott and J. R. Huber, "Pulsed laser vaporization and deposition," *Rev. Mod. Phys.*, vol. 72, no. 1, p. 315, 2000.

[31]   D. M. Mattox, *Handbook of physical vapor deposition (PVD) processing*. William Andrew, 2010.

[32]   D. Mergel, D. Buschendorf, S. Eggert, R. Grammes, and B. Samset, "Density and refractive index of TiO2films prepared by reactive evaporation," *Thin Solid Films*, vol.

371, no. 1, pp. 218–224, Aug. 2000.

[33] M. F. Al-Kuhaili, M. Saleem, and S. M. A. Durrani, "Optical properties of iron oxide (α-Fe 2O 3) thin films deposited by the reactive evaporation of iron," *J. Alloys Compd.*, vol. 521, pp. 178–182, Apr. 2012.

[34] Y. Golan, L. Margulis, and I. Rubinstein, "Vacuum-deposited gold films," *Surf. Sci.*, vol. 264, no. 3, pp. 312–326, 1992.

[35] J. Zhujing, L. Changqing, Y. Li, and W. Weitao, "Corrosion performance of ion-plated titanium and yttrium-modified TiN coatings," *Surf. Coatings Technol.*, vol. 46, no. 3, pp. 307–315, 1991.

[36] J. J. Garrido, D. Gerstenberg, and R. W. Berry, "Effect of angle of incidence during deposition on Ti-Pd-Au conductor film adhesion," *Thin Solid Films*, vol. 41, no. 1, pp. 87–103, 1977.

[37] P. J. Kelly and R. D. Arnell, "Magnetron sputtering: A review of recent developments and applications," *Vacuum*, vol. 56, no. 3, pp. 159–172, Mar. 2000.

[38] F. M. d'Heurle, "Aluminum films deposited by rf sputtering," *Metall. Mater. Trans. B*, vol. 1, no. 3, pp. 725–732, 1970.

[39] C. Nouvellon, M. Michiels, J. P. Dauchot, C. Archambeau, F. Laffineur, E. Silberberg, S. Delvaux, R. Cloots, S. Konstantinidis, and R. Snyders, "Deposition of titanium oxide films by reactive High Power Impulse Magnetron Sputtering (HiPIMS): Influence of the peak current value on the transition from metallic to poisoned regimes," *Surf. Coatings Technol.*, vol. 206, no. 16, pp. 3542–3549, Apr. 2012.

[40] W. Khan, Q. Wang, X. Jin, and T. Feng, "The Effect of Sputtering Parameters and Doping of Copper on Surface Free Energy and Magnetic Properties of Iron and Iron Nitride Nano Thin Films on Polymer Substrate," *Materials (Basel).*, vol. 10, no. 2, p. 217, 2017.

[41] F. Kurdesau, G. Khripunov, A. F. Da Cunha, M. Kaelin, and A. N. Tiwari, "Comparative study of ITO layers deposited by DC and RF magnetron sputtering at room temperature," *J. Non. Cryst. Solids*, vol. 352, no. 9, pp. 1466–1470, 2006.

[42] T. Kumura, K. Yamauchi, and T. Kobayashi, "Properties of Fe-Al-Si-N thin films prepared by N2 reactive sputtering," *J. Appl. Phys.*, vol. 61, no. 8, pp. 3844–3846, 1987.

[43] C. H. Hsu, M. L. Chen, and K. L. Lai, "Corrosion resistance of TiN/TiAlN-coated ADI by cathodic arc deposition," *Mater. Sci. Eng. A*, vol. 421, no. 1–2, pp. 182–190, Apr. 2006.

[44] H. Randhawa and P. C. Johnson, "Technical note: A review of cathodic arc plasma deposition processes and their applications," *Surf. Coatings Technol.*, vol. 31, no. 4, pp. 303–318, Oct. 1987.

[45] D. M. Sanders and A. Anders, "Review of cathodic arc deposition technology at the start of the new millennium," *Surf. Coatings Technol.*, vol. 133–134, pp. 78–90, Nov. 2000.

[46] D. Mattox, "Fundamentals of ion plating," *J. Vac. Sci. Technol.*, vol. 10, no. 1, pp. 47–52, 1973.

[47] D. M. Mattox, "Film deposition using accelerated ions," Sandia Lab., Albuquerque, N. Mex., 1963.

[48] D. M. Mattox, "Ion plating—past, present and future," *Surf. Coatings Technol.*, vol. 133, pp. 517–521, 2000.

[49] B. Zega, M. Kornmann, and J. Amiguet, "Hard decorative TiN coatings by ion plating," *Thin Solid Films*, vol. 45, no. 3, pp. 577–582, Sep. 1977.

[50] Tsutomu Ikeda and Hiroshi Satoh, "Phase formation and characterization of hard coatings in the TiAlN system prepared by the cathodic arc ion plating method," *Thin Solid Films*, vol. 195, no. 1–2, pp. 99–110, Jan. 1991.

[51] A. M. Chaze and C. Coddet, "The role of nitrogen in the oxidation behaviour of titanium and some binary alloys," *J. Less-Common Met.*, vol. 124, no. 1–2, pp. 73–84, Oct. 1986.

[52] A. Zhecheva, S. Malinov, and W. Sha, "Titanium alloys after surface gas nitriding," *Surf. Coatings Technol.*, vol. 201, no. 6, pp. 2467–2474, 2006.

[53] H. Shibata, K. Tokaji, T. Ogawa, and C. Hori, "The effect of gas nitriding on fatigue behaviour in titanium alloys," *Int. J. Fatigue*, vol. 16, no. 6, pp. 370–376, Aug. 1994.

[54] W. Sha, Ak Muhd Fu'Ad Pg Haji Ali, and X. Wu, "Gas nitriding of titanium alloy Timetal 205," *Surf. Coatings Technol.*, vol. 202, no. 24, pp. 5832–5837, Aug. 2008.

[55] S. Mridha and T. N. Baker, "Effects of nitrogen gas flow rates on the microstructure and properties of laser-nitrided IMI318 titanium alloy (Ti–4V–6Al)," *J. Mater. Process. Technol.*, vol. 77, no. 1–3, pp. 115–121, May 1998.

[56] A. Zhecheva, W. Sha, S. Malinov, and A. Long, "Enhancing the microstructure and properties of titanium alloys through nitriding and other surface engineering methods," *Surf. Coatings Technol.*, vol. 200, no. 7, pp. 2192–2207, Dec. 2005.

[57] P. A. Coulon and G. Alsthom, "Resistance to wear of nitriding on titanium alloy using the laser-irradiation technique," *J. Mater. Process. Tech.*, vol. 38, no. 1–2, pp. 247–263, Feb. 1993.

[58] A. Grill, "Ion beam nitriding of titanium and titanium alloy," *Vacuum*, vol. 33, no. 6, pp. 333–337, Jun. 1983.

[59] U. Ebersbach, F. Henny, U. Winckler, G. Reisse, and C. Weissmantel, "Ion beam nitriding of high purity iron surfaces," *Thin Solid Films*, vol. 112, no. 1, pp. 29–40, 1984.

[60] A. Gicquel, N. Laidani, and P. Saillard, "Plasma and nitrides: application to the nitriding of titanium," *Pure Appl. Chem.*, vol. 62, no. 9, pp. 1743–1750, 1990.

[61] M. Mubarak Ali, S. Ganesh Sundara Raman, S. D. Pathak, and R. Gnanamoorthy, "Influence of plasma nitriding on fretting wear behaviour of Ti-6Al-4V," *Tribol. Int.*, vol. 43, no. 1–2, pp. 152–160, Jan. 2010.

[62] T. M. Muraleedharan and E. I. Meletis, "Surface modification of pure titanium and Ti6A14V by intensified plasma ion nitriding," *Thin Solid Films*, vol. 221, no. 1–2, pp. 104–113, Dec. 1992.

[63] T. Bell, H. W. Bergmann, J. Lanagan, P. H. Morton, and A. M. Staines, "Surface engineering of titanium with nitrogen," *Surf. Eng.*, vol. 2, no. 2, pp. 133–143, 1986.

[64] K. C. Chen and G. J. Jaung, "Dc diode ion nitriding behavior of titanium and Ti-6Al-4V," *Thin Solid Films*, vol. 303, no. 1–2, pp. 226–231, 1997.

[65] K. S. Fancey and A. Matthews, "Process effects in ion plating," *Vacuum*, vol. 41, no. 7–9, pp. 2196–2200, 1990.

[66] W. D. Davis and T. A. Vanderslice, "Ion Energies at the Cathode of a Glow Discharge," *Phys. Rev.*, vol. 131, no. 1, pp. 219–228, Jul. 1963.

[67] J. Rickards, "Energies of particles at the cathode of a glow discharge," *Vacuum*, vol. 34, no. 5, pp. 559–562, 1984.

[68] K. Wagatsuma and K. Hirokawa, "Effect of oxygen addition to an argon glow-discharge plasma source in atomic emission spectrometry," *Anal. Chim. Acta*, vol. 306, no. 2, pp. 193–200, 1995.

[69] A. Matthews and D. G. Teer, "Characteristics of a thermionically assisted triode ion-plating system," *Thin Solid Films*, vol. 80, no. 1–3, pp. 41–48, 1981.

[70] A. Leyland, K. S. Fancey, and A. Matthews, "Plasma nitriding in a low pressure triode discharge to provide improvements in adhesion and load support for wear resistant coatings," *Surf. Eng.*, vol. 7, no. 3, pp. 207–215, 1991.

[71] J. C. Avelar-Batista, E. Spain, J. Housden, A. Matthews, and G. G. Fuentes, "Plasma nitriding of Ti6Al4V alloy and AISI M2 steel substrates using DC glow discharges under a triode configuration," *Surf. Coatings Technol.*, vol. 200, no. 5, pp. 1954–1961, 2005.

[72] A. Leyland, K. S. Fancey, A. S. James, and A. Matthews, "Enhanced plasma nitriding at low pressures: a comparative study of dc and rf techniques," *Surf. Coatings Technol.*, vol. 41, no. 3, pp. 295–304, 1990.

[73] D. B. Lee, I. Pohrelyuk, O. Yaskiv, and J. C. Lee, "Gas nitriding and subsequent oxidation of Ti-6Al-4V alloys," *Nanoscale Res. Lett.*, vol. 7, no. 1, p. 21, Jan. 2012.

[74] A. Leyland, "Design and plasma synthesis of tribological surface for titanium," in *ICMCTF Conference*, 2012.

[75] J. Qian, K. Farokhzadeh, and A. Edrisy, "Ion nitriding of a near-β titanium alloy: Microstructure and mechanical properties," *Surf. Coatings Technol.*, vol. 258, pp. 134–141, 2014.

[76] W. Sha, M. A. Haji Mat Don, A. Mohamed, X. Wu, B. Siliang, and A. Zhecheva, "X-ray diffraction, optical microscopy, and microhardness studies of gas nitrided titanium alloys and titanium aluminide," *Mater. Charact.*, vol. 59, no. 3, pp. 229–240, 2008.

[77] I. Pohrelyuk and V. Fedirko, "Chemico-Thermal Treatment of Titanium Alloys-Nitriding," in *Titanium Alloys-Towards Achieving Enhanced Properties for Diversified Applications*, InTech, 2012.

[78] R. G. and B. S. and R. P. and M.-L. Antti, "Study of alpha-case depth in Ti-6Al-2Sn-4Zr-2Mo and Ti-6Al-4V," *IOP Conf. Ser. Mater. Sci. Eng.*, vol. 48, no. 1, p. 12002,

2013.

[79]   Y.-Z. Xing, G. Wang, Y. Zhang, Y.-N. Chen, and M. Dargusch, "Development in plasma surface diffusion techniques of Ti-6Al-4V alloy: a review," *Int. J. Adv. Manuf. Technol.*, vol. 92, no. 5–8, pp. 1901–1912, 2017.

[80]   R. Abbaschian and R. E. Reed-Hill, *Physical metallurgy principles*. Cengage Learning, 2008.

[81]   V. Fouquet, L. Pichon, M. Drouet, and A. Straboni, "Plasma assisted nitridation of Ti-6Al-4V," *Appl. Surf. Sci.*, vol. 221, no. 1–4, pp. 248–258, Jan. 2004.

[82]   C. I. Costescu and B. J. Heuser, "The effect of a nitrogen-rich surface layer on the sub-surface deuterium (hydrogen) concentration distribution in titanium," *Surf. Sci.*, vol. 450, no. 3, pp. 242–250, 2000.

[83]   T. Morita, H. Takahashi, M. Shimizu, and K. Kawasaki, "Factors controlling the fatigue strength of nitrided titanium," *Fatigue Fract. Eng. Mater. Struct.*, vol. 20, no. 1, pp. 85–92, 1997.

[84]   M. Rahman, I. Reid, P. Duggan, D. P. Dowling, G. Hughes, and M. S. J. Hashmi, "Structural and tribological properties of the plasma nitrided Ti-alloy biomaterials: Influence of the treatment temperature," *Surf. Coatings Technol.*, vol. 201, no. 9, pp. 4865–4872, 2007.

[85]   F. Yildiz, A. F. Yetim, A. Alsaran, and A. Çelik, "Plasma nitriding behavior of Ti6Al4V orthopedic alloy," *Surf. Coatings Technol.*, vol. 202, no. 11, pp. 2471–2476, 2008.

[86]   P. Jacquot, M. Buvron, and J. P. Souchard, "Plasma Nitriding and Plasma Carburizing of Pure Titanium and Ti6Al4V Alloy," in *Materials Science Forum*, 1992, vol. 102, pp. 301–318.

[87]   F. J. Gil, R. Canedo, A. Padrós, and E. Sada, "Enhanced Wear Resistance of Ball-And-Socket Joints of Dental Implants by Means of Titanium Gaseous Nitriding," *J. Biomater. Appl.*, vol. 17, no. 1, pp. 31–43, 2002.

[88]   G. G. Maksimovich, I. N. Pogrelyuk, and V. N. Fedirko, "Structure formation in nitrided layers of titanium alloys," *Met. Sci. Heat Treat.*, vol. 28, no. 6, pp. 393–397, Jun. 1986.

[89]   V. M. Fedirko, I. M. Pogrelyuk, V. A. Lopushan'skii, and V. I. Kalyandruk, "Nitriding VT35 β-titanium alloy," *Mater. Sci.*, vol. 29, no. 2, pp. 165–169, Mar. 1993.

[90]   N. G. Boriskina, D. P. Shashkov, E. M. Kenina, and V. M. Mikhalin, "Effect of nitriding on the structure of the surface layers and properties of titanium alloys AT3 and AT6," *Met. Sci. Heat Treat.*, vol. 23, no. 7, pp. 503–506, Jul. 1981.

[91]   K.-T. Rie, T. Stucky, R. A. Silva, E. Leit≈ao, K. Bordji, J.-Y. Jouzeau, and D. Mainard, "Plasma surface treatment and PACVD on Ti alloys for surgical implants," *Surf. Coatings Technol.*, vol. 74–75, pp. 973–980, 1995.

[92]   C. Badini, C. Gianoglio, T. Bacci, and B. Tesi, "Characterization of surface layers in ion-nitrided titanium and titanium alloys," *J. Less Common Met.*, vol. 143, no. 1–2, pp. 129–141, 1988.

[93] B. S. Yilbas, A. Z. Sahin, A. Z. Al-Garni, S. A. M. Said, Z. Ahmed, B. J. Abdulaleem, and M. Sami, "Plasma nitriding of Ti-6Al-4V alloy to improve some tribological properties," *Surf. Coatings Technol.*, vol. 80, no. 3, pp. 287–292, Apr. 1996.

[94] S. G. Lakshmi, D. Arivuoli, and B. Ganguli, "Surface modification and characterisation of Ti–Al–V alloys," *Mater. Chem. Phys.*, vol. 76, no. 2, pp. 187–190, 2002.

[95] F. Galliano, E. Galvanetto, S. Mischler, and D. Landolt, "Tribocorrosion behavior of plasma nitrided Ti–6Al–4V alloy in neutral NaCl solution," *Surf. Coatings Technol.*, vol. 145, no. 1, pp. 121–131, Aug. 2001.

[96] C. Anandan, P. D. Babu, and L. Mohan, "Effect of Gas Composition on Nitriding and Wear Behavior of Nitrided Titanium Alloy Ti-15V-3Cr-3Al-3Sn," *J. Mater. Eng. Perform.*, vol. 22, no. 9, pp. 2623–2633, Sep. 2013.

[97] Y. V. Borisyuk, N. M. Oreshnikova, M. A. Berdnikova, A. V. Tumarkin, G. V. Khodachenko, and A. A. Pisarev, "Plasma nitriding of titanium alloy Ti5Al4V2Mo," in *Physics Procedia*, 2015, vol. 71, pp. 105–109.

[98] G. Cassar, J. C. A.-B. Wilson, S. Banfield, J. Housden, A. Matthews, and A. Leyland, "A study of the reciprocating-sliding wear performance of plasma surface treated titanium alloy," *Wear*, vol. 269, no. 1, pp. 60–70, 2010.

[99] S. L. R. Da Silva, L. O. Kerber, L. Amaral, and C. A. Dos Santos, "X-ray diffraction measurements of plasma-nitrided Ti–6Al–4V," *Surf. Coatings Technol.*, vol. 116, pp. 342–346, 1999.

[100] A. Zhecheva, S. Malinov, I. Katzarov, and W. Sha, "Modelling of kinetics of nitriding titanium alloys," *Surf. Eng.*, vol. 22, no. 6, pp. 452–454, 2006.

[101] A. Zhecheva, S. Malinov, and W. Sha, "Surface gas nitriding of Ti-6Al-4V and Ti-6Al-2Sn-4Zr-2Mo-0.08 Si alloys," *Zeitschrift für Met.*, vol. 94, no. 1, pp. 19–24, 2003.

[102] J. Dossett and G. E. Totten, "Introduction to Surface Hardening of Steels," *ASM Handb.*, vol. 4, 2013.

[103] J. Morgiel and T. Wierzchoń, "New estimate of phase sequence in diffusive layer formed on plasma nitrided Ti-6Al-4V alloy," *Surf. Coatings Technol.*, vol. 259, pp. 473–482, 2014.

[104] K. S. Fancey and A. Matthews, "Some fundamental aspects of glow discharges in plasma-assisted processes," *Surf. Coatings Technol.*, vol. 33, pp. 17–29, 1987.

[105] A. Matthews, K. S. Fancey, A. S. James, and A. Leyland, "Ionization in plasma-assisted physical vapour deposition systems," *Surf. Coatings Technol.*, vol. 61, no. 1, pp. 121–126, 1993.

[106] T. Czerwiec, H. Michel, and E. Bergmann, "Low-pressure, high-density plasma nitriding: mechanisms, technology and results," *Surf. Coatings Technol.*, vol. 108–109, pp. 182–190, 1998.

[107] H. J. Spies, "Surface engineering of aluminium and titanium alloys: an overview," *Surf. Eng.*, vol. 26, no. 1–2, pp. 126–134, 2010.

[108] K. T. Rie and T. Lampe, "Thermochemical surface treatment of titanium and titanium alloy Ti6Al4V by low energy nitrogen ion bombardment," *Mater. Sci. Eng.*, vol. 69, no. 2, pp. 473–481, 1985.

[109] K. T. Rie, T. Lampe, and S. Eisenberg, "Plasma Heat Treatment of Titanium and Titanium Alloy Ti-6Al-4V: Effect of Gas Composition and Temperature," *Surf. Eng.*, vol. 1, no. 3, pp. 198–202, 1985.

[110] H. J. Spies, B. Reinhold, and K. Wilsdorf, "Gas nitriding–process control and nitriding non-ferrous alloys," *Surf. Eng.*, vol. 17, no. 1, pp. 41–54, 2001.

[111] H. J. Brading, P. H. Morton, T. Bell, and L. G. Earwaker, "Plasma nitriding with nitrogen, hydrogen, and argon gas mixtures: structure and composition of coatings on titanium," *Surf. Eng.*, vol. 8, no. 3, pp. 206–212, 1992.

[112] G. Cassar, S. Banfield, J. C. A.-B. Wilson, J. Housden, A. Matthews, and A. Leyland, "Tribological properties of duplex plasma oxidised, nitrided and PVD coated Ti–6Al–4V," *Surf. Coatings Technol.*, vol. 206, no. 2, pp. 395–404, 2011.

[113] G. Cassar, S. Banfield, J. C. A.-B. Wilson, J. Housden, A. Matthews, and A. Leyland, "Impact wear resistance of plasma diffusion treated and duplex treated/PVD-coated Ti–6Al–4V alloy," *Surf. Coatings Technol.*, vol. 206, no. 10, pp. 2645–2654, 2012.

[114] S. Taktak and H. Akbulut, "Diffusion kinetics of explosively treated and plasma nitrided Ti–6Al–4V alloy," *Vacuum*, vol. 75, no. 3, pp. 247–259, 2004.

[115] S. Taktak and H. Akbulut, "Dry wear and friction behaviour of plasma nitrided Ti–6AL–4V alloy after explosive shock treatment," *Tribol. Int.*, vol. 40, no. 3, pp. 423–432, 2007.

[116] K. Farokhzadeh, J. Qian, and A. Edrisy, "Effect of SPD surface layer on plasma nitriding of Ti–6Al–4V alloy," *Mater. Sci. Eng. A*, vol. 589, pp. 199–208, 2014.

[117] S. M. Johns, T. Bell, M. Samandi, and G. A. Collins, "Wear resistance of plasma immersion ion implanted Ti6Al4V," *Surf. Coatings Technol.*, vol. 85, no. 1, pp. 7–14, 1996.

[118] V. Fouquet, L. Pichon, A. Straboni, and M. Drouet, "Nitridation of Ti6Al4V by PBII: study of the nitrogen diffusion and of the nitride growth mechanism," *Surf. Coatings Technol.*, vol. 186, no. 1, pp. 34–39, 2004.

[119] V. Pecharsky and P. Zavalij, *Fundamentals of Powder Diffraction and Structural Characterization of Materials*. Springer US, 2005.

[120] C. Quaeyhaegens, L. M. Stals, M. Van Stappen, and L. De Schepper, "Interface study of TiN- and Ti-TiN-coated stainless steel AISI 304 with asymmetric glancing angle X-ray diffraction and classical Bragg-Brentano X-ray diffraction," *Thin Solid Films*, vol. 197, no. 1–2, pp. 37–46, Mar. 1991.

[121] D. B. Murphy, *Fundamentals of light microscopy and electronic imaging*. John Wiley & Sons, 2002.

[122] P. J. Goodhew, J. Humphreys, and R. Beanland, *Electron microscopy and analysis*. CRC Press, 2000.

[123] L. Reimer, "Scanning electron microscopy: physics of image formation and microanalysis." IOP Publishing, 2000.

[124] I. M. Watt, *The principles and practice of electron microscopy*. Cambridge University Press, 1997.

[125] J. C. Russ, *Fundamentals of Energy Dispersive X-Ray Analysis: Butterworths Monographs in Materials*. Butterworth-Heinemann, 2013.

[126] D. Shindo and T. Oikawa, *Analytical electron microscopy for materials science*. Springer Science & Business Media, 2013.

[127] J. Goldstein, D. E. Newbury, P. Echlin, D. C. Joy, A. D. Romig Jr, C. E. Lyman, C. Fiori, and E. Lifshin, *Scanning electron microscopy and X-ray microanalysis: a text for biologists, materials scientists, and geologists*. Springer Science & Business Media, 2012.

[128] A. C. Fischer-Cripps, *Nanoindentation*. Springer New York, 2011.

[129] W. C. Oliver and G. M. Pharr, "An improved technique for determining hardness and elastic modulus using load and displacement sensing indentation experiments," *J. Mater. Res.*, vol. 7, no. 6, pp. 1564–1583, 1992.

[130] W. C. Oliver and G. M. Pharr, "Measurement of hardness and elastic modulus by instrumented indentation: Advances in understanding and refinements to methodology," *J. Mater. Res.*, vol. 19, no. 1, pp. 3–20, 2004.

[131] S. Liu and Q. J. Wang, "Determination of Young's modulus and Poisson's ratio for coatings," *Surf. Coatings Technol.*, vol. 201, no. 14, pp. 6470–6477, 2007.

[132] N. A. Sakharova, J. V Fernandes, J. M. Antunes, and M. C. Oliveira, "Comparison between Berkovich, Vickers and conical indentation tests: A three-dimensional numerical simulation study," *Int. J. Solids Struct.*, vol. 46, no. 5, pp. 1095–1104, 2009.

[133] E384-11, "ASTM-Standard Test Method for Knoop and Vickers Hardness of Materials." .

[134] K. Herrmann, *Hardness testing: principles and applications*. ASM International, 2011.

[135] K. L. Rutherford and I. M. Hutchings, "Theory and application of a micro-scale abrasive wear test," *J. Test. Eval.*, vol. 25, no. 2, pp. 250–260, 1997.

[136] R. I. Trezona and I. M. Hutchings, "Three-body abrasive wear testing of soft materials," *Wear*, vol. 233, pp. 209–221, 1999.

[137] J. C. A. Batista, M. C. Joseph, C. Godoy, and A. Matthews, "Micro-abrasion wear testing of PVD TiN coatings on untreated and plasma nitrided AISI H13 steel," *Wear*, vol. 249, no. 10–11, pp. 971–979, 2001.

[138] J. C. A. Batista, C. Godoy, and A. Matthews, "Micro-scale abrasive wear testing of duplex and non-duplex (single-layered) PVD (Ti, Al) N, TiN and Cr–N coatings," *Tribol. Int.*, vol. 35, no. 6, pp. 363–372, 2002.

[139] M. M. Stack and M. Mathew, "Micro-abrasion transitions of metallic materials," *Wear*,

vol. 255, no. 1–6, pp. 14–22, 2003.

[140] M. H. Staia, C. E. Enriquez, E. S. Puchi, D. B. Lewis, and M. Jeandin, "Application of Ball Cratering Method To Study Abrasive Wear," *Surf. Eng.*, vol. 14, no. 1, pp. 49–54, 1998.

[141] A. J. Gant and M. G. Gee, "A review of micro-scale abrasion testing," *J. Phys. D. Appl. Phys.*, vol. 44, no. 7, p. 73001, 2011.

[142] J. D. Gates, "Two-body and three-body abrasion: A critical discussion," *Wear*, vol. 214, no. 1, pp. 139–146, 1998.

[143] "Fine Ceramics (advanced ceramics, advanced technical ceramics)-Determination of the abrasion resistance of coatings by a micro-scale abrasion test -BS-ISO 26424:2008."

[144] K. L. Rutherford and I. M. Hutchings, "A micro-abrasive wear test, with particular application to coated systems," *Surf. Coatings Technol.*, vol. 79, no. 1–3, pp. 231–239, 1996.

[145] D. Culliton, A. Betts, S. Carvalho, and D. Kennedy, "Improving tribological properties of cast Al-Si alloys through application of wear-resistant thermal spray coatings," *J. Therm. spray Technol.*, vol. 22, no. 4, pp. 491–501, 2013.

[146] D. H. Buckley, *Surface effects in adhesion, friction, wear, and lubrication*, vol. 5. Elsevier, 1981.

[147] M. Niinomi, "Mechanical properties of biomedical titanium alloys," *Mater. Sci. Eng. A*, vol. 243, no. 1, pp. 231–236, 1998.

[148] A. Akbari, R. Mohammadzadeh, C. Templier, and J. P. Riviere, "Effect of the initial microstructure on the plasma nitriding behavior of AISI M2 high speed steel," *Surf. Coatings Technol.*, vol. 204, no. 24, pp. 4114–4120, 2010.

[149] E. D. Gonzalez, C. R. M. Afonso, and P. A. P. Nascente, "Influence of Nb content on the structure, morphology, nanostructure, and properties of titanium-niobium magnetron sputter deposited coatings for biomedical applications," *Surf. Coatings Technol.*, vol. 326, pp. 424–428, Oct. 2017.

[150] V. Starý, L. Cvrček, S. Daniš, J. Krčil, J. Málek, and Z. Tolde, "Characterization of TiNb Films on Ti Alloys for Hard Tissue Replacement," in *Solid State Phenomena*, 2017, vol. 258, pp. 345–349.

[151] L. L. Chang, Y. D. Wang, and Y. Ren, "In-situ investigation of stress-induced martensitic transformation in Ti–Nb binary alloys with low Young's modulus," *Mater. Sci. Eng. A*, vol. 651, pp. 442–448, 2016.

[152] T. Ahmed and H. J. Rack, "Martensitic transformations in Ti-(16-26 at %) Nb alloys," *J. Mater. Sci.*, vol. 31, no. 16, pp. 4267–4276, Jan. 1996.

[153] D. L. Moffat and D. C. Larbalestier, "The compctition between martensite and omega in quenched Ti-Nb alloys," *Metall. Trans. A*, vol. 19, no. 7, pp. 1677–1686, Jul. 1988.

[154] E. D. Gonzalez, T. C. Niemeyer, C. R. M. Afonso, and P. A. P. Nascente, "Ti-Nb thin films deposited by magnetron sputtering on stainless steel," *J. Vac. Sci. Technol. A*

Vacuum, Surfaces, Film., vol. 34, no. 2, p. 021511, Mar. 2016.

[155] D. Photiou, N. T. Panagiotopoulos, L. Koutsokeras, G. A. Evangelakis, and G. Constantinides, "Microstructure and nanomechanical properties of magnetron sputtered Ti − Nb films," *Surf. Coatings Technol.*, vol. 302, pp. 310–319, 2016.

[156] R. Mohammadzadeh, A. Akbari, and M. Drouet, "Microstructure and wear properties of AISI M2 tool steel on RF plasma nitriding at different N2-H2gas compositions," *Surf. Coatings Technol.*, vol. 258, pp. 566–573, Nov. 2014.

[157] R. Wuhrer and W. Y. Yeung, "Effect of target–substrate working distance on magnetron sputter deposition of nanostructured titanium aluminium nitride coatings," *Scr. Mater.*, vol. 49, no. 3, pp. 199–205, 2003.

[158] I. Y. Burmakinskii and A. V Rogov, "Effect of resonance charge exchange between argon ions on the effective sputtering rate in a magnetron discharge," *Tech. Phys.*, vol. 49, no. 1, pp. 119–122, Jan. 2004.

[159] Y. Yamamura and H. Tawara, "Energy Dependence of Ion-Induced Sputtering Yields from Monatomic Solids at Normal Incidence," *At. Data Nucl. Data Tables*, vol. 63, no. 0016, p. 1996, 1996.

[160] Y. Pauleau and P. Barna, *Protective Coatings and Thin Films: Synthesis, Characterization and Applications.*, vol. 21. Springer Science & Business Media, 1997.

[161] V. Valvoda, "Structure of thin films of titanium nitride," *J. Alloys Compd.*, vol. 219, no. 1, pp. 83–87, 1995.

[162] A. Karimi, O. R. Shojaei, T. Kruml, and J. L. Martin, "Characterisation of TiN thin films using the bulge test and the nanoindentation technique," *Thin Solid Films*, vol. 308–309, pp. 334–339, 1997.

[163] G. Abadias, S. Dub, and R. Shmegera, "Nanoindentation hardness and structure of ion beam sputtered TiN, W and TiN/W multilayer hard coatings," *Surf. Coatings Technol.*, vol. 200, no. 22, pp. 6538–6543, 2006.

[164] L. Shan, Y. Wang, J. Li, H. Li, X. Wu, and J. Chen, "Tribological behaviours of PVD TiN and TiCN coatings in artificial seawater," *Surf. Coatings Technol.*, vol. 226, pp. 40–50, 2013.

[165] A. Leyland and A. Matthews, "On the significance of the H/E ratio in wear control: a nanocomposite coating approach to optimised tribological behaviour," *Wear*, vol. 246, no. 1, pp. 1–11, 2000.

[166] J. Lawal, P. Kiryukhantsev-Korneev, A. Matthews, and A. Leyland, "Mechanical properties and abrasive wear behaviour of Al-based PVD amorphous/nanostructured coatings," *Surf. Coatings Technol.*, vol. 310, pp. 59–69, 2017.

[167] F. W. Wood and O. G. Paasche, "Dubious details of nitrogen diffusion in nitrided titanium," *Thin Solid Films*, vol. 40, pp. 131–137, 1977.

[168] A. C. Fernandes, F. Vaz, E. Ariza, L. A. Rocha, A. R. L. Ribeiro, A. C. Vieira, J. P. Rivière, and L. Pichon, "Tribocorrosion behaviour of plasma nitrided and plasma nitrided + oxidised Ti6Al4V alloy," *Surf. Coatings Technol.*, vol. 200, no. 22–23 SPEC.

ISS., pp. 6218–6224, Jun. 2006.

[169] A. Wilson, A. Matthews, J. Housden, R. Turner, and B. Garside, "A comparison of the wear and fatigue properties of plasma-assisted physical vapour deposition TiN, CrN and duplex coatings on Ti-6Al-4V," *Surf. Coatings Technol.*, vol. 62, no. 1–3, pp. 600–607, Dec. 1993.

[170] A. Fossati, F. Borgioli, E. Galvanetto, and T. Bacci, "Corrosion resistance properties of plasma nitrided Ti-6Al-4V alloy in nitric acid solutions," *Corros. Sci.*, vol. 46, no. 4, pp. 917–927, Apr. 2004.

[171] W. L. Finlay and J. A. Snyder, "Effects of three interstitial solutes (nitrogen, oxygen, and carbon) on the mechanical properties of high-purity, alpha titanium," *JOM*, vol. 2, no. 2, pp. 277–286, Feb. 1950.

[172] F. Vaz, J. Ferreira, E. Ribeiro, L. Rebouta, S. Lanceros-Méndez, J. A. Mendes, E. Alves, P. Goudeau, J. P. Rivière, F. Ribeiro, I. Moutinho, K. Pischow, and J. de Rijk, "Influence of nitrogen content on the structural, mechanical and electrical properties of TiN thin films," *Surf. Coatings Technol.*, vol. 191, no. 2–3, pp. 317–323, Feb. 2005.

[173] J. P. Bars, D. David, E. Etchessahar, and J. Debuigne, "Titanium α- nitrogen solid solution formed by high temperature nitriding: diffusion of nitrogen, hardness, and crystallographic parameters," *Metall. Trans. A*, vol. 14, no. 8, pp. 1537–1543, Aug. 1983.

[174] G. Cassar, J. C. Avelar-Batista Wilson, S. Banfield, J. Housden, M. Fenech, A. Matthews, and A. Leyland, "Evaluating the effects of plasma diffusion processing and duplex diffusion/PVD-coating on the fatigue performance of Ti-6Al-4V alloy," *Int. J. Fatigue*, vol. 33, no. 9, pp. 1313–1323, Sep. 2011.

[175] J. Keinonen, J. Räisänen, and A. Anttila, "Diffusion of nitrogen in vanadium and niobium," *Appl. Phys. A*, vol. 34, no. 1, pp. 49–56, 1984.

[176] F. J. M. Boratto and R. E. Reed-Hill, "Oxygen and nitrogen diffusion in vanadium," *Scr. Metall.*, vol. 11, no. 12, pp. 1107–1111, 1977.

[177] F. A. Schmidt and J. C. Warner, "Diffusion of carbon, nitrogen and oxygen in vanadium between 60 and 1825° C," *J. Less Common Met.*, vol. 26, no. 2, pp. 325–326, 1972.

[178] F. J. M. Boratto and R. E. Reed-Hill, "On the calculations of the diffusion coefficients of oxygen and nitrogen in niobium," *Metall. Trans. A*, vol. 8, no. 8, pp. 1233–1238, 1977.

[179] C. Y. Ang, "Activation energies and diffusion coefficients of oxygen and nitrogen in niobium and tantalum," *Acta Metall.*, vol. 1, no. 2, pp. 123–125, 1953.

[180] F. J. M. Boratto and R. E. Reed-Hill, "Oxygen and nitrogen diffusion in tantalum," *Scr. Metall.*, vol. 11, no. 3, pp. 1107–1111, 1978.

[181] J. Keinonen, J. Räisänen, and A. Anttila, "Diffusion of nitrogen in ion-implanted chromium and tungsten," *Appl. Phys. A*, vol. 35, no. 4, pp. 227–232, 1984.

[182] R. Frauenfelder, "Permeation, Diffusion, and Solution of Nitrogen in Tungsten and Molybdenum," *The Journal of chemical physics.*, vol. 48, no. 9. pp. 3966–3971, 1968.

[183] E. A. Gulbransen and K. F. Andrew, "Kinetics of the Reactions of Zirconium with O 2, N 2 and H 2," *JOM*, vol. 1, no. 8, pp. 515–525, 1949.

[184] A. Lussi, *Dental erosion: from diagnosis to therapy*, vol. 20. Karger Medical and Scientific Publishers, 2006.

[185] T. Bacci, G. Pradelli, B. Tesi, C. Gianoglio, and C. Badini, "Surface engineering and chemical characterization in ion-nitrided titanium and titanium alloys," *J. Mater. Sci.*, vol. 25, no. 10, pp. 4309–4314, Oct. 1990.

[186] K. Farokhzadeh, A. Edrisy, G. Pigott, and P. Lidster, "Scratch resistance analysis of plasma-nitrided Ti–6Al–4V alloy," *Wear*, vol. 302, no. 1, pp. 845–853, 2013.

[187] B. Podgornik, J. Vižintin, and V. Leskovšek, "Wear properties of induction hardened, conventional plasma nitrided and pulse plasma nitrided AISI 4140 steel in dry sliding conditions," *Wear*, vol. 232, no. 2, pp. 231–242, 1999.

[188] D. Batory, W. Szymanski, M. Panjan, O. Zabeida, and J. E. Klemberg-Sapieha, "Plasma nitriding of Ti6Al4V alloy for improved water erosion resistance," *Wear*, vol. 374, pp. 120–127, 2017.

[189] A. Czyrska-Filemonowicz, P. A. Buffat, M. Łucki, T. Moskalewicz, W. Rakowski, J. Lekki, and T. Wierzchoń, "Transmission electron microscopy and atomic force microscopy characterisation of titanium-base alloys nitrided under glow discharge," *Acta Mater.*, vol. 53, no. 16, pp. 4367–4377, 2005.

[190] M. K. Khalaf, B. T. Chiad, T. L. Al-Zubaydi, and Z. T. Alani, "Surface Modification of Ti6Al4V Alloy by Glow Dicharge-Plasma Nitriding," *Iraqi J. Phys.*, vol. 9, no. 16, pp. 34–40, 2011.

[191] P. J. Bania, "Beta titanium alloys and their role in the titanium industry," *JOM*, vol. 46, no. 7, pp. 16–19, Jul. 1994.

[192] D. M. Gordin, A. Guillou, I. Thibon, M. Bohn, D. Ansel, and T. Gloriant, "Duplex nitriding treatment of a beta-metastable Ti94Mo6 alloy for biomedical applications," *J. Alloys Compd.*, vol. 457, no. 1, pp. 384–388, 2008.

[193] D. M. Gordin, I. Thibon, A. Guillou, D. Ansel, and T. Gloriant, "Gas Nitriding of Biocompatible Beta Titanium Alloys," *Ti-2007, Sci. Technol. Proc. 11th World Conf. Titan. held Kyoto Int. Conf. Center, Kyoto, Japan, 3-7 June 2007 / Ed. by M. Niinomi .*, pp. 1731–1734, 2007.

[194] W. Lenguaer and P. Ettmayer, "Investigations of phase equilibria in the Ti-N and Ti-Mo-N systems," *Mater. Sci. Eng. A*, vol. 106, pp. 257–263, 1988.

[195] L. Mohan and C. Anandan, "Effect of gas composition on corrosion behavior and growth of apatite on plasma nitrided titanium alloy Beta-21S," *Appl. Surf. Sci.*, vol. 268, pp. 288–296, 2013.

[196] T. Akahori, M. Niinomi, M. Nakai, H. Nishimura, Y. Takei, H. Fukui, and M. Ogawa, "Wear and Mechanical Properties, and Cell Viability of Gas-Nitrided Beta-Type Ti-Nb-Ta-Zr System Alloy for Biomedical Applications," *Mater. Trans.*, vol. 49, no. 1, pp. 166–174, 2008.

[197] R. Maas, M. Koch, N. R. Harris, N. M. White, and A. G. R. Evans, "Thick-film printing of PZT onto silicon," *Mater. Lett.*, vol. 31, no. 1, pp. 109–112, 1997.

[198] S. Divinski, F. Hisker, C. Klinkenberg, and C. Herzig, "Niobium and titanium diffusion in the high niobium-containing Ti–54Al–10Nb alloy," *Intermetallics*, vol. 14, no. 7, pp. 792–799, 2006.

[199] A. E. Pontau and D. Lazarus, "Diffusion of titanium and niobium in bcc Ti-Nb alloys," *Phys. Rev. B*, vol. 19, no. 8, pp. 4027–4037, Apr. 1979.

[200] K. Bose and R. J. K. Wood, "Optimum tests conditions for attaining uniform rolling abrasion in ball cratering tests on hard coatings," *Wear*, vol. 258, no. 1–4, pp. 322–332, 2005.

[201] K. Adachi and I. M. Hutchings, "Sensitivity of wear rates in the micro-scale abrasion test to test conditions and material hardness," *Wear*, vol. 258, no. 1–4, pp. 318–321, 2005.

[202] M. Bromark, M. Larsson, P. Hedenqvist, and S. Hogmark, "Wear of PVD Ti/TiN multilayer coatings," *Surf. Coatings Technol.*, vol. 90, no. 3, pp. 217–223, 1997.

[203] M. Diserens, J. Patscheider, and F. Lévy, "Improving the properties of titanium nitride by incorporation of silicon," *Surf. Coatings Technol.*, vol. 108–109, pp. 241–246, 1998.

[204] J. C. A. Batista, A. Matthews, and C. Godoy, "Micro-abrasive wear of PVD duplex and single-layered coatings," *Surf. Coatings Technol.*, vol. 142–144, pp. 1137–1143, 2001.

[205] P. Hedenqvist, M. Bromark, M. Olsson, S. Hogmark, and E. Bergmann, "Mechanical and tribological characterization of low-temperature deposited PVD TiN coatings," *Surf. Coatings Technol.*, vol. 63, no. 1, pp. 115–122, 1994.

[206] K. L. Rutherford, S. J. Bull, E. D. Doyle, and I. M. Hutchings, "Laboratory characterisation of the wear behaviour of PVD-coated tool steels and correlation with cutting tool performance," *Surf. Coatings Technol.*, vol. 80, no. 1, pp. 176–180, 1996.

[207] Y. Kirmanidou, M. Sidira, M.-E. Drosou, V. Bennani, A. Bakopoulou, A. Tsouknidas, N. Michailidis, and K. Michalakis, "New Ti-Alloys and Surface Modifications to Improve the Mechanical Properties and the Biological Response to Orthopedic and Dental Implants: A Review," *Biomed Res. Int.*, vol. 2016, p. 2908570, Jan. 2016.

[208] Y. Kusano, K. Van Acker, and I. M. Hutchings, "Methods of data analysis for the micro-scale abrasion test on coated substrates," *Surf. Coatings Technol.*, vol. 183, no. 2–3, pp. 312–327, 2004.

[209] D. N. Allsopp, R. I. Trezona, and I. M. Hutchings, "The effects of ball surface condition in the micro-scale abrasive wear test," *Tribol. Lett.*, vol. 5, no. 4, pp. 259–264, 1998.

[210] S. Banfield, J. C. A.-B. Wilson, G. Cassar, A. Leyland, A. Matthews, and J. Housden, "An investigation into the effect of Triode Plasma Oxidation (TPO) on the tribological properties of Ti6Al4V," *Surf. Coatings Technol.*, vol. 206, no. 7, pp. 1955–1962, 2011.

[211] G. Cassar, J. C. A.-B. Wilson, S. Banfield, J. Housden, A. Matthews, and A. Leyland, "Surface modification of Ti–6Al–4V alloys using triode plasma oxidation treatments," *Surf. Coatings Technol.*, vol. 206, no. 22, pp. 4553–4561, 2012.

[212] M. F. C. Andrade, R. P. Martinho, F. J. G. Silva, R. J. D. Alexandre, and A. P. M. Baptista, "Influence of the abrasive particles size in the micro-abrasion wear tests of TiAlSiN thin coatings," *Wear*, vol. 267, no. 1, pp. 12–18, 2009.

[213] F. J. G. Silva, R. B. Casais, R. P. Martinho, and A. P. M. Baptista, "Role of abrasive material on micro-abrasion wear tests," *Wear*, vol. 271, no. 9, pp. 2632–2639, 2011.

[214] F. Marques, W. M. da Silva, J. M. Pardal, S. S. M. Tavares, and C. Scandian, "Influence of heat treatments on the micro-abrasion wear resistance of a superduplex stainless steel," *Wear*, vol. 271, no. 9, pp. 1288–1294, 2011.